



THE THERAPEUTIC USE OF
MESENCHYMAL STEM CELLS FOR
TREATING KIDNEY DISEASE



Andrea Frances Wise

Bachelor of Science (Honours)

Department of Anatomy and Developmental Biology
Monash University,
Melbourne, Australia

October 2014

Submitted to Monash University in total fulfilment
of the requirements for the degree of Doctor of Philosophy

Notice 1

Under the Copyright Act 1968, this thesis must be used only under the normal conditions of scholarly fair dealing. In particular no results or conclusions should be extracted from it, nor should it be copied or closely paraphrased in whole or in part without the written consent of the author. Proper written acknowledgement should be made for any assistance obtained from this thesis.

Notice 2

I certify that I have made all reasonable efforts to secure copyright permissions for third-party content included in this thesis and have not knowingly added copyright content to my work without the owner's permission.

TABLE OF CONTENTS

List of Figures	I
List of Tables	II
Summary	III
General Declaration	V
Acknowledgments	VI
Research Output	VIII
Abbreviations	XI
Chapter 1: Literature Review	
1.1 Introduction	1
1.2 The Kidney	3
1.2.1 Kidney Disease: a global health problem	6
1.2.2 Acute Kidney Injury	8
1.2.3 Renal ischaemia/reperfusion injury	9
1.2.3.1 Rodent models of IR injury	10
1.2.3.2 Cellular pathophysiology following IR injury	10
1.2.3.3 Regeneration and repair of the tubular epithelium following IR injury	12
1.3 The mononuclear phagocyte system	16
1.3.1 Monocytes	16
1.3.1.1 Murine monocyte subsets (Ly6C ^{high} and Ly6C ^{low})	17
1.3.1.2 Human monocyte subsets (CD14 and CD16)	19
1.3.2 Macrophages	22
1.3.2.1 Macrophage polarisation: M1 vs. M2	24
1.3.2.2 The pathogenic and protective roles of macrophages in acute kidney disease	26
1.4 Kidney, stem cells and regeneration	29
1.4.1 Mesenchymal stem cells	29
1.4.2 Mesenchymal stem cells in tissue regeneration and repair	31
1.4.3 Mesenchymal stem cells in acute kidney disease	32
1.4.4 Homing of mesenchymal stem cells	36
1.4.5 Do mesenchymal stem cells act via macrophages?	38
1.5 Hypothesis and aims	41

Chapter 2: The characterisation of MSCs and the development of an intravenous MSC therapy for mice with acute ischaemic kidney injury

2.1 Introduction	42
2.2 Materials and Methods	44
2.2.1 Mesenchymal stem cells	44
2.2.1.1 Colony-forming unit-fibroblasts assay	44
2.2.1.2 MSC multilineage differentiation	45
2.2.2 Animals and Ethics Approval	45
2.2.2.1 Renal ischaemia/reperfusion injury	45
2.2.2.2 Structural analysis	46
2.2.2.3 Flow cytometry	47
2.2.3 Statistical analysis	49
2.3 Results	50
2.3.1 Characterisation of mouse MSCs	50
2.3.2 Characterisation of human MSCs	50
2.3.3 Dose curve of MSC administration to mice with unilateral IR injury	55
2.3.4 Semi-quantification of histopathology	56
2.3.5 Apoptosis	58
2.3.6 Assessment of EpCAM ⁺ proximal TECs	58
2.4 Discussion	61

Chapter 3: Human mesenchymal stem cells alter macrophage phenotype and promote regeneration via homing to the kidney following ischemia/reperfusion injury

3.1 Introduction	66
3.2 Materials and Methods	68
3.2.1 Mesenchymal stem cell culture	68
3.2.2 Experimental design	68
3.2.3 Bioluminescence imaging	69
3.2.4 Histology and immunofluorescence labeling	69
3.2.5 Hydroxyproline, SDS-PAGE and zymography analysis	70
3.2.6 MSC and macrophage co-culture	71
3.2.7 Real-time quantification PCR and gene analysis	72
3.2.8 Statistical analysis	73

3.3 Results	74
3.3.1 MSCs home to the injured kidney following unilateral and bilateral IR injury	74
3.3.2 MSCs promote structural and functional regeneration	78
3.3.3 MSCs reduce collagen accumulation in the injured kidney	81
3.3.4 MSCs alter macrophage phenotype following <i>in vitro</i> co-culture	83
3.4 Discussion	86
Chapter 4: Human mesenchymal stem cells alter the phenotype and gene profile of monocytes from type 2 diabetic patients with end-stage renal disease	
4.1 Introduction	90
4.2 Subjects and Methods	93
4.2.1 Study population	93
4.2.2 Monocyte purification	93
4.2.3 Flow cytometry	95
4.2.4 Monocyte and MSC co-culture	95
4.2.5 RNA isolation and microarray analysis	97
4.2.6 Statistical analysis	97
4.3 Results	98
4.3.1 The proportions of blood monocyte subsets are altered in type 2 diabetic patients with ESRD	98
4.3.2 MSCs alter the inflammatory profile of monocytes	100
4.3.3 Monocytes co-cultured with MSCs have distinct gene expression profiles	104
4.3.4 MSCs induce an M2-like gene expression profile in monocytes	108
4.4 Discussion	117
Chapter 5: General Discussion	122
References	131
Appendices	156

LIST OF FIGURES

CHAPTER 1:

Figure 1.1	Schematic of the kidney	5
Figure 1.2	Multilineage potential of MSCs	30
Figure 1.3	Representative diagram depicting MSC homing to a kidney with acute damage	37

CHAPTER 2:

Figure 2.1	Mouse mesenchymal stem cells	51
Figure 2.2	The differentiation potential of mouse MSCs	52
Figure 2.3	Human mesenchymal stem cells	53
Figure 2.4	The characterisation of human MSCs	54
Figure 2.5	Human MSC dose curve in mice with unilateral IR injury	57
Figure 2.6	Treatment with MSCs reduces apoptosis following IR injury	59
Figure 2.7	MSC treatment increases TEC regeneration	60

CHAPTER 3:

Figure 3.1	Isolation of enhanced green fluorescent protein ⁺ firefly luciferase ⁺ (eGFP ⁺ fluc ⁺) MSCs and experimental design for <i>in vivo</i> bioluminescence tracing	76
Figure 3.2	MSCs traffic to the injured kidney(s) following unilateral and bilateral IR injury	77
Figure 3.3	MSC treatment following IR injury accelerates structural repair in adult mice	79
Figure 3.4	MSCs improve kidney function and reduce the expression and excretion of Kim-1 in the kidney following IR injury	80
Figure 3.5	MSCs reduce collagen accumulation in the kidney following IR injury	82
Figure 3.6	MSCs can alter macrophage phenotype following <i>in vitro</i> co-culture ...	84

CHAPTER 4:

Figure 4.1	Schematic of the isolation and <i>in vitro</i> culture of human monocytes ...	96
Figure 4.2	Comparison of CD14/CD16 monocyte populations isolated from control and type 2 diabetic subjects	99
Figure 4.3	Control and type 2 diabetic-derived monocytes following 48 hours of co-culture with MSCs	102
Figure 4.4	MSCs alter the phenotype of human monocytes	103
Figure 4.5	Transcription profiling of human monocytes	105
Figure 4.6	MSCs alter the gene expression profile of monocytes	110
Figure 4.7	Signalling pathways upregulated in monocytes co-cultured with MSCs	111
Figure 4.8	MSCs upregulate signalling associated with an M2 macrophage response	114
Figure 4.9	MSCs upregulate classical monocyte and M2 macrophage-associated phagocytic receptors	115
Figure 4.10	MSCs downregulate MHC class II molecules	116

LIST OF TABLES
CHAPTER 1:

Table 1.1	Classification of murine monocyte subsets based on phenotype and function	18
Table 1.2	Classification of human monocyte subsets based on phenotype and function	19
Table 1.3	Classification of macrophages based on phenotype and function	23
Table 1.4	Summary of studies using mesenchymal stem cells (MSCs) isolated from various sources to treat acute kidney injury	34

CHAPTER 3:

Table 3.1	The injury scale used to grade kidney damage following IR injury	69
Table 3.2	Real-time PCR TaqMan gene expression assays	72
Table 3.3	Human cytokines secreted following 24 hours of MSC and mouse bone marrow-derived macrophage co-culture <i>in vitro</i>	85

CHAPTER 4:

Table 4.1	Baseline characteristics of control and type 2 diabetic subjects	94
Table 4.2	Top genes upregulated in MSC-treated monocytes compared to monocytes alone	106
Table 4.3	Top genes downregulated in MSC-treated monocytes compared to monocytes alone	107
Table 4.4	Top 10 canonical signalling pathways significantly over-represented in MSC-treated monocytes	111
Table 4.5	Top 10 canonical pathways merged gene list	112

Summary

A surge in the prevalence of chronic diseases, including chronic kidney disease (CKD), has caused a major shift in the developed world's disease profile. The increasing incidence of CKD is in part due to the escalating incidence of type 2 diabetes. For end-stage renal disease (ESRD) patients, the only renal replacement therapy options for kidney disease patients are dialysis and kidney transplantation. However, dialysis places a substantial burden on patient quality of life and the global healthcare systems, and there is a shortage of donor organs for transplantation. Together, these issues highlight the urgent need for new therapeutic approaches.

The adult kidney has the capacity, although somewhat limited, to undergo regeneration and repair following injury. This process is primarily governed by the surrounding microenvironment, with the nature of the inflammatory response playing a large part in determining disease outcome. Monocytes and macrophages are the principal immune cells that infiltrate the diseased kidney, where signals from the local milieu determine their activation and functional state. Therefore, given a favourable environment, monocytes and macrophages have the ability to resolve inflammation and promote repair, leading to the restoration of renal architecture and function.

Mesenchymal stem (stromal) cells (MSCs) possess unique immunomodulatory and cytoprotective properties, making them an ideal candidate for a range of therapeutic applications, including kidney disease. This thesis investigated the reparative potential of MSCs to promote kidney regeneration in ischaemia/reperfusion injury (IR), a model of acute kidney disease, and evaluated the mechanisms involved in the attenuation of structural injury and functional decline of the kidneys. Additionally, the effect MSCs have on the polarisation of murine macrophages and monocytes isolated from type 2 diabetic patients with ESRD were assessed.

In Chapter 2, MSCs derived from human bone marrow were characterised and compared to murine bone marrow-derived MSCs. Following administration to mice with IR injury, human MSC treatment promoted structural repair resulting in reduced apoptosis and increased re-epithelisation of the damaged tubular epithelium. In Chapter 3, the renoprotective mechanisms by which the human MSCs promoted repair were examined. It was shown that following administration to mice with IR injury, MSCs homed to the injured kidney where they afforded protection, indicated by reduced blood urea nitrogen, serum creatinine and proximal and urinary kidney injury molecule-1. MSC treatment increased matrix metalloproteinase-9 activity, which coincided with a reduction in collagen accumulation. *In vitro*, MSCs promoted the polarisation of murine bone marrow-derived macrophages towards a reparative ‘M2’ phenotype, a process mediated by paracrine mechanisms. In Chapter 4, the effects of MSCs on human monocytes isolated from patients with type 2 diabetes and ESRD or control subjects were determined. MSCs were found to retain the ability to alter the gene profile and phenotype of monocytes, even when isolated from this chronic inflammatory environment.

Overall, results from this thesis show that MSCs hold great promise as a treatment strategy for kidney disease. Therapeutic manipulation of the kidney microenvironment with MSCs could alter the polarisation of monocytes and macrophages towards a reparative phenotype, halt disease progression and even promote kidney regeneration, providing a potential new treatment option for kidney disease patients.

General Declaration

In accordance with Monash University Doctorate Regulation 17.2 Doctor of Philosophy and Research Master's regulations the following declarations are made:

I hereby declare that this thesis contains no material which has been accepted for the award of any other degree or diploma at any university or equivalent institution and that, to the best of my knowledge and belief, this thesis contains no material previously published or written by another person, except where due reference is made in the text of the thesis.

This thesis includes 2 original papers, 1 published and 1 under consideration in peer reviewed journals and 1 unpublished publication. In addition, a published invited review constitutes part of the literature review. The core theme of the thesis is the therapeutic use of mesenchymal stem cells for treating kidney disease. The ideas, development and writing up of all the papers in the thesis were the principal responsibility of myself, the candidate, working within The Department of Anatomy and Developmental Biology, Faculty of Medicine, Nursing and Health Sciences, under the supervision of Associate Professor Sharon Ricardo. The inclusion of co-authors reflects the fact that the work came from active collaboration between researchers and acknowledges input into team-based research.

In the case of chapters 1, 3 and 4 my contribution to the work involved the following:

Thesis chapter	Publication title	Publication status	Nature and extent of candidate's contribution
1	Mesenchymal stem cells in kidney inflammation and repair	Published	95%
3	Human mesenchymal stem cells alter macrophage phenotype and promote regeneration via homing to the kidney following ischemia-reperfusion injury	Published	85%
4	Human mesenchymal stem cells alter the phenotype and gene profile of monocytes from type 2 diabetic patients with end-stage renal disease	Submitted	85%

I have renumbered sections of submitted or published papers in order to generate a consistent presentation within the thesis.

Signed: 
Andrea Frances Wise

Date: 06.10.14

Acknowledgements

As I sit here, about to write the last section of this PhD thesis, I reflect back on the past 5 years and cannot believe this day has finally come. As gruelling as writing this thesis was, I am finding this section, by far, the most difficult to write as words cannot express how extremely appreciative I am for those who have helped me along this PhD rollercoaster.

First and foremost, I would like to thank my supervisor, Associate Professor Sharon Ricardo. I cannot express how glad I am that I ended up in your lab and I will forever be grateful for you taking me in. You provide every single one of your students with amazing opportunities and push us all to be the best we can be. Thank you for guidance, support and all of the opportunities you have given me. I have definitely grown as a person while being a member of your lab and am I indebted to you for that. You have an amazing lab and I have absolutely loved being apart of it!

I am extremely appreciative to a number of collaborators and members of the Monash community who have helped me with their scientific expertise. Thank you to Stephen Firth and his team at Monash Micro Imaging, Ian Boundy, Camilla Cohen and Steph Tombs at histology, and Andrew Fryga and the FlowCore team. Thank you to Professor Claude Bernard for donating both the human and mouse MSCs used in this project. A special thank you to Associate Professor Chrishan Samuel, for all of your help with performing, analysing and interpreting the collagen and zymography assays. To Dr Michelle Kett for your assistance with the renal function assays. Thank you Professor Peter Kerr and the dialysis nurses at Monash Medical Centre, for helping us obtain patient samples. Thank you also to Dr Stephen Rudd and Associate Professor Christine Wells for your help with the microarray study.

To the past and present members of the Kidney Regeneration and Stem Cell Laboratory, coming to work each day was so enjoyable because of you all. Thank you to Liz for welcoming me into the lab and providing hours of entertainment, laughter and 'Liz

moments'. Vingo, I really appreciate your patience and helping hand with all of my cell culture. To Mali and Tina, you were great mentors who taught me many of the technical skills I know today. Thank you for all of the help and guidance that you provided over the years, I will forever appreciate it. To the Monash Immunology and Stem Cell Laboratories crew, there are endless fond memories that were created over the years that I will never forget. MISCL was definitely a special workplace with an amazing vibe and bunch of people whom I have made life long friends with. Thank you particularly Marco, Jonny, Leona, Jen, Dan, Mel, Robi, Chris, Jade, Emerald and Renae for all the fun times and great memories. Also a big thank you to Marky Mark for solving all computer related crises.

To my dearest Sacred Heart girls, Cait, Jess, Shaz and Sar, you were my pick-me-ups during the lowest points of my PhD. Thank you for checking up on me, reminding me there is life outside a PhD and for being such an amazing support. To Tránt and Clari Hart's thank you for the endless entertainment and laughter you never fail to provide.

Timothy, words cannot express how grateful I am for everything you have done for me. You were by my side during the toughest of PhD times; the 5am starts, the all-nighters and the nightmare of patient sample collections, to name a few. You made me push on when I was experiencing my PhD lows and were there to share all my PhD highs. You spent countless hours in the lab helping me with big experiments and read all of my drafts along the way. I do not know what I would have done without you, all of your wisdom, help and support and I will forever be extremely thankful.

Last but not least, I would like to thank my family – mum, dad and Jo. Thank you for always providing me with the opportunities to do whatever I wanted to do. Thank you for encouraging and supporting me over the years and years of study, it is finally coming to an end! You made life at home easy for me so I could always focus entirely on my work. You endured the grumpy side of me during the times of PhD blues. I will forever be grateful for everything you have done for me over the years and I dedicate this thesis to you.

Research Output

Published manuscripts included in this PhD thesis

Invited Review: Wise AF and Ricardo SD (2012). "Mesenchymal stem cells in kidney inflammation and repair." Nephrology. 17(1): 1-10. Review. (Appendix)

Impact factor: 1.864

Times cited: 17

JCR Category	Rank in category	Quartile in category
Urology & Nephrology	37 of 75	Q2

Wise AF, Williams TM, Kiewiet MB, Payne NL, Siatskas C, Samuel CS, Ricardo SD (2014). "Human mesenchymal stem cells alter macrophage phenotype and promote regeneration via homing to the kidney following ischemia-reperfusion injury." *Am J Physiol Renal Physiol.* 306(10): F1222-F1235. (Appendix)

Impact Factor: 3.300

Times cited: 0

JCR Category	Rank in category	Quartile in category
Physiology	22 of 81	Q2
Urology & Nephrology	15 of 75	Q1

Wise AF, Williams TM, Rudd S, Wells CA, Kerr PG, Ricardo SD. "Mesenchymal stem cells alter the phenotype and gene profile of monocytes from type 2 diabetic patients with end-stage renal disease." Submitted to *Clinical Science*.

Additional publications

Williams TM, **Wise AF**, Alikhan MA, Layton DS, Ricardo SD (2014). "Establishing the flow cytometric assessment of myeloid cells in kidney ischemia/reperfusion injury." *Cytometry A.* 85(3): 256-267. (Appendix)

Impact factor: 3.066

Times cited: 0

JCR Category	Rank in category	Quartile in category
Biochemical Research Methods	26 of 78	Q2
Cell Biology	102 of 185	Q3

Huuskes BM, **Wise AF**, Cox AJ, Lim EX, Payne NL, Kelly DJ, Samuel CS, Ricardo SD. "Combination therapy of mesenchymal stem cells and serelaxin effectively attenuates renal fibrosis in obstructive nephropathy." In Press *FASEB J.*

Impact factor: 5.480

JCR Category	Rank in category	Quartile in category
Biology	7 of 83	Q1
Biochemistry & Molecular Biology	47 of 291	Q1
Cell Biology	45 of 185	Q1

Conference abstracts and presentations

International

Wise AF, Alikhan MA, Zhuang J, Ricardo SD (2011). "The in vitro and in vivo alteration of macrophage polarisation via mesenchymal stem cells." *American Society of Nephrology Annual Meeting*, Philadelphia, USA

Wise AF, Williams TM, Zhuang J, Samuel CS, Ricardo SD (2012). "Mesenchymal stem cells promote renal regeneration via alteration of macrophage phenotype." *American Society of Nephrology Annual Meeting*, San Diego, USA

Wise AF, Kiewiet MB, Samuel CS, Ricardo SD (2012). "Mesenchymal stem cells promote regeneration via homing to the kidney and altering macrophage phenotype following ischemia-reperfusion injury." *International Society of Nephrology*, Florence, Italy

Wang B, **Wise AF**, Huuskes B, Ricardo SD (2014). "An innovative microRNA delivery system using engineered mesenchymal stem cells to combat kidney fibrosis." *The 14th Asia Pacific Congress of Nephrology*, Tokyo, Japan

Wise AF, Williams TM, Rudd S, Wells CA, Kerr PG, Ricardo SD (2014). "Human mesenchymal stem cells promote alternative activation of monocytes isolated from healthy and type 2 diabetic subjects." *American Society of Nephrology Annual Meeting*, Philadelphia, USA

Huuskes BM, **Wise AF**, Samuel CS, Ricardo SD (2014). "Attenuation of renal fibrosis through the combined therapy of mesenchymal stem cells and the hormone serelaxin." *American Society of Nephrology Annual Meeting*, Philadelphia, USA

Wang B, **Wise AF**, Huuskes B, Ricardo SD (2014). "MicroRNA Let-7C delivery using engineered mesenchymal stem cells to combat kidney fibrosis." *American Society of Nephrology Annual Meeting*, Philadelphia, USA

Williams TM, **Wise AF**, Barbuto J, Samuel CS, Layton DS, Hamilton JA, Ricardo SD (2014). "Blocking myeloid growth factors to protect against ischemia/reperfusion injury." *American Society of Nephrology Annual Meeting*, Philadelphia, USA

National

Wise AF, Zhuang J, Ricardo SD (2010). "Therapeutic application of human bone marrow mesenchymal stem cells in ischemia-reperfusion injury." *The 46th Annual Scientific Meeting of the Australia and New Zealand Society of Nephrology*, Perth, WA
Abstract published in: *Nephrology* 15 (Supp. S4); 164.

Wise AF, Alikhan MA, Zhuang J, Ricardo SD (2011). "Mesenchymal stem cells modulate macrophage phenotype in vitro and in vivo." *The 47th Annual Scientific Meeting of the Australia and New Zealand Society of Nephrology*, Adelaide, South Australia
Abstract published in: *Nephrology* 16(Supp. S1); A107.

Wise AF, Williams TM, Zhuang J, Samuel CS, Ricardo SD (2012). “The regenerative potential of mesenchymal stem cells following ischemia-reperfusion injury.” *The 48th Annual Scientific Meeting of the Australia and New Zealand Society of Nephrology*, Auckland, New Zealand Abstract published in: *Nephrology* 17(Supp. S2); A064.

Huuskes BM, **Wise AF**, Jones CV, Lim EX, Payne NL, Siatskas C, Samuel CS, Ricardo SD (2013). “A novel strategy to attenuate renal fibrosis using the combination of mesenchymal stem cells and relaxin in obstructive nephropathy.” *The Annual Scientific Meeting of the Australasian Society for Stem Cell Research*, Brisbane, Queensland

Wise AF, Williams TM, Wells CA, Kerr PG, Ricardo SD (2014). “Human bone marrow-derived mesenchymal stem cells alter the phenotype and gene profile of monocytes from type 2 diabetic patients.” *The 50th Annual Scientific Meeting of the Australia and New Zealand Society of Nephrology*, Melbourne, Victoria
Abstract published in: *Nephrology* 19(Supp. S4).

Huuskes BM, **Wise AF**, Cox AJ, Lim EX, Payne NL, Samuel CS, Ricardo SD (2014). “Combined therapy of mesenchymal stem cells and the hormone relaxin attenuate renal fibrosis.” *The 50th Annual Scientific Meeting of the Australia and New Zealand Society of Nephrology*, Melbourne, Victoria
Abstract published in: *Nephrology* 19(Supp. S4).

Wang B, **Wise AF**, Yao K, Huuskes B, Ricardo SD (2014). “An innovative microRNA delivery system using engineered mesenchymal stem cells to combat kidney fibrosis.” *The 50th Annual Scientific Meeting of the Australia and New Zealand Society of Nephrology*, Melbourne, Victoria
Abstract published in: *Nephrology* 19(Supp. S4).

Williams TM, **Wise AF**, Barbuto J, Samuel CS, Layton DS, Hamilton JA, Ricardo SD (2014). “Tissue repair and fibrosis in kidney ischemia/reperfusion injury is dependent on the timing of CSF-1 signalling to myeloid cells.” *The 50th Annual Scientific Meeting of the Australia and New Zealand Society of Nephrology*, Melbourne, Victoria
Abstract published in: *Nephrology* 19(Supp. S4).

Awards

Australia and New Zealand Society of Nephrology Travel Award to attend the ANZSN Annual Scientific Meeting Perth, WA – 2010

Australia and New Zealand Society of Nephrology Travel Award to attend the ANZSN Annual Scientific Meeting Adelaide, SA – 2011

Australia and New Zealand Society of Nephrology Travel Award to attend the ANZSN Annual Scientific Meeting Auckland, New Zealand – 2010

Australia and New Zealand Society of Nephrology Travel Award to attend the ASN Annual Scientific Meeting Philadelphia, USA – 2014

Abbreviations

α-MEM	α-minimum essential medium	ERA-EDTA	European Renal Association-European Dialysis and Transplant Association
βig-H3	transforming growth factor-β-induced protein	ES	Embryonic stem
A2M	Alpha-2-macroglobulin	ESRD	End-stage renal disease
ABC	Avidin-biotin complex	FABP-4	Fatty acid binding protein-4
AKI	Acute kidney injury	F13A1	Coagulation factor XIII A1 polypeptide
ANOVA	Analysis of variance	FACS	Fluorescence activated cell sorting
APOC1	Apolipoprotein C-1	FBS	Foetal bovine serum
APOE	Apolipoprotein E	FcγR	Fcγ receptor
ARF	Acute renal failure	FDR	False discovery rate
Arg1	Arginase 1	Fizz1	Found in inflammatory zone 1
ATN	Acute tubular necrosis	FLOT1	Flotillin 1
bFGF	Basic fibroblast growth factor	FLNA	Filamin A
BM	Bone marrow	FLNB	Filamin B
BrdU	Bromodeoxyuridine	Fluc	Firefly luciferase
BSA	Bovine serum albumin	FN	Fibronectin
BUN	Blood urea nitrogen	FPR	Formyl peptide receptor
C2	Complement component 2	GDNF	Glial cell-derived neurotrophic factor
C3	Complement component 3	GFR	Glomerular filtration rate
CIITA	Class II major histocompatibility complex transactivator	GM-CSF	Granulocyte macrophage colony-stimulating factor
CASP5	Caspase 5	GMSCs	Gingiva-derived MSCs
CCL	Chemokine (C-C motif) ligand	GvHD	Graft-versus-host disease
CCR	Chemokine (C-C motif) receptor	H&E	Haematoxylin and eosin
cDNA	Complementary deoxyribonucleic acid	HA	Hyaluronic acid
CFU-U	Colony-forming unit-fibroblasts	HBSS	Hank's balanced salt solution
Chi3l3	Chitinase 3-like-3	HGF	Hepatocyte growth factor
CKD	Chronic kidney disease	HGF-huMSCs	Human umbilical cord-derived MSCs overexpressing HGF
CLEC4D	C-type lectin domain family 4	HIF1α	Hypoxic inducible factor 1α
CLP	Cecal ligation and puncture	HLA	Human leukocyte antigen
COX-2	Cyclooxygenase-2	huMSCs	Human umbilical cord-derived MSCs
CSF	Colony stimulating factor	ICAM1	Intracellular adhesion molecule 1
Ct	Threshold cycle	IDO	Indoleamine 2,3-dioxygenase
CXCL	Chemokine (C-X-C motif) ligand	IFN	Interferon
CXCR	Chemokine (C-X-C motif) receptor	IGF	Insulin-like growth factor
CX3CR1	Chemokine (C-X3-C motif) receptor 1	IL	Interleukin
DAB	3,3'-diaminobenzidine	IL1RA	Interleukin-1 receptor antagonist
DAMPs	Danger-associated molecular patterns	iNOS	Inducible nitric oxide synthase
DCs	Dendritic cells	IPA	Ingenuity pathway analysis
DC-SIGN	Dendritic cell-specific intracellular adhesion molecule-3 grabbing non-integrin	iPS	induced pluripotent stem
DN	Diabetic nephropathy	IR	Ischaemia/reperfusion
DNase	Deoxyribonuclease	ITGA9	Integrin, α 9
EAE	Experimental autoimmune encephalomyelitis	ITGAL	Integrin, α L
ECM	Extracellular matrix	ITGAX	Integrin, α X
EDNRB	Endothelin receptor type B	i.p.	Intraperitoneal
EDTA	Ethylenediaminetetraacetic acid	i.v.	Intravenous
EGF	Epidermal growth factor	Kim-1	Kidney injury molecule-1
eGFP	Enhanced green fluorescent protein	LILRB1	Leukocyte immunoglobulin like receptor subfamily B member 1
EP	E-prostanoid	LPL	Lipoprotein lipase
EpCAM	Epithelial cell adhesion molecule		

LPS	Lipopolysaccharide	SERPINF1	Serpin peptidase inhibitor clade F member 1
Ly6C	Lymphocyte antigen 6 complex	SOCS3	Suppressor of cytokine signalling 3
M1	Classically activated macrophage	SOD2	Superoxide dismutase 2
M2	Alternatively activated macrophage	SPN	Sialophorin
MACS	Magnetic activated cell sorting	STAT4	Signal transducer and activator of transcription 4
MCP-1	Monocyte chemoattractant protein-1	T2D	Type 2 diabetes
MFI	Mean fluorescence intensity	TECs	Tubular epithelial cells
MHC	Major histocompatibility complex	TGF	Transforming growth factor
MIP	Monocyte inflammatory protein	TLR	Toll-like receptor
MMP	Matrix metalloproteinase	TNF	Tumour necrosis factor
MOG	Myelin oligodendrocyte glycoprotein	TREM	Triggering receptor expressed on myeloid cells
MR	Mannose receptor	UUO	Unilateral ureteral obstruction
Mrc1	Mannose receptor, C type 1	Veh	Vehicle
MSCs	Mesenchymal stem (stromal) cells	VEGF-hMSCs	Human embryonic MSCs overexpressing VEGF
MSR1	Macrophage scavenger receptor 1	VLDLR	Very low density lipoprotein receptor
NCAM	Neural cell adhesion molecule	WHO	World health organization
NO	Nitric oxide	Wnt	Wingless-type MMTV integration site family
OTT	Orthotopic tracheal transplantation		
PAMPs	Pathogen-associated molecular patterns		
Pax2	Paired box gene 2		
PBMCs	Peripheral blood mononuclear cells		
PBS	Phosphate buffered saline		
PC	Principal component		
PCA	Principal component analysis		
PCNA	Proliferating cell nuclear antigen		
PDGF	Platelet-derived growth factor		
PFA	Paraformaldehyde		
PGE ₂	Prostaglandin E ₂		
Pmp	Per million population		
PPARG	Peroxisome proliferator-activated receptor γ		
PRKCA	Protein kinase C α		
PRR	Pattern recognition receptor		
PTGER2	Prostaglandin E2 receptor		
PTGS2	Prostaglandin-endoperoxide synthase 2		
qPCR	Quantitative polymerase chain reaction		
RANTES	Regulated and normal T cell expressed and secreted		
RBP1	Retinol binding protein 1		
Retnla	Resistin-like molecule alpha		
RFP	Red fluorescent protein		
RNA	Ribonucleic acid		
ROIs	Regions of interest		
ROS	Reactive oxygen species		
Rpm	Revolutions per minute		
RPMI	Roswell Park Memorial Institute		
SCID	Severe combined immunodeficiency		
SDF-1	Stromal cell-derived factor-1		
SDS-PAGE	Sodium dodecyl sulphate polyacrylamide gel electrophoresis		
SEM	Standard error of the mean		
SERPINA1	Serpin peptidase inhibitor clade A member 1		
SERPINB2	Serpin peptidase inhibitor clade B member 2		

Symbols

α	alpha
β	beta
γ	gamma
Δ	delta; change in
+	positive
-	negative
~	approximately
AU\$	Australian dollar
US\$	United States dollar
°C	degrees Celsius
μ l	microlitre
μ m	micrometre
mg	milligram
ml	millilitre
mM	millimolar
ng	nanogram
g/L	gram pre litre
w/v	weight per volume

CHAPTER 1

Literature Review

Declaration for Thesis Chapter 1

Declaration by candidate

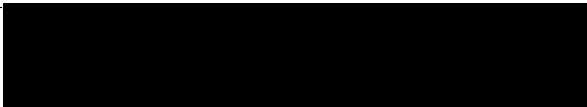
Part of this chapter was published in Nephrology:

Wise AF and Ricardo SD (2012). "Mesenchymal stem cells in kidney inflammation and repair" Nephrology 17(1): 1-10.

In the case of Chapter 1, the nature and extent of my contribution to the work was the following:

Nature of contribution	Extent of contribution (%)
Design, preparation of manuscript	95%

The undersigned hereby certify that the above declaration correctly reflects the nature and extent of the candidate's and co-authors' contributions to this work.

Candidate's Signature		Date: 06.10.14
Main Supervisor's Signature		Date: 06.10.14

1.1 Introduction

Chronic kidney disease (CKD) is the progressive loss of kidney function ultimately resulting in end-stage renal disease (ESRD). In this instance, kidney function is reduced to 10% capacity or less and patients require renal replacement therapy. It is estimated there are approximately 3,010,000 ESRD patients receiving renal replacement therapy worldwide. Currently the only renal replacement therapy options for these patients are kidney transplantation or dialysis. However, dialysis presents a significant healthcare burden whereby in the United States, the total Medicare expenditure for haemodialysis is US\$87,945 per patient per annum and in Australia AU\$79,072 per patient per annum. Further, CKD and ESRD account for 24% of the total annual healthcare budget in the United States, costing US\$79.9 billion. Moreover, in Australia only 6% of dialysis patients receive a kidney transplant each year due to the significant shortage of organ donations.

In addition, the incidence of CKD and consequent ESRD is escalating. Currently, the leading cause of ESRD worldwide is due to complications from diabetes mellitus. This is in part due to the surge in diabetes, or more specifically type 2 diabetes (T2D), which accounts for 90% of all diabetic cases. Given the incidence of CKD is dramatically rising, the poor quality of life that these patients endure, and the enormous economic burden the disease places on the healthcare system, there is an urgent need for a more efficient and cost effective therapeutic approach for the treatment of kidney disease.

In contrast to CKD, following acute injury, the kidney has the capacity to undergo endogenous repair to a certain extent. The most common cause of acute kidney injury (AKI) is ischaemic insult. The experimental model of acute ischaemic injury, known as ischaemia/reperfusion (IR) injury, enables the study of pathophysiological processes that mediate injury and repair. Monocytes and their tissue-derived progeny, macrophages, play a

crucial role in determining the outcome of kidney disease as they can both contribute to tissue inflammation and promote remodelling and repair.

Mesenchymal stem (stromal) cells (MSCs) possess extraordinary immunomodulatory and tissue regenerative properties. Following *in vivo* administration, these cells home to the site of injury where they secrete an array of factors that can alter the course of disease. For this reason, MSCs have been used in a range of biomedical disciplines. Following AKI, MSC therapy could promote tubular epithelial cell (TEC) regeneration and remodelling of the damaged tissue architecture through the secretion of regenerative growth factors. In addition, MSCs could alter the polarisation of infiltrating monocytes and macrophages towards a tissue reparative phenotype. Understanding the processes in which MSCs coordinate repair could lead to a more effective treatment option for patients with kidney disease.

1.2 The Kidney

The human adult kidney is a highly complex organ with its primary function essentially being to filter the blood, remove waste and excess fluid along with reabsorbing nutrients. This coordinated interplay of functions results in the critical regulation of the body's fluid and electrolyte balance (1). However, the kidneys also carry out several other functions that play a vital role in maintaining the body's homeostatic state, that include regulating the production of red blood cells, controlling blood pressure, maintaining blood calcium levels and producing calcitriol, the active form of vitamin D, which promotes high bone density (2-5). The kidney's morphologically complex and highly differentiated anatomical structure is key to successfully accomplishing this diverse range of specialised functions (6).

The kidney parenchyma is divided into two major compartments, the outer cortex and the inner medulla. Spanning the renal cortex and medulla is the nephron, the functional unit of the kidney, which is comprised of a precise structural arrangement of over 30 different specialised cells types. Nephrogenesis, the process of nephron development, ceases by 36 weeks of gestation in humans, after which no new nephrons can be generated (7). At term birth, the normal human kidney contains on average one million nephrons (8). However, this can vary by 13-fold and is believed to be affected by birth weight, body size, gender, race, hypertension and the length of gestation, all of which are risk factors associated with the development of kidney disease (8).

The nephron is comprised of two main components: the renal corpuscle and the renal tubule. The renal corpuscle, located in the cortex, is the initial filtering segment. The tubule, which follows the renal corpuscle, passes from the cortex into the medulla. The renal corpuscle is made up of the glomerulus, a clustered network of capillaries, which is surrounded by a glomerular capsule, known as the Bowman's capsule. As blood passes through this network at high pressure, waste products, water and various solutes are filtered

out and allowed to pass into the tubular region. The renal tubule segment consists of the proximal convoluted tubule, the loop of Henle and the distal convoluted tubule. From the glomerulus, the filtrate enters and passes through the proximal convoluted tubule, where the majority of reabsorption of electrolytes, nutrients and water occurs. It then passes through the loop of Henle, of which the main function is to maintain an osmotic gradient in order to concentrate the urine. Finally, the filtrate passes through the distal convoluted tubule where blood pressure, calcium levels and the blood pH are all regulated. From the distal convoluted tubule the filtrate enters into the collecting duct where it is transported through the medulla, into the renal pelvis and ultimately the ureter where it is then emptied into the bladder as urine (Figure 1.1).

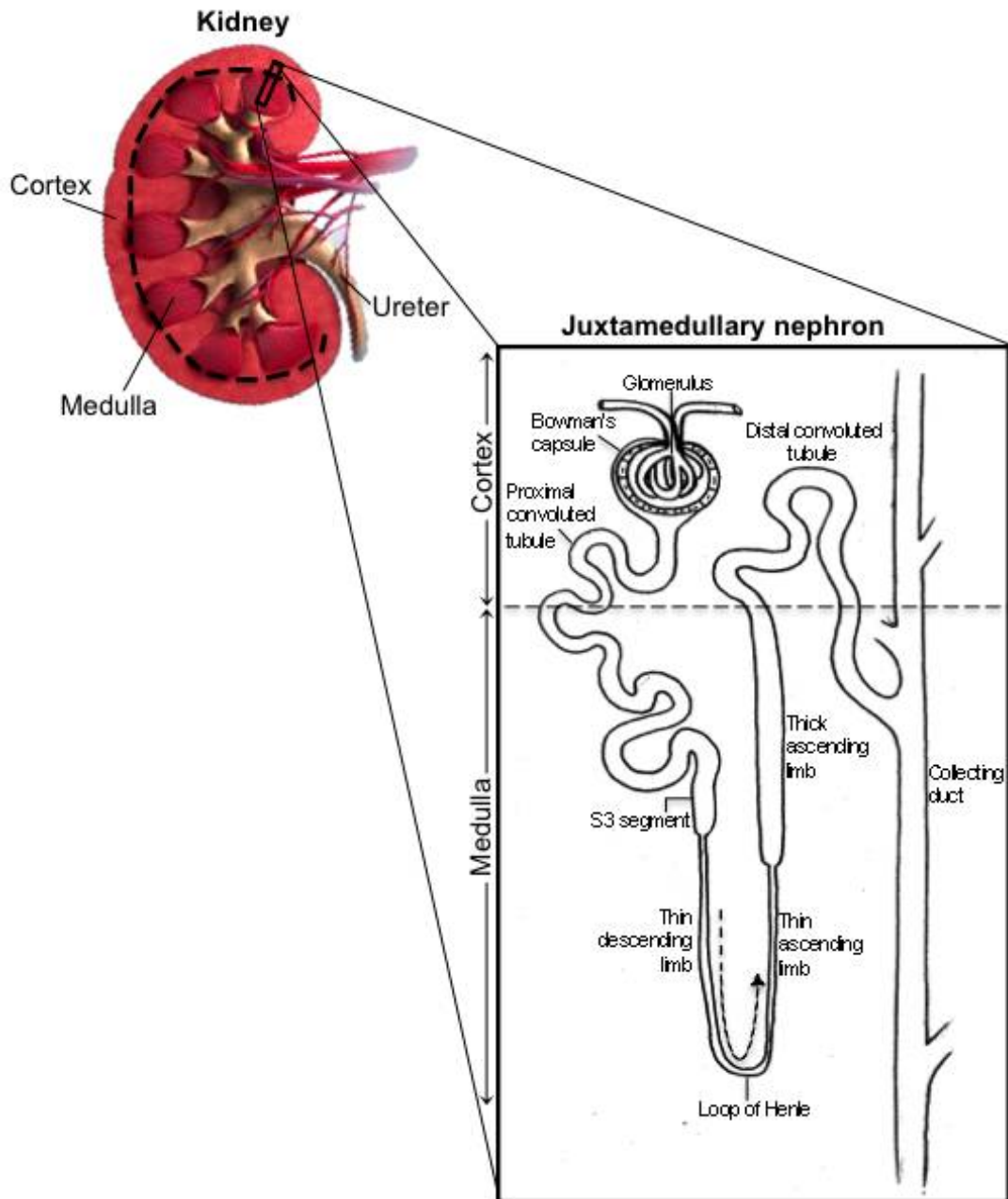


Figure 1.1 Schematic of the kidney. The kidney parenchyma is comprised of two major compartments, the outer cortex and inner medulla. Spanning the renal cortex and medulla is the functional unit of the kidney, the nephron. The nephron is made up of the renal corpuscle, and the renal tubule, which consists of the proximal convoluted tubule, loop of Henle and distal convoluted tubule. The dotted arrow depicts the direction in which the kidney filtrate flows.

1.2.1 Kidney Disease: a global health problem

The 21st century has seen a profound increase in the prevalence of chronic diseases, such as CKD, making them the leading cause of morbidity and mortality worldwide (9). CKD is defined as either a reduction in kidney function (glomerular filtration rate (GFR) < 60ml/min/1.73m²) or the presence of kidney damage for ≥ 3 months (10). The disease is categorised into 5 stages (stages 1-5) according to the level of reduced kidney function or evident kidney damage, with stage 5 being ESRD (9). At this stage, kidney function is reduced to 10% capacity or less (GFR < 15ml/min/1.73m²) and patients require renal replacement therapy, with the only two options being dialysis or kidney transplantation, in order to sustain life (10). Unfortunately, kidney disease can quite commonly progress to this stage before any symptoms present and for this reason CKD is often termed a 'silent killer'.

The increasing incidence of CKD is in part linked with the shift in the developed world's disease profile, where the incidence of T2D is dramatically increasing. Today, the principle cause of ESRD worldwide is diabetes mellitus, primarily T2D, which accounts for approximately 90% of all diabetic cases (9, 11). In 2004 in Australia, diabetes overtook glomerulonephritis as the leading cause of CKD. Currently these account for approximately 35% and 23% of all cases respectively, followed by hypertension, which accounts for 15% (12, 13). In the United States diabetes accounts for 42% of CKD patients (14). In 2013, the prevalence of diabetes was estimated to be 382 million worldwide and is further predicted to reach an alarming 471 million by 2035 (11). Of this 382 million, 80% were from low- and middle-income countries including China (98.4 million) and India (65.1 million; 11).

Due to the drastically escalating T2D epidemic, in conjunction with an ageing population, it is predicted that there will be a surge in the number of patients with CKD and ESRD requiring renal replacement therapies over the next decade (12). Between 1991 and 2009 the number of Australian patients being treated for ESRD nearly tripled and it is projected to increase by an additional 80% between 2009 and 2020 (12, 15). This will result in a

significant financial burden on our healthcare systems. At the end of 2009, 7962 ESRD patients were receiving hospital dialysis in Australia, costing approximately AU\$79,072 per patient (16, 17). In 2010, the Australian Government expenditure on renal replacement therapies alone was almost AU\$1 billion and it is estimated to cost an additional AU\$12 billion between 2009 and 2020 (17). The prevalence of ESRD in the United States is 1,901 patients per million population (pmp). In 2011, the United States Medicare expenditure for CKD and ESRD was US\$45.4 billion and US\$34.4 billion respectively, representing 24% of their total Medicare budget (14, 18). According to the 2010 European Renal Association-European Dialysis and Transplant Association (ERA-EDTA) registry annual report, the average prevalence of ESRD in 29 countries in Europe was 741 pmp, representing 551,005 patients, with dialysis treatment alone consuming 2% of the national healthcare budget (19, 20). The situation is substantially worse in developing countries where renal replacement therapy is often unaffordable or unavailable, resulting in ESRD claiming the lives of nearly 1 million patients each year (9).

Moreover, while renal replacement therapies are able to prolong the lives of ESRD patients, their quality of life remains poor. Haemodialysis is the predominant form of dialysis, requiring patients to attend a satellite or hospital based centre three times per week for three to four hours per session. For this reason, as well as the substantial economic burden associated with dialysis, kidney transplantation is the preferred option. However, likewise this provides a treatment option and not a cure for ESRD. Unfortunately, there is a significant shortage of organ donations in Australia with only 6% of patients on dialysis receiving a kidney transplant each year, making the average waiting time for an organ donation four to seven years (13). Furthermore, following transplantation, patients are still at risk of transplant rejection. ESRD patients also have a 20- to 30-fold increased risk of developing cardiovascular diseases such as hypertension, angina, myocardial infarction, heart failure, stroke, peripheral vascular disease and arrhythmias (9). Additionally, they are at higher risk of developing anaemia as well as increased risk of premature mortality (9, 21).

As the incidence of CKD and consequent ESRD necessitating renal replacement therapies continues to escalate, the associated costs impose an enormous financial burden on global healthcare systems and threaten to reach unsustainable levels. Therefore, there is an urgent need for more effective therapeutic approaches to delay the progression of kidney disease. Understanding the cellular and molecular mechanisms that regulate kidney injury and subsequent repair in acute experimental models of kidney disease will provide important insight that could potentially lead to the development of novel therapeutic approaches that can be applied to the CKD setting.

1.2.2 Acute Kidney Injury

AKI, previously known as acute renal failure (ARF), is defined as an abrupt loss of kidney function resulting in an acute increase in nitrogenous waste in the blood (22). It is particularly common among the elderly, patients of the intensive care unit and hospital inpatients, and like CKD it too is becoming increasingly common (23, 24). Even a small decrease in kidney function is associated with an increased risk of morbidity and carries an approximate 40% to 80% chance of mortality (25). Currently, the only treatment options for AKI involve supportive interventions, with dialysis utilised in severe cases (25).

AKI is classified according to the site of injury, such as the tubules, glomeruli, vasculature or interstitium (26). Injury of the renal tubules is termed acute tubular necrosis (ATN) and is the most common form of AKI (27, 28). The pathophysiology of ATN comprises three main phases: initiation, maintenance and recovery (28). The initiation phase involves the initial insult to the TECs causing injury and dysfunction. This injury, followed by cell death and detachment from the basement membrane, leads to the formation of tubular casts, which obstruct the tubular lumen. This subsequently results in an acute reduction in GFR concomitant with an increase in serum creatinine and blood urea nitrogen (BUN) concentrations. Renal injury is established prior to the maintenance phase, which is characterised by a sustained, severe reduction in GFR and further increases in serum

creatinine and BUN. The reduction in renal function causes fluid retention, electrolyte imbalances and decreased urine output. This occurs concurrently with the infiltration of inflammatory cells into the interstitium. In the recovery phase, there is re-epithelialisation and regeneration of the injury site governing a gradual return of kidney function, a decrease in serum creatinine and BUN and an increase in urine volume (27, 28).

ATN is principally caused by ischaemia, sepsis and nephrotoxins (26-28). Due to its rich blood supply and the processing of the filtrate, the kidney is exposed to drugs and chemicals present in the body, some of which can be nephrotoxic. Common nephrotoxic agents include antibiotics such as aminoglycosides, radiocontrast agents and chemotherapy agents such as cisplatin (29-31). Ischaemic AKI usually occurs as a result of hypertension, sepsis, hypovolemia, vasoconstrictive drugs and organ transplantation (32, 33). The pathophysiology of ischaemic ATN is similar to the nephrotoxic form and often ischaemia and nephrotoxins will manifest together to cause ARF in critically ill patients (26). However, ischaemia is the leading cause of ATN and will be discussed further (1).

1.2.3 Renal ischaemia/reperfusion injury

Each kidney receives approximately 20% to 25% of the cardiac output (34). The renal cortex, containing the glomeruli, receives the majority of the renal blood flow, with the medulla only receiving approximately 10% (1). The kidney is able to adapt to reduced levels of blood flow to a certain extent. However, when oxygen levels become inadequate subsequent dysfunction and cellular injury occurs (35).

Renal IR injury occurs as a result of an abrupt decline in renal blood flow causing an impairment of oxygen and nutrient delivery, followed by the re-establishment of circulation, reperfusion (33). The hypoxic conditions that occur as a result of ischaemia trigger an inflammatory response. This is exacerbated following reperfusion, resulting in a complex cascade of events. Following ischaemia, the impact of the reduced blood flow is greatest in

the medulla, particularly at the corticomedullary junction, due to the smaller proportion of blood flow supplied to this region, and therefore it is more susceptible to ischaemic damage (1). More specifically, it is the S3 segment of the proximal tubule and the medullary thick ascending limb of the loop of Henle that are most vulnerable due to the high oxygen demands required to carry out the tubular transport processes (1).

1.2.3.1 Rodent models of IR injury

The experimental model of renal IR injury involves occluding the renal pedicle with a microvasculature clamp for a defined duration to induce ischaemia, followed by removing the clamp to allow for reperfusion. *In vivo* whole animal experimental models of IR injury comprise two forms: bilateral or unilateral. The bilateral model is considered more closely related to the human condition, where the blood supply is affected in both kidneys (36). In mice, the duration of bilateral IR injury typically ranges between 20-30 minutes and in unilateral IR injury, 30-60 minutes (37). Experimental models of IR injury result in more widespread and severe damage than what typically manifests in humans (38, 39). However, patients with ischaemic AKI often present with pre-existing co-morbidities and multifactorial aetiology and thus the prolonged ischaemic damage in rodents is required to reproduce the similar renal failure that occurs in humans (40). Nevertheless, rodent models of IR injury have become indispensable in studying the pathophysiological processes that are involved in injury and repair and have led to great advances in the field.

1.2.3.2 Cellular pathophysiology following IR injury

Under normal physiological conditions, proximal TECs are highly polarised. The apical surface is covered in microvilli, which form the brush border that extends into the tubular lumen. The microvilli contain actin filaments that connect to the actin cytoskeleton, which is located in the cytoplasm. TECs are connected to each other via tight junctions and adherens junctions. The basolateral surface of the TECs are firmly adhered to the underlying tubular basement membrane by integrins and adhesion molecules and contain Na⁺/K⁺-ATPase

pumps, which are responsible for Na⁺ reabsorption from the tubular lumen to the renal interstitium (40).

Following IR injury, there is apical bleb formation and shedding of the brush border into the tubular lumen (41). This is followed by a loss of TEC polarity and integrity of the actin cytoskeleton leading to the disruption of the cellular junction complexes. Furthermore, there is mislocalisation of the integrins and membrane proteins, such as the Na⁺/K⁺-ATPase and β -integrins, from the basolateral surface to the apical domain (42, 43). This results in desquamated, flattened, non-polarised TECs that lack cell-to-cell attachments to each other and to the basement membrane (35). These damaged proximal TECs highly express kidney injury molecule (Kim)-1 on the apical surface until recovery from injury has occurred. Additionally, the Kim-1 ectodomain is cleaved and excreted in the urine and thus its presence in the urine can be used as a direct measure of kidney injury (44). Severely injured TECs undergo apoptosis or necrosis (45). Consequently, there is sloughing of both viable and non-viable cells into the tubular lumen leaving a denuded basement membrane, which remains as the only barrier between the renal interstitium and tubular filtrate. The detached cells interact with proteins such as fibronectin and Tamm-Horsfall protein, which are also present in the lumen, resulting in the formation of tubular casts (33, 46). The casts obstruct the lumen and cause increased intratubular pressure. The increased pressure along with increased permeability, due to the denuded basement membrane, leads to backleak of the tubular filtrate into the interstitium, which is subsequently reabsorbed into the blood resulting in a reduced GFR and renal function (47).

The extent of kidney damage occurring after IR injury is dependent on the duration of the insult. However, if the underlying cause is corrected and the resulting damage is not too severe, the kidney has the ability to undergo endogenous regeneration and repair ultimately leading to the restoration of both renal architecture and function.

1.2.3.3 Regeneration and repair of the tubular epithelium following IR injury¹

Understanding the process of endogenous kidney regeneration is important for the development of new therapeutic strategies. Tissue stem/progenitor cells play a vital role in maintaining homeostasis, a process of self-renewal (48). The rate at which this occurs varies amongst tissues. For example, epithelial cells of the intestine (48) and skin (49) have a high cell turnover rate and can completely self-renew within days. In contrast, the kidney has a considerably lower cell turnover rate, with proliferative abilities that differ depending on the specialised cell type (50, 51).

Unlike mammalian kidneys, where the formation of nephrons ceases at birth, cartilaginous fish have the capacity to form new nephrons after birth through de novo nephrogenesis (52). Moreover, following partial nephrectomy, skate fish show proliferation of progenitor cells that results in ongoing kidney development (53). In contrast, mammalian adult kidneys undergo compensatory hypertrophy following uninephrectomy without the formation of new nephrons. The mammalian kidney, therefore, has a limited capacity to undergo endogenous cellular replacement and tissue remodelling under normal conditions. Nevertheless, in response to acute injury the adult kidney does have some capacity for repair and remodelling that can ultimately lead to restoration of renal structure and function (54).

Whilst it is well known that proximal TECs can regenerate, the underlying reparative mechanisms still remain elusive. Therefore, over the past decade numerous studies have investigated the origin of the cell responsible for replacing damaged TECs after AKI with three sources having been proposed: 1) immigrating bone marrow-derived cells, 2) renal stem or progenitor cells and 3) surviving proximal TECs.

¹ Exerts of the text in Section 1.2.3.3 have been published in: Wise and Ricardo, *Nephrology*, 2012.

It was originally hypothesised that bone marrow-derived stem cells integrated and differentiated into TECs, thereby contributing to regeneration via a process of cell transdifferentiation. Studies have shown that kidneys transplanted from a female donor into a male patient contained Y-chromosome positive TECs. However, this only accounted for 1% or less of TECs (55, 56). Poulsom et al. (55) demonstrated that female mice who had received a male bone marrow transplant had Y-chromosome containing cells within the kidney, and therefore concluded that the bone marrow cells contribute to TEC turnover and regeneration. This finding was confirmed by the demonstration of the presence of Y-chromosome β -galactosidase-positive cells in the renal tubules of female non-transgenic mice who had received a transplant of male bone marrow-derived cells from β -galactosidase transgenic Rosa mice (57). However, follow-up studies have been unable to reproduce these results, suggesting that the previous results were erroneous due to technical limitations, and subsequently it has been shown and now accepted that bone marrow-derived cells do not significantly contribute to the repair of damaged kidney TECs (58, 59).

It is currently unclear if the kidney contains resident stem cells (60), although there have been reports to suggest that progenitor cell population/s originally identified in embryonic kidneys (CD24+CD133+Oct-4+Bml-1+) exist within the urinary pole of the glomerular parietal epithelium of the Bowman's capsule (61-63). These cells, expressing CD24, a surface antigen commonly used for the identification of human stem cells (64, 65), and CD133, a surface antigen specific for a variety of adult stem cells (66-68), were thought to represent a residual kidney progenitor cell population within the parietal epithelium (69). The CD24+CD133+podocalyxin+ cells localised to the urinary pole of the parietal epithelium may be responsible for podocyte replacement after injury (61, 62), a cell type once thought to be post-mitotic and unable to divide. *In vitro*, clonally expanded CD24+CD133+podocalyxin- cells were able to generate podocytes and tubular cells and after administration to mice with AKI, these cells contributed to the regeneration of the damaged tubules (62, 63). In addition, human CD24+CD133+CD106- cells localised to the

proximal tubules when administered to severe combined immune deficiency (SCID) mice with AKI (70). This population has also been shown to proliferate in kidneys of patients with acute and chronic kidney tubular damage, contributing to TEC regeneration (70, 71). However, recent studies have suggested that these parietal epithelial cells do not significantly contribute to podocyte turnover or regeneration in ageing kidneys, in response to glomerular hypertrophy or nephron loss (72-74). It has also been proposed that the renal papilla may contain a resident kidney stem/progenitor cell population (75, 76). Pulse-chase studies using bromodeoxyuridine (BrdU), a nucleotide analogue that is incorporated into the DNA of proliferating cells, revealed a population of BrdU-retaining cells within in the papilla of the healthy rat kidney. Following ischaemic injury these cells disappeared from the papilla, although this was not due to apoptosis (75). In a subsequent study it was shown that the upper papilla contained chains of proliferating cells which, following AKI, migrated to the injured site and generated new kidney cells (76).

However, in contrast to these findings Humphreys et al. (77, 78) demonstrated that kidney regeneration of the tubular compartment was predominately attributed to surviving epithelial cells undergoing proliferative expansion. It has long been established that surviving TECs repopulate the damaged regions of the tubule following IR injury through a process that to some extent parallels renal development, with a high rate of apoptosis and proliferation and the upregulation of genes that are highly expressed in the developing kidney but absent in the healthy adult kidney [for review see (79)]. Following IR injury, surviving proximal TECs have been shown to dedifferentiate into an immature mesenchymal phenotype, resulting in the upregulation of the mesenchymal markers vimentin, neural cell adhesion molecule (NCAM) and paired box gene 2 (Pax2), all of which are involved in nephron development (80-82). These immature cells spread and migrate along the denuded areas of the basement membrane where they then proliferate, re-differentiate and re-establish polarity resulting in a mature functional epithelial cell.

Recently, transgenic fate mapping and DNA analogue-based approaches have been used to verify this hypothesis (58, 77, 78, 83). Humphreys et al. (77) genetically labelled mesenchyme-derived TECs with β -galactosidase or red fluorescent protein (RFP). Two days after IR injury, 50.5% of epithelial cells co-expressed RFP and the proliferation marker Ki67. Furthermore, following repair, 94% of epithelial cells expressed RFP, without dilution of the cell fate marker occurring (77). Using a DNA analogue-based lineage analysis technique these authors demonstrated in a subsequent study that the majority of these newly generated epithelial cells were derived from self-duplicating TECs, which were injured and dedifferentiated, rather than uninjured neighbouring cells (78). Berger et al. (83) additionally demonstrated that following IR injury there is a sharp increase in newly generated TECs occurring in a small time frame and therefore it is unlikely these cells were derived from a small stem/progenitor pool.

Therefore, it is most likely that endogenous repair of the injured tubular epithelium, following ischaemic damage, predominately results from the dedifferentiation and proliferation of surviving injured TECs. The factors and mechanisms driving this process remain poorly understood. However, macrophages and macrophage-derived factors have both been shown to signal to TECs and play a pivotal role in mediating tubular regeneration following AKI.

1.3 The mononuclear phagocyte system

The kidney tubular epithelium is not purely a victim of injury following an ischaemic insult but also actively participates in the inflammatory response by generating several pro-inflammatory and chemotactic cytokines, such as tumour necrosis factor (TNF)- α , monocyte chemoattractant protein (MCP)-1, interleukin (IL)-1 β and IL-8, expressing various Toll-like receptors (TLRs), complement, complement receptors and co-stimulatory molecules, which recruit and activate inflammatory cells from both the innate and adaptive immune systems (33). The inflammatory response, however, is a crucial event that if regulated properly can mediate repair of the damaged kidney tissue leading to restoration in kidney function. Of importance, monocytes and their tissue-derived progeny, macrophages, have both been shown to play an imperative role in this regenerative process leading to cellular replacement of somatic cells. The heterogeneity of monocytes and tissue macrophages, the identifying cell surface markers and genes, and their functional roles that contribute to both tissue destruction and regeneration following kidney injury will be discussed in turn.

1.3.1 Monocytes

Circulating peripheral blood monocytes are a highly plastic, phenotypically and functionally heterogeneous population equipped with a vast repertoire of receptors that enable them to recognise foreign material and dying cells. Monocytes originate from a myeloid precursor cell in the bone marrow and extravasate into the peripheral blood through mechanisms that still remain unknown. In steady state, proportions of monocyte subsets remain stable. However, increased monocytosis occurs in response to inflammation (84, 85). Following stimulation from an inflammatory insult such as tissue damage, these cells are able to rapidly adapt their phenotype and home to the inflammatory/injury site where they subsequently differentiate into their tissue-derived progeny (84). Furthermore, recent studies have revealed that increased proportions of circulating peripheral blood monocytes

are present in mice and humans with acute and chronic kidney disease, such as IR injury and diabetic nephropathy (86-89).

1.3.1.1 Murine monocyte subsets (Ly6C^{high} and Ly6C^{low})

Once released from the bone marrow, monocytes typically exist as one of three subsets known as classical, intermediate and non-classical (Table 1.1). In mice, these subsets are defined based on the expression of the cell surface receptor lymphocyte antigen 6 complex (Ly6C; 90). Under homeostatic conditions, Ly6C⁺ monocytes that egress from the bone marrow initially express high levels of chemokine (C-C motif) receptor type 2 (CCR2), however, once in circulation the expression of Ly6C and CCR2 are both downregulated and the expression of the fractalkine receptor, chemokine (C-X3-C motif) receptor 1 (CX3CR1) is concomitantly upregulated (91). These subsequent non-classical Ly6C^{low}CCR2⁻CX3CR1⁺ cells form the mature 'resident' monocyte pool, with their primary function being immune surveillance. Therefore, they predominantly reside around the vascular endothelium where they patrol the blood vessel lumen (92). It has also been proposed that this subset may be the precursor of resident macrophages (93).

In contrast, classical Ly6C^{high} monocytes are the more immature subset and express the chemokine receptor CCR2 at high levels, although lack the expression of CX3CR1. Following an inflammatory insult, this subset exits the bone marrow via a CCR2 dependent mechanism and is preferentially recruited to the injury site during the early stages of inflammation through chemokine (C-C motif) ligand 2 (CCL2; also known as MCP-1). Following recruitment, this subset possesses a more inflammatory phenotype with enhanced phagocytosis capabilities and elevated secretion of inflammatory mediators such as TNF- α , nitric oxide (NO) and reactive oxygen species (ROS). Following AKI, there is an influx of Ly6C^{high} monocytes, as opposed to Ly6C^{low} monocytes, in the damaged kidney (89, 94). Interestingly, adoptive transfer of the Ly6C^{high} monocyte population to mice with unilateral ureteral obstruction (UUO) revealed that this subset had the potential to differentiate into

different tissue-derived macrophage subpopulations upon entering the damaged kidney (94). However, during steady state there are relatively equal proportions of the classical and non-classical monocyte subsets in mice.

Additionally there is also a minor ‘intermediate’ monocyte population, known as Ly6C^{int}, reported to be a transitioning population between the immature Ly6C^{high} and more mature Ly6C^{low} monocyte subsets (90).

Table 1.1 Classification of murine monocyte subsets based on phenotype and function

Monocyte subset	Surface markers	Functions	Circulating proportion
Classical (Inflammatory) Ly6C ^{high}	CCR2 ^{high} , CD62L, CX3CR1 ^{low/-}	<ul style="list-style-type: none"> • Immature phenotype • High migratory capacity to inflammatory stimuli • ↑ during early stages of inflammation and home to sites of inflammation in response to CCL2 and CCL7 • High antimicrobial capacity • Highly phagocytic • Produce ROS, TNF-α, NO, IL-1β, type 1 IFN • More likely to differentiate into an M1 phenotype 	50%
Intermediate Ly6C ^{int}	CCR2, CD62L, CCR7, CCR8, CX3CR1	<ul style="list-style-type: none"> • Intermediate ‘transitioning’ phenotype between the Ly6C^{high} and Ly6C^{low} subsets • Precise functions not well defined 	Not defined
Non-classical (Resident/Patrolling) Ly6C ^{low/-}	CX3CR1 ^{high}	<ul style="list-style-type: none"> • Mature phenotype • Patrol blood vessel walls and possibly contribute to resident tissue macrophage populations • More likely to differentiate into an M2 phenotype 	50%

All data are derived from references cited in the main text. CCL, chemokine (C-C motif) ligand; CCR, chemokine (C-C motif) receptor; CX3CR1, chemokine (C-X3-C motif) receptor 1; IFN, interferon; IL, interleukin; Ly6C, lymphocyte antigen 6 complex; M1, classically activated macrophage; M2, alternatively activated macrophage; NO, nitric oxide; ROS, reactive oxygen species; TNF, tumour necrosis factor.

1.3.1.2 Human monocyte subsets (CD14 and CD16)

In humans, monocyte heterogeneity is categorised based on the expression of the lipopolysaccharide (LPS) co-receptor, CD14 and the Fcγ receptor III (FcγRIII), CD16. Three major subsets have been described, consisting of the classical CD14^{high/+ +}CD16⁻, intermediate CD14^{high/+ +}CD16⁺ and non-classical CD14^{dim/+}CD16^{high/+ +} monocytes (Table 1.2; 95, 96). Of note, the latter two subsets are also referred to as CD16⁺ monocytes.

Table 1.2 Classification of human monocyte subsets based on phenotype and function

Monocyte subset	Surface markers	Functions	Circulating proportion
Classical (inflammatory) CD14 ^{high/+ +} CD16 ⁻	CCR1, CCR2 ^{high} , CCR4, CCR7, CXCR1, CXCR2, CXCR4, CD32, CD33, CD36, CD64, CD62L (L-selectin), CD93, CSF3R, HLA-DR, CX3CR1 ^{low}	<ul style="list-style-type: none"> • Immature phenotype • ↑ during early/acute inflammation and home to sites of inflammation in response to CCL2 • Highly phagocytic • Low lymphocyte proliferation ability • Better antimicrobial capacity • Respond to TLR2 and TLR4 • Produce ROS • Secrete high levels of IL-10 and low levels of TNF-α in response to LPS • Express genes involved in angiogenesis and wound healing 	Majority of circulating monocytes comprising ~90%
Intermediate CD14 ^{high/+ +} CD16 ⁺	CCR1, CCR2, CCR5, CD64, CX3CR1, HLA-DR ^{high}	<ul style="list-style-type: none"> • Intermediate 'transitioning' phenotype • ↑ during inflammation and home to sites of inflammation in response to CCL2 • Highly phagocytic • Respond to TLR2 and TLR4 • Produce ROS • Secrete pro-inflammatory IL-1β and TNF-α 	~5%
Non-classical (resident/patrolling) CD14 ^{dim/+} CD16 ^{high/+ +}	CX3CR1, CCR5, CD31, CD32, CXCR4, CSF1R, HLA-DR ^{high}	<ul style="list-style-type: none"> • Mature phenotype • Low phagocytic activity • High lymphocyte proliferation ability • High antigen presentation activity • Patrol blood vessel walls and possibly contribute to resident macrophage populations • ↑ during chronic inflammation in response to CX3CL1 • Secrete pro-inflammatory IL-1β, TNF-α, IL-6, IL-8 • Respond to viral stimuli through TLR7 and TLR8 	<10%

All data are derived from references cited in the main text. CCL, chemokine (C-C motif) ligand; CCR, chemokine (C-C motif) receptor; CSF1R, colony stimulating factor-1 receptor; CSF3R, colony stimulating factor-3 receptor; CX3CR1, chemokine (C-X3-C motif) receptor 1; CXCR, chemokine (C-X-C motif) receptor; HLA-DR, human leukocyte antigen-DR complex; IL, interleukin; LPS, lipopolysaccharide; ROS, reactive oxygen species; TLR, toll-like receptor; TNF, tumour necrosis factor.

The CD14⁺⁺CD16⁻ monocytes comprise the main peripheral blood monocyte population in healthy adults, representing approximately 90% of the total monocyte pool, and therefore are termed the 'classical' monocyte subset (96). This population is the equivalent of the mouse Ly6C^{high} subset that express high levels of CCR2 and CD62L, also known as L-selectin, and express low levels of CX3CR1. Following injury, CD14⁺⁺CD16⁻ monocytes are the first to mobilise from the bone marrow and infiltrate the damaged tissue via a CCR2/CCL2 dependent mechanism and analogous to Ly6C^{high} monocytes in mice, this is the most immature subset (93). Functionally, they are highly phagocytic, exhibit high antimicrobial capabilities and peroxidase activity, secrete high levels of IL-10 and low levels of TNF- α (97, 98). Additionally, gene expression profiling revealed that CD14⁺⁺CD16⁻ monocytes express several genes associated with angiogenesis, wound healing and coagulation, indicating they may play a role in mediating tissue repair (98).

The human CD14⁺CD16⁺⁺ non-classical monocyte subset forms approximately 5-10% of the total peripheral blood monocyte pool in healthy individuals (95, 96). Non-classical monocytes have a more mature phenotype compared to the classical subset and like the murine equivalent, express high levels of CX3CR1 and patrol the vascular endothelium in a 'crawling' manner, playing a crucial role in mediating immune surveillance (93, 99). In contrast to the classical subset, non-classical monocytes have low phagocytic capabilities, express high levels of human leukocyte antigen (HLA)-DR and thus exhibit a higher capacity for antigen presentation. They also respond strongly to TLR7 and TLR8 ligands, secrete high levels of the pro-inflammatory molecules IL-1 β and TNF- α and are weak producers of the anti-inflammatory IL-10 (97, 98, 100). In addition, they are recruited to the injury site during the later stages of the inflammatory response where they have been shown to accumulate and promote inflammation in varying disease settings (101).

The intermediate CD14⁺⁺CD16⁺ monocytes are the least characterised of the human monocyte subsets. This subset is believed to be an intermediate between the classical and non-classical monocyte populations, expressing the same level of CD14 as the classical monocytes but also expressing CD16 (96, 99). Like classical monocytes, the intermediate subset can home to the site of injury during the early stages of the inflammatory response via a CCR2/CCL2 or CCR5/CCL5 dependent mechanism (84). However, they can also possess a pro-inflammatory phenotype analogous to the non-classical subset; secreting high levels of TNF- α and IL- β , expressing high levels of HLA-DR, possessing high lymphocyte proliferative abilities and demonstrating low phagocytic activity (97, 98, 102).

It is important to note that although the CD14⁺⁺CD16⁻ and CD14⁺CD16⁺⁺ subsets in humans have been suggested to resemble the Ly6C^{high} and Ly6C^{low} monocyte subsets in mice respectively, in a setting of chronic inflammation, the more mature CD14⁺CD16⁺⁺ subset has been shown to be pro-inflammatory and contribute to the pathogenesis of disease (101). Studies have shown that the CD16-expressing intermediate and non-classical monocyte subsets accumulate in patients with chronic inflammatory conditions, such as CKD (86, 101, 103). Patients with ESRD receiving haemodialysis have been shown to have higher proportions of intermediate and non-classical monocyte subsets compared to age-matched control patients with normal kidney function (104). Interestingly, these ESRD patients receiving haemodialysis have a significantly greater number of CD16⁺ monocytes compared to patients receiving peritoneal dialysis or patients with advanced CKD who are yet to commence dialysis (104, 105). Additionally, monocytes isolated from haemodialysis patients secrete elevated levels of pro-inflammatory cytokines with these elevated levels in the plasma correlating with an increased risk of mortality (86, 106, 107). Taken together, these studies indicate that the CD16⁺ monocyte subsets may be directly or indirectly contributing to the pathogenesis of CKD. Therefore future studies are required to further investigate monocyte phenotype and function and their involvement in the progression of kidney disease.

1.3.2 Macrophages

Upon entering the kidney, monocytes receive cues from the local milieu that promote their differentiation into tissue-derived macrophages. Like monocytes, macrophages are highly plastic and heterogeneous cells whose phenotype changes in response to the surrounding microenvironmental cues, including those from damaged cells and microbial products. During homeostatic conditions, macrophages play an important role in tissue homeostasis and surveillance, clearing apoptotic debris and acting as sentinels for the kidney (108). Following kidney damage, macrophages can either further contribute to tissue injury and the progression of kidney disease or mediate wound healing leading to the restoration of renal architecture and function. Based on the varying activation and functional polarisation states, macrophages have been classified into two major categories known as classically activated 'M1' pro-inflammatory macrophages and alternatively activated 'M2' anti-inflammatory macrophages (Table 1.3).

Table 1.3. Classification of macrophages based on phenotype and function

Macrophage activation state	Stimuli	Surface markers	Cytokine and inflammatory profile	Functions
Classical – M1	IFN- γ , TNF- α , DAMPs, PAMPs (such as LPS)	IFNGR, TLRs, MHC class II, CD80, CD86	IL-1 β , IL-6, IL-12, IL-23, TNF- α , MCP1/CCL2, CCL5, MIG/CXCL9, CXCL10, CXCL11, iNOS, NO, ROS	<ul style="list-style-type: none"> • Host defence • Induce inflammatory response
Alternative – M2 Wound-healing M2a	IL-4, IL-13	IL-4Ra, MHC class II, Arg-1, MR (CD206), SR (CD163), DC-SIGN, Fizz1/Retnla, Chi3l3/Ym1	IGF-1, β ig-H3, FN-1, PDGF, TGF- β , CCL2, CCL13, CCL14, CCL17, CCL18, CCL23, CCL26, MMP-9, MMP-12	<ul style="list-style-type: none"> • Wound healing • ECM remodelling
Alternative – M2 Regulatory M2b	TLR ligands, immune complexes	MHC class II, CD86	IL-10, CCL1, CCL20, CXCL1, CXCL2, CXCL3	<ul style="list-style-type: none"> • Immune regulation
Alternative – M2 Regulatory M2c	IL-10, TGF- β , glucocorticoids	MR (CD206), SR (CD163), Arg-1	IL-6, IL-10, TGF- β , CCL18	<ul style="list-style-type: none"> • Immune regulation • ECM remodelling • Tissue repair

All data are derived from references cited in the main text. Arg-1, arginase-1; β ig-H3, transforming growth factor- β -induced protein; CCL, chemokine (C-C motif) ligand; Chi3l3, chitinase-like protein; CXCL, chemokine (C-X-C motif) ligand; DAMPs, danger-associated molecular patterns; DC-SIGN, dendritic cell-specific intracellular adhesion molecule-3 grabbing non-integrin; ECM, extracellular matrix; Fizz1, found in inflammatory zone; FN, fibronectin; IGF, insulin-like growth factor; IFN, interferon; IFNGR, interferon gamma receptor complex; IL, interleukin; IL-4Ra, interleukin-4 receptor α ; iNOS, inducible nitric oxide synthase; LPS, lipopolysaccharide; MCP, monocyte chemoattractant protein; MHC, major histocompatibility; MIG, monocyte induced by IFN- γ ; MMP, matrix metalloproteinase; MR, mannose receptor; NO, nitric oxide; PAMPs, pathogen-associated molecular patterns; Retnla, resistin-like molecule alpha; ROS, reactive oxygen species; SR, scavenger receptor; TGF, transforming growth factor; TLRs, toll-like receptors; TNF, tumour necrosis factor; PDGF, platelet-derived growth factor.

1.3.2.1 Macrophage polarisation: M1 versus M2

M1 macrophages accumulate during the early stages of inflammation where they are involved in sustaining the inflammatory response to mediate the clearance of pathogens, apoptotic cells and debris (109, 110). M1 macrophage activation is mediated by stimulation with interferon (IFN)- γ alone or in combination with pathogen-derived products (termed pathogen-associated molecular patterns; PAMPs), such as LPS, or factors released from the injured host cells (termed danger-associated molecular patterns; DAMPs; (109). Following activation, M1 macrophages secrete high levels of several pro-inflammatory cytokines, including IL-1 β , IL-12, IL-23 and TNF- α , and chemokines, including CCL2, CCL5, CXCL9, CXCL10 and CXCL11 (110, 111). This induces the downstream production of reactive nitrogen and oxygen intermediates that further promotes Th1 and Th17 immune responses (110-112). M1 macrophages have high phagocytic and antigen presentation capabilities due to their high expression of major histocompatibility complex (MHC) class II and the co-stimulatory molecules CD80 and CD86 (110, 113). M1 macrophages are equipped to rapidly respond to stress and microbial stimuli and their recruitment is essential for host defence. However, their pro-inflammatory functions can cause host tissue damage and therefore their response must be tightly regulated (114).

In contrast, M2 macrophages counteract the M1 pro-inflammatory response and are associated with the resolution of inflammation and wound healing. Due to their diverse range of functions, M2 macrophages have notionally been further classified into M2a, M2b and M2c subsets (115). However, considerable overlap between these subsets is likely to exist.

Activation of M2a wound healing macrophages is primarily induced by the cytokines IL-4 and/or IL-13 binding to the IL-4Ra, which in turn activate the M2-associated genes arginase 1 (*Arg1*), chitinase 3-like-3 (*Chi3l3* or *Ym1*), found in inflammatory zone 1 (*Fizz1* or *Retnla*) and mannose receptor, C type 1 (*Mrc1*; 116). Arginase-1 activation inhibits the production of

NO and promotes proline and polyamine synthesis. Proline is required for extracellular matrix synthesis and polyamines stimulate cell proliferation, both important factors for tissue repair (117). M2a macrophages produce matrix metalloproteinases (MMPs), which mediate extracellular matrix remodelling and are characterised by the upregulated expression of pattern recognition receptors (PRRs), such as mannose receptor (CD206), scavenger receptor (CD163) and dendritic cell-specific intracellular adhesion molecule-3 grabbing non-integrin (DC-SIGN; 113, 118). These PRRs are capable of binding and internalising collagens, a major structural component that accumulates as a result of kidney injury and has to subsequently be degraded. Additionally they generate factors such as insulin-like growth factor (IGF)-1, platelet-derived growth factor (PDGF), transforming growth factor (TGF)- β , transforming growth factor- β -induced protein (β ig-H3) and fibronectin (FN)-1, which promote angiogenesis and provide signals for regeneration and repair of the damaged tissue (113).

The M2b and M2c macrophage subsets are also known as regulatory macrophages as their primary function is to modulate the immune response in order to limit tissue damage, promote wound healing and re-establish tissue homeostasis (114, 119). However, the mode of activation between these two subsets differs, with TLR ligands and immune complexes driving M2b activation and exposure to IL-10, TGF- β or glucocorticoids mediating M2c activation (115). Regulatory macrophages produce high levels of the anti-inflammatory cytokine IL-10, which is responsible for dampening the inflammatory response (119, 120). Additionally, IL-10 induces the expression of interleukin-1 receptor antagonist (IL-1RA), which subsequently inhibits the production of the pro-inflammatory cytokine IL-1 (121, 122). Regulatory macrophages possess enhanced phagocytic capabilities, allowing them to clear cellular debris and apoptotic cells. M2b macrophages express increased levels of the Fc γ R1, which bind immune complexes and leads to the deactivation of the pro-inflammatory cytokine IL-12 (123). They also express high levels of MHC class II and co-stimulatory molecules and thus are capable of efficiently presenting antigens (124). Phagocytosis of

apoptotic cells also triggers the production of TGF- β by M2c macrophages, which itself inhibits the production of pro-inflammatory cytokines as well as mediating extracellular matrix remodelling and tissue repair (113, 125).

1.3.2.2 The pathogenic and protective roles of macrophages in acute kidney disease

The initial characterisation of macrophage polarisation states was based on *in vitro* stimulation experiments. However, the *in vivo* microenvironment is much more complex than the *in vitro* setting due to the broad range of signals and stimuli produced in the diseased kidney that vary greatly throughout the different stages of injury and repair. Infiltrating monocytes and macrophages are subsequently affected by the changing dynamics of the local kidney inflammatory milieu resulting in differential activation of these cells (109).

Regardless of the insult, numerous studies have shown that at the onset of AKI the Ly6C^{high} monocyte subset dominates the initial infiltration to the kidney (89, 94, 126). Once recruited, the fate of these cells is determined by the cues received from the kidney microenvironment. Monocyte recruitment peaks at 24 hours following IR injury, with macrophage accumulation occurring as early as 2 hours post-ischaemic injury (127). The initial reperfusion phase, in which tubular injury occurs, is characterised by the production of IFN- γ and ROS, as well as DAMPs secreted from the injured TECs themselves (128). Consequently, early infiltrating macrophages acquire a pro-inflammatory M1 activation state and further contribute to the disease (129). Studies have demonstrated that macrophage ablation prior to IR injury is renoprotective, significantly reducing kidney injury and improving kidney function (129-131). In addition, the adoptive transfer of unstimulated or M1-induced macrophages at the time of IR injury to macrophage depleted mice has been reported to restore kidney damage (129, 130). M1 macrophages contribute to the pathogenesis of IR injury by enhancing the inflammatory response through promoting neutrophil infiltration and further monocyte and macrophage recruitment. This is associated

with the secretion of pro-inflammatory cytokines and chemokines including TNF- α , IFN- γ , IL-1, IL-6, MCP-1 and macrophage inflammatory protein (MIP)-2 (also known as CXCL2), which ultimately leads to TEC apoptosis (128, 130, 132, 133).

In contrast, M2 macrophages infiltrate the IR damaged kidney at a latter stage and play a vital role in the tissue repair process (129). The kidney starts undergoing endogenous repair approximately 72 hours after the initial ischaemic insult (134). The inhibition of tubular regeneration and functional recovery have been reported in two experimental settings of macrophage depletion, namely using clodronate liposomes or when CD11b-diphtheria toxin receptor transgenic mice are injected with diphtheria toxin during the repair phase (48 – 72 hours post-IR) of IR injury (129, 134, 135). Vinuesa et al. (134) verified the role macrophages play during the repair phase of IR injury by re-infusing macrophages at 48 hours post-IR to mice that had undergone macrophage depletion prior to IR surgery. Interestingly, macrophage repletion during the repair phase of IR injury significantly promoted renal regeneration and improved kidney function, implying that macrophages do have a protective role and are associated with promoting renal repair (134). Cytokine profiling of the kidney environment further revealed elevated levels of pro-inflammatory cytokines during the initial IR injury phase, however, there was an upregulation of the anti-inflammatory cytokine IL-10, that is associated with tissue remodelling and cellular replacement, during the subsequent repair phase (134). The adoptive transfer of M2-induced macrophages to macrophage depleted mice also stimulated TEC proliferation and structural repair (129). Furthermore, when M1-induced macrophages were administered to mice during the repair phase of IR injury, the cells migrated to the injured kidney and switched phenotype to an M2 polarisation state (129). The precise mechanisms that dictate macrophage polarisation and the subsequent process of kidney repair are not fully understood. Lin et al. (135) demonstrated that macrophage-derived Wnt7b is crucial for macrophage-mediated kidney repair. Following IR injury, macrophages produced increased levels of Wnt7b, which signalled to the surviving epithelial cells and promoted regeneration

of the basement membrane and TEC proliferation (135). The exogenous administration of colony stimulating factor (CSF)-1, a growth factor produced by the kidney tubular epithelium that controls the survival, proliferation and differentiation of macrophages, has also been shown to have beneficial effects (136, 137). When delivered to mice with established IR injury, CSF-1 promoted renal repair via polarising macrophages towards an M2 phenotype (138).

Collectively, these studies provide evidence that the signals produced in the kidney microenvironment play an important role in governing macrophage polarisation and phenotypic switching from a pro-inflammatory to anti-inflammatory activation state and *vice versa*. Therefore, identifying the specific signals and factors produced by the local environment that mediate this process would be essential in providing further insight into the process of endogenous kidney repair. Furthermore, therapeutic manipulation of the kidney microenvironment with the use of cytokines or immunomodulatory MSCs may provide a novel method to promote the alternative activation of monocytes and macrophages and additional treatment options for patients with kidney disease.

1.4 Kidney, stem cells and regeneration²

As mentioned above, cellular loss most often leads to the infiltration of bone marrow-derived inflammatory cells that may contribute to both tissue destruction or repair depending on the extent of injury (139). MSCs, derived from the bone marrow, have initiated considerable excitement in their role to promote kidney repair and tissue remodelling through the secretion of mitogenic and angiogenic factors.

1.4.1 Mesenchymal stem cells

MSCs were originally identified in the bone marrow stroma by Friedenstein and colleagues (140, 141). MSC therapy has since been reported to ameliorate kidney injury and promote structural repair (142). These undifferentiated adult stem cells are of mesodermal origin and constitute only 0.001-0.01% of the total bone marrow cell population (143). They can be easily isolated from other bone marrow cells *ex vivo* due to their propensity to adhere to plastic and their ability to extensively proliferate *in vitro* (143, 144). Furthermore, these characteristics allow for the cell expansion of adequate numbers of MSCs for potential therapeutic use (51). However, as the extensive expansion of MSCs in culture can lead to alterations in both phenotype and function, it remains uncertain if *in vitro* cultured MSCs differ significantly from the *in vivo* populations (144-146).

MSCs form a heterogeneous population in culture that consists of small immature rapidly self-renewing cells, large, more mature, slowly replicating cells and in some confluent cultures, cuboidal cells (147). Interestingly, it has been shown that single cell-derived clones of MSCs can vary in phenotype, gene expression and their differentiation abilities (148, 149). *The Mesenchymal and Tissue Stem Cell Committee of the International Society of Cellular Therapy* have outlined a combination of morphological, phenotypical and functional characteristics that are required to define these cells (150). As part of their definition, it is

² Pages 26 – 32 have been published in: Wise and Ricardo, *Nephrology*, 2012.

essential that MSCs adhere to plastic in standard tissue culture conditions, exhibit a fibroblast-like morphology and have the ability to undergo extensive proliferation, resulting in the formation of colonies of fibroblastic cells, termed colony-forming unit-fibroblasts (CFU-F; Figure 1.2A; 150-152). Furthermore, MSCs should express the surface antigens CD73, CD90 and CD105 and lack the expression of the haematopoietic markers CD45, CD34, CD14 or CD11b, CD79 α or CD19 and MHC class II (150). They also typically express intermediate levels of MHC class I and are negative for the co-stimulatory molecules CD40, CD80 and CD86 (153). However, when exposed to inflammatory stimuli, such as IFN- γ , their expression of MHC class I and II has been reported to be upregulated (154). Finally, when exposed to the appropriate differentiation conditions, MSCs should have the capacity to differentiate into adipocytes, osteocytes and chondrocytes *in vitro* (Figure 1.2 B-D; 150). More recently MSCs have also been detected in adipose, umbilical cord and a number of post-natal organs and tissues, including the kidney, and they have shown a promising ability to protect against tissue injury and facilitate endogenous tissue repair (155-158). Unlike embryonic stem (ES) cells and induced pluripotent stem (iPS) cells, MSCs do not form teratomas following transplantation in rodents (159).

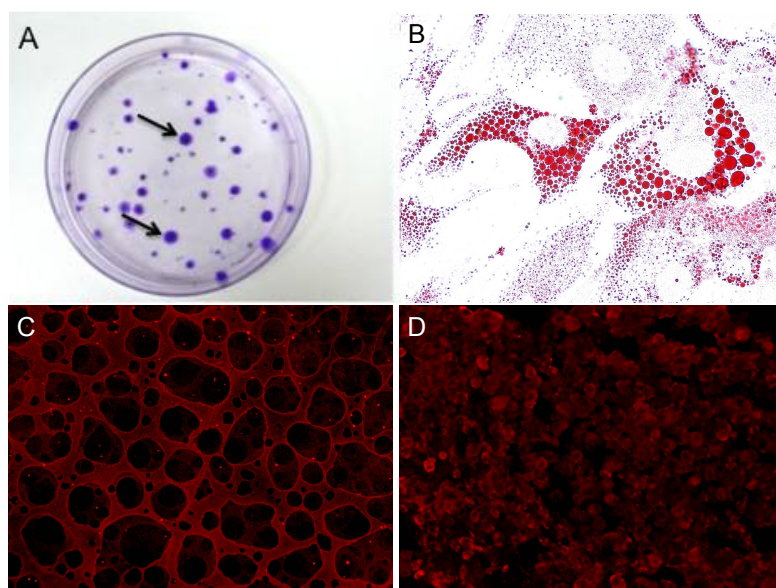


Figure 1.2 Mesenchymal stem cells (MSCs) show multipotent potential and form colony-forming unit-fibroblasts (CFU-F) in culture (A; arrows) that can differentiate into adipocytes (B), where lipid droplets stain red with Oil Red O (Mag x1000); bone (C), shown in red with immunostaining for osteopontin (Mag x400); and cartilage (Mag x200) stained with collagen II (D).

1.4.2 Mesenchymal stem cells in tissue regeneration and repair

MSCs have been found to exert a therapeutic effect in a wide array of diseases, acting through their unique immunomodulatory abilities that can alter the pro-inflammatory course of injury. This may involve the secretion of paracrine factors that dampen inflammation and in turn promote tissue remodelling and repair (157). Their ability to modulate the immune response *in vivo* was first reported by Bartholomew et al. (160) who demonstrated that the intravenous administration of allogeneic MSCs to baboons resulted in prolonged skin-graft survival. MSCs have also been reported to be beneficial in an autoimmune disease setting. In a mouse model of multiple sclerosis termed experimental autoimmune encephalomyelitis (EAE), the administration of MSCs at the onset of disease induced peripheral T-cell anergy against the pathogenic peptide myelin oligodendrocyte glycoprotein (MOG), resulting in the amelioration of the progression of injury (161). Furthermore, the administration of MSCs to mice with type 1 diabetes resulted in the recovery of damaged insulin producing pancreatic islets and β -cells and decreased blood glucose levels (162). Two mechanisms appear to be aiding this recovery. In addition to the production of trophic growth factors, MSCs also inhibit the β -cell specific T-cell immune reaction (163). In a mouse model of lung fibrosis, MSCs reduced local inflammation, collagen accumulation and consequently fibrosis (164). Subsequent studies demonstrated that MSCs conferred this protection by inhibiting the release of IL-1 α and TNF- α through the secretion of IL-1RA (165). The local injection of MSCs to mice following coronary ligation induced the regeneration of cardiac tissue and improved myocardial function (166). Following intravenous administration, MSCs preferentially homed to the infarct site where they promoted angiogenesis and myogenesis and mediated myocardial repair via paracrine mechanisms (167). The first phase I clinical trial in humans involved the intravenous infusion of MSCs into patients with haematologic malignancies in complete remission resulting in no adverse events (168). Subsequent trials in breast cancer patients showed that MSC infusion, following high dose chemotherapy and peripheral-blood progenitor-cell infusion, resulted in enhanced haematopoietic engraftment and recovery (169). The immunosuppressive effects of MSCs has also effectively been used

to treat a leukaemia patient with severe treatment-resistant grade IV acute graft-versus-host disease (GvHD; 170). Following the promising results obtained from these trials, MSCs have since been clinically trialled in a diverse range of other conditions. Numerous Phase I-II and III clinical trials exploring the therapeutic potential of MSCs in conditions such as type 1 diabetes, myocardial infarction, ischaemic stroke, Crohn's disease, cirrhosis and osteoarthritis have been completed or are currently in progress (see www.clinicaltrials.gov).

Furthermore, a dose-escalating phase I clinical trial was carried out in on-pump cardiac surgery patients undergoing coronary artery bypass or valve repair, who were at high risk of developing postoperative acute kidney injury (www.clinicaltrials.gov; NCT00733876). Preliminary results have demonstrated that the MSC therapy resulted in no adverse effects. The postoperative length of stay and readmission rate of MSC-treated patients compared to historical matched controls was reduced by approximately 40%. All MSC-treated patients exhibited normal renal function in comparison to approximately 20% of the historical matched controls that developed AKI (171). Clinical trials investigating the use of MSC transplantation for the prevention of kidney transplant rejection and graft tolerance (www.clinicaltrials.gov; NCT00752479, NCT00658073 and NCT00734396), and the treatment of lupus nephritis (www.clinicaltrials.gov; NCT00698191 and NCT00659217) are also currently underway.

1.4.3 Mesenchymal stem cells in acute kidney disease

Despite the current data showing clinical efficacy, the precise manner in which MSCs confer renoprotection is not understood. Initial experimental studies carried out by Morigi et al. (142) and Herrera et al. (172) reported that the exogenous administration of MSCs to mice with acute renal injury could promote both structural and functional renal repair via the transdifferentiation of MSCs into tubular epithelium. However, follow-up studies revealed that only 2 – 2.5% of the injected MSCs showed engraftment (173), opposed to a previously reported 22% of cells (172). These reports demonstrate that the direct engraftment of

exogenously administered, transdifferentiating MSCs is not the predominant mechanism in which MSCs enhance renal repair.

There is increasing evidence that MSCs can elicit repair through paracrine and/or endocrine mechanisms, where they release trophic growth factors that modulate the immune response and consequently mediate repair (174-181). The ability of MSCs to inhibit the release of pro-inflammatory cytokines and secrete a variety of trophic growth factors that, promote angiogenesis, mitogenesis and proliferation whilst reducing apoptosis may collectively mediate the protective and regenerative effects in the kidney of laboratory rodents (summarised in Table 1.4; 142, 172-187).

Recent studies have shown that the administration of MSCs following IR injury result in a significant downregulation of the expression of pro-inflammatory cytokines such as IL-1 β , TNF- α , IFN- γ and suppression of inducible nitric oxide synthase (iNOS) at 24 hours post-IR injury (177, 179). This was coupled with an upregulation of the anti-inflammatory cytokines IL-4, IL-10, basic fibroblast growth factor (bFGF), TGF- α and Bcl-2, which resulted in a reduction in renal injury, increased tubular epithelial proliferation and improved renal function. These findings indicate that MSCs are capable of modulating the inflammatory immune response soon after the initiation of injury, shifting it from a pro-inflammatory Th1 profile to an anti-inflammatory Th2 one (177, 179). Moreover, the areas of the kidney where MSCs were still present at 24 hours post-IR injury were associated with reduced apoptosis compared to regions that no longer contained these cells (180). This suggests that MSCs are capable of secreting anti-apoptotic factors that protect surrounding renal cells from undergoing apoptosis following renal insult. To further elucidate their protective mechanisms, MSCs, were co-cultured *in vitro* with cisplatin-treated proximal TECs (176). These co-culture assays, using Transwell membranes, showed that the protective effects of MSCs on proximal TEC proliferation were not due to cell-to-cell contact but more likely the production of MSC-derived trophic factors (176).

Table 1.4 Summary of studies using mesenchymal stem cells (MSCs) isolated from various sources to treat acute kidney injury

Injury model	MSC source	Administration	Features	Reference
Glycerol-induced kidney injury	1x10 ⁶ GFP+ mouse BM-MSC – female C57BL6/J mice	i.v. injection	↑ proliferation, ↑ morphological recovery, ↑ renal function	(142)
Cisplatin-induced kidney injury	2x10 ⁵ mouse BM-MSC – male C57BL6/J mice	i.v. injection	↑ renal function, ↑ tubular proliferation, ↑ morphological recovery	(172)
40 min bilateral IR	1.5x10 ⁶ rat BM-MSC – Sprague-Dawley rats	Infused into thoracic aorta via a carotid artery	↑ renal function, ↓ injury score, ↑ preservation of proximal tubular brush border	(185)
40 min bilateral IR	1x10 ⁶ rat BM-MSC	Intra-aortic delivery via left carotid artery	↑ renal function, ↑ proliferative indexes, ↓ apoptotic indexes, ↓ renal injury, ↓ IL-1β, TNF-α, IFN-γ, iNOS, ↑IL-10, bFGF, TGF-α, Bcl-2	(179)
Cisplatin-induced kidney injury	2x10 ⁵ mouse BM-MSC – male C57BL6/J mice	Tail vein or i.p. injection	↑ renal function, ↑ tubular cell proliferation, ↓ tubular cell apoptosis	(174)
Glycerol-induced kidney injury	1x10 ⁶ mouse CD44+ or CD44-/- BM-MSC – C57BL6/J or Cd44tm1Hbg/J mice	Tail vein	CD44+ BM-MSC: ↑ morphological and functional recovery CD44-/- BM-MSC: no significant morphological or functional recovery	(173)
Cisplatin-induced kidney injury	2x10 ⁵ mouse IGF-1 gene silenced BM-MSC – male C57BL6/J mice	i.v. injection	Limited protection of renal function (BUN) and tubular injury	(176)
60 min bilateral IR	2x10 ⁵ rat BM-MSC – male Wistar rats	i.v. injection	↓ serum creatinine and plasma urea, ↑ PCNA nuclei in MSC treated kidneys, ↑ IL-4, ↓ IL-1β	(187)
30 min unilateral IR	1x10 ⁵ rat MSC	Intra-arterially infused	↓ apoptosis in kidney regions with MSC still present in microvasculature 24hrs post-IR	(180)
40 min bilateral IR	1x10 ⁶ Kallikrein-modified BM-MSC – male Wistar rats	Intra-aortic delivery via left carotid artery	↓ serum creatinine and urea nitrogen, ↓ apoptosis, ↓ tubular injury	(184)
Cisplatin-induced kidney injury	5x10 ⁵ human BM-MSC	Tail vein	↑ renal function, ↑ proliferative score, ↓ proximal tubular epithelial cell injury, ↓ apoptotic score, ↓ mortality	(186)
60 min bilateral IR	2x10 ⁵ rat BM-MSC – male Wistar rats	i.v. injection	↓ serum creatinine, ↑ renal function, low expression of IL-1β, IL-6, TNF-α, high expression IL-4 and IL-10	(177)
58 min bilateral IR	VEGF knockdown BM-MSC – hPAP transgenic F344 rats	Intra-aortic delivery via left carotid artery	↑ mortality, delayed functional recovery	(178)
60 min bilateral IR	1x10 ⁶ human umbilical cord-MSC	Intra-aortic delivery via left carotid artery	↓ serum creatinine and urea nitrogen, ↓ caspase-3, IL-1β and TNF-α, ↑ proliferative score	(182)
Cisplatin-induced kidney injury	5x10 ⁶ human BM-MSC	i.p. injection	Prolonged survival, ↓ urea nitrogen, ↓ apoptosis, ↑ proliferation	(183)
Cisplatin-induced kidney injury	5x10 ⁵ VEGF-hMSC	Tail vein	↑ proliferation, ↓ apoptosis, ↑ renal function, improved morphology and prolonged survival	(181)
60 min bilateral IR	1x10 ⁶ human umbilical cord HGF-MSC	Intra-aortic delivery via left carotid artery	↓ apoptosis, ↓ tubular casts, ↑ proliferation, ↑ renal function	(175)

bFGF, basic fibroblast growth factor; BM-MSC, bone marrow-mesenchymal stem cell; BUN, blood urea nitrogen; HGF, hepatic growth factor; IGF, insulin-like growth factor; IL, interleukin; iNOS, inducible nitric oxide synthase; i.p., intraperitoneal; IR, ischemia reperfusion; i.v., intravenous; PCNA, proliferating cell nuclear antigen; TGF, transforming growth factor; TNF, tumour necrosis factor; VEGF, vascular endothelial growth factor.

Importantly, the administration of MSC-conditioned medium to mice with cisplatin-induced injury was also found to reduce tubular cell apoptosis and improve kidney structure and function (174). This further supports the notion that MSCs secrete factors that mediate renoprotection in a paracrine manner. MSC-conditioned medium has been reported to contain hepatocyte growth factor (HGF), IGF-1 and vascular endothelial growth factor (VEGF; 179, 180). Both HGF and IGF-1 have anti-apoptotic and mitogenic properties that can accelerate cellular repair when administered to mice with kidney IR injury (188-191). In addition to the cellular survival effects of VEGF that decrease apoptosis and promote endothelial and epithelial proliferation, VEGF can also mediate vasodilation, matrix remodelling, monocyte chemotaxis and angiogenesis (180, 192).

Imberti et al. (176) provided *in vitro* evidence that MSC-derived IGF-1 is the principle mediator responsible for renal repair. The addition of an anti-IGF-1 antibody to MSC and proximal TEC co-cultures resulted in the attenuation of proximal TEC proliferation. Furthermore, the co-culture of IGF-1 silenced MSCs and proximal TECs also resulted in the attenuation of proximal TEC proliferation and increased apoptosis. The *in vivo* administration of IGF-1 silenced MSCs to mice with cisplatin-induced injury resulted in limited improvements in renal regeneration and repair (176). Furthermore, human umbilical cord-derived MSCs (hucMSCs) overexpressing HGF (HGF-hucMSCs) showed enhanced therapeutic effects when administered to mice with IR injury, compared to hucMSC treatment (175). In addition, Yuan et al. (181) demonstrated that the *in vitro* co-culture of human embryonic MSCs overexpressing VEGF (VEGF-hMSCs) with cisplatin-injured tubular epithelial cells (TCMK-1) resulted in enhanced protection, in comparison with co-cultures involving hMSCs. Moreover, the administration of VEGF-hMSCs to mice with cisplatin-induced injury, resulted in decreased apoptosis and increased proliferation, enhanced functional recovery and prolonged survival compared to hMSC treated mice (181). Togel et al. (178) also demonstrated that the administration of VEGF knockdown MSCs to animals with IR injury resulted in a decline in the rate of functional renal repair and increased

mortality rates.

Whilst results in the laboratory have shown great potential for MSCs to exert immunomodulatory effects and promote regeneration and repair following disease, it should not be ignored that some studies have demonstrated that the therapeutic effect of MSCs can vary (183, 193).

1.4.4 Homing of mesenchymal stem cells

In steady state, intravenously injected MSCs migrate to the bone marrow (194, 195). In the setting of inflammatory damage, MSCs preferentially home to the site of inflammation where they then migrate across the endothelium and enter the injured organ (164, 173, 196-198), to some extent analogous to leukocyte trafficking (Figure 1.4). The *in vivo* tracking of fluorescently labelled MSCs have demonstrated that these cells infiltrate the peritubular capillaries and glomeruli of kidneys with IR injury within 10 minutes of injection, with no cells evident by 72 hours (179). The precise mechanisms of MSC homing to sites of tissue injury are not fully understood. However, Bi et al. (174) reported that the beneficial effects of administering MSCs to mice with cisplatin-induced injury were also observed when MSC-conditioned media was administered without the cells. This implies that the mechanisms in which MSCs confer protection is not entirely attributed to their ability to home and engraft to the site of kidney damage. The study highlights that MSCs are also capable of mediating protection via an endocrine manner (174).

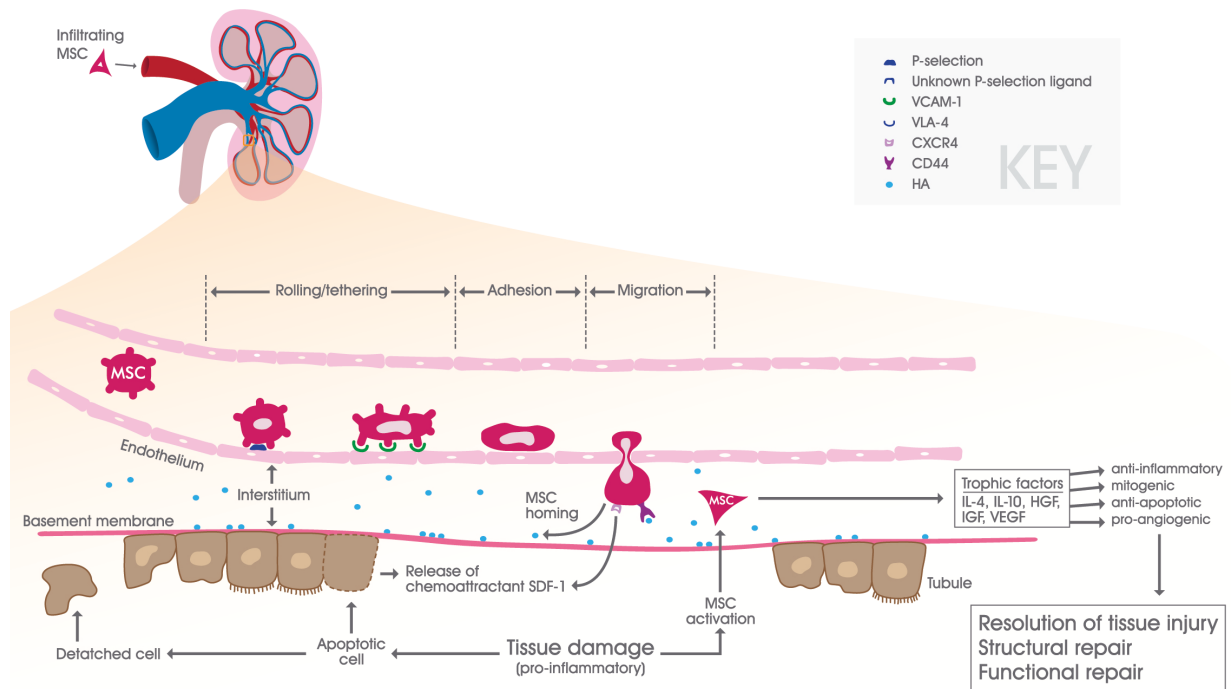


Figure 1.3 Representative diagram depicting MSC homing to a kidney with acute damage. The precise mechanisms that facilitate MSC homing are still unclear. However, various growth factors, cytokines, chemokines and chemokine receptors are proposed to play key roles in the migratory process. Following acute insult, there is upregulation of SDF-1 and HA within the kidney. MSC express CXCR4 and CD44, which bind SDF-1 and HA, respectively. Following intravenous administration, MSC can bind to P-selectin and roll along the endothelium of blood vessels, preferentially migrating along the SDF-1 and HA gradient to sites of inflammation. Thereafter, MSC firmly adhere to the endothelial wall via VLA-4 and VCAM-1 and transmigrate across the endothelium into the kidney where they secrete an array of trophic factors that promote structural and functional repair and mediate tissue remodelling. HA, hyaluronic acid; MSC, mesenchymal stem cell; SDF-1, stromal cell-derived factor-1; VCAM-1, vascular cell adhesion molecule-1; VLA-4, very late antigen-4. IL, interleukin; HGF, hepatocyte growth factor; IGF, insulin-like growth factor; VEGF, vascular endothelial growth factor.

MSCs have numerous chemokine receptors that may assist in their migration to sites of inflammation (199, 200). Following ischaemic injury, the expression of the chemokine stromal cell-derived factor-1 (SDF-1), also known as chemokine (C-X-C motif) ligand (CXCL)12, is upregulated within the kidney (201). MSCs express the SDF-1 receptor chemokine (C-X-C motif) receptor (CXCR)4, which is further upregulated under hypoxic conditions (201, 202). In addition, when MSCs are pre-incubated with TNF- α they show an increased migratory capacity towards SDF-1 indicating that a SDF-1/CXCR4 interaction may mediate the localisation of exogenously injected MSCs to sites of tissue injury (203, 204). Ponte et al. (204) tested the ability of MSCs to home towards 16 different growth factors and chemokines *in vitro* and found that PDGF and IGF-1 were the most potent chemoattractants for MSCs. CD44 is another candidate that has been shown to play a vital role in MSC trafficking (173, 205). CD44 on MSCs binds to hyaluronic acid (HA), which is significantly upregulated in the kidney following ischaemic injury (173, 206). Supportive studies by Herrera et al. (173) show that the injection of either MSCs derived from CD44 null mice, or MSCs incubated with a CD44 blocking antibody or soluble hyaluronic acid (HA), did not migrate to the kidney following glycerol induced damage. However, MSC homing was restored when these CD44-negative cells were transfected with wild-type CD44, indicating that CD44/HA interactions are required for the migration of MSCs to the kidney following injury (173).

1.4.5 Do mesenchymal stem cells act via macrophages?³

As discussed in Section 1.3 in detail, monocyte-derived macrophages comprise a heterogeneous population of cells that play a fundamental role in immune and non-immune-mediated renal disease, host defence and allograft responses. Recent studies have demonstrated that MSCs interact with macrophages and have the potential to promote M2 polarisation (207-224). The *in vitro* co-culture of human MSCs and macrophages resulted in an alternatively activated macrophage phenotype described as mannose receptor (MR)^{high},

³ Exerts of the text in Section 1.4.5 have been published in: Wise and Ricardo, *Nephrology*, 2012.

IL-10^{high}, IL-6^{high}, TNF- α ^{low} and IL-12^{low} which exhibit enhanced phagocytic activity, increased secretion of IL-10 and VEGF and decreased secretion of pro-inflammatory cytokines (207, 211, 214, 216). Furthermore, when MSCs were co-cultured with macrophages, that had been polarised *in vitro* to an M1 phenotype, the MSCs retained their ability to shift macrophage polarisation towards an M2 phenotype (220). It has also been shown that MSC-conditioned medium can promote macrophages to adapt a regulatory-like M2 phenotype characterised by a significantly reduced production of pro-inflammatory cytokines and an enhanced production of IL-10 and phagocytic function (208, 224). MSCs may switch macrophage phenotype toward an M2 phenotype via cyclooxygenase-2 (COX-2), indoleamine 2,3-dioxygenase (IDO) and prostaglandin E₂ (PGE₂) mediated mechanisms (208, 209, 214, 217, 218). Ablating PGE₂ or blocking the PGE₂ receptors, E-prostanoid (EP)2 or EP4, inhibits the MSCs ability to drive macrophage polarisation towards the M2 phenotype (209, 217).

Several recent studies have revealed that these *in vitro* findings translate to an *in vivo* setting. The *in vivo* treatment of wounds with bone marrow-MSC conditioned medium has been reported to enhance wound healing, a process associated with an increased infiltration of macrophages (212). Following the systemic administration of human gingiva-derived MSCs (GMSCs) to mice with an excisional skin wound, GMSCs homed to the wound site and were found in close propinquity with macrophages. Subsequent analysis of this macrophage phenotype revealed an increased expression of the M2 macrophage markers Fizz1 and arginase-1, highlighting the ability of MSCs to interact with macrophages and promote M2 polarisation (211). In a mouse model of transient global ischaemia, the administration of bone marrow-MSCs resulted in neuroprotection. Further investigation demonstrated an up-regulation of the M2 markers Ym-1, IGF-1, galactin-3 and MHC class II in the microglia/macrophages (210). Following the administration of MSCs to rats with spinal cord injury, induced by contusion to vertebrae T9-T10, the MSCs migrated to the spinal cord where they promoted an increase in IL-4 and IL-13 concomitant with a decrease in TNF- α

and IL-6. Furthermore, MSC treatment resulted in increased M2 and decreased M1 macrophage accumulation (215). Nemeth et al. (209) showed that MSCs administered to mice with cecal ligation and puncture (CLP)-induced sepsis homed to the lung where they were found surrounded by macrophages. To further support the argument for the importance of macrophages in the MSC reparative response, when MSCs were administered to mice with CLP-induced sepsis following macrophage depletion, injury protection was lost (209). Transplantation of MSCs in an experimental model of myocardial infarction promoted an increase in the proportion of M2 macrophages in circulation and the infarcted heart resulting in a decrease in apoptotic cardiomyocytes, pro-inflammatory IL-1 β and IL-6, and an increase in anti-inflammatory IL-10 expression (213, 221, 223). Interestingly, the beneficial effect of MSCs were eliminated when macrophages were depleted prior to myocardial infarction (221). In the setting of lung disease, MSCs have been shown to reduce airway hyperresponsiveness and eosinophil accumulation in a mouse model of ovalbumin-induced allergic asthma (222). In a model of orthotopic tracheal transplantation (OTT), MSCs inhibited the development of obliterative bronchiolitis, the narrowing of the airways (218). Interestingly, MSC treatment significantly promoted IL-10 secretion in both of these models, however, following macrophage depletion the increase in IL-10 and the protective effect of the MSCs were abolished (218, 222). Following the administration of MSCs to mice with IR injury, Li et al. (219) showed that the proportion of M2 macrophages within the kidney was increased along with improved renal architecture and function. However, this MSC-induced renoprotection was abrogated when the macrophages were depleted 24 hours post-IR injury indicating the MSC-mediated repair is dependent on the infiltrating macrophages (219).

1.5 Hypothesis and Aims

The preceding introduction has outlined the pathophysiology of acute ischaemic kidney injury, with focus on the pathogenic and protective roles of monocytes and macrophages in both inflammation and repair. Moreover, the promising therapeutic properties of MSCs and their potential to alter the inflammatory response and promote kidney repair has been reviewed. The present PhD thesis has investigated the mechanisms in which MSCs exert their therapeutic benefits in an acute experimental mouse model of IR injury and determined the effect they had on the polarisation of monocytes and macrophages isolated from mice and patients with ESRD.

The overall hypothesis of this PhD project is that MSCs can attenuate AKI via homing to the damaged kidney where they secrete soluble factors that promote regeneration of the damaged tubular epithelium leading to functional recovery through alteration of monocyte and macrophage phenotype.

The specific aims of the studies described in this thesis are:

- 1) To characterise the identity of mouse and human bone marrow-derived MSCs.
To optimise the therapeutic dose of human bone marrow-derived MSCs for mice with kidney IR injury and assess the potential for this therapy to promote structural repair.
- 2) To determine the mechanisms by which exogenously administered human bone marrow-derived MSCs promote structural and functional repair of the kidney following IR injury.
To determine the effect human bone marrow-derived MSCs have on the polarisation of murine bone marrow-derived macrophages.
- 3) To examine the effects human bone marrow derived-MSCs have on the phenotype of monocytes isolated from a chronic inflammatory setting (type 2 diabetic patients with ESRD), following *in vitro* co-culture.

CHAPTER 2

*The characterisation of mesenchymal stem cells and
the development of an intravenous therapy for
mice with acute ischaemic kidney injury*

Chapter 2: The characterisation of MSCs and the development of an intravenous MSC therapy for mice with acute ischaemic kidney injury

2.1 Introduction

Renal IR injury is a leading cause of AKI, the incidence of which is rising rapidly (24). In many cases, ischaemic injury occurs following hypovolemia, sepsis, cardiac surgery or kidney transplantation (1). Treating the kidney disease resulting from these triggers comes with great difficulty due to the structural and functional complexity of the kidney. In addition, the pathophysiology of IR injury is multifactorial, involving the interplay between numerous tubular and inflammatory factors (225). Several attempts have been made to target specific mediators that contribute to ischaemic AKI with the use of pharmacological agents delivered to experimental animal models (38). However, the clinical translation of these therapies has been disappointing to date (26, 38). Consequently, there is still no effective treatment for AKI, with only supportive therapy, such as dialysis, available. As a result, there is a growing interest in stem cell-based treatments, including MSCs, as new therapeutic options for the treatment of AKI.

MSCs comprise a heterogeneous population that was originally identified in the bone marrow stroma (140, 141, 226). However, MSCs have since been isolated from a variety of tissues using various isolation and expansion protocols (156). The formal identification of MSCs proved to be difficult due to the lack of any MSC specific markers. Therefore, to aid in the classification of MSCs, the *Mesenchymal and Tissue Stem Cell Committee of the International Society for Cellular Therapy* devised a minimal criteria to be used by researchers to confirm the true identity of the MSCs (150). As part of this criteria, MSCs must adhere to plastic *in vitro*, with $\geq 95\%$ of MSCs expressing CD73, CD90 and CD105 and with $\leq 2\%$ expressing the haematopoietic markers CD45, CD34, CD14 or CD11b, CD79a or CD19 and

MHC class II. MSCs must also possess trilineage differentiation potential that is evidenced following the *in vitro* differentiation into osteocytes, adipocytes and chondrocytes. In terms of cell function, MSCs secrete a broad spectrum of soluble factors that exert immunomodulatory and tissue regenerative effects. As a result, MSCs hold great promise as a new cell-based therapy for AKI as they have the potential to target several aspects of the disease simultaneously. Additionally, following allogeneic or xenogeneic transplantation MSCs remain 'immune tolerated' and are capable of exerting their therapeutic effects across MHC and species barriers (227, 228). Hence, numerous preclinical and clinical studies have exploited these unique properties and have demonstrated therapeutic efficacy with autologous, allogeneic and xenogeneic MSCs in a wide range of disorders (229).

This study used the minimal criteria outlined by Dominici et al. (150) to define the identity of MSCs isolated from murine and human bone marrow. Additionally, the feasibility of using human MSCs in a mouse model of AKI was investigated. This pilot study incorporated a treatment dose curve using human bone marrow-derived MSCs in a mouse model of unilateral IR injury. The therapeutic potential of the human MSCs was assessed through analysis of apoptosis, quantification of epithelial cell adhesion molecule (EpCAM) and the semi-quantification of tissue architecture disruption and interstitial inflammatory cell infiltration.

2.2 Materials and Methods

2.2.1 Mesenchymal stem cells

A frozen vial of mouse MSCs at passage 5, isolated from the bone marrow of C57BL6/J mice, was kindly provided by Professor Claude Bernard (Monash University). Mouse MSCs were cultured in α -minimum essential media (α -MEM; Invitrogen, Camarillo, CA) supplemented with 9.8% foetal bovine serum (FBS; GIBCO, Grand Island, NY), 9.8% horse serum (Sigma-Aldrich, St. Louis, MO), 2mM L-glutamine, 100U/ml penicillin and 100 μ g/ml streptomycin (all from Invitrogen) until approximately 70% confluence was reached. Frozen vials of human bone marrow-derived MSCs at passage 1 were purchased from the Tulane Centre for Stem Cell Research and Regenerative Medicine (Tulane University, New Orleans, LA). Human bone marrow-derived MSCs at passage 2 were kindly provided by Professor Claude Bernard. Human MSCs were cultured in α -MEM supplemented with 16.5% foetal bovine serum, 2mM L-glutamine, 100U/ml penicillin and 100 μ g/ml streptomycin (all from Invitrogen) until approximately 70% confluence was reached. Karyotype analysis was performed on mouse MSCs at passage 6 and human MSCs at passage 3 by Southern Cross Pathology (Clayton, Australia).

2.2.1.1 Colony-forming unit-fibroblasts assay

The clonogenic potential of MSCs was tested using a CFU-F assay. One hundred mouse MSCs or human MSCs were plated in 100x20mm tissue culture-treated dishes (BD Biosciences, San Jose, CA) containing 10ml of MSC media. The cells were cultured at 37°C with 5% humidified CO₂ for 14 days. The MSC media was changed every 3-4 days. Following 14 days of culture the media was aspirated and the plates washed with 10ml of phosphate buffered saline (PBS). The colonies were stained with 3% (w/v) crystal violet (Sigma-Aldrich) dissolved in 100% methanol (Merck, Darmstadt, Germany) for 10 minutes at room temperature. The plates were washed with deionised water until the washes became clear then air-dried.

2.2.1.2 MSC multilineage differentiation

To demonstrate multilineage differentiation potential, mouse MSCs and human MSCs were differentiated towards adipogenic, osteogenic and chondrogenic lineages using a mouse MSC functional identification kit or a human MSC functional identification kit, respectively, according to the manufacturer's guidelines (R&D Systems Inc., Minneapolis, MN). Following differentiation, adipocytes were stained with fatty acid binding protein-4 (FABP-4; R&D Systems) or Oil Red O (Sigma-Aldrich), osteocytes were stained with osteopontin (R&D Systems) or Alizarin Red S (Sigma-Aldrich) and chondrocytes with collagen II (R&D Systems) or aggrecan (R&D Systems).

2.2.2 Animals and Ethics Approval

All animal procedures were approved by the Monash University Animal Ethics Committee in accordance with the ethics number SOBSA/MIS/2009/41 and were carried out under the strict guidelines of the "*Australian Code of Practice for the Care and Use of Animals for Scientific Purpose*". Male 6 – 8 week old (weighing 20 – 25g) C57BL6/J mice were obtained from the Monash Animal Research Platform (Monash University, Clayton) and were housed at the Animal Research Laboratories (Monash University, Clayton) under controlled temperature and light conditions, with free access to food and water.

2.2.2.1 Renal ischaemia/reperfusion surgery

To perform renal unilateral IR injury, mice were anaesthetised with 2.5% (v/v) inhaled isoflurane (Abbott Australasia Pty, Kurnell, Australia) mixed with medical EP grade oxygen (BOC, North Ryde, NSW) via a Stinger Veterinary Anaesthetic machine (Advanced Anaesthesia Specialists, Gladesville, NSW). Once sufficient sedation was reached where the mice no longer had pedal reflexes, the hair was shaved on the flank region on the left side and the skin cleansed with 70% ethanol. Mice were placed on a heated mat to maintain a core body temperature of 37°C throughout the procedure. A flank incision was made through the skin and peritoneum on the left side and the left renal pedicle (left renal artery and vein)

was clamped for 40 minutes using an atraumatic microaneurysm vascular clamp (0.4-1.0 mm; S&T Fine Science Tools, Foster City, CA) to induce ischaemia. Following 40 minutes of ischaemia, the microvascular clamp was removed and reperfusion was visually confirmed. Following reperfusion, 1×10^5 , 5×10^5 or 1×10^6 human bone marrow-derived MSCs re-suspended in 120 μ l of PBS or a vehicle control (120 μ l of PBS alone; $n = 3$ /group) were injected using a 0.5ml syringe and 29-gauge needle (BD biosciences) directly into the renal vein. The side flank incision was then sutured with surgical silk (5-0; Ethicon, Johnson & Johnson, North Ryde, NSW) and mice were removed from anaesthesia and allowed to recover. A third group of mice served as a sham-operated control group, whereby the animals were anaesthetised and a flank incision was made without clamping the renal pedicle. Mice were culled from all 3 treatment groups via CO₂ asphyxiation on days 3 or 7 post-IR and the left kidneys were removed for histological assessment.

2.2.2.2 Structural analysis

Following removal of the left kidneys, the organs were decapsulated prior to being dissected transversally and immersion-fixed in 4% paraformaldehyde (PFA) solution overnight at 4°C. Kidneys were processed by the Histology Laboratory, Department of Anatomy and Developmental Biology, Monash University, according to their short cycle protocol and embedded in paraffin wax. Paraffin-embedded kidneys were sectioned at 4 μ m using a microtome (Leitz Wetzlar, Germany), mounted on SuperFrost Plus glass slides (Menzel-Glaser, Braunschweig, Germany) and baked overnight at 37°C. Prior to staining, paraffin sections were dewaxed in xylene (3 x 3 minutes), rehydrated through absolute alcohol (3 x 3 minutes) and rinsed in distilled water for 3 minutes. For haematoxylin and eosin (H&E) staining, sections were stained for 5 minutes in Mayer's Haematoxylin (Amber Scientific, Midvale, WA), rinsed thoroughly with distilled water, to remove excess haematoxylin, dipped in 0.1% acid alcohol for 10 seconds to remove non-specific staining in the cytoplasm, and washed in Scott's tap water for 10 seconds to blue the nuclei. Slides were then thoroughly rinsed with distilled water and counterstained with eosin for 3 minutes to stain

the cytoplasm. Following staining, sections were rehydrated through graded alcohols (5 minutes in 80% ethanol, 5 minutes in 95% ethanol, 5 minutes in absolute ethanol), cleared in three changes of xylene before a coverslip was applied. To assess apoptosis, kidney sections were stained with rabbit anti-mouse active caspase-3 (BD Biosciences) followed by a Alexa Fluor 555 goat anti-rabbit (Molecular Probes, Eugene, OR) secondary antibody. Kidney sections were visualised on a Provis AX70 microscope (Olympus, Tokyo, Japan) and images captured with a DP70 digital colour camera (Olympus).

For semi-quantification of histopathology, five fields of view per kidney section ($n = 3$; 3 sections/mouse) at a magnification of x400 were analysed within the corticomedullary region of the kidney. Disruption of tissue architecture and interstitial inflammatory cell infiltration were graded on a scale of 0 to 4, with 0 representing normal tubules, no protein casts and normal interstitial inflammatory cell infiltrate; 0.5, minor tubular damage, protein cast formation and minor interstitial inflammatory cell infiltration; 1, involvement of <10% corticomedullary region; 2, involvement of 11 to 25% of corticomedullary region; 2.5, involvement of 26% to 50% of corticomedullary region; 3, involvement of 51 to 75% of corticomedullary region; and 4, widespread damage, involving >75% of the corticomedullary region.

2.2.2.3 Flow cytometry

Mice were killed 7 days post-IR surgery and the left kidneys were isolated and placed in cold fluorescence activated cell sorting (FACS) buffer [PBS supplemented with 0.2% bovine serum albumin (BSA), 0.02% NaN₃ and 5mM ethylenediaminetetraacetic acid (EDTA)]. The kidneys were removed from the FACS buffer, decapsulated and transferred into a 1.7ml Eppendorf tube where they were chopped finely with surgical scissors prior to enzymatic digestion in 1ml of pre-heated dissociation media (Hank's balanced salt solution (HBSS; Sigma-Aldrich) supplemented with 3mg/ml collagenase/dispase (Roche Applied Science, Penzberg, Germany), 0.2mg/ml deoxyribonuclease (DNase) type 1 (Roche Applied Science)

and 50 μ M CaCl₂). The kidney samples were mixed on a rotary tube suspension mixer (20 revolutions per minute (rpm); Ratek Instruments, Melbourne Australia) at 37°C for 20 minutes and then mechanically digested using a 1000 μ l pipette tip. The samples were mixed for two further 5 minute periods (20rpm) with mechanical dissociation using a 1000 μ l pipette tip in between. After 30 minutes, samples were mechanically digested with an 18-gauge needle until a single cell suspension was achieved. The kidney single cell suspensions were then transferred into 15ml Falcon tubes and 9ml of cold FACS buffer was added in order to inhibit the enzymatic digestion. Samples were centrifuged at 1500rpm for 5 minutes at 4°C, the supernatants were removed and the pellet re-suspended in 1ml of pre-heated red blood cell lysis buffer (8.3g/L Na₄Cl, 10mM Tris-HCl, pH7.5) for 1 minute in order to remove the red blood cells. The cells were washed with 9ml of FACS buffer and centrifuged at 1500rpm for 5 minutes at 4°C. The supernatant was removed, the pellet re-suspended with 1ml of FACS buffer and the cell suspension filtered through a 40 μ m nylon cell strainer (BD Bioscience). An additional 1ml of FACS buffer was used to rinse the cell strainer and the samples were then centrifuged at 1500rpm for 5 minutes at 4°C. Following centrifugation, the supernatants were removed and the pellet re-suspended in 1ml of FACS buffer. A Z2 Coulter Counter (Beckman Coulter, USA) was used to calculate the viable and total cell counts of each sample prior to antibody labelling. Three million cells from each kidney sample were incubated with anti-mouse CD45 PE-Cy5 (clone 30-F11; BD Biosciences), EpCAM PE-Cy7 (CD326; clone G8.8; BioLegend, San Diego, CA) and Fc receptor (anti-CD16/CD32) block for 20 minutes at 4°C in the dark. Isotype matched controls were used for each antibody in a fluorescence minus one (FMO) manner. Cell samples were acquired on a FACSCanto II flow cytometer (BD Biosciences) with the FACS Diva acquisition software (BD Biosciences). Flow cytometric data were analysed using the FlowLogic FCS analysis software (Inivai Technologies, Melbourne, Australia).

2.2.3 Statistical analysis

Statistical analyses of the data were performed using GraphPad Prism software version 5.0 (GraphPad Software Inc., San Diego, CA). An unpaired *t*-test was used to analyse data between two groups. Comparisons between three groups were performed using a one-way analysis of variance (ANOVA) followed by Tukey's multiple comparison tests. All data were expressed as mean \pm standard error of the mean (SEM). $P < 0.05$ was considered statistically significant.

2.3 Results

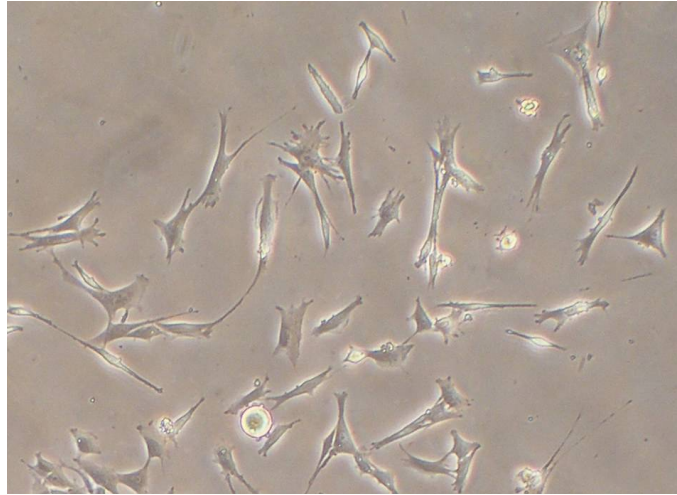
2.3.1 Characterisation of mouse MSCs

Mouse MSCs were initially characterised to confirm their cellular identity using the minimal criteria established by Dominici et al. (150). *In vitro*, the mouse MSCs adhered to plastic, had a spindle-shaped morphology (Figure 2.1A) and formed CFU-F (Figure 2.1B). Using *in vitro* standard differentiation culture conditions, the mouse MSCs differentiated into adipocytes as shown by the presence of lipid vacuoles stained with FABP-4 and Oil Red O (Figure 2.2A; i and ii), osteocytes as evidenced by osteopontin staining and extracellular mineral deposition stained with Alizarin Red S (Figure 2.2B; iii and iv) and chondrocytes as demonstrated with collagen II staining (Figure 2.2C; v). However, the mouse MSCs at passage 6 had an extremely abnormal karyotype (Figure 2.1C).

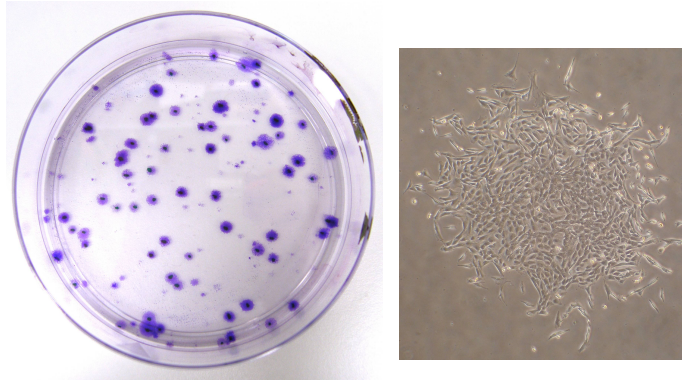
2.3.2 Characterisation of human MSCs

In vitro, human MSCs at passage 3 adhered to plastic, possessed a spindle-shaped morphology (Figure 2.3A), formed CFU-F (Figure 2.3B) and displayed a normal karyotype (Figure 2.3C). The cells were shown to possess true MSC functionality, being able to differentiate into adipocytes, osteocytes and chondrocytes (Figure 2.4A) as evidenced by positive staining with FABP-4 and Oil Red O (Figure 2.4A; i and ii), Alizarin Red S (Figure 2.4A; iii) and aggrecan (Figure 2.4A; iv), respectively. Finally, these MSCs were uniformly positive for the canonical MSC markers CD73, CD90 and CD105, and lacked the expression of the haematopoietic markers CD14, CD19, CD34, CD45 and HLA-DR (Figure 2.4B). As the mouse MSCs exhibited an abnormal karyotype all subsequent experiments in this PhD thesis were performed using the human bone marrow-derived MSCs at passage 3.

A



B



C

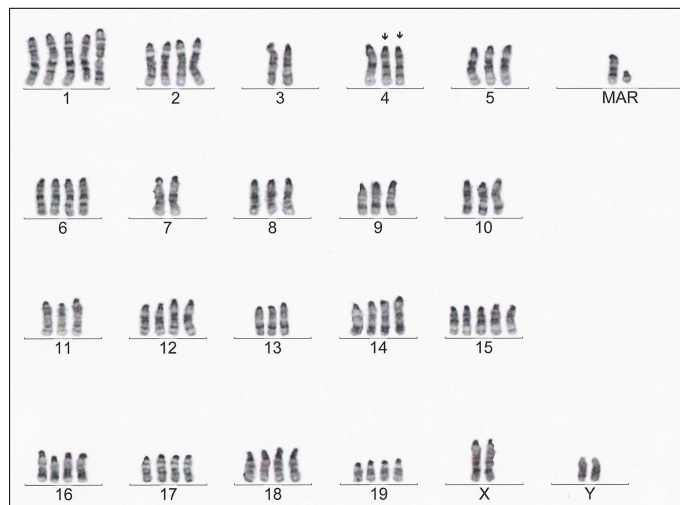


Figure 2.1 Mouse mesenchymal stem cells

Mouse MSCs (passage 6) adhered to plastic in standard tissue culture conditions (**A**; original magnification x100), formed CFU-F following 14 days of *in vitro* culture (**B**; stained with crystal violet) and had an abnormal karyotype (**C**). CFU-F, colony-forming unit-fibroblasts; MSCs, mesenchymal stem cells.

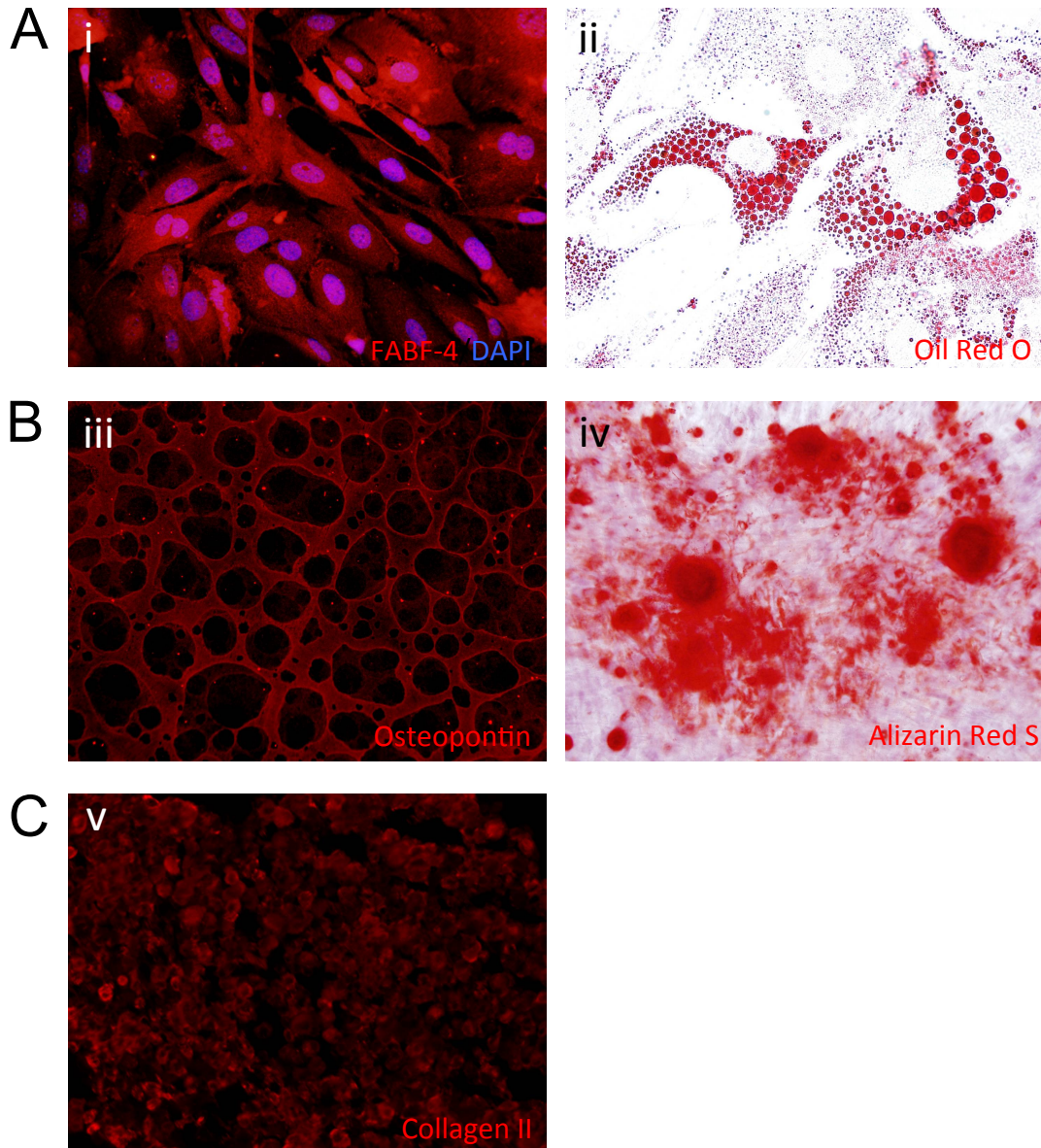
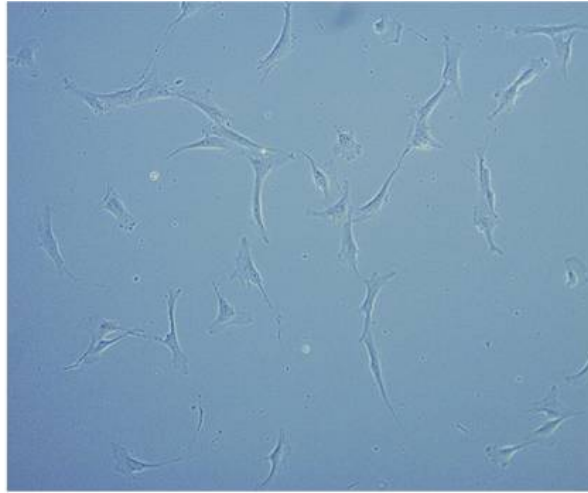


Figure 2.2 The differentiation potential of mouse MSCs

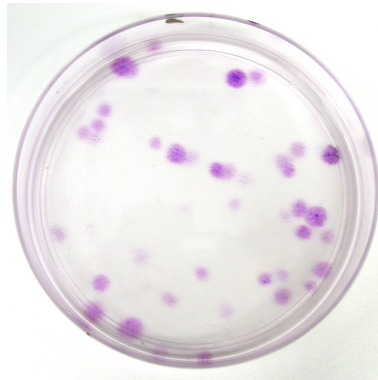
Mouse MSCs demonstrated multilineage potential, differentiating into adipocytes (**A**); stained with FABP-4 (**i**; magnification x400) and Oil Red O (**ii**; magnification x1000), osteocytes (**B**); stained with osteopontin (**iii**; magnification x400) and Alizarin Red S (**iv**; magnification x200) and chondrocytes (**C**); stained with collagen II (**v**; magnification x200). FABP-4; fatty acid binding protein-4; MSCs, mesenchymal stem cells.

(Images in Figure 2.2 (excluding 2.2Ai and 2.2Biv) were published in Wise and Ricardo, *Nephrology*, 2012. See Appendices.)

A



B



C

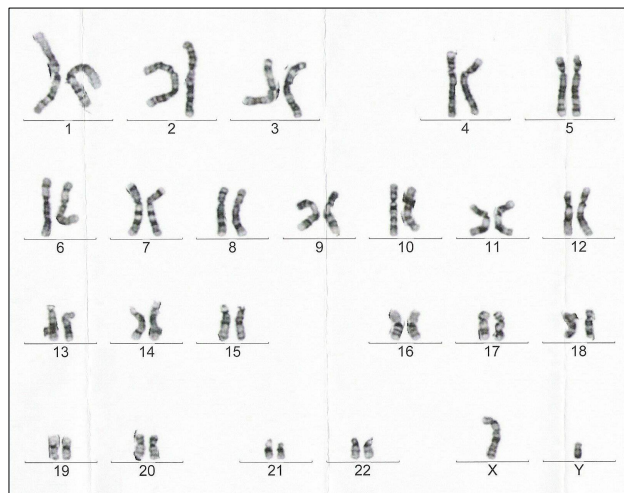


Figure 2.3 Human mesenchymal stem cells

Human MSCs adhered to plastic in standard tissue culture conditions (**A**; original magnification x200), formed CFU-F, demonstrated by crystal violet staining, following 14 days of *in vitro* culture (**B**) and displayed a normal 46XY karyotype (**C**). CFU-F, colony-forming unit-fibroblasts; MSCs, mesenchymal stem cells.

(Data in Figure 2.3 were published in Wise et al., *Am J Physiol Renal Physiol*, 2014. See Appendices.)

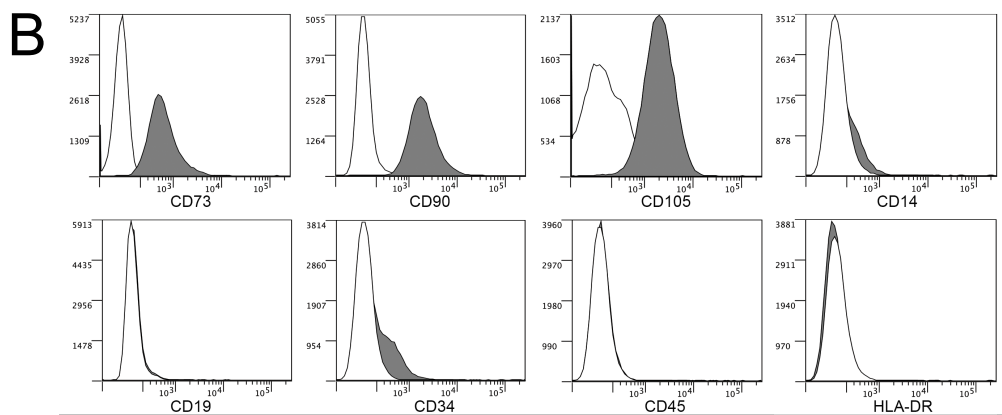
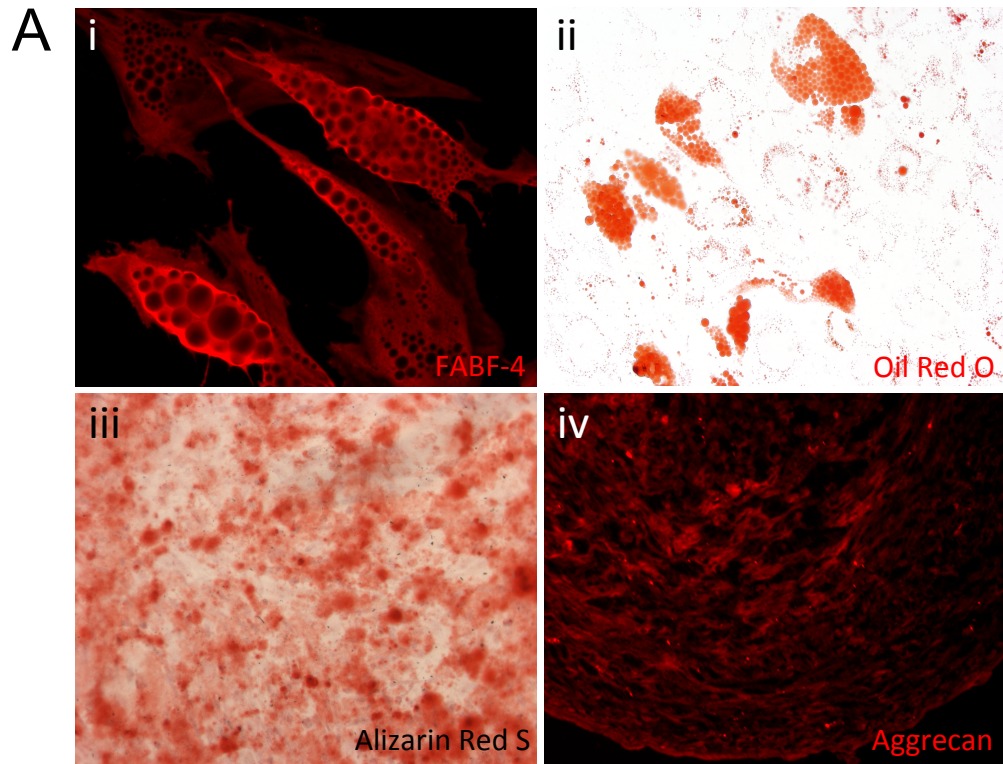


Figure 2.4 The characterisation of human MSCs

Human MSCs possessed multilineage differentiation potential *in vitro* (**A**), differentiating into adipocytes, identified by the presence of FABP-4 staining (**i**; magnification x400) and lipid vacuoles stained with Oil Red O (**ii**; magnification x400), osteocytes, indicated by the formation of calcium-rich deposits detected using Alizarin Red S staining (**iii**; magnification x50) and chondrocytes, visualised due to the presence of aggrecan staining (**iv**; magnification x200). MSCs expressed the cell surface antigens CD73, CD90, and CD105, however, lacked the expression of CD14, CD19, CD34, CD45, and HLA-DR (**B**). Surface marker expression (grey) is overlaid with an isotype control (white). FABP-4, fatty acid binding protein-4; HLA-DR, human leukocyte antigen-DR, MSCs, mesenchymal stem cells.

(Data in Figure 2.4 (excluding 2.4Aii) were published in Wise et al., *Am J Physiol Renal Physiol*, 2014. See Appendices.)

2.3.3 Dose curve of MSC administration to mice with unilateral IR injury

The therapeutic effect of human MSC administration was investigated using a murine model of unilateral IR injury. Following IR injury, kidney damage peaks at approximately 3 days after the initial insult, followed by a reparative phase that allows endogenous regeneration given appropriate environmental cues. In order to establish the optimal dose of MSCs to be delivered to the mice, IR injury was induced prior to the administration of one of three different doses of MSCs. The doses included 1×10^5 MSCs, 5×10^5 MSCs, 1×10^6 MSCs or a vehicle PBS control, injected intravenously on day 0, after reperfusion had visually been confirmed. The histoarchitecture of the kidneys was analysed 3 and 7 days post-treatment (see diagram in Figure 2.5A).

As shown in Figure 2.5B; vi, H&E staining of the kidneys isolated from sham-operated control mice exhibited normal renal histoarchitecture in the corticomedullary region. Figure 5B; vi shows an intact glomerulus and the straight S3 segments of the proximal tubules, which are lined with cuboidal epithelial cells and surrounded by the interstitium comprising a delicate framework of connective tissue. At 7 days following IR injury and vehicle treatment, widespread TEC damage was evident in the kidney (Figure 2.5B; i; magnification x200). Interstitial matrix expansion was evident in conjunction with a vast number of infiltrating inflammatory cells (double ended arrows). At a higher magnification (Figure 2.5B; ii; magnification x400), a loss of the brush border on the luminal surface and flattening of the proximal TECs was observed. In addition, desquamation of the TEC into the kidney lumen was evident resulting in a denuded basement membrane (oval). This was further accompanied with intratubular protein cast formation (asterisk) and an overall widespread loss of tissue architecture. In contrast, the administration of MSCs to mice with IR injury resulted in improved kidney structure (Figure 2.5B; iii-v; magnification x200). At 7 days post-MSC treatment, histological assessment revealed a marked reduction in tissue

damage with all three doses of MSCs. In comparison to the vehicle-treated kidneys, MSC treatment resulted in an attenuation of extracellular matrix expansion and a marked reduction in inflammatory cell infiltrate. There were very few proteinaceous casts present in the tubular compartment and re-epithelialisation of the basement membrane or preserved tubular morphology was widespread. A greater degree of regeneration in the MSC-treated kidneys correlated with the increasing MSC dose that had been administered to mice. This is evident in Figure 5B, which shows that mice administered with 1×10^6 MSCs (Figure 2.5B; v) demonstrated the greatest degree of repair with no mortality.

2.3.4 Semi-quantification of histopathology

Histological observation of the kidney tissue allows for the identification of global and isolated changes in the tissue architecture however, quantifying these changes in the kidney pathology is important as it provides a measure of the extent of injury or improvements achieved as a result of treatment. Therefore, in order to validate the initial histological observations, the overall disruption of kidney tissue architecture was quantified in addition to the infiltration of inflammatory cells. Semi-quantification was performed on the corticomedullary region of the kidneys isolated from vehicle- and MSC-treated (1×10^6 MSCs) mice, 7 days post-IR (Figure 2.5C). At 7 days after IR injury, MSC treatment had significantly reduced damage of the kidney tissue architecture compared to vehicle-treated mice (1.39 ± 0.45 vs. 3.89 ± 0.11 ; $P < 0.01$). Additionally, MSC treatment significantly reduced the extent of inflammatory cells infiltrating the kidney interstitium (1.67 ± 0.58 vs. 3.89 ± 0.11 ; $P < 0.05$).

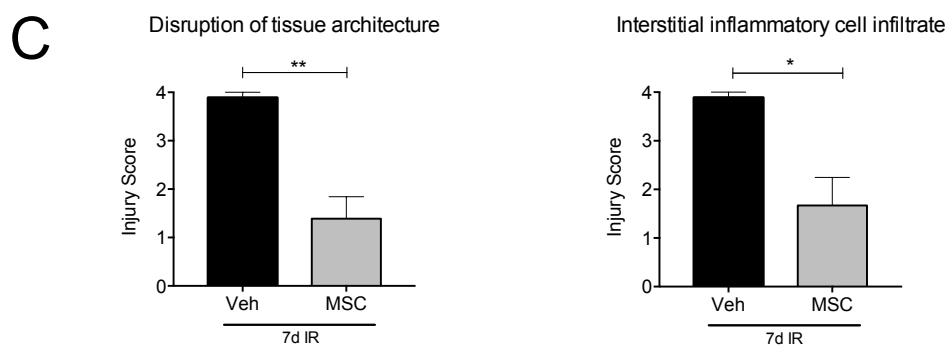
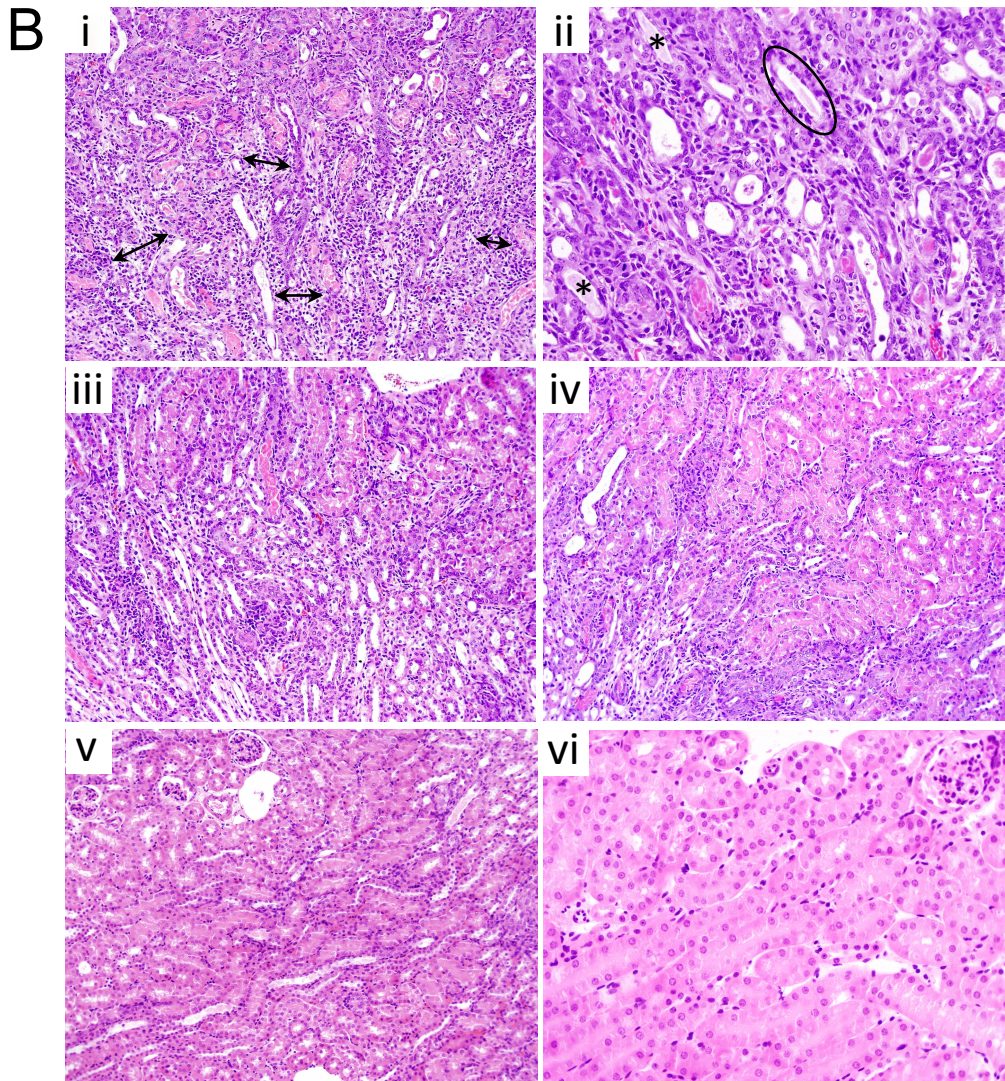
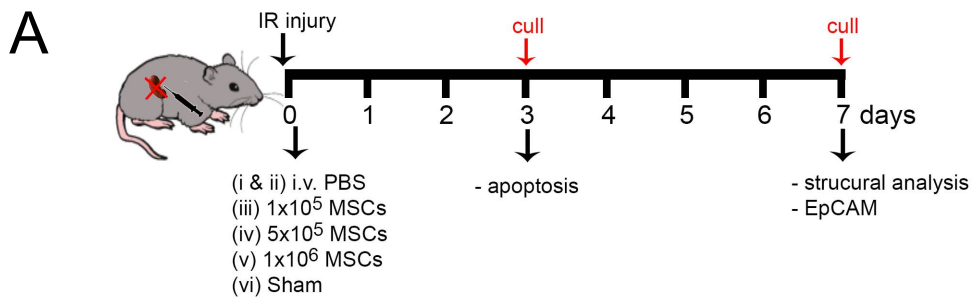


Figure 2.5 Human MSC dose curve in mice with unilateral IR injury

MSCs (P3) were administered intravenously following IR injury and at 3 and 7 days post-injury the histoarchitecture of the kidney was analysed (**A**). In comparison to the 7 day IR+PBS kidney where interstitial matrix expansion, infiltration of inflammatory cells (double arrow head), denuded tubules (oval) and protein casts (asterisks) were evident (**B**; **i**; magnification x200; and **ii**; magnification x400), the administration of 1×10^5 (**iii**), 5×10^5 (**iv**) and 1×10^6 (**v**) MSCs resulted in improved renal architecture (magnification x200) comparable to the sham-operated control kidney (**vi**; magnification x400). Semi-quantitative analysis of the disruption of the tissue architecture and interstitial inflammatory cell infiltration in IR kidneys with and without 1×10^6 MSCs 7 days post-IR are displayed graphically (**C**). Data are means \pm SEM; $n = 3$. * $P < 0.05$, ** $P < 0.01$. EpCAM, epithelial cell adhesion molecule; IR, ischaemia/reperfusion; MSCs, mesenchymal stem cells; P3, passage 3; PBS, phosphate buffered saline; Veh, vehicle.

2.3.5 Apoptosis

One characteristic of IR injury is an increased occurrence of cell death. It is possible that MSCs help preserve cell viability. Therefore apoptosis within the corticomedullary region of the kidney was analysed with the use of immunofluorescence microscopy 3 days post-IR, the time-point at which injury peaks. As a result of ischaemic injury, there was widespread apoptosis within the corticomedullary region of the kidney 3 days following vehicle treatment (Figure 2.6A). In contrast, MSC-treated mice had far less apoptotic cells present within the kidney at this same time-point (Figure 2.6B).

2.3.6 Assessment of EpCAM⁺ proximal TECs

Following ischaemic injury, surviving TECs undergo proliferation resulting in regeneration and repair of the damaged kidney tubules. EpCAM is expressed on the surface of kidney epithelial cells and has been shown to play an important role in both nephrogenesis and kidney regeneration (230, 231). Therefore, EpCAM expression was analysed in order to assess the extent of epithelial cell regeneration following IR injury within the kidneys of vehicle- and MSC-treated mice (Figure 2.7). The gating procedure used to analyse the EpCAM⁺ cells is outlined in Williams et al. (89). As evident in H&E stained kidney sections, there is a dramatic loss of TECs seen at 7 days following IR injury (Figure 2.7A; ii). In comparison, kidneys from MSC-treated mice (Figure 2.7A; iii) have a relatively intact tubular epithelium with re-epithelisation comparable to the sham-operated kidneys (Figure 2.7A; i). Flow cytometric analysis of EpCAM expression supported this finding, revealing that at 7 days post-IR injury there was a significant decrease in the proportion of EpCAM⁺ cells in the vehicle-treated kidneys compared to the sham-operated control kidneys (Figure 2.7B; sham: 27.31% vs. IR: 16.12%; $P < 0.0001$). However, MSC treatment resulted in a greater proportion of EpCAM⁺ cells compared to the vehicle-treated control group (Figure 2.7B; MSC: 20.89% vs. 16.12%; $P < 0.01$). Although the proportion of EpCAM⁺ cells had not yet

returned to the levels observed in the sham group, these results confirm that MSC treatment was promoting TEC regeneration or preserving tubular morphology.

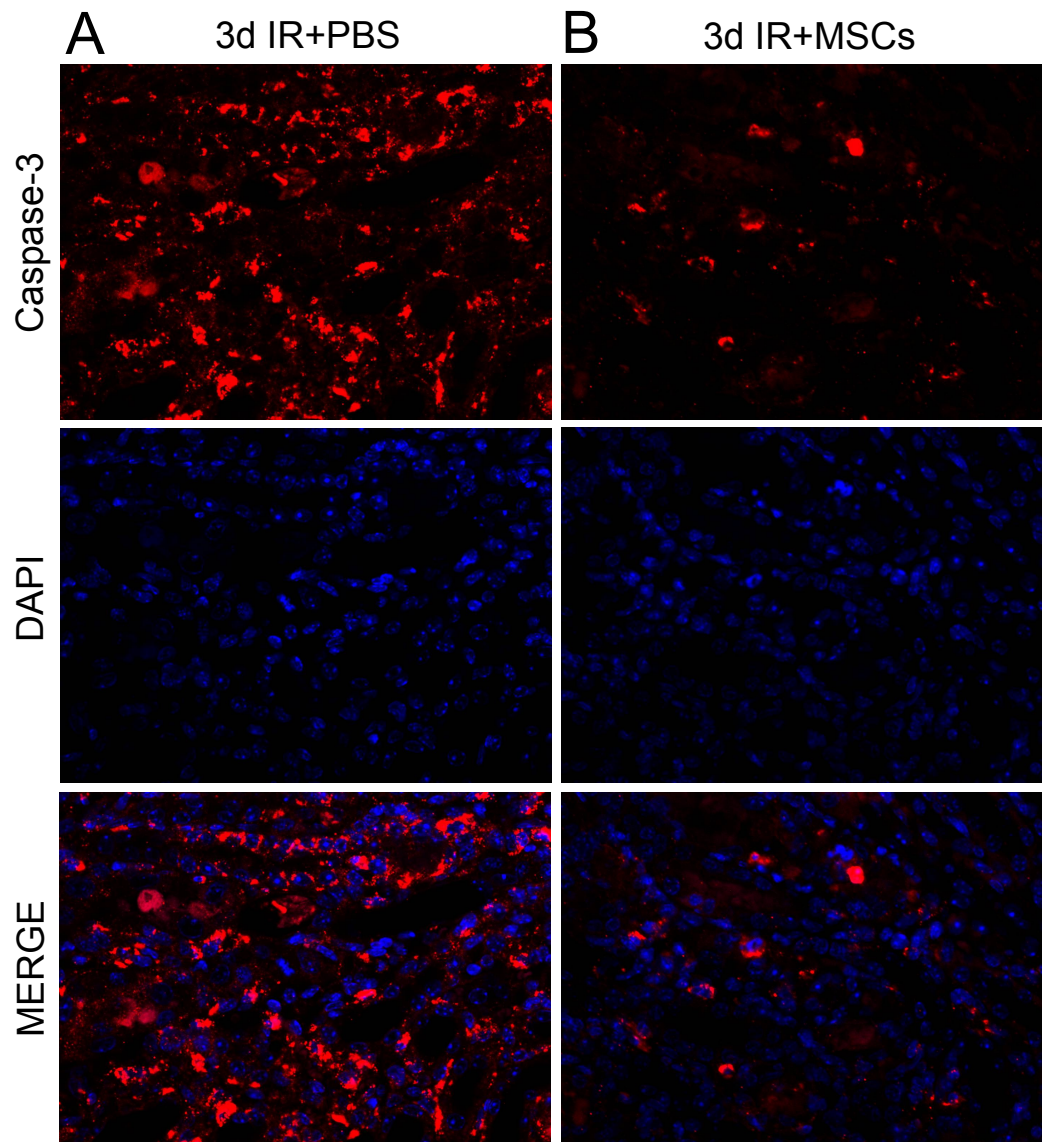


Figure 2.6 Treatment with MSCs reduces apoptosis following IR injury

Representative immunofluorescence photomicrographs (magnification x400) of 3 day post-IR kidneys following vehicle (A) and MSC (B) treatment show that MSCs reduced the amount of caspase-3⁺ (activated form; red) apoptotic cells within the kidney. Kidney sections are counterstained with DAPI nuclear stain (blue). IR, ischaemia/reperfusion; MSCs, mesenchymal stem cells; PBS, phosphate buffered saline.

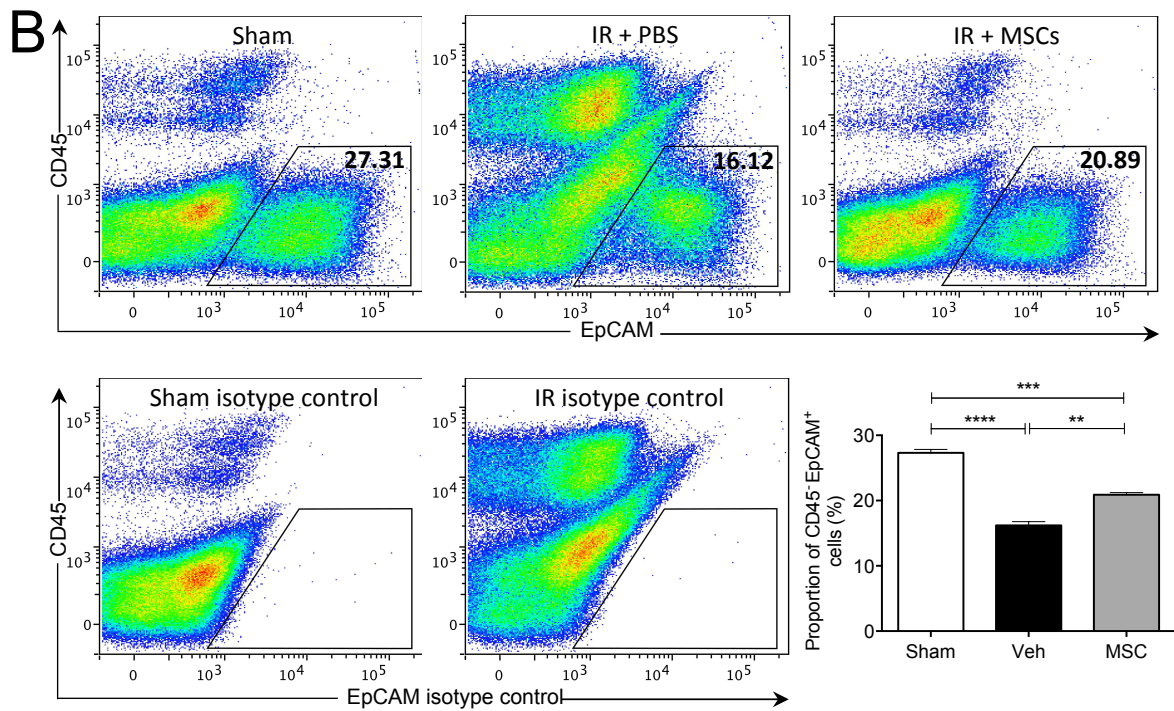
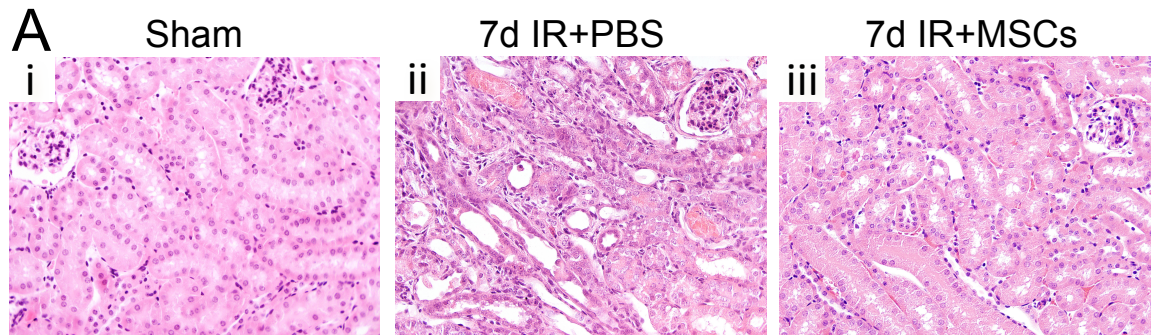


Figure 2.7 MSC treatment increases TEC regeneration

Representative photomicrographs of H&E staining in sham (i) and 7 day post-IR kidneys following vehicle (ii) and MSC (iii) treatment show that following IR injury there is a loss of TECs, however, MSCs promote TEC regeneration, comparable to the sham kidneys (**A**; magnification x400). Flow cytometric analysis of the proportion of EpCAM⁺ cells in sham and 7 day post-IR kidneys following vehicle and MSC treatment (**B**). Data are means \pm SEM, $n = 6$. ** $P < 0.01$, *** $P < 0.001$, **** $P < 0.0001$. IR, ischaemia/reperfusion; MSCs, mesenchymal stem cells; PBS, phosphate buffered saline; TECs, tubular epithelial cells; Veh, vehicle.

2.4 Discussion

Friedenstein and colleagues (232) were the first to isolate MSCs from the mouse bone marrow stroma. They identified these cells as a spindle-shaped, clonogenic population capable of regenerating bone (141). MSCs have since been shown to exist in virtually all postnatal and perinatal (such as amnion, placenta, umbilical cord and Wharton's jelly) tissues, however their precise anatomical location within these tissues and intrinsic physiological role are yet to be fully elucidated (156, 229). Nevertheless, due the immense therapeutic potential of *ex vivo* expanded MSCs, there has a dramatic rise in MSC research in a multitude of medical disciplines. Due to the growing interest, the discovery and use of MSCs isolated from various tissue sources, and the lack of a single MSC specific marker, a criteria was formulated for MSC researchers to adopt to ensure a standardised MSC population was being used amongst research laboratories (150). The minimum criteria outlined by Dominici et al. (150) were achieved in this study for both the mouse- and human-derived MSCs. It is vital that the cells to be used were verified as MSCs prior to experimentation so that comparison of the research findings could be made with other studies in the field.

Interestingly, the mouse-derived MSCs by passage 6 displayed an abnormal karyotype. Several recent studies have reported that mouse-derived MSCs have an increased susceptibility to spontaneously transform following isolation and *ex vivo* expansion, resulting in immortalisation and an abnormal karyotype (233-236). Further, these transformed MSCs form tumours following administration to mice (233, 234, 236). The spontaneous transformation of mouse MSCs may be attributable to the longer telomere length in mice, 30-40kb, compared to humans, 5-10kb (237). Consequently, mouse MSCs can undergo extended proliferation before they reach their telomere length limit, increasing their susceptibility to mutations (237). Miura et al. (233) proposed that the mouse MSC transformations were due to an upregulation of c-myc expression, which induced increased

telomerase activity. It may also be due to the highly inbred nature of experimental mouse colonies, making them genetically unstable. Additionally, mice have a shorter life-span in comparison to humans and subsequently their genome maintenance is not as tightly regulated, allowing them to regularly escape senescence (237, 238). In contrast to mouse MSCs, human MSCs are genetically much more stable *in vitro* and eventually enter senescence after long-term *in vitro* expansion (239). It has been estimated that the probability that human MSCs would emerge from senescence is $<10^{-9}$ (240). Therefore, their tumorigenic potential following *in vivo* infusion would also most likely be very low.

MSCs have long been thought to be immune privileged as they express low levels of MHC class I and lack the expression of MHC class II and the co-stimulatory molecules CD40, CD80 and CD86 (153, 241). As a result, MSCs fail to induce allogeneic PBMC or T-cell proliferation *in vitro* and instead suppress the proliferation of these cells in an MHC independent manner (153, 241). Following *in vivo* administration to MHC-mismatched baboons, Bartholomew et al. (160) demonstrated that MSCs could prolong skin graft survival. Further, in 2004 Le Blanc and colleagues successfully treated a 9 year old boy with acute lymphoblastic leukaemia suffering from severe treatment-resistant grade IV acute GvHD with allogeneic MSCs (170). However, it has been shown that upon exposure to IFN- γ , MHC class I and MHC class II can be upregulated on MSCs (154). Thus in an *in vivo* setting of inflammation, it is most likely these molecules are upregulated, exposing them to the host's immune system. Interestingly, it has been shown that following the transplantation of human MSCs into immunocompetent and immunosuppressed mice, the MSCs persist for the same duration (210). Several studies have also now demonstrated that human MSCs successfully exert therapeutic benefits following xenogeneic transplantation in an array of experimental disease models including retinal degeneration (242), myocardial infarction (243), streptozotocin-induced diabetes (244), acute lung injury (245), asthma (222) and EAE (246), to name a few [for review see (228)].

These findings provide support for using human MSCs in studies aimed at developing a cell-based therapy to promote kidney regeneration. Importantly, as mouse MSCs have an unstable karyotype we concluded that it is not feasible to administer the mouse MSCs at passage 6 to mice, due to the increased safety risks. This pilot study was therefore carried out to determine the feasibility of using a xenogeneic transplant model, whereby *ex vivo* culture expanded human bone marrow-derived MSCs were administered to immunocompetent mice with AKI. We demonstrated that following administration to mice with unilateral IR injury, a single dose of 1×10^5 , 5×10^5 or 1×10^6 human bone marrow-derived MSCs promoted structural regeneration of the kidney, without any mortality occurring. The extent of renal repair appeared greatest with the highest dose of 1×10^6 MSCs. Therefore, additional analyses investigating the renoprotective potential of human MSCs (using the 1×10^6 MSC dosage) were performed to validate the initial findings. At 3 days post-IR injury, when widespread tubular damage is most apparent, MSC treatment reduced apoptosis within the kidney, in comparison to vehicle treatment. By 7 days, the histoarchitecture of the kidney from MSC-treated mice were comparable to sham kidneys, with few intratubular casts, reduced interstitial matrix expansion and re-epithelialisation of the denuded basement membrane. This was accompanied with a significant reduction in infiltrating inflammatory cells.

The reasons why MSCs are not immediately detected and cleared by the host's immune system but instead persist following allogeneic or xenogeneic transplantation are yet to be elucidated. This, though, may prove to be a key characteristic in the development of a successful MSC therapy. It is also worth investigating whether this characteristic can itself be manipulated, thereby improving the efficacy of treatment. Although there may be concerns regarding the implications of xenogeneic transplantation, using human MSCs in experimental mouse models is extremely beneficial and of clinical relevance due to documentation of species variation in mouse and human MSC-mediated immunosuppression (247). Therefore, using human MSCs in mouse models can allow for a better understanding

of the migratory capabilities of human MSCs to sites of inflammation, their effects on endogenous cells and the resultant therapeutic consequences, further delineating the mechanisms by which human MSCs exert therapeutic effects.

A key feature of acute and chronic kidney disease is the accumulation of collagen resulting in fibrosis and a subsequent loss in renal function. Regardless of the insult, kidney injury most often results in a rapid influx of macrophages (248). In many CKD models, in both mice and humans, macrophage accumulation has been shown to promote fibrosis. Furthermore, the degree of macrophage accumulation directly correlates to the extent of renal dysfunction and subsequent disease progression (249-253). However, following AKI, such as IR injury, macrophages can also mediate regeneration through the phagocytosis of apoptotic cells, extracellular matrix and debris and by secreting anti-inflammatory and wound healing-related soluble factors that resolve inflammation and promote tissue remodelling (discussed in detail in Section 1.3.2.2). We therefore propose that MSCs exert their therapeutic effects by secreting soluble factors that not only promote TEC proliferation, but also promote a reparative macrophage phenotype. Following on from the present study, the mechanisms in which MSCs mediate endogenous renal repair following acute ischaemic injury will be investigated together with the specific effect MSCs have on macrophage polarisation.

In summary, this initial investigation into MSC suitability for promoting kidney regeneration demonstrated that the administration of human MSCs to mice is feasible, compared to using mouse-derived MSCs, which have considerable limitations. The administration of 1×10^6 human MSCs to adult mice with IR injury was established as a safe and effective dose. MSC treatment of IR injury with 1×10^6 human MSCs accelerated endogenous renal repair resulting in reduced apoptosis, increased re-epithelialisation of the damaged tubular epithelium, attenuation of extracellular matrix expansion and a reduced infiltration of inflammatory cells. MSCs have extraordinary tissue regenerative capabilities and thus hold great promise as a potential new cell-based treatment option for promoting tissue repair and regeneration. However, understanding the underlying renoprotective mechanisms in which MSCs promote kidney repair is required to develop specific and targeted treatments.

CHAPTER 3

*Human mesenchymal stem cells alter macrophage phenotype
and promote regeneration via homing to the kidney
following ischemia-reperfusion injury*

Declaration for Thesis Chapter 3

Declaration by candidate

This chapter was published as is, in the American Journal of Physiology Renal Physiology:

Wise AF, Williams TM, Kiewiet MB, Payne NL, Siatskas C, Samuel CS, Ricardo SD (2014). "Human mesenchymal stem cells alter macrophage phenotype and promote regeneration via homing to the kidney following ischemia/reperfusion injury" *Am J Physiol Renal Physiol.* 306(10): F1222-F1235. Figure 1 from this manuscript was included in Chapter 2 of this thesis.

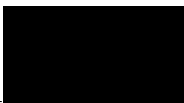
In the case of Chapter 3, the nature and extent of my contribution to the work was the following:

Nature of contribution	Extent of contribution (%)
Study design, execution of experiments, data analysis, interpretation of results, preparation of manuscript	85%

The following co-authors are students at Monash University and the extent of their contribution in percentage terms are stated below.

Name	Nature of contribution	Extent of contribution (%) for student co-authors only
Timothy Williams	Technical assistance and intellectual input	3%

The undersigned hereby certify that the above declaration correctly reflects the nature and extent of the candidate's and co-authors' contributions to this work.

Candidate's Signature		Date: 06.10.14
Main Supervisor's Signature		Date: 06.10.14

Chapter 3: Human mesenchymal stem cells alter macrophage phenotype and promote regeneration via homing to the kidney following ischemia/reperfusion injury

3.1 Introduction

Since the initial excitement surrounding the multi-lineage potential and self-renewal properties of mesenchymal stem (stromal) cells (MSCs), their therapeutic potential to elicit tissue regeneration has been explored experimentally and in a wide range of clinical applications (254). MSCs are capable of modulating inflammation through interacting with a variety of immune cells (255, 256). These immunomodulatory properties, in combination with their tissue regenerative capabilities, have created great enthusiasm for these cells to be used as a treatment for a wide variety of pathological conditions ranging from autoimmune to chronic inflammatory diseases [for review (254, 256, 257)]. MSCs reside in most postnatal organs and tissues, and can be isolated and expanded in culture (156). Unlike embryonic stem (ES) cells and induced pluripotent stem (iPS) cells, MSCs typically do not form tumors following transplantation in rodents and are free of the ethical limitations associated with ES cell research.

Human MSCs have been shown to ameliorate the symptoms of inflammatory diseases in rodent models (186, 258-262) however, the mechanisms responsible for their protective and regenerative effects are not completely understood. The interaction of MSCs with macrophages may play a vital role in their downstream anti-inflammatory and immunomodulatory effects, yet the specific cell cross-talk MSCs have with infiltrating macrophages and damaged kidney cells, along with the cytokines that contribute to their unique immunomodulatory properties, remain poorly defined.

MSCs secrete a broad range of cytokines, including macrophage chemoattractants, as well as a variety of factors with renoprotective and reparative capabilities. These include anti-inflammatory, anti-apoptotic, mitogenic, anti-fibrotic and pro-angiogenic agents, which most likely govern repair via paracrine and endocrine pathways (51, 174, 263, 264). In a setting of acute kidney injury (AKI), transplanted MSCs localized within peritubular capillaries, adjacent to the renal tubules, and glomeruli (179). However, the survival of MSCs and timing of administration leading to the interplay between MSCs and macrophages, along with their ability to modify the tissue microenvironment in a setting where aberrant wound healing-induced collagen accumulation leads to fibrosis has yet to be elucidated.

Macrophages comprise a heterogeneous population that is governed by the inflammatory cues in the surrounding microenvironment (265). Although initially recognized as contributing to the pathogenesis of kidney injury, macrophages may also play a vital role in the remodeling phase of kidney regeneration following acute damage (113, 129, 134). Subsequently, macrophages have been broadly classified into one of two opposing polarization states: classically activated 'M1' and alternatively activated 'M2' populations (266). M1 macrophages secrete numerous pro-inflammatory cytokines and are involved in pathogen clearance whereas M2 macrophages secrete anti-inflammatory cytokines that mediate wound healing and tissue remodeling (266).

This study investigated the therapeutic potential of human bone marrow (BM)-derived MSCs in conjunction with their homing patterns following intravenous administration to mice with ischemia/reperfusion (IR) injury using whole body bioluminescence imaging. In addition, the effect of MSCs on macrophage phenotype and the soluble factors produced following direct and indirect co-culture experiments were assessed.

3.2 Materials and Methods

3.2.1 Mesenchymal stem cell culture

Human BM-derived MSCs purchased from the Tulane Centre for Stem Cell Research and Regenerative Medicine (Tulane University, New Orleans, LA) and enhanced green fluorescent protein (eGFP) and firefly luciferase (fluc) eGFP⁺fluc⁺MSCs were cultured as previously described (246).

3.2.2 Experimental design

All animal studies were approved by the Monash University Animal Ethics Committee, which adheres to the Australian Code of Practice for the Care and Use of Animals for Scientific Purposes. For IR injury, male 6-8 week old C57BL/6J mice (Monash Animal Services, Clayton, Australia) were anesthetized with 2.5%(v/v) inhaled isoflurane (Abbott Australasia Pty Ltd., Kurnell, Australia) and injury induced by clamping the left renal pedicle for 40 minutes (unilateral) or both renal pedicles for 25 minutes (bilateral) with a microvascular clamp (0.4 to 0.1mm; S&T Fine Science Tools, Foster City, CA) through a flank incision. Following reperfusion, mice were injected with 1×10^6 MSCs (i.v.) re-suspended in 120 μ l PBS or a vehicle control (120 μ l PBS alone). A third group of mice served as a sham-operated control group whereby the animals were anaesthetized and a flank incision was made without clamping the renal pedicle. Mice that received bilateral IR injury were placed in metabolic cages to obtain 24hr urine samples. Urinary kidney injury molecule (Kim)-1 was measured with a Kim-1 mouse ELISA (Abcam, Cambridge, United Kingdom). Concentrations of blood urea nitrogen (BUN) and serum creatinine were measured 3 days post-IR using the i-STAT CHEM8+ cartridges and the i-STAT system ($n=8$; Abbott, Ontario, Canada).

3.2.3 Bioluminescence imaging

Mice ($n=5$) were anesthetized with 2.5%(v/v) isoflurane, injected intraperitoneally (i.p.) with 200 μ l D-luciferin (15mg/mL in PBS; VivoGlo Luciferin, Promega, San Luis Obispo, CA) and imaged 10 minutes after injection using a Xenogen IVIS 200 system (Xenogen, Alameda, CA) on days 0 (1hr post-MSC injection), 1 and 3 post-IR. Regions of Interest (ROIs) were drawn and luciferase luminescent signal intensities were analyzed using Living Image 3.2 software (Xenogen; 246).

3.2.4 Histology and immunofluorescence labeling

Histopathology was assessed on formalin fixed, 4 μ m thick paraffin sections stained with hematoxylin and eosin (H&E). Semi-quantification of histopathology was performed after taking 5 fields of view/kidney section within the corticomedullary region ($n=3$; 3 sections/mouse; x400). Proximal tubular damage and protein cast formation was assessed and the percentage of kidney damage was graded on a scale of 0 to 4 (refer to Table 3.1).

Table 3.1 The injury scale used to grade kidney damage following IR injury.

Scale	Percentage of kidney damage
0	Normal tubules and no protein casts
0.5	Minor tubular damage and protein cast formation
1.0	Involvement of <10% corticomedullary region
2.0	Involvement of 10% to 25% of corticomedullary region
2.5	Involvement of 26% to 50% of corticomedullary region
3.0	Involvement of 51% to 75% of corticomedullary region
4.0	Widespread damage >75% of corticomedullary region

IR, ischaemia/reperfusion.

To assess proliferation, kidney sections were stained with mouse anti-PCNA (DakoCytomation, Glostrup, Denmark) and rabbit anti-mouse Ki67 (Abcam) primary antibodies followed by an Alexa Fluor 488 donkey anti-mouse (Molecular Probes, Eugene, OR) and Alexa Fluor 555 goat anti-rabbit (Molecular Probes) secondary antibodies. For proximal tubule Kim-1 expression, immunohistochemical staining was performed with rat anti-mouse Kim-1 (R&D Systems) using the avidin-biotin complex (ABC) method as described previously (267). The area of 3,3'-diaminobenzidine (DAB) staining per unit area of tissue was measured using a custom macro from the image analysis software ImageJ/FIJI version 1.48d. Areas of positive staining were quantified in five non-overlapping randomly selected fields of view ($n=3$, 3 sections/mouse; x400 magnification).

For the visualization of type IV collagen, kidney sections were stained with a goat anti-human collagen type IV primary antibody (Southern Biotech, Birmingham, Al) followed by an Alexa Fluor 647 chicken anti-goat antibody (Molecular Probes) and for macrophage staining, a rat anti-mouse F4/80 antibody (AbD Serotec, Oxford, UK) followed by an Alexa Fluor 555 goat anti-rat antibody (Molecular Probes). Sections were counterstained with DAPI (Molecular Probes) and viewed with a Provis AX70 fluorescence microscope (Olympus, Tokyo, Japan). Fluorescence images were captured with the F-view II digital camera (Soft Imaging System, Munster, Germany).

3.2.5 Hydroxyproline, SDS-PAGE and zymography analyses

The kidney from each animal was divided into portions containing both cortex and medulla for use in each assay. The total collagen content (% collagen content/dry weight tissue) in the kidney ($n=3$ /group) was measured using a hydroxyproline assay as previously described (268). In brief, kidneys were lyophilized to measure dry weight, hydrolyzed in 6M hydrochloric acid and hydroxyproline levels determined by measuring the absorbance of hydrolyzed samples at 558nm, using a Digital Spectrophotometer (Varian, Palo Alto, CA)

(269). Total collagen content was determined by multiplying the hydroxyproline measurements by a factor of 6.94.

SDS-PAGE analysis was used to detect changes in interstitial collagen subtypes within the kidney (269). The supernatants from pepsin-digested kidneys were analyzed on 5%(w/v) acrylamide gels with 3.5%(w/v) acrylamide stacking gels. The $\alpha 1$ (III) chains were separated from the $\alpha 1$ (I) collagen chains with interrupted electrophoresis with delayed reduction of type III collagen. The gels were stained with 0.1% Coomassie Blue R-250 overnight at 4°C and then destained with 30%(v/v) methanol containing 7%(v/v) acetic acid. Densitometry was performed with a calibrated imaging densitometer (Gel Scan-710, Bio-Rad, Hercules, CA) and data analyzed using Quantity-One software (Bio-Rad).

Matrix metalloproteinase (MMP)-2 and MMP-9 activity was assessed by gelatin zymography (270). Zymographs consisted of 7.5%(w/v) acrylamide gels containing 1mg/ml gelatin. The gels were stained with 0.1%(w/v) Coomassie Blue R-250 overnight at 37°C and then destained with 7%(v/v) acetic acid. Clear bands indicated gelatinolytic activity, where the enzymes had digested the substrate. Densitometry of these MMP bands was performed and data analyzed using Quantity-One software.

3.2.6 MSC and macrophage co-culture

BM was isolated from male 6-8 week old C57BL/6J mice and cultured in DMEM/F12 (Invitrogen, Camarillo, CA) supplemented with 10% FBS, 10mM L-glutamine, 100 μ g/ml penicillin/streptomycin and 100U/ml mouse recombinant colony stimulating factor (CSF)-1 (Chiron Corporation) in order to generate macrophages. On day 7 the purity of the BM-derived macrophages was >95% when checked by flow cytometry.

For co-culture experiments, macrophages were primed with 120ng/ml of IFN- γ (R&D Systems) and 10ng/ml LPS (Sigma-Aldrich, St. Louis, MO) to induce an ‘M1’ phenotype or with 20ng/ml IL-4 (Invitrogen) to induce an ‘M2’ phenotype. The macrophages were then washed with PBS before MSCs were plated indirectly, on a 0.4 μ m pore size transwell (Corning Life Sciences, Pittson, PA), or directly and cultured for 48hr. Following 24hr of co-culture, 1ml of the co-culture supernatant was collected and screened for human MSC-derived cytokines, using the MILLIPLEX_{MAP} Human Cytokine/Chemokine Panel (Millipore).

3.2.7 Real-time quantification PCR gene expression analysis

Macrophages were FACS sorted from the co-cultures using the conjugated anti-mouse antibodies CD45-FITC (BD Biosciences) and F4/80-APC (BD Biosciences). RNA was extracted using the RNeasy Micro Kit (Qiagen, Hilden, Germany) according to the manufacturer’s guidelines. RNA samples were reverse transcribed using the High Capacity cDNA Reverse Transcription Kit (Applied Biosystems, Foster City, CA) and real-time quantitative PCR (qPCR) for each target gene was performed in duplicate on cDNA samples using the TaqMan Universal PCR Master Mix (Applied Biosystems) and TaqMan Gene Expression Assays (refer to Table 3.2; Applied Biosystems). The threshold cycle (Ct) values were normalized against the endogenous control β -actin to determine the Δ Ct.

Table 3.2 Real-time PCR TaqMAN gene expression assays

Gene symbol	Assay ID
<i>Actb</i>	Mm00607939_s1
<i>Arg1</i>	Mm00475988_m1
<i>Chi3l3</i>	Mm00657889_m1
<i>Fizz1 (Retnla)</i>	Mm00445108_m1
<i>Ccl2</i>	Mm00441242_m1
<i>Mrc1</i>	Mm00485148_m1

Actb, actin beta; *Arg1*, arginase 1; *Chi3l3*, chitinase 3-like 3; *Fizz1*, found in inflammatory zone 1; *Ccl2*, chemokine (C-C motif) ligand 2; *Mrc1*, mannose receptor, C type 1

3.2.8 Statistical analyses

Statistical analyses of the data were performed using GraphPad Prism software version 5.0 (GraphPad Software Inc., San Diego, CA). The unpaired *t*-test was used to analyze data between 2 groups. Comparisons between 3 groups were performed by one-way ANOVA followed by Tukey's multiple comparison tests. All data were expressed as mean \pm SEM. $P < 0.05$ was considered statistically significant.

3.3 Results

3.3.1 MSCs home to the injured kidney following unilateral and bilateral IR injury

eGFP⁺fluc⁺MSCs were FACS sorted to enrich for the number of eGFP⁺fluc⁺MSCs (Figure 3.1A), with the purity of the post-sorted cells also determined by flow cytometry (Figure 3.1A). eGFP expression was confirmed visually using fluorescence microscopy (Figure 3.1B). Using a non-invasive bioluminescent imaging technique, eGFP⁺fluc⁺MSCs were tracked *in vivo* following intravenous (i.v.) administration immediately following surgery in mice with unilateral or bilateral IR injury and in sham-operated control mice (see diagram in Figure 3.1C).

Following sham surgery, MSCs accumulated only in the lungs, likely the result of being trapped in the pulmonary capillaries (Figure 3.2A). Bioluminescence measurements in the sham-operated control mice decreased over the 3 day time-course (2.038×10^7 photons \cdot s⁻¹ \cdot cm⁻² \cdot sr⁻¹ on day 0 to 3.362×10^6 photons \cdot s⁻¹ \cdot cm⁻² \cdot sr⁻¹ on day 1 as per mouse in Figure 3.2A). No signal was detected at day 3. In contrast, following unilateral and bilateral IR injury, MSCs homed to the site of damage via two routes: directly to the kidney(s), as detected at the day 0 imaging time-point (Figure 3.2B and 3.2D respectively), or to the kidney(s) via the lungs (Figure 3.2C and 3.2E respectively). The localization of the MSCs in the kidney was confirmed by imaging the lateral aspect of the mouse (images not shown) before the kidneys were excised and imaged *ex vivo*. Examples of each of the MSC homing patterns with detected fluc signals in sham and IR mice are shown in Figure 3.2. The fluc signal following direct homing to the kidney with unilateral IR injury was marginally decreased from day 0 to day 1, (4.436×10^7 to 3.828×10^7 photons \cdot s⁻¹ \cdot cm⁻² \cdot sr⁻¹) and further by day 3 (1.953×10^7 photons \cdot s⁻¹ \cdot cm⁻² \cdot sr⁻¹; Figure 3B). In contrast to the unilateral model, the fluc signal with bilateral IR injury gradually increased from 5.109×10^7 photons \cdot s⁻¹ \cdot cm⁻² \cdot sr⁻¹ on day 1 to 1.706×10^8 photons \cdot s⁻¹ \cdot cm⁻² \cdot sr⁻¹ on day 3. At 7 days post-IR, the fluc signal was no longer

detected in either the unilateral or bilateral models. In the mice where MSCs were observed to accumulate in the lungs prior to migrating to the damaged kidney(s) following unilateral or bilateral IR injury (Figure 3.2C and 3.2E), the majority of injected cells had localized in the lungs at 1hr post-administration. However, the MSCs further migrated from the lungs to the injured kidney(s) (imaged on day 1 and 3), with the majority of cells being present in the kidney(s) at day 3. Again, at day 7, no cells were detected.

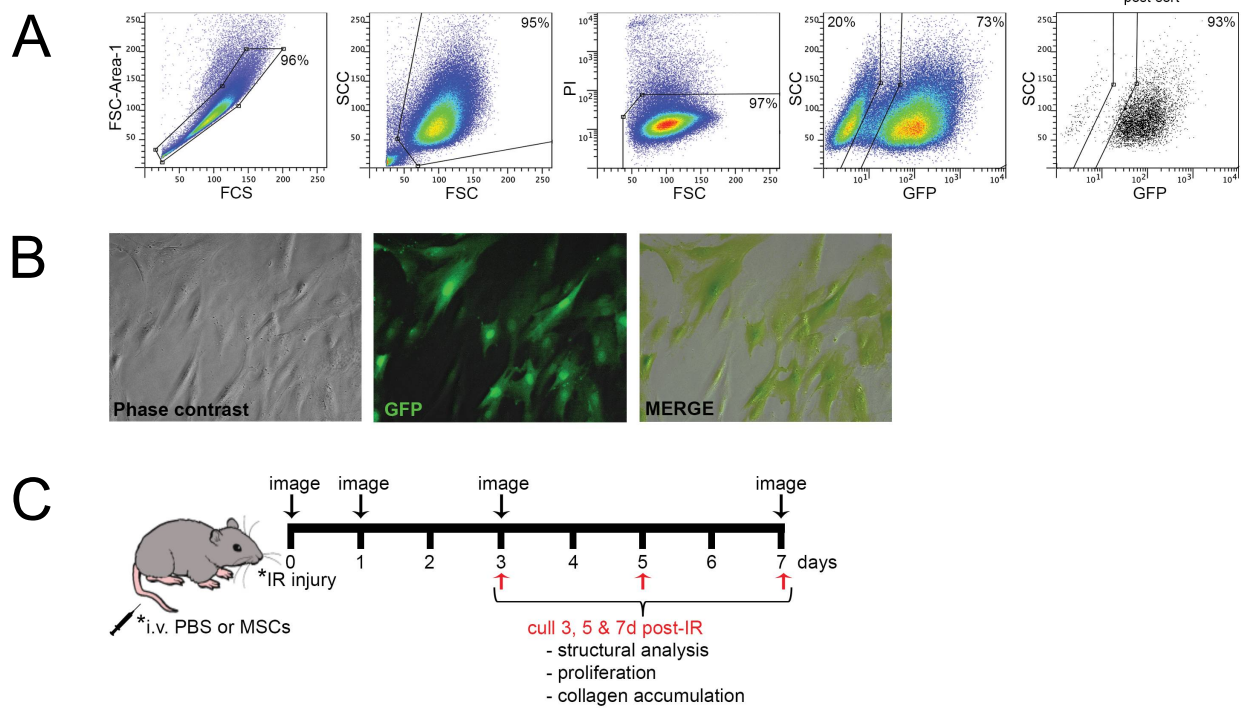


Figure 3.1 Isolation of enhanced green fluorescent protein⁺ firefly luciferase⁺ (eGFP⁺fluc⁺) MSCs and experimental design for *in vivo* bioluminescence tracing

eGFP⁺fluc⁺MSCs were FACS sorted based on their forward and side light-scattering properties, viability using propidium iodide (PI) and eGFP expression (**A**). Representative micrographs are shown of the MSCs demonstrating eGFP expression (magnification x200; **B**) and a schematic diagram of the experimental timeline following the induction of unilateral (40 minutes) or bilateral (25 minutes) ischemia/reperfusion (IR) injury with and without MSC treatment (**C**).

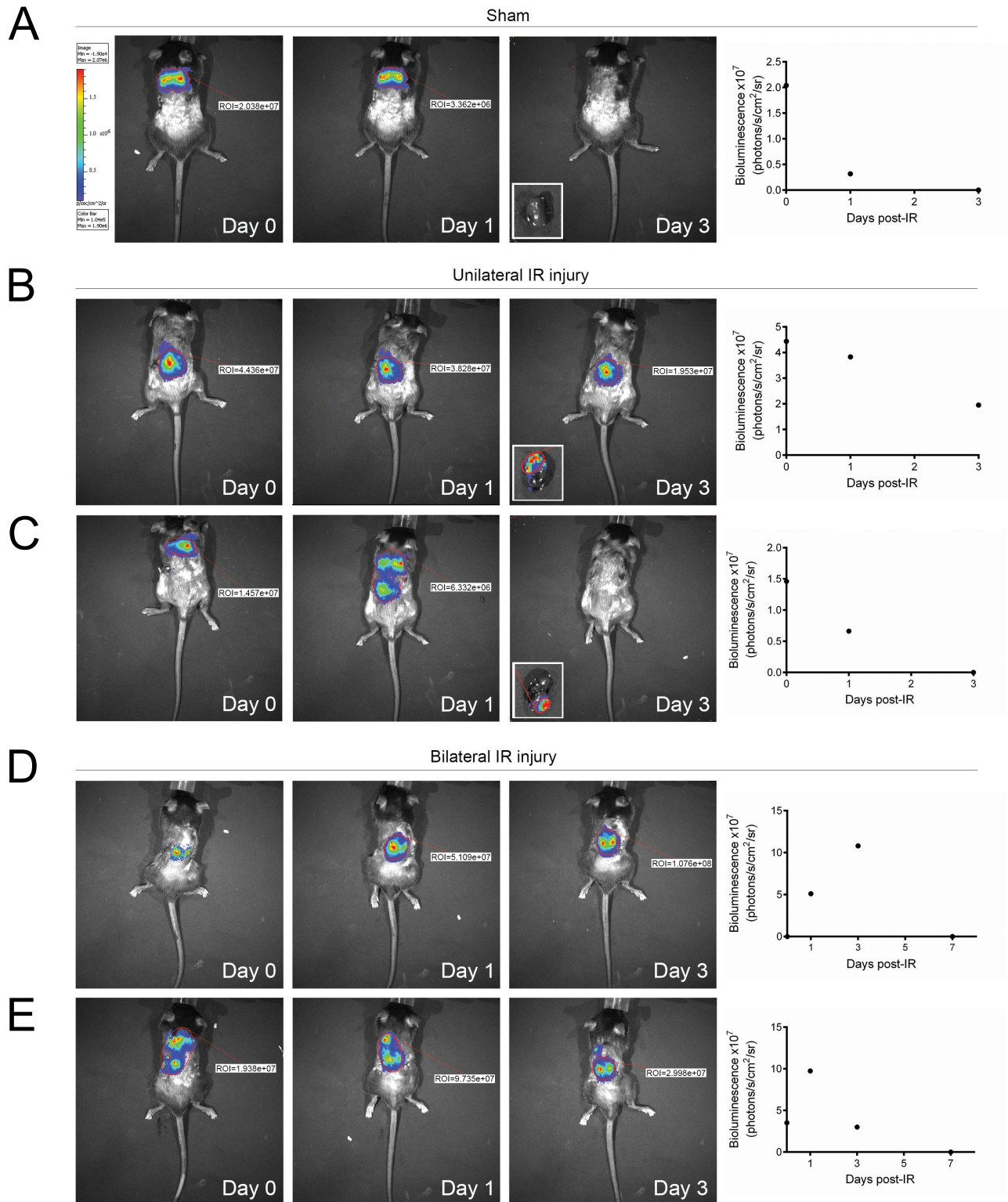


Figure 3.2 MSCs traffic to the injured kidney(s) following unilateral and bilateral IR injury

Representative images of the distribution of MSCs 0, 1 and 3 days post-intravenous injection in sham-operated control mice, showing the accumulation of these cells in the lungs (**A**) and in mice with unilateral or bilateral IR injury, where the cells homed directly to the injured kidney (**B** and **D**, respectively) or to the injured kidney via the lungs (**C** and **E**, respectively). The region of interest (ROI) indicates photon emission within the red-encircled area. Red indicates areas with the highest photon emission density, and blue indicates the areas with the lowest. The *in vivo* ROIs for each animal on days 0, 1 and 3 are displayed in each corresponding graph.

3.3.2 MSCs promote structural and functional regeneration

Compared to sham-operated mice, at 7 days following IR injury there was widespread tubular epithelial cell damage within the kidney, evidenced by numerous protein casts, interstitial matrix expansion and extracellular matrix deposition along with a marked infiltration of inflammatory cells (Figure 3.3A). In contrast, the administration of MSCs to mice with IR injury promoted structural regeneration, including reduced inflammation and re-establishment of the tubular epithelium. Semi-quantitative examination of kidney sections revealed a significant reduction in the number of protein casts ($P < 0.001$) and proximal tubule epithelial cell damage ($P < 0.001$; Figure 3.3B) by 5 days following MSC injection. Structural regeneration of the MSC-treated kidneys was associated with a significant increase in tubular epithelial cell proliferation demonstrated at the 3 day time-point, as assessed with Ki67 and PCNA immunostaining (Figure 3.3C and 3.3D). This MSC-mediated repair was further evidenced by functional recovery. BUN and serum creatinine concentrations were measured 3 days post-MSC administration (Figure 3.4A and 3.4B). At 3 days after bilateral IR surgery BUN levels had increased over two-fold compared to sham-operated controls (18.1 ± 1.9 versus 8.4 ± 0.4 mmol/L; $P < 0.001$) and serum creatinine 1.5-fold higher than sham levels (34.7 ± 3.1 versus 22.4 ± 2.1 μ mol/L; $P < 0.05$). In MSC-treated mice, both the BUN and serum creatinine concentrations were comparable to baseline measurements and were significantly lower than the vehicle-treated controls (Figure 3.4A and 3.4B). In addition, immunohistochemical staining revealed increased expression of Kim-1, a marker of proximal tubular injury, on the apical membrane of proximal tubule cells 3 days after IR injury, compared with sham-operated kidneys (Figure 3.4C), while Kim-1 expression was markedly reduced in MSC-treated mice. Notably, urinary Kim-1, assessed by an ELISA, was significantly increased at 7 days post-IR compared to sham-operated control mice ($P < 0.001$) but returned to baseline levels in MSC-treated mice ($P < 0.01$; Figure 5D).

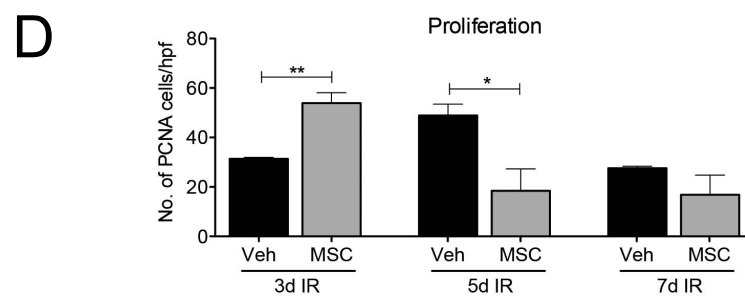
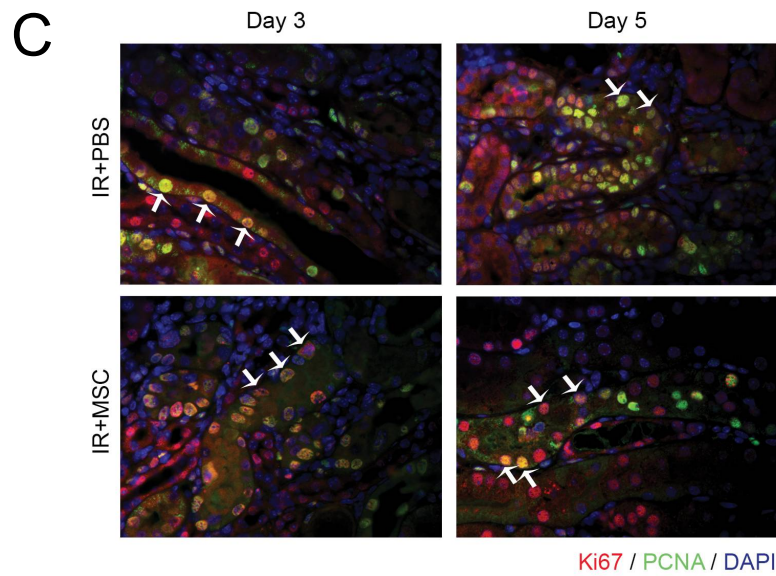
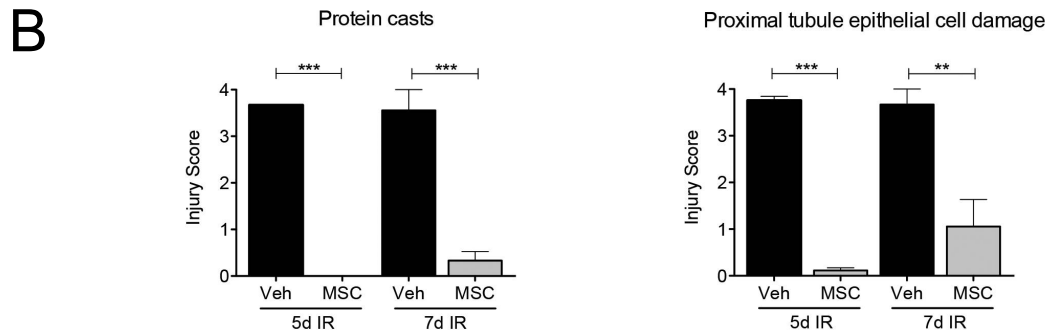
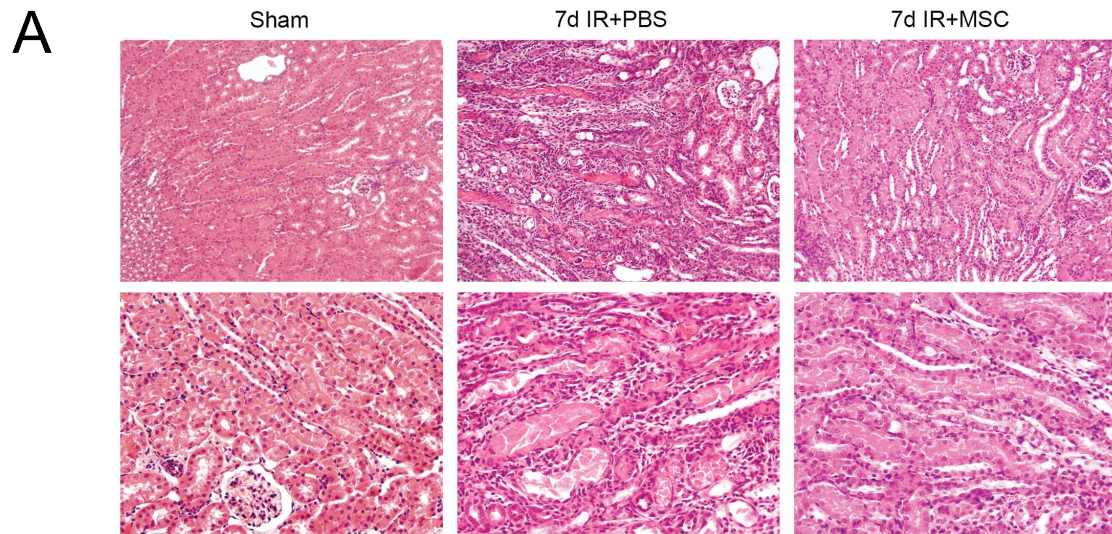


Figure 3.3 MSC treatment following IR injury accelerates structural repair in adult mice

Representative micrographs of hematoxylin and eosin (H&E)-stained sections show the histoarchitecture of the corticomedullary region from sham and unilateral IR kidneys with and without MSC treatment, 7 days post-injury (magnification x200 and x400; **A**). Semi-quantitative analysis of kidney injury from IR kidneys with and without MSC treatment 5 and 7 days post-IR is displayed graphically (**B**). Tubular epithelial cell proliferation was demonstrated with Ki67 (red) and PCNA (green) immunofluorescence labeling in kidneys with and without MSC treatment (**C**). PCNA expression was quantified at 3, 5 and 7 days following IR injury (magnification x400; **D**). Veh, vehicle; cells/hpf, cells per high-power field. Data are means \pm SEM; $n=3$. * $P<0.05$, ** $P<0.01$, *** $P<0.001$.

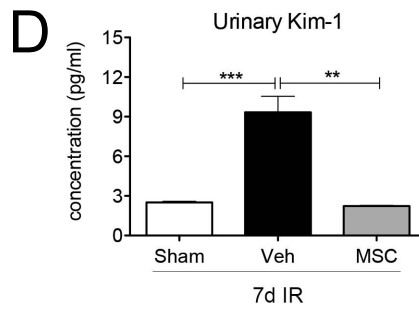
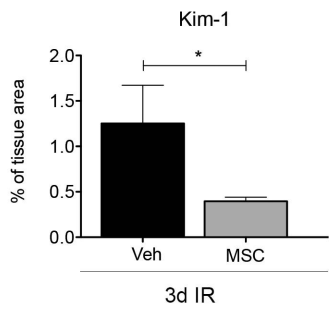
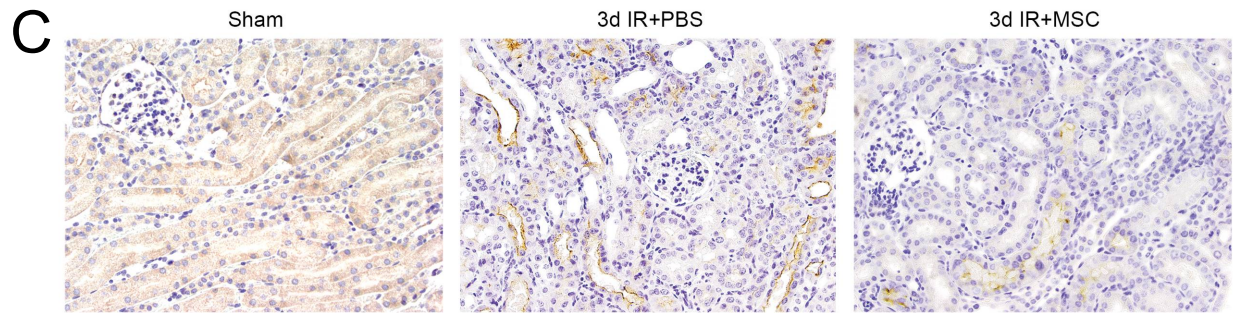
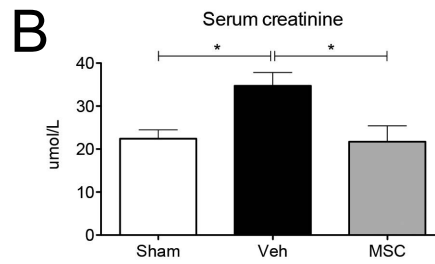
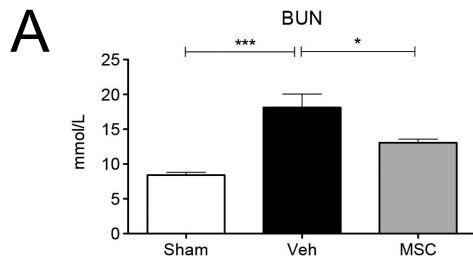


Figure 3.4 MSCs improve kidney function and reduce the expression and excretion of Kim-1 in the kidney following IR injury

Functional analysis is shown measuring blood urea nitrogen (BUN; **A**) and serum creatinine (**B**) in sham and bilateral IR mice with and without MSC treatment 3 days post-injury. Representative micrographs and semi-quantification of Kim-1 expression in sham and IR kidneys 3 days following MSC treatment are shown (magnification x400; **C**). Urinary Kim-1 levels from days 6-7 was significantly increased in mice with IR but returned to baseline levels following MSC treatment (**D**). Veh, vehicle. Data are means \pm SEM. ** $P < 0.01$, *** $P < 0.001$.

3.3.3 MSCs reduce collagen accumulation in the injured kidney

MSC therapy following IR injury reduced interstitial collagen accumulation as assessed by hydroxyproline assay, SDS-PAGE and type IV collagen immunofluorescence labeling. IR injury resulted in a gradual but significant increase in the total collagen concentration at 3 ($P<0.05$), 5 ($P<0.001$) and 7 ($P<0.001$) days post-injury compared to sham-operated controls (Figure 3.5A). At 5 days post-IR injury, MSC treatment significantly decreased the total renal collagen concentration ($P<0.05$), compared to vehicle-treated mice. SDS-PAGE revealed the predominant interstitial collagen subtypes within the kidney were type I collagen [$\alpha 1(I)$ and $\alpha 2(I)$ monomers and dimers of two $\alpha 1(I)$ chains ($\beta 11$) or $\alpha 1(I)$ and $\alpha 2(I)$ monomers ($\beta 12$)], and a small amount of type V collagen (Figure 6B). Scanning densitometry further revealed a decrease in the accumulation of the collagen subtype $\alpha 1(I)$ in MSC-treated kidneys compared to the vehicle-treated controls at 5 and 7 days post-injury (Figure 3.5B), which reached significance ($P<0.05$) at day 7. Immunofluorescence microscopy was utilized to visualize type IV collagen and macrophage (F4/80) localization within the kidney (Figure 3.5D). At day 7, an accumulation of interstitial collagen was evident in vehicle-treated kidneys. In comparison, type IV collagen appeared as a delicate framework surrounding the glomeruli and re-epithelialized tubules of MSC-treated kidneys, with a pattern of expression comparable to kidneys from sham-operated control mice.

Gelatin zymography revealed that IR injury resulted in a significant increase in latent and active MMP-2 levels compared to sham-operated control kidneys at both 5 ($P<0.001$) and 7 ($P<0.001$) days post-injury (Figure 3.5C). In comparison, the latent and active forms of MMP-2 in the MSC-treated kidneys remained significantly lower than the vehicle-treated kidneys at both days 5 and 7. Active MMP-9 was also significantly increased in vehicle-treated kidneys at 3 ($P<0.001$), 5 ($P<0.01$) and 7 ($P<0.05$) days post-injury compared to the sham-operated kidneys (Figure 3.5C). Notably, MSC treatment resulted in a significant increase in active MMP-9 at 3 days post-injury ($P<0.05$) compared to its vehicle-treated counterpart.

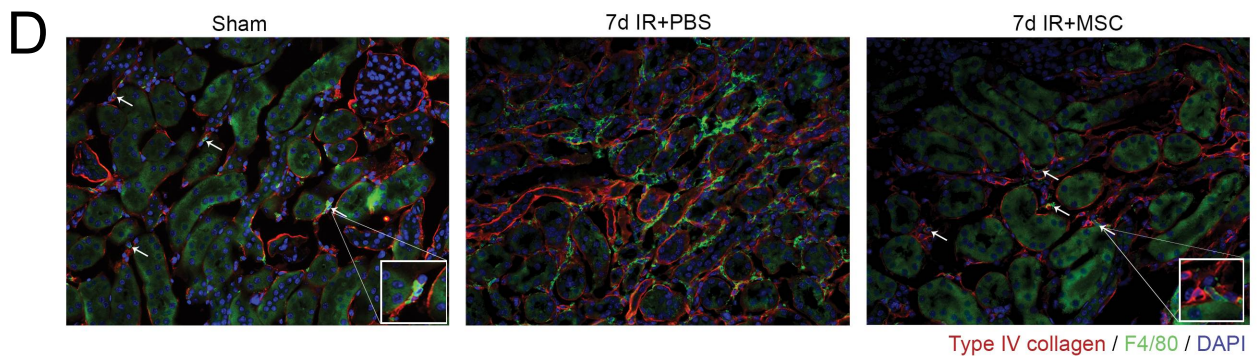
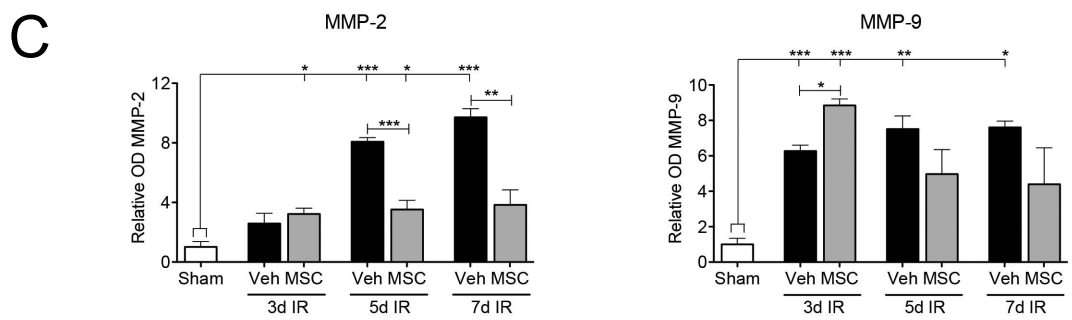
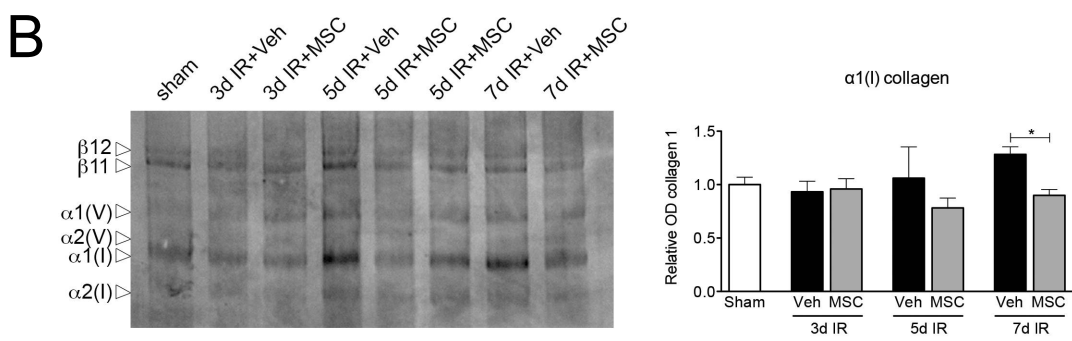
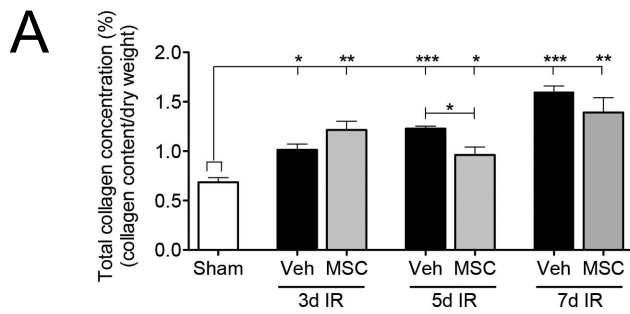


Figure 3.5 MSCs reduce collagen accumulation in the kidney following IR injury

Total kidney collagen concentration (% collagen content/dry weight tissue) in sham and IR kidneys with and without MSC treatment (**A**). SDS-PAGE analysis and densitometry of sham and IR kidneys 3, 5 and 7 days after vehicle or MSC treatment (**B**). Densitometry of MMP-2 and MMP-9 in sham and IR kidneys 3, 5 and 7 days following IR injury with vehicle or MSC treatment (**C**). Representative fluorescence micrographs showing type IV collagen (red) and F4/80 (green) staining in sham and IR kidneys 7 days after vehicle or MSC treatment (magnification x200; **D**). Veh, vehicle; OD, optical density. Data are means \pm SEM. ($n=3$). * $P<0.05$, ** $P<0.01$, *** $P<0.001$.

3.3.4 MSCs alter macrophage phenotype following *in vitro* co-culture

Direct and indirect co-culture of MSCs with macrophages resulted in an MSC-dependent polarization of macrophages towards an 'M2' phenotype. BM-derived murine macrophages that had been stimulated to display an M1 or M2 phenotype *in vitro* were co-cultured with MSCs for 48hr either directly or indirectly using a transwell co-culture system (see diagram in Figure 3.6A). qPCR analysis of macrophage gene expression showed that the direct co-culture of M1 macrophages with MSCs caused an upregulation of the M2-associated gene, *Arg1* (Figure 3.6B). Another M2-associated gene, *Ccl2*, was also upregulated following the indirect co-culture of M1 macrophages with MSCs (Figure 3.6B). Furthermore, an enhanced expression of the M2-associated genes, *Arg1*, *Chi3l3*, *Ccl2* and *Fizz1* (also known as *Retnla*), was observed following both the direct and indirect co-culture of M2 macrophages with MSCs (Figure 3.6B).

The MSC-macrophage co-culture medium was then screened using a panel of human cytokines and chemokines (Table 3.3). The human soluble factors EGF, granulocyte macrophage colony-stimulating factor (GM-CSF), CXCL1, IL-6, IL-8, monocyte chemotactic protein (MCP)-1, PDGF-AA and CCL5 were detected in the co-culture supernatants, suggesting these factors may play a role in the MSC-mediated shift in macrophage polarization.

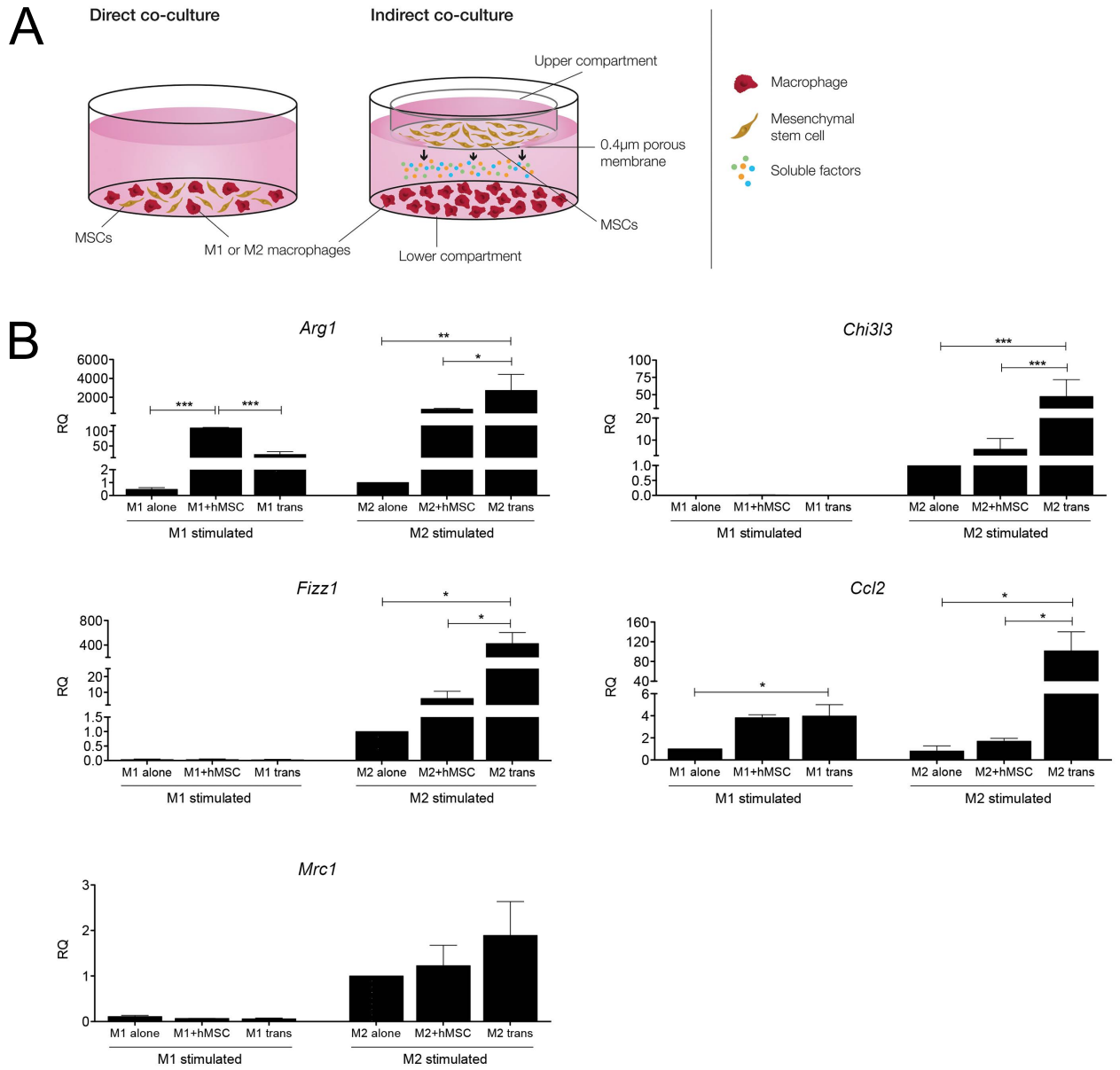


Figure 3.6 MSCs can alter macrophage phenotype following *in vitro* co-culture

A schematic diagram of the co-culture system used to culture macrophages and MSCs (**A**). qPCR analysis of anti-inflammatory 'M2' gene expression in mouse bone marrow-derived M1- and M2-stimulated macrophages co-cultured for 48hr either directly (M1 or M2+MSC) or indirectly (M1 or M2 trans) with MSCs (**B**). RQ, relative quantification; trans, transwell. Data are means \pm SEM. ($n=3$). * $P<0.05$, ** $P<0.01$, *** $P<0.001$.

Table 3.3 Human cytokines secreted following 24 hours of MSC and mouse bone marrow-derived macrophage co-culture *in vitro*

Cytokine (pg/mL)	Co-culture conditions					
	M1+MSC direct	M1+MSC transwell	significance	M2+MSC direct	M2+MSC transwell	significance
EGF	8.3 ± 5.0	16.6 ± 3.2	NS	2.57 ± 2.6	0	NS
eotaxin	0	0	NS	0	0	NS
FGF2	0	0	NS	0	0	NS
Flt-3L	0	0	NS	0	0	NS
Fractalkine	0	0	NS	0	0	NS
G-CSF	0	0	NS	0	0	NS
GM-CSF	3.5 ± 0.2	0	***	0	0	NS
GRO (CXCL1)	67.8 ± 3.6	0	***	30.8 ± 5.1	0	***
IFNα2	0	0	NS	0	0	NS
IFN-γ	0	0	NS	0	0	NS
IL-1α	0	0	NS	0	0	NS
IL-1β	0	0	NS	0	0	NS
IL-1RA	0	0	NS	0	0	NS
IL-2	0	0	NS	0	0	NS
IL-3	0	0	NS	0	0	NS
IL-4	0	0	NS	0	0	NS
IL-5	0	0	NS	0	0	NS
IL-6	732.6 ± 22.6	193.9 ± 10.7	***	423.2 ± 38.3	88.7 ± 3.7	***
IL-7	0	0	NS	0	0	NS
IL-8	133.5 ± 7.7	23.2 ± 4.0	***	68.3 ± 11.9	6.8 ± 0.4	**
IL-9	0	0	NS	0	0	NS
IL-10	0	0	NS	0	0	NS
IL12p40	0	0	NS	0	0	NS
IL12p70	0	0	NS	0	0	NS
IL-13	0	0	NS	0	0	NS
IL-15	0	0	NS	0	0	NS
IL-17A	0	0	NS	0	0	NS
IP10 (CXCL10)	0	0	NS	0	0	NS
MCP-1 (CCL2)	433.1 ± 16.1	103.9 ± 8.7	***	86.1 ± 11.8	51.3 ± 2.7	***
MCP-3 (CCL7)	0	0	NS	0	0	NS
MDC (CCL22)	0	0	NS	0	0	NS
MIP-1α (CCL3)	0	0	NS	0	0	NS
MIP-1β (CCL4)	0	0	NS	0	0	NS
PDGF-AA	38.1 ± 2.5	13.5 ± 1.0	***	35.2 ± 1.0	15.5 ± 0.2	***
PDGF-BB	0	0	NS	0	0	NS
RANTES (CCL5)	0	16.2 ± 1.0	***	0	3.58 ± 0.9	**
sCD40La	0	0	NS	0	0	NS
sIL2Ra	0	0	NS	0	0	NS
TGFα	0	0	NS	0	0	NS
TNFα	0	0	NS	0	0	NS
TNFβ	0	0	NS	0	0	NS

Abbreviations: EGF, epidermal growth factor; FGF2, basic fibroblast growth factor; G-CSF, granulocyte colony-stimulating factor; GM-CSF, granulocyte macrophage colony-stimulating factor; IFNα2, interferon-alpha; IFN-γ; interferon-gamma; IL, interleukin; IL-1RA, interleukin-1 receptor antagonist; IP-10, interferon gamma-induced protein; MCP-1, monocyte chemotactic protein; MDC, macrophage derived chemokine; MIP, monocyte inflammatory protein; PDGF, platelet-derived growth factor; RANTES, regulated and normal T cell expressed and secreted; sCD40L, soluble CD40 ligand; sIL2Ra, soluble IL-2 receptor alpha; TGF, transforming growth factor; TNF, tumor necrosis factor; MSC, mesenchymal stem cell; NS, not significant. Data are means ± SEM. (*n*=3). ***P*<0.01, *** *P*<0.001.

3.4 Discussion

The therapeutic efficacy of MSCs derived from various sources including BM (186), adipose (271), umbilical cord (182), embryos (181) and Wharton's jelly (272) to treat cisplatin- (172, 174, 186), glycerol- (142, 173), unilateral ureteral obstruction (UUO)- (273-276) and IR- (177-179, 185) induced experimental models of AKI have been investigated [for review see (277)]. However, the mechanisms by which MSCs elicit repair remain largely unknown. Following injury, MSCs have the capacity to migrate along an inflammatory cytokine gradient, governed largely by chemokines and their receptors, to the site of damage (173, 201, 278, 279). The present study demonstrated that MSCs administered to sham-operated mice migrated directly to the lungs, where they remained and were cleared within 3 days. In comparison, MSCs administered to mice following IR had the potential to home directly to the injured kidney(s) where they remained for up to 3 days post-administration and exerted beneficial effects over the longer-term. These findings are consistent with previously published work (280). While some MSCs still traveled to the lung, these cells retained the ability to migrate to the injured kidney(s) within the first 3 days following IR injury. The localization of the MSCs in the lungs of mice has been confirmed in previous studies in other experimental models (281, 282). Cell size is believed to contribute to the initial entrapment of the MSCs within the pulmonary capillaries, due to the small diameter of the vessels. In addition, adhesion molecules expressed by MSCs and the corresponding receptors expressed on the lung endothelia may also contribute to the MSC-lung entrapment and dislodgement (281). Although tissue-specific homing has been demonstrated in a number of different conditions, long-term engraftment of the MSCs has rarely been shown. Consequently, several studies have investigated strategies aimed at enhancing the MSC migratory properties, survival and consequently regenerative capacity through pre-conditioning with various growth factors such as IGF-1 (283), glial cell-derived neurotrophic factor (GDNF) (284), melatonin (285), exposure to hypoxia (286), or genetic modification (175, 181, 184, 287, 288).

The current study utilized the xenogeneic transplantation of MSCs into immunocompetent mice without the use of immunosuppressant agents. Although there is extensive data demonstrating the immunomodulatory properties of MSCs *in vitro*, it is unclear why these cells remain tolerated by the host's immune system following xenogeneic transplantation (227). In the current study, the possibility that the host's immune system cleared the transplanted MSCs by the day 7 time-point cannot be discounted. Nevertheless, numerous studies have demonstrated extraordinary regenerative efficacy following successful transplantation of human MSCs into mice in several disease models (228). However, the type of MSC transplantation (allogeneic vs. autologous), tissue of origin (BM, adipose, umbilical cord), isolation method (enzymatic vs. mechanical), delivery route (systemic vs. local), dose and timing of administration are also key factors that may influence the renoprotective effect of MSC therapy and need to be carefully considered prior to clinical application. For example, in an experimental model of glomerulonephritis, the administration of MSCs improved renal function but resulted in long-term maldifferentiation into glomerular adipocytes (289). These findings raise considerable concerns surrounding the safety of MSC-based therapies and so it is imperative that studies looking into their long-term safety and unwanted differentiation are performed.

In this study we demonstrate that following migration to the kidney in response to IR injury, MSCs promoted tubular epithelial cell proliferation, resulting in structural repair and tissue remodeling concurrent with a reduction in collagen. MMPs are enzymes that are involved in extracellular matrix remodeling via collagen degradation (290). The identification of an MSC-induced increase in MMP-9 at day 3 and decrease in MMP-2 at days 5 and 7 provides insight into the temporal pattern of MSC-mediated tissue remodeling. In addition to structural improvement, proximal tubular Kim-1 expression and urinary Kim-1 levels were assessed, as a direct measure of kidney injury. Both demonstrated significant improvements in the severity of injury at 3 and 7 days post-MSCTreatment. Kim-1 is a sensitive AKI

biomarker useful for detecting early disease onset and can provide useful insight into the state of injury prior to the production of classical indicators of nephrotoxicity, such as serum creatinine levels (291, 292).

MSCs have unique immunomodulatory properties and their trophic effects on T, B, natural killer and dendritic cells have been thoroughly investigated (255, 256). However, the effect of MSCs on macrophage polarization and the consequences of this cell-cell interaction in altering the pro-inflammatory course of injury remains largely unknown. Our findings are consistent with other studies that have demonstrated the ability of MSCs to polarize macrophages towards an M2 phenotype *in vitro* (207, 208, 216, 219, 293). However, the influence MSCs have on the phenotypic and functional characteristics of macrophages is often variable. For example, MSCs have been shown to both up-regulate and inhibit the expression of IL-6. Similarly, macrophage phagocytic activity has been both enhanced and suppressed by MSCs (207, 208, 216, 219).

Li et al. (219) demonstrated that MSC repair requires the infiltration of macrophages after the induction of IR injury. Given this important observation, we show herein that MSCs significantly enhanced the expression of M2 associated macrophage genes in both M1 and M2 macrophage subsets *in vitro*. Furthermore, MSC-induced M2 polarization was evident in both direct and indirect co-culture systems, indicating that the alteration of macrophage phenotype was mediated through paracrine mechanisms. Screening of the co-culture supernatants detected the presence of MSC-derived EGF, GM-CSF, CXCL1, IL-6, IL-8, MCP-1/CCL2, PDGF-AA and RANTES/CCL5, all of which, except for EGF, GM-CSF, CXCL1 and PDGF-AA, have previously been shown to promote M2 polarization (216, 294-297). Interestingly, CXCL1 was only detected in the direct co-culture system, indicating that its production required direct cell-to-cell contact. Conversely, RANTES/CCL5 was only detected in the transwell co-culture system, signifying that the direct cell-to-cell contact inhibited the

release of this chemokine. Although the enhancement of an M2 phenotype was facilitated through paracrine mechanisms, with the exception of EGF and RANTES/CCL5, direct co-culture did result in increased levels of MSC secreted soluble factors.

In summary, whole body bioluminescence imaging to trace MSCs delivered to mice with unilateral or bilateral IR injury demonstrated a unique pattern of infiltration where MSCs either homed directly to the injured kidney(s) or mobilized from the lungs to the injured kidney(s). MSC therapy was renoprotective and promoted kidney repair as indicated by decreased proximal tubule Kim-1 expression and urinary Kim-1 levels. In addition, MSC therapy stimulated somatic tubular epithelial cell proliferation and significantly reduced aberrant collagen accumulation resulting in improved kidney function. This highlights the therapeutic potential of MSCs in ameliorating the progression of kidney disease, of which established fibrosis is a common characteristic. MSCs are thought to elicit repair through paracrine and/or endocrine mechanisms that modulate the immune response, leading to tissue repair and cellular replacement. Our results provide important insights into the production of various cytokines, chemokines and enzymes resulting from macrophage-MSC interactions and how these govern the inflammatory and remodeling phases of AKI. However, determining the optimal delivery methods for engraftment, testing long-term safety and understanding their ability to modify the tissue microenvironment in a setting of progressive fibrosis require further consideration.

CHAPTER 4

Human mesenchymal stem cells alter the phenotype and gene profile of monocytes from type 2 diabetic patients with end-stage renal disease

Declaration for Thesis Chapter 4

Declaration by candidate

This chapter has been submitted to Clinical Science:

Wise AF, Williams TM, Rudd S, Wells CA, Kerr PG, Ricardo SD (2014). “Human mesenchymal stem cells alter the phenotype and gene profile of monocytes from type 2 diabetic patients with end-stage renal disease”.

In the case of Chapter 4, the nature and extent of my contribution to the work was the following:

Nature of contribution	Extent of contribution (%)
Study design, execution of experiments, data analysis, interpretation of results, preparation of manuscript	85%

The following co-authors are students at Monash University and the extent of their contribution in percentage terms have been stated below.

Name	Nature of contribution	Extent of contribution (%) for student co-authors only
Timothy Williams	Technical assistance and intellectual input	3%

The undersigned hereby certify that the above declaration correctly reflects the nature and extent of the candidate’s and co-authors’ contributions to this work.

Candidate’s Signature		Date: 06.10.14
Main Supervisor’s Signature		Date: 06.10.14

Chapter 4: Human mesenchymal stem cells alter the phenotype and gene profile of monocytes from type 2 diabetic patients with end-stage renal disease

4.1 Introduction

T2D is a metabolic disorder perpetuated by a peripheral resistance to insulin that leads to an increased production of insulin by pancreatic β -cells, which forces the uptake of glucose in peripheral tissues (298). This consequently results in β -cell exhaustion and subsequently a decline in β -cell function, insufficient insulin secretion and a deficient uptake of blood glucose (299). T2D accounts for approximately 90% of diabetic cases worldwide and is recognised by the International Diabetes Federation and World Health Organization (WHO) as a global epidemic (11). Despite this, its incidence is continuing to rise due to an ageing population, increasing obesity, physical inactivity and unhealthy diet (300).

Diabetic nephropathy (DN) is a progressive kidney disease that results from enduring diabetes, characterised by the accumulation of extracellular matrix and eventual glomerular and interstitial fibrosis leading to declining renal function (301). DN is the leading cause of ESRD worldwide, which requires life-saving dialysis or kidney transplantation (302). Chronic inflammation is a key factor promoting the development and progression of DN (300, 303). More specifically, monocytes and monocyte-derived macrophages are the main inflammatory cells that infiltrate the diabetic kidney, and the number of monocyte-derived macrophages correlates with declining renal function in both humans and mice (251, 304). Recent studies have also demonstrated that T2D in humans is characterised by an increased number of circulating $CD14^+CD16^+$ monocytes that display a pro-inflammatory profile (87, 88, 305).

Monocytes show considerable heterogeneity in both phenotype and function; for review see (306). The classification of human peripheral blood monocytes is centred on the expression of the LPS co-receptor, CD14 and the FcγRIII, CD16 (96). Three major subsets exist: CD14^{high/++}CD16⁻ (classical), CD14^{high/++}CD16⁺ (intermediate) and CD14^{dim/+}CD16^{high/++} (non-classical; 96). Classical CD14^{high/++}CD16⁻ monocytes traffic to the site of inflammation via a CCR2-dependant mechanism during the early stages of inflammation where they exhibit functions related to a typical inflammatory response, such as phagocytosis and ROS production (306, 307). In contrast, non-classical CD14^{dim/+}CD16^{high/++} monocytes predominantly patrol blood vessel walls and are believed to contribute to resident macrophage populations (92). These cells also accumulate in a variety of inflammatory diseases where they are recruited at a later stage of the inflammatory response via a CX3CR1-dependant pathway (101, 306). The third subset, CD14^{high/++}CD16⁺, is believed to be an intermediate phenotype between the classical and non-classical subsets (96). Importantly, although functionally and phenotypically distinct monocyte subsets exist, these subsets may denote the same cell at different stages of maturation. Supporting evidence confirms that classical CD14^{high/++}CD16⁻ monocytes are the most immature phenotype but are capable of developing into the intermediate CD14^{high/++}CD16⁺ subset, which in turn mature into the CD14^{dim/+}CD16^{high/++} non-classical subset, characterised by the downregulation of CD14 and CCR2 expression and the upregulation of CD16 and CX3CR1 (308).

Current therapeutic approaches have been able to reduce proteinuria in patients with diabetic nephropathy, but have shown limited success in attenuating disease progression. MSCs have been used in several clinical trials including kidney transplantation, renal allograft rejection and T2D, demonstrating promising results with no adverse side effects (309-312). Pre-clinical studies show that administered MSCs home to sites of injury where they ameliorate renal injury and accelerate repair through paracrine and/or endocrine mechanisms; for review see (277). It has been well documented that MSCs have remarkable

immunomodulatory abilities, capable of altering dendritic cell phenotype and function, and macrophage phenotype and function (207, 208, 313-315).

Despite the interest in MSC-based approaches for the treatment of human kidney injury, there is limited information on the effects MSCs have on circulating human monocytes, the progenitors of dendritic cells and macrophages, particularly under chronic inflammatory conditions. This study therefore investigated the effects of human bone marrow-derived MSCs on human monocytes isolated from healthy (control) subjects and type 2 diabetic patients with ESRD. To achieve this, microarray analysis and flow cytometry were used to assess the genetic and phenotypic profile of isolated diabetic and non-diabetic monocytes co-cultured with and without MSCs. This data demonstrates that MSCs can influence the phenotype of monocytes, even when isolated from a setting of chronic T2D and ESRD, and lends support for the development of MSC-based therapies as a treatment strategy to reduce inflammation and promote kidney remodelling in DN patients.

4.2 Subjects and Methods

4.2.1 Study population

Blood was obtained from five type 2 diabetic patients with ESRD receiving haemodialysis at the Monash Medical Centre. Control blood was obtained from four donors from the Australian Red Cross Blood Service. Donor details are summarised in Table 4.1. Informed consent was obtained from all participants and the studies were approved by the Monash Health Human Research Ethics Committee (Monash 10179B) and Monash University Human Research Ethics Committee (CF07/3495 – 2007001798), which conform to the *National Statement on Ethical Conduct in Human Research*.

4.2.2 Monocyte purification

20ml of type 2 diabetic patient blood was collected in VACUETTE Premium K2E K2EDTA tubes (Greiner bio-one, Kremsmünster, Austria) and diluted with PBS. Diluted blood was layered onto Ficoll-Paque PLUS (GE Healthcare Life Sciences, Uppsala, Sweden) and centrifuged at 400g for 30 minutes at room temperature (Figure 4.1A). Peripheral blood mononuclear cells (PBMCs) were harvested and transferred into a 50ml Falcon tube and cells were washed twice by the addition of PBS followed by centrifugation at room temperature for 10 minutes at 100g. PBMCs were re-suspended in 40 μ l of magnetic activated cell sorting (MACS) buffer (PBS supplemented with 0.5% FBS and 2mM EDTA) and 10 μ l of human anti-CD14 conjugated microbeads (Miltenyi Biotec, Auburn, CA) per 10⁷ total cell count. Cells were incubated for 15 minutes at 4°C with continuous mixing. Following incubation, cells were washed with MACS buffer and centrifuged at 300g for 10 minutes at 4°C. The supernatant was aspirated and the cells were re-suspended in MACS buffer prior to sorting the cells on a QuadroMACS (Miltenyi Biotec) separator (Figure 4.1B). The purity of the CD14⁺ sorted cells was >90% when confirmed by flow cytometry (Figure 4.1B).

Table 4.1 Baseline characteristics of control and type 2 diabetic subjects

	Gender	Age	Creatinine	WBC (x10 ⁹ /litre)	Monocytes (x10 ⁹ /litre)	CRP	Duration (years)	Disease
Control	Female	25	-	-	-	-	-	-
	Male	29	-	-	-	-	-	-
	Female	25	-	-	-	-	-	-
	Male	29	-	-	-	-	-	-
T2D	Male	63	680	7.3	0.63	25	30	<ul style="list-style-type: none"> • Type 2 diabetes • Dialysis dependent
	Female	74	>1000	5.6	0.71	12	Unknown	<ul style="list-style-type: none"> • End-stage type 2 diabetes • Dialysis dependent
	Male	65	400-500	6.4	0.49	17	20	<ul style="list-style-type: none"> • End-stage type 2 diabetes • Dialysis dependent
	Male	64	>1000	7.1	0.60	23	21	<ul style="list-style-type: none"> • Type 2 diabetes • Dialysis dependent
	Male	85	793	11.3	0.70	14	6	<ul style="list-style-type: none"> • Type 2 diabetes • Dialysis dependent

T2D, type 2 diabetes; WBC, white blood cells; CRP, C-reactive protein.

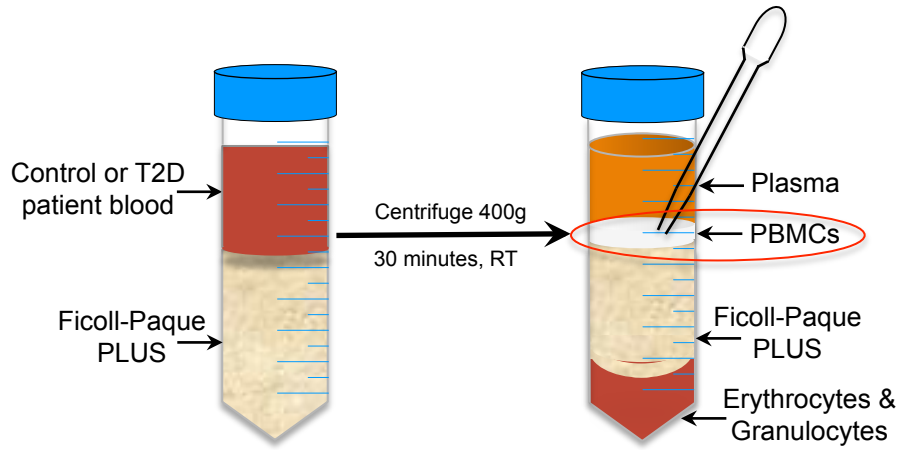
4.2.3 Flow cytometry

Immunophenotypic analysis of monocytes on day 0 and day 2 by flow cytometry was performed using the following fluorochrome-conjugated anti-human antibodies: CD45-FITC, CD14-APC, CD16-eFluor450 and HLA-DR-PE. All antibodies were purchased from eBioscience Inc (San Diego, CA). Cell population data was acquired using a FACSCanto II flow cytometer (BD Biosciences, San Jose, CA) with the FACS Diva acquisition software (BD Biosciences) and analysed using FlowLogic FCS analysis software (Inivai Technologies, Melbourne, Australia).

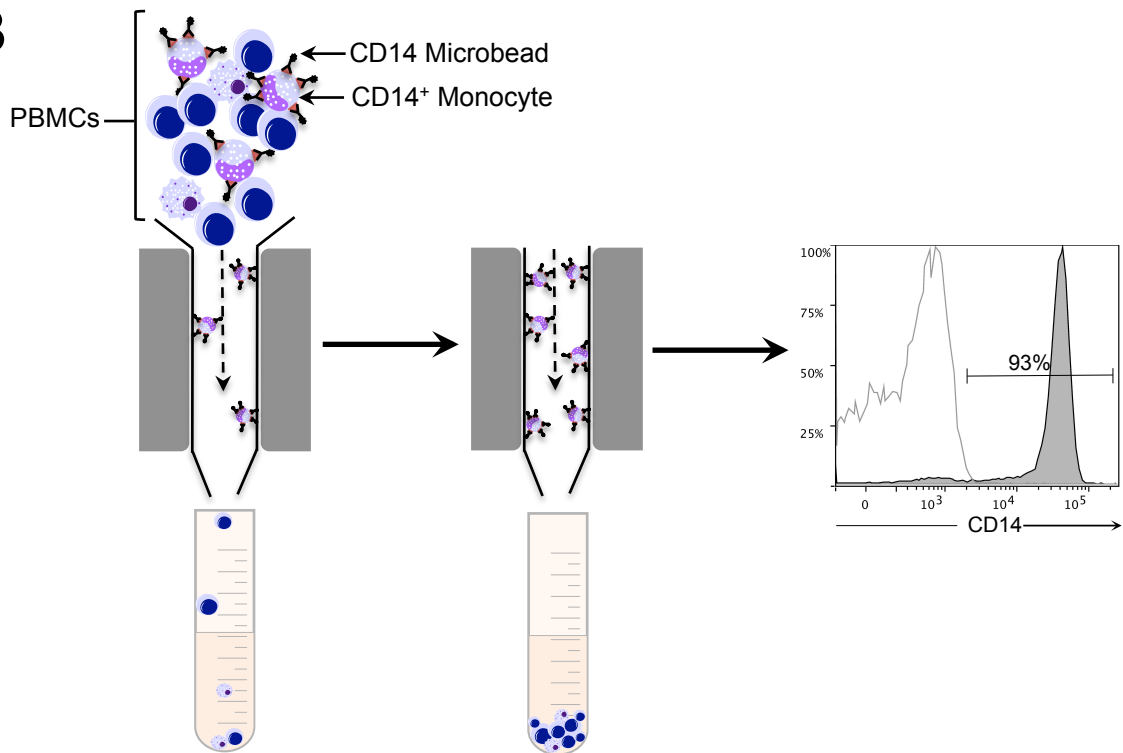
4.2.4 Monocyte and MSC co-culture

Human bone marrow-derived MSCs purchased from the Tulane Centre for Stem Cell Research and Regenerative Medicine (Tulane University, New Orleans, LA) were cultured as previously described in Chapter 2. For co-culture experiments, 3×10^5 CD14⁺ monocytes were plated in 6-well plates and MSCs plated indirectly on a 0.4 μ m pore size Transwell (Figure 4.1C; Millipore Corporation, Billerica, MA). Cells were co-cultured for 48 hours in Roswell Park Memorial Institute (RPMI) 1640 medium supplemented with 10% FBS (Sigma-Aldrich, St. Louis, MO), 1% L-glutamine and 1% penicillin-streptomycin (Gibco, Grand Island, NY; Figure 4.1C). Monocytes were visualised on an Olympus IX81 microscope and images captured with an Olympus IX2-UCB camera.

A



B



C

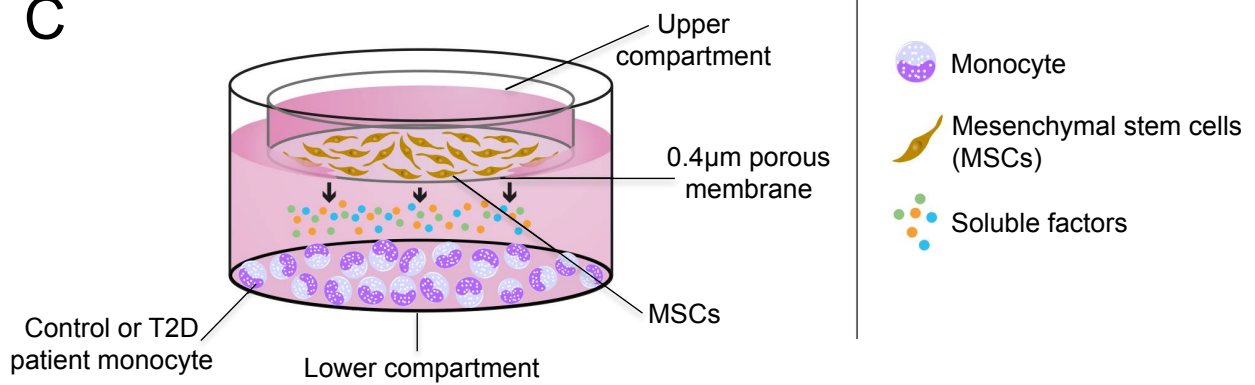


Figure 4.1 Schematic of the isolation and *in vitro* culture of human monocytes

The isolation of PBMCs from whole blood by Ficoll-Paque PLUS centrifugation (**A**). CD14⁺ cells were magnetically sorted from the PBMCs using CD14 microbeads on a QuadroMACS separator. The histogram depicts the purity of the CD14⁺ sorted monocytes by flow cytometry. The isotype control (white) is overlaid with surface marker expression (grey). The proportion on the histogram is the % of viable, sorted CD14⁺ cells (**B**). Co-culture system used to culture human monocytes and MSCs (**C**) MSCs, mesenchymal stem cells; PBMCs, peripheral blood mononuclear cells; RT, room temperature; T2D, type 2 diabetes.

4.2.5 RNA isolation and microarray analysis

RNA was extracted using the RNeasy Micro Kit (Qiagen, Hilden, Germany) according to the manufacturer's guidelines. Any contaminating DNA was removed by using 50U DNase I (Qiagen). RNA quantity was measured using a Nanodrop ND 1000 spectrophotometer (Rockland, DE), quality was determined with an Agilent 2100 electrophoresis bioanalyser (Agilent, Santa Clara, CA) and an RNA integrity number threshold of ≥ 0.8 was used for all samples. Samples (5ng RNA per sample) were prepared using an Ovation Pico WTA system V2 (NuGEN Technologies Inc., Bemmell, The Netherlands) and Encore Biotin Module V2 (NuGEN Technologies Inc.). 5 μ g of biotin labelled fragmented cDNA was hybridised to an Affymetrix GeneChip Human Gene 2.0 ST array (Affymetrix, Santa Clara, CA). Data were background corrected, \log_2 transformed and quantile normalised using the bioconductor packages for gene expression profiling in R. A linear model was then fitted to the normalised data and differential gene expression was when samples had a \log_2 -fold change of < -0.75 and > 0.75 . False discovery rate (FDR) correction was performed on the *P*-values according to methods described by Benjamini Hochberg (1995) using the *limma* bioconductor package. A FDR *P*-value of ≤ 0.05 was considered statistically significant. The list of differentially expressed genes was then subjected to pathway analysis using Ingenuity Pathway Analysis (IPA) software (Ingenuity Systems, Redwood City, CA).

4.2.6 Statistical analysis

All statistical analyses, except for the microarray analysis, were performed using GraphPad Prism software version 5.0 (GraphPad Software Inc., San Diego, CA). Comparisons between two groups were made with a Student's *t*-test (unpaired, 2-tailed). All data are expressed as means \pm SEM. A *P*-value of < 0.05 was considered statically significant.

4.3 Results

4.3.1 The proportions of blood monocyte subsets are altered in type 2 diabetic patients with ESRD

To understand the impact of T2D on blood monocytes, flow cytometry was used to assess and compare the phenotypes and relative proportions of freshly purified monocytes from control and diabetic subjects based on the expression of the monocyte markers CD14 and CD16. The baseline clinical parameters of the diabetic study participants are shown in Table 4.1. All diabetic subjects had T2D with ESRD and were receiving haemodialysis at the time of blood collection. Representative dot plots show CD45⁺CD14⁺CD16^{+/-} monocytes from control and type 2 diabetic subjects on the day of blood collection (Figure 4.2A). Three monocyte populations, corresponding to those reported in the literature, were identified in both patient groups. The CD14⁺⁺CD16⁻ ‘classical’ monocytes formed the predominant subset, while the transitioning ‘intermediate’ and more mature non-classical subsets constituted smaller proportions of the monocyte pool. Significant differences in the proportions of each of these subsets were observed when compared between the two subject groups. Within the monocyte pool, there were a significantly greater proportion of classical monocytes from control subjects, compared to those from type 2 diabetic patients (Figure 4.2B; control: 73.9±3.6% vs. T2D: 56.3±4.9%; $P<0.05$). In contrast, the type 2 diabetic patients had a higher proportion of intermediate (Figure 4.2C; control: 19.2±3.3% vs. T2D: 32.2±3.6%; $P<0.05$) and non-classical (Figure 4.2D; control: 2.8±0.5% vs. T2D: 7.5±1.3; $P<0.05$) monocytes, compared to the control subjects. Purified monocytes were also cytopun and subjected to Giemsa staining. Representative bright field images of monocytes from both subject groups (included in the dot plots in Figure 4.2A) confirmed normal monocyte morphology.

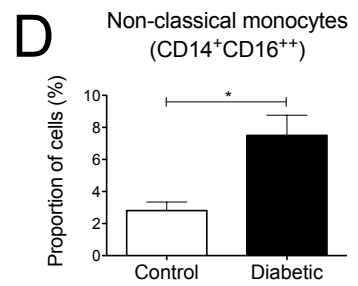
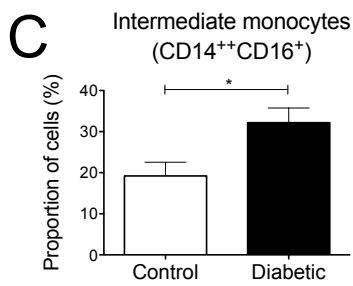
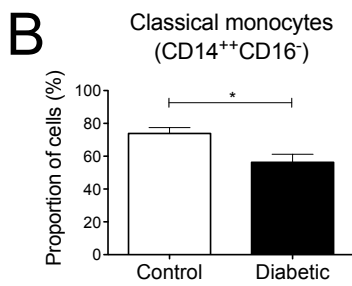
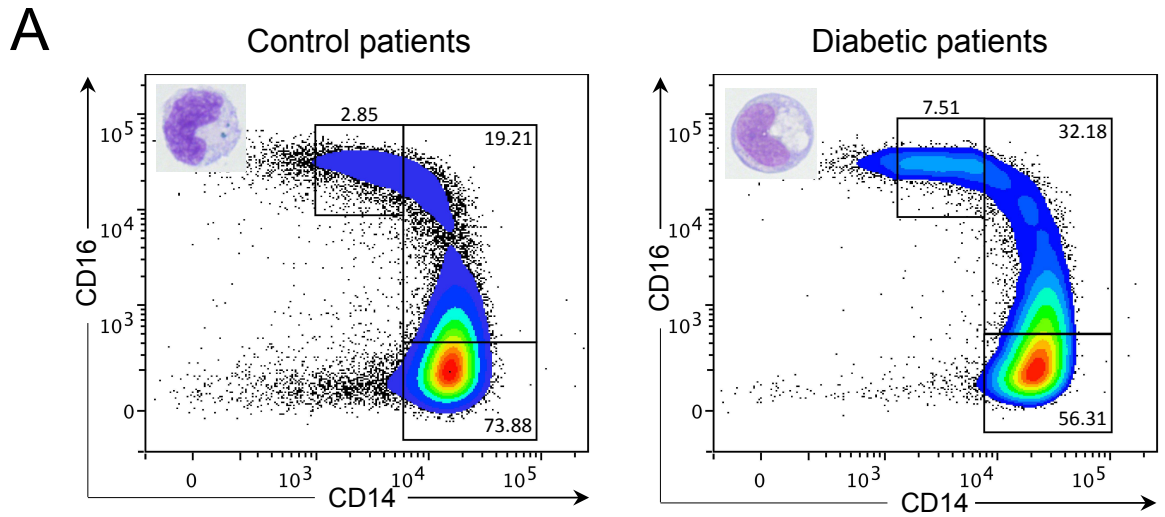


Figure 4.2 Comparison of CD14/CD16 monocyte populations isolated from control and type 2 diabetic subjects

Freshly isolated CD14⁺ cells from control and type 2 diabetic subjects were subjected to Giemsa staining to observe morphology (magnification x1000) and analysed by flow cytometry for their expression of CD14 and CD16 on day 0. Representative dot plots are shown. Numbers on dot plots represent the proportion of viable, sorted CD14⁺ cells (A). Proportion of CD14⁺⁺CD16⁻ classical (B), CD14⁺⁺CD16⁺ intermediate (C) and CD14⁺CD16⁺⁺ non-classical (D) monocytes from control and type 2 diabetic subjects. Data are means ± SEM. **P*<0.05.

This data has identified the shift in the proportions of the different monocyte subsets at the time of T2D-mediated ESRD. The inflammatory monocyte populations from type 2 diabetic patients could be either perpetuating the underlying inflammation, or may provide an indicator of disease state. Nonetheless, this data provides a useful benchmark for which to assess potential treatments for T2D and DN. One such therapy is the administration of MSCs, as they have previously demonstrated immunomodulatory and regenerative capabilities in a number of animal models of inflammatory diseases (209, 246, 315, 316). As such, the effect that MSCs have on these particular monocytes was assessed.

4.3.2 MSCs alter the inflammatory profile of monocytes

MSCs are believed to exert their immunomodulatory and regenerative effects through the release of soluble factors. In order to test this, monocytes from healthy control subjects and type 2 diabetic patients were co-cultured with MSCs for 48hrs using a Transwell system, as depicted in Figure 4.1C.

Following 48hrs of co-culture, MSCs significantly promoted the expansion of the T2D monocytes compared to the T2D monocytes alone (Figure 4.3B; T2D monocytes alone: $6.0 \times 10^4 \pm 9.6 \times 10^3$ vs. T2D monocytes+MSCs: $19.4 \times 10^4 \pm 7.97^4$; $P < 0.01$). However, there was no significant difference between the control monocytes alone and control monocytes+MSCs following co-culture (Figure 4.3A). Initial flow cytometric analysis revealed that following *in vitro* co-culture, both the control and T2D monocytes displayed a more uniform and mature CD14⁺CD16⁺ phenotype (Figure 4.3C). The level of CD14 and CD16 expression is an indicator of a cell's maturation state. Further, a decrease in CD14 and an increase in CD16 and MHC class II antigen expression is associated with the maturation of monocytes towards macrophages (317). Interestingly, additional analysis revealed that co-culture of monocytes with MSCs caused a significant upregulation of CD14 and CD16 expression on the type 2 diabetic patient monocytes, as depicted by an increased mean fluorescence intensity (MFI) of the CD14 (Figure 4.4A; T2D monocytes alone: $2.3 \times 10^4 \pm 0.7 \times 10^3$ vs. T2D monocytes+MSCs:

$3.3 \times 10^4 \pm 1.5 \times 10^3$; $P < 0.001$) and CD16 (Figure 4.4B; T2D monocytes alone: $2.5 \times 10^3 \pm 26.4$ vs. T2D monocytes+MSCs: $3.0 \times 10^3 \pm 233.4$; $P < 0.05$) parameters. This trend was also observed in the control group, however, was not statistically significant. In contrast, the MFI of the HLA-DR parameter was significantly lower in both the control (Figure 4.4C; control monocytes alone: $1.2 \times 10^4 \pm 2.4 \times 10^3$ vs. control monocytes+MSCs: $4.9 \times 10^3 \pm 0.6 \times 10^3$; $P < 0.05$) and T2D (Figure 4.4C; T2D monocytes alone: $1.4 \times 10^4 \pm 3.1 \times 10^3$ vs. T2D monocytes+MSCs: $5.6 \times 10^3 \pm 1.2 \times 10^3$; $P < 0.05$) monocytes following co-culture with MSCs. These results indicate that the MSCs are capable of restricting, retarding or impairing the differentiation of the monocytes towards the pro-inflammatory, non-classical phenotype. To understand the level and nature of the control the MSCs possess over the monocytes, microarray expression profiling was used to assess alterations in the genetic profile and biological signalling pathways in the monocytes following co-culture with MSCs.

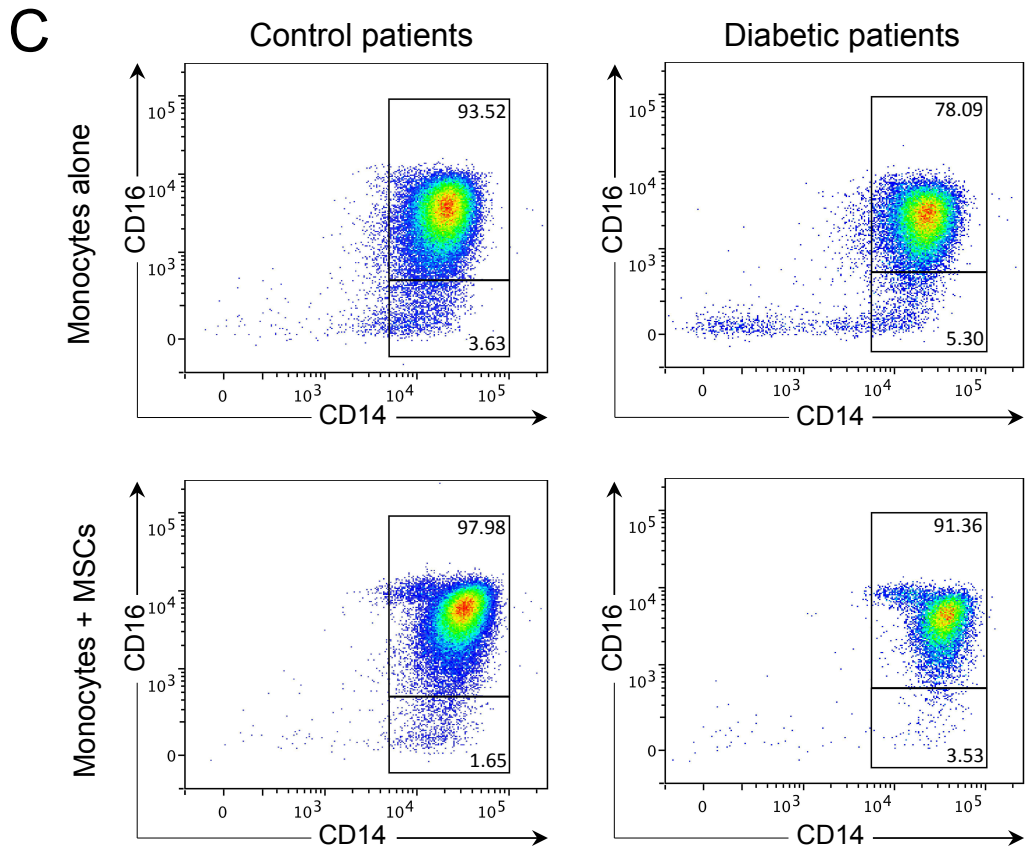
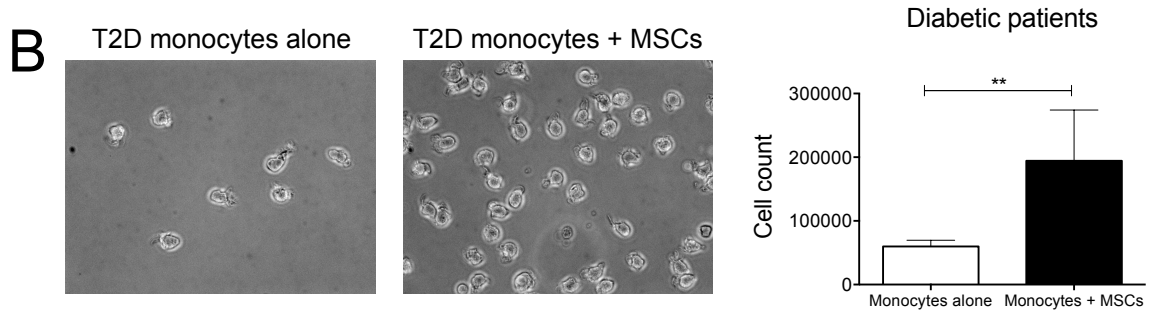
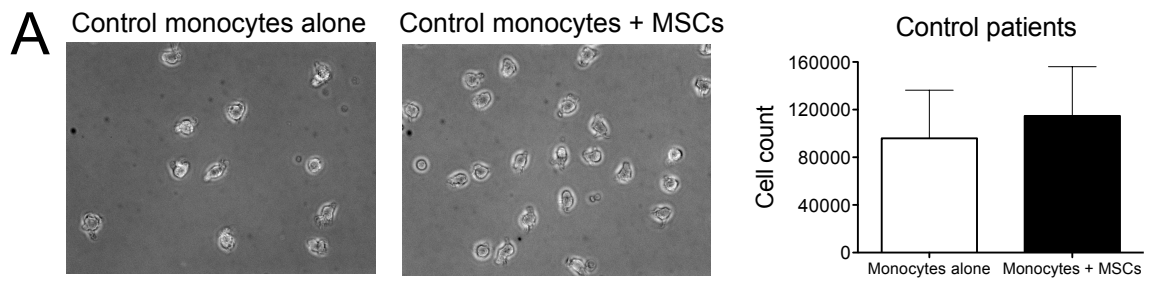


Figure 4.3 Control and type 2 diabetic-derived monocytes following 48 hours of co-culture with MSCs

Representative photomicrographs (magnification x400) and total cell counts of monocytes isolated from control (**A**) and type 2 diabetic (**B**) subjects following 48 hours of culture with and without MSCs. Representative flow cytometry dot plots showing the expression of CD14 and CD16 in monocytes following 48 hours of co-culture with and without MSCs. Numbers on dot plots represent the proportion of viable, sorted CD14⁺ cells (**C**). Data are means \pm SEM. ** $P < 0.01$. MSCs, mesenchymal stem cells; T2D, type 2 diabetes.

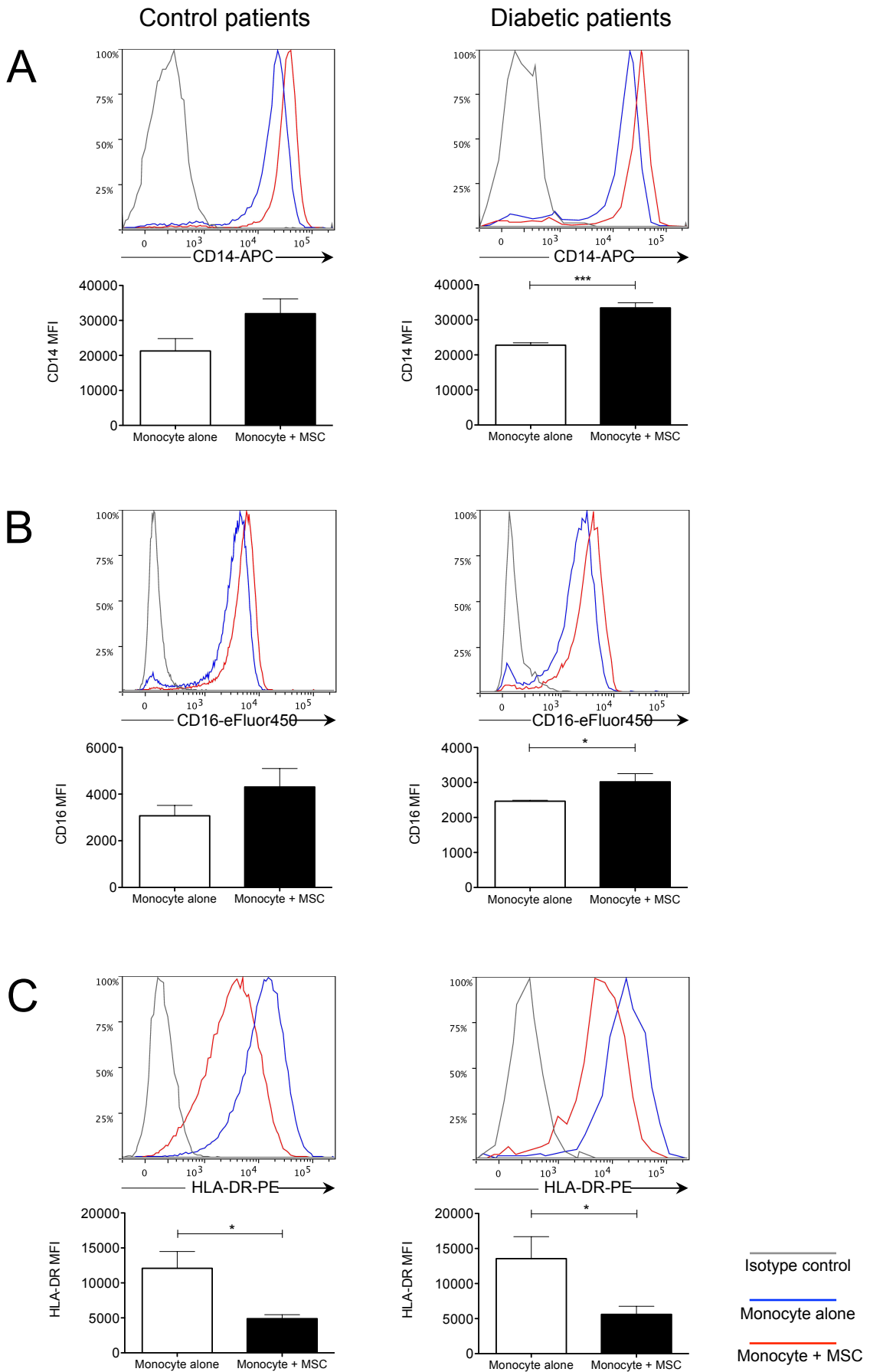


Figure 4.4 MSCs alter the phenotype of human monocytes

The CD14-APC (A), CD16-eFluor450 (B) and HLA-DR-PE (C) MFIs, representing surface marker expression level, of monocytes isolated from control and type 2 diabetic subjects following 48 hours of co-culture with and without MSCs. Data are means \pm SEM. * $P < 0.05$; *** $P < 0.001$. MFI, mean fluorescence intensity; MSCs, mesenchymal stem cells.

4.3.3 Monocytes co-cultured with MSCs have distinct gene expression profiles

Monocytes from control subjects and type 2 diabetic patients, that had been co-cultured with and without MSCs, were subjected to microarray gene expression profiling and multiple analysis methods were utilised to highlight the relationship between the gene expression profiles. The global relationship between the monocyte samples were first examined through principal component analysis (PCA). PCA simplifies multidimensional expression data into a lower set of orthogonal variables, known as principal components, each of which accounts for a proportion of variance. PCA revealed that the MSC-treated monocytes from both the control and type 2 diabetic subjects clustered separately from their respective untreated monocyte groups, indicating differences in gene expression intensity (Figure 4.5A). Hierarchical clustering of the genes reinforced that MSC-treated monocytes shared similarities in gene expression, although, displayed distinct patterns of gene expression compared to the monocytes that were not co-cultured with MSCs (Figure 4.5B). Following co-culture with MSCs, a total of 324 genes were differentially expressed, with 212 genes significantly upregulated (red) and 112 genes significantly downregulated (green) in both MSC-treated monocyte groups, compared to the monocyte alone groups (Figure 4.5C). The volcano plot in Figure 4.5C shows the distribution of gene signal intensity differences that occurred as a result of MSC treatment in both the control and diabetic monocytes. Tables 4.2 and 4.3 list the top ranked upregulated and downregulated genes, respectively, displaying the greatest differential expression (with a cut-off threshold of >2-fold and P -value <0.05) resulting from MSC co-culture in both control and diabetic monocytes compared to untreated monocytes.

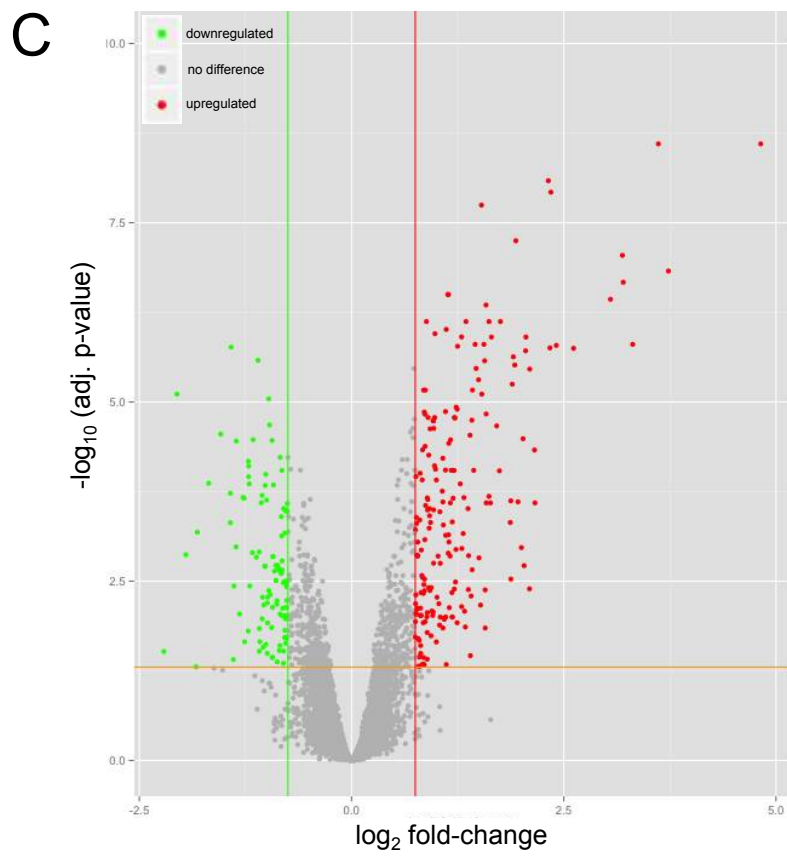
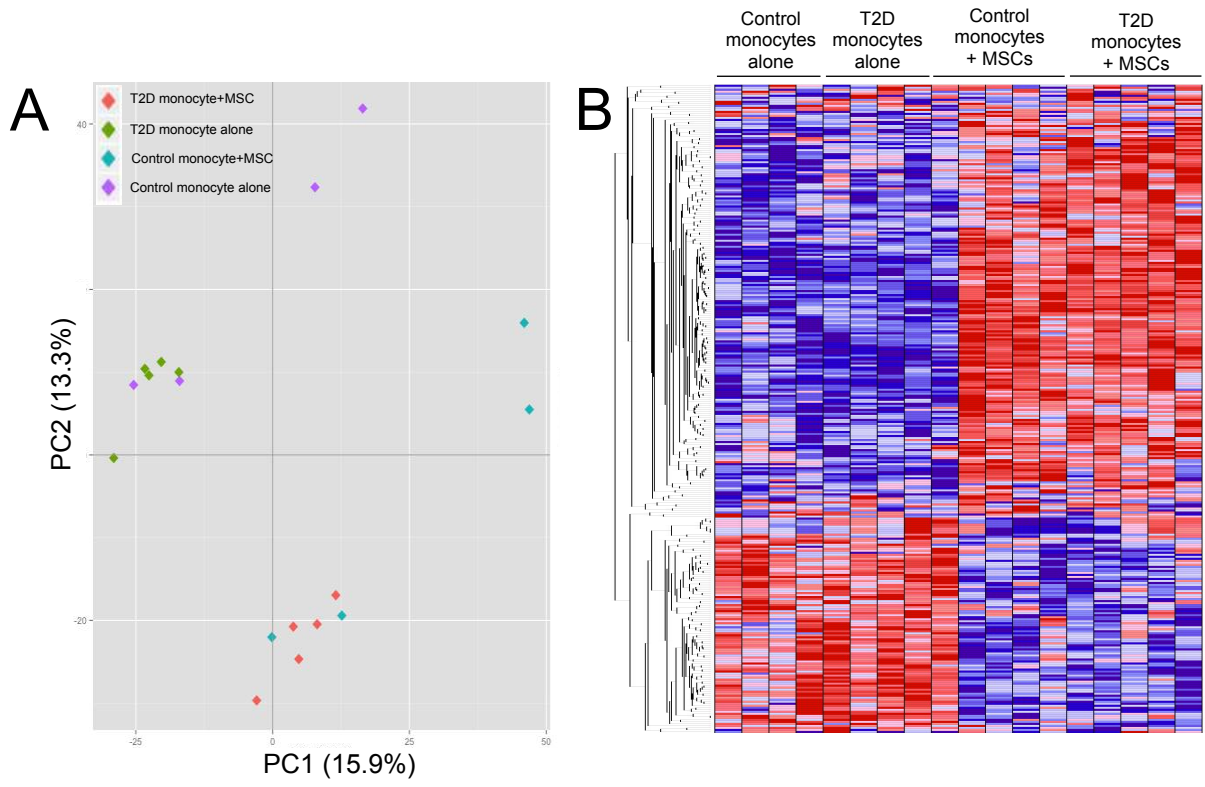


Figure 4.5 Transcription profiling of human monocytes

PCA of monocytes isolated from control and type 2 diabetic subjects, following 48 hours of co-culture with and without MSCs, demonstrating the relationship between samples for the first two principal components. The variance explained by each principal component is shown within the brackets of the axis labels **(A)**. Clustered heatmap of differentially expressed genes in monocytes isolated from control and type 2 diabetic subjects following co-culture with and without MSCs. Each gene is coloured according to their expression; red indicates upregulated, blue indicates downregulated. The intensity of the colour indicates the level of gene expression **(B)**. Volcano plot showing the \log_2 fold-change and *P*-value of differentially expressed genes for the comparison of MSC-treated monocytes versus untreated monocytes (LFC of <-0.75 or >0.75 ; FDR *P*-value <0.05) **(C)**. FDR, false discovery rate; LFC, \log_2 -fold change; MSCs, mesenchymal stem cells; PCA, principal component analysis; T2D, type 2 diabetes.

Table 4.2. Top genes upregulated in MSC-treated monocytes compared to monocytes alone

Gene symbol	Gene name	Log ₂ fold-change	P-value
<i>SERPINB2</i>	serpin peptidase inhibitor, clade B (ovalbumin), member 2	4.8204	<0.0001
<i>VCAN</i>	versican	3.7329	<0.0001
<i>ENPP2</i>	ectonucleotide pyrophosphatase/phosphodiesterase 2	3.6144	<0.0001
<i>THBS1</i>	thrombospondin 1	3.3122	<0.0001
<i>F13A1</i>	coagulation factor XIII, A1 polypeptide	3.2009	<0.0001
<i>NRG1</i>	neuregulin 1	3.1909	<0.0001
<i>CD226</i>	CD226 molecule	3.0500	<0.0001
<i>CCL2</i>	chemokine (C-C motif) ligand 2	2.6148	<0.0001
<i>EREG</i>	epiregulin	2.4116	<0.0001
<i>FAM20A</i>	family with sequence similarity 20, member A	2.3481	<0.0001
<i>CR1</i>	complement component (3b/4b) receptor 1 (Knops blood group)	2.3365	<0.0001
<i>MIR21</i>	microRNA 21	2.3178	<0.0001
<i>AQP9</i>	aquaporin 9	2.1604	0.0003
<i>KCNJ15</i>	potassium inwardly-rectifying channel, subfamily J, member 15	2.1551	<0.0001
<i>DHRS3</i>	dehydrogenase/reductase (SDR family) member 3	2.0984	<0.0001
<i>CXCL5</i>	chemokine (C-X-C motif) ligand 5	2.0964	0.0040
<i>DSC2</i>	desmocollin 2	2.0539	<0.0001
<i>SLC16A10</i>	solute carrier family 16 (aromatic amino acid transporter), member 10	2.0505	<0.0001
<i>PCOLCE2</i>	procollagen C-endopeptidase enhancer 2	2.0328	0.0019
<i>RNASE2</i>	ribonuclease, RNase A family, 2 (liver, eosinophil-derived neurotoxin)	2.0198	<0.0001
<i>CD38</i>	CD38 molecule	2.0003	0.0011
<i>LOC154761</i>	family with sequence similarity 115, member C pseudogene	1.9606	0.0002
<i>OLFML2B</i>	olfactomedin-like 2B	1.9351	<0.0001
<i>FPR2</i>	formyl peptide receptor 2	1.9227	<0.0001
<i>SLC2A3</i>	solute carrier family 2 (facilitated glucose transporter), member 3	1.9055	<0.0001
<i>TMEM26</i>	transmembrane protein 26	1.8933	<0.0001
<i>ECRP</i>	ribonuclease, RNase A family, 2 (liver, eosinophil-derived neurotoxin) pseudogene	1.8767	0.0030
<i>SOCS3</i>	suppressor of cytokine signaling 3	1.8759	0.0002
<i>LYVE1</i>	lymphatic vessel endothelial hyaluronan receptor 1	1.8695	0.0005
<i>SH3PXD2B</i>	SH3 and PX domains 2B	1.7537	<0.0001
<i>FPR1</i>	formyl peptide receptor 1	1.7419	<0.0001
<i>BNIP3</i>	BCL2/adenovirus E1B 19kDa interacting protein 3	1.7096	<0.0001
<i>ZNF704</i>	zinc finger protein 704	1.6477	<0.0001
<i>FCGR1B</i>	Fc fragment of IgG, high affinity Ib, receptor (CD64)	1.6356	0.0003
<i>HIVEP2</i>	human immunodeficiency virus type I enhancer binding protein 2	1.6191	0.0002
<i>VSIG4</i>	V-set and immunoglobulin domain containing 4	1.6188	<0.0001
<i>MS4A4A</i>	membrane-spanning 4-domains, subfamily A, member 4A	1.5863	0.0003
<i>FCGR1A</i>	Fc fragment of IgG, high affinity Ia, receptor (CD64)	1.5854	<0.0001
<i>TNIK</i>	TRAF2 and NCK interacting kinase	1.5835	<0.0001
<i>IGF1</i>	insulin-like growth factor 1 (somatomedin C)	1.5744	0.0142
<i>CD163L1</i>	CD163 molecule-like 1	1.5733	0.0042
<i>KIAA0226L</i>	KIAA0226-like	1.5681	<0.0001
<i>PIM1</i>	pim-1 oncogene	1.5596	<0.0001
<i>HIF1A-AS2</i>	HIF1A antisense RNA 2	1.5338	<0.0001
<i>S100A9</i>	S100 calcium binding protein A9	1.5303	<0.0001
<i>BEX1</i>	brain expressed, X-linked 1	1.5192	0.0068
<i>FCAR</i>	Fc fragment of IgA, receptor for	1.5011	0.0015
<i>PMP22</i>	peripheral myelin protein 22	1.4962	<0.0001
<i>LOC100506114</i>	uncharacterized LOC100506114	1.4667	<0.0001
<i>HIF1A</i>	hypoxia inducible factor 1, alpha subunit (basic helix-loop-helix transcription factor)	1.4558	<0.0001

Table 4.3. Top genes downregulated in MSC-treated monocytes compared to monocytes alone

Gene symbol	Gene name	Log ₂ fold-change	P-value
<i>LOC100653057</i>	liver carboxylesterase 1-like	-2.2113	0.0300
<i>FABP3</i>	fatty acid binding protein 3, muscle and heart (mammary-derived growth inhibitor)	-2.0570	<0.0001
<i>APOC1</i>	apolipoprotein C-I	-1.9524	0.0014
<i>CLEC12A</i>	C-type lectin domain family 12, member A	-1.8336	0.0495
<i>ALDH1A1</i>	aldehyde dehydrogenase 1 family, member A1	-1.8172	0.0007
<i>SERPINF1</i>	serpin peptidase inhibitor, clade F (alpha-2 antiplasmin, pigment epithelium derived factor), member 1	-1.6829	0.0001
<i>FFAR4</i>	free fatty acid receptor 4	-1.5411	<0.0001
<i>C3</i>	complement component 3	-1.4277	0.0005
<i>SPN</i>	sialophorin	-1.4274	0.0002
<i>IPCEF1</i>	interaction protein for cytohesin exchange factors 1	-1.4188	<0.0001
<i>CES1</i>	carboxylesterase 1	-1.3931	0.0392
<i>CIITA</i>	class II, major histocompatibility complex, transactivator	-1.3857	0.0037
<i>A2M</i>	alpha-2-macroglobulin	-1.3609	0.0011
<i>ITGAL</i>	integrin, alpha L (antigen CD11A (p180), lymphocyte function-associated antigen 1; alpha polypeptide)	-1.3581	<0.0001
<i>CD52</i>	CD52 molecule	-1.3202	0.0091
<i>GCLC</i>	glutamate-cysteine ligase, catalytic subunit	-1.2777	0.0002
<i>P2RX7</i>	purinergic receptor P2X, ligand-gated ion channel, 7	-1.2665	0.0002
<i>CXCR2P1</i>	chemokine (C-X-C motif) receptor 2 pseudogene 1	-1.2601	0.0222
<i>ZNF366</i>	zinc finger protein 366	-1.2182	0.0157
<i>HLA-DMB</i>	major histocompatibility complex, class II, DM beta	-1.2162	<0.0001
<i>ALCAM</i>	activated leukocyte cell adhesion molecule	-1.2062	0.0001
<i>CST6</i>	cystatin E/M	-1.1998	0.0037
<i>OLFML3</i>	olfactomedin-like 3	-1.1682	0.0013
<i>RASAL2</i>	RAS protein activator like 2	-1.1594	<0.0001
<i>MYOF</i>	myoferlin	-1.1210	0.0015
<i>LOC100506928</i>	uncharacterized LOC100506928	-1.1025	<0.0001
<i>DHCR24</i>	24-dehydrocholesterol reductase	-1.0871	0.0012
<i>OLR1</i>	oxidized low density lipoprotein (lectin-like) receptor 1	-1.0863	0.0145
<i>CD83</i>	CD83 molecule	-1.0861	0.0299
<i>APOE</i>	apolipoprotein E	-1.0801	0.0221
<i>IFI6</i>	interferon, alpha-inducible protein 6	-1.0535	0.0106
<i>QPRT</i>	quinolinate phosphoribosyltransferase	-1.0491	0.0053
<i>MMP2</i>	matrix metalloproteinase 2 (gelatinase A, 72kDa gelatinase, 72kDa type IV collagenase)	-1.0422	0.0265
<i>SLC1A3</i>	solute carrier family 1 (glial high affinity glutamate transporter), member 3	-1.0347	0.0068
<i>HLA-DPB1</i>	major histocompatibility complex, class II, DP beta 1	-1.0201	0.0019
<i>FLNA</i>	filamin A, alpha	-1.0182	0.0001
<i>OPHN1</i>	oligophrenin 1	-1.0109	0.0001
<i>MIR54802</i>	microRNA 548o-2	-1.0100	0.0241
<i>C14orf159</i>	chromosome 14 open reading frame 159	-1.0014	0.0002

4.3.4 MSCs induce an M2-like gene expression profile in monocytes

Hierarchical clustering and heatmap visualisation of the differentially expressed genes further demonstrates that MSC co-culture lead to the downregulation (blue) of the non-classical monocyte markers integrin, α L (*ITGAL*; also known as *CD11a*) and sialophorin (*SPN*; also known as *CD43*) and the upregulation (red) of the classical monocyte markers *FCGR2A* and *FCGR2B* (both associated with CD64), *CD163*, *CD93*, *CD38*, C-type lectin domain family 4 (*CLEC4D*), hypoxia inducible factor 1 α (*HIF1A*) and formyl peptide receptor 1 (*FPR1*; Figure 4.6A). In addition, MSC treatment also significantly upregulated several markers associated with an M2 macrophage phenotype including the cytokines *IL10*, *IGF1*, *CCL2* and *VEGF-A*; membrane receptors *MRC1* (also known as *CD206*), *CD163*, *CD163L1*, *CD226*, *CD93*, leukocyte immunoglobulin-like receptor subfamily B member 1 (*LILRB1*) and prostaglandin E2 receptor (*PTGER2*; also known as *EP2*); and enzymes *MMP9*, *MMP19*, coagulation factor XIII A1 polypeptide (*F13A1*), serpin peptidase inhibitor clade B member 2 (*SERPINB2*) and prostaglandin-endoperoxide synthase 2 (*PTGS2*; also known as *COX2*; Figure 4.6B). The list of differentially expressed genes was then subjected to pathway over-representation analyses. Over-representation analyses determines the biological pathways that are significantly over-represented in the dataset and measures the probability that the differentially expressed gene list contains more genes of the biological pathway that would have occurred by chance alone. The top 10 canonical signalling pathways significantly over-represented in the MSC-treated monocytes are shown in Figure 4.7. The genes involved in the top 10 canonical signalling pathways overlapped in their expression profiles (Table 4.4). As such, the top pathways shared several common genes indicative of cell maturation including, Fc γ receptors (*FCGR1B*, *FCGR2A*, *FCGR2B* and *FCGR3A*), MHC class II molecules (*HLA-DMB* and *HLA-DQB1*) and adhesion molecules (*ITGAL*, *ITGAX*, *ITGA9* and *ICAM1*). Interestingly, the MHC class II molecules and many of the adhesion molecules were in fact downregulated by the MSC treatment (Table 4.5). Studies examining the gene expression profiles associated with monocyte-to-macrophage differentiation have shown that proteins involved in lipid metabolism, such as apolipoprotein E (*APOE*), apolipoprotein C-1 (*APOC1*),

lipoprotein lipase (*LPL*) and peroxisome proliferator-activated receptor γ (*PPARG*), are induced in macrophages (318, 319). In this study, these same genes were collectively downregulated in the MSC-treated monocytes (Table 4.5). Altogether, these results are consistent with the phenotypic data, indicating that MSCs impaired the maturation of the monocytes towards a non-classical or mature macrophage phenotype.

A number of genes associated with an M2 macrophage response were also upregulated (Table 4.5). To further characterise the functional changes associated with MSC-mediated monocyte polarisation, IPA software was used to generate network hubs showing the common differentially expressed genes involved within the top 10 signalling pathways (Figure 4.8 – 4.10). This enabled the identification of the differential networks and key regulators involved. As shown in Figure 4.8, the M2-associated, anti-inflammatory, regenerative molecules *IL10*, *IGF1*, *MMP9* and *VEGF* were upregulated. This was accompanied by an upregulation of classical monocyte and M2 macrophage-associated phagocytic receptors *FCGR1B*, *FCGR2A*, *FCGR2B* and *CD163* (Figure 4.9), coinciding with a downregulation of MHC class II molecules (Figure 4.10). Microarray analysis was used to determine the global effects MSCs had on the genome-wide gene expression profiles of monocytes, as this could not have been detected through phenotypic analysis, using techniques such as flow cytometry. Interestingly, microarray analysis revealed that the MSCs did alter the genetic profile of the monocytes, whereby the MSCs promoted the upregulation of several classical monocyte and M2 macrophage-associated genes, therefore promoting an alternatively activated monocyte phenotype. Further, this occurred regardless of the environment the monocytes were originally isolated from, namely control or T2D patients.

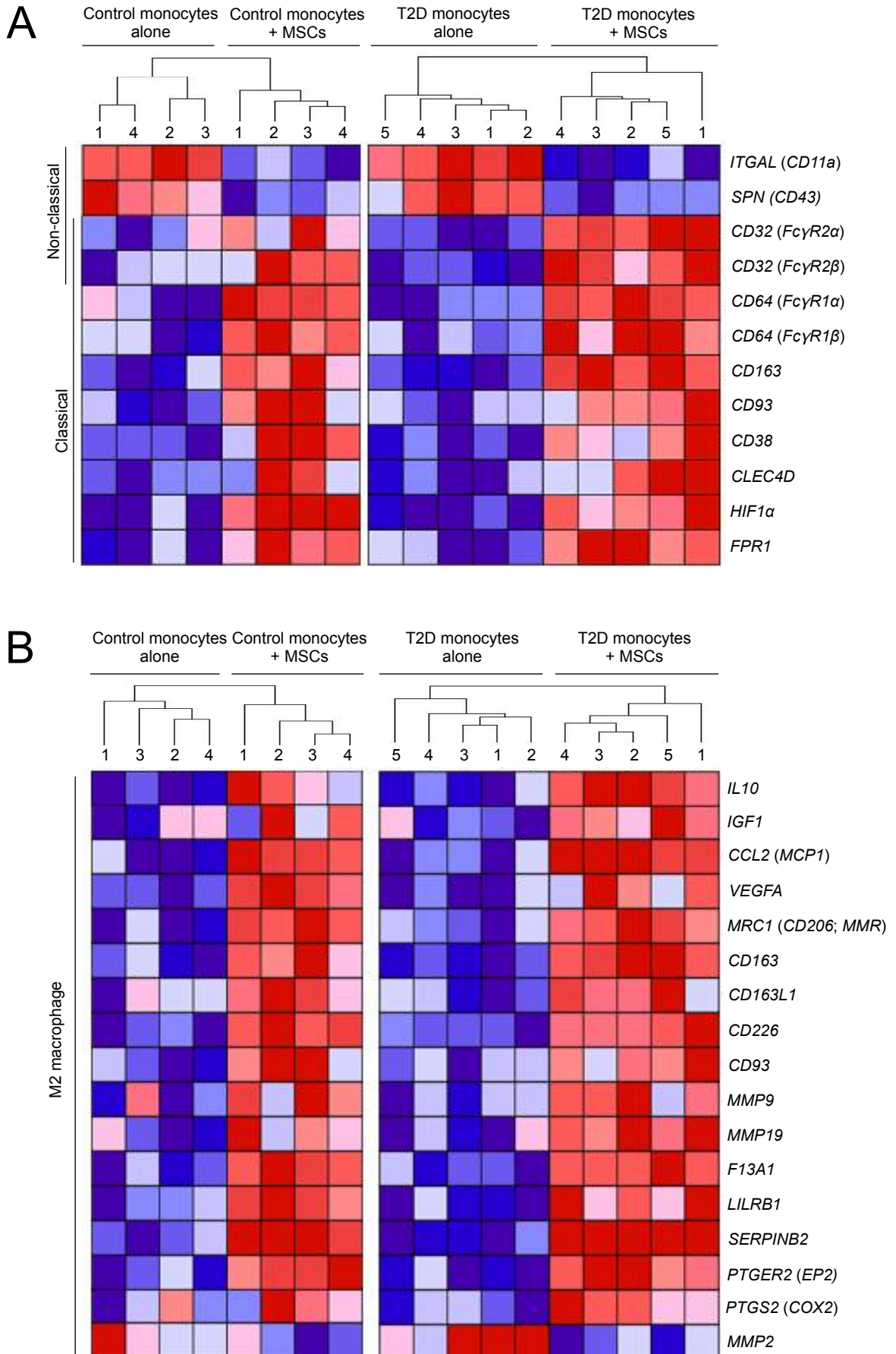
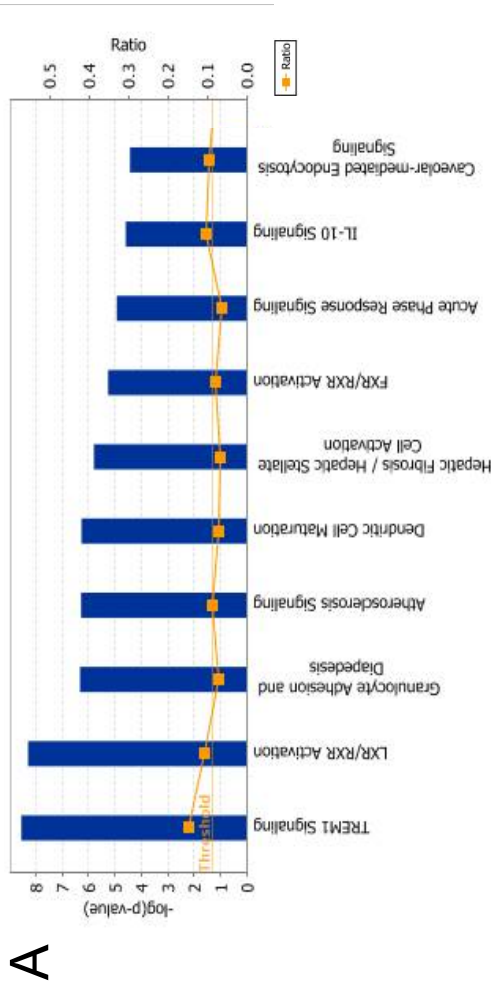


Figure 4.6 MSCs alter the gene expression profile of monocytes

Hierarchical clustering and heatmap visualisation of known classical and non-classical monocyte (A) and M2 macrophage (B) markers differentially expressed on monocytes co-cultured with and without MSCs for 48 hours. Numbers at the top of the heatmap correspond to subject number (Defined in Table 4.1). Each gene is coloured according to their expression; red indicates upregulated, blue indicates downregulated. The intensity of the colour indicates the level of gene expression. CCL2, chemokine (C-C motif) ligand 2/MCP-1, monocyte chemoattractant protein-1; CLEC4D, C-type lectin domain family 4; F13A1, coagulation factor XIII, A1 polypeptide; FPR1, formyl peptide receptor 1; HIF1 α , hypoxia inducible factor 1 alpha, IGF1, insulin-like growth factor 1; IL, interleukin; ITGAL, integrin alpha L; LILRB1, leukocyte immunoglobulin-like receptor, subfamily B, member 1; MMP, matrix metalloproteinase; MRC1, mannose receptor, C type 1; MSCs, mesenchymal stem cells; PTGER2, prostaglandin E receptor 2; PTGS2, prostaglandin-endoperoxide synthase 2/COX-2, cyclooxygenase-2; SERPINB2, serpin peptidase inhibitor, clade B, member 2; SPN, sialophorin; T2D, type 2 diabetes; VEGFA, vascular endothelial growth factor A.



B Table 4.4 Top 10 canonical signalling pathways significantly over-represented in MSC-treated monocytes

Canonical signalling pathway	P-value	Differentially expressed genes
TREM1 signalling	2.83×10^{-9}	<i>CASP5, CCL2, CD83, CIITA, CXCL8, FCGR2B, ICAM1, IL10, IL1B, ITGAX, TREM1</i>
Liver X receptor/retinoid X receptor activation	1.55×10^{-9}	<i>APOC1, APOE, C3, CCL2, IL1A, IL1B, IL1RAP, LPL, MMP9, MSRI, PTGS2, SERPINA1, SERPINF1</i>
Granulocyte adhesion and diapedesis	4.74×10^{-7}	<i>CCL2, CXCL5, CXCL8, FPR1, FPR2, ICAM1, IL1A, IL1B, IL1RAP, ITGAL, MMP2, MMP9, MMP19</i>
Atherosclerosis signalling	5.20×10^{-7}	<i>APOC1, APOE, CCL2, CXCL8, ICAM1, IL1A, IL1B, LPL, MMP9, MSRI, SERPINA1</i>
Dendritic cell maturation	5.93×10^{-7}	<i>CD83, FCGR1B, FCGR2A, FCGR2B, FCGR3A/FCGR3B, HLA-DMB, HLA-DQB1, ICAM1, IL10, IL1A, IL1B, STAT4, TREM2</i>
Hepatic fibrosis/hepatic stellate cell activation	1.59×10^{-6}	<i>A2M, CCL2, CXCL8, EDNRB, ICAM1, IGF1, IL10, IL1A, IL1B, IL1RAP, MMP2, MMP9, VEGFA</i>
Farnesoid X receptor/retinoid X receptor activation	5.48×10^{-6}	<i>APOC1, APOE, C3, IL1A, ILB, LPL, PPARG, SERPINA1, SERPINF1, VLDLR</i>
Acute Phase response signalling	1.16×10^{-5}	<i>A2M, C2, C3, IL1A, IL1B, IL1RAP, RBP1, SERPINA1, SERPINF1, SOCS3, SOD2</i>
IL-10 signalling	2.55×10^{-5}	<i>FCGR2A, FCGR2B, IL10, IL1A, IL1B, IL1RAP, SOCS3</i>
Caveolar-mediated endocytosis signalling	3.72×10^{-5}	<i>FLNA, FLNB, FLOT1, ITGA9, ITGAL, ITGAX, PRKCA</i>

Figure 4.7 Signalling pathways upregulated in monocytes co-cultured with MSCs

The top 10 canonical signalling pathways significantly over-represented in control and T2D monocytes co-cultured with MSCs compared to the monocyte alone groups (**A**). The threshold line refers to the cut-off probability ($P < 0.05$) and the ratio line indicates the number of genes from the gene list that pass the cut-off criteria in the pathway divided by the total number of genes in the pathway. Differentially expressed genes in the top 10 canonical signalling pathways significantly over-represented in MSC-treated monocytes compared to untreated monocytes (**B**; Table 4.4). The P -values were calculated using a right-tailed Fisher's exact test within the IPA software.

Table 4.5 Top 10 canonical pathways merged gene list

Gene symbol	Gene name	Log ₂ fold change	P-value	Pathways implicated
Phagocytosis				
<i>FCGR1B</i>	Fc fragment of IgG, high affinity IB, receptor (CD64)	1.64	2.56x10 ⁻⁴	Dendritic cell maturation
<i>FCGR2A</i>	Fc fragment of IgG, low affinity IIa, receptor (CD32)	0.85	0.0035	Dendritic cell maturation, IL10 signalling
<i>FCGR2B</i>	Fc fragment of IgG, low affinity IIb, receptor (CD32)	1.37	3.08x10 ⁻⁴	TREM1 signalling, Dendritic cell maturation, IL10 signalling
<i>FCGR3A</i>	Fc fragment of IgG, low affinity IIIa, receptor (CD16a)	1.11	8.93x10 ⁻⁵	Dendritic cell maturation
Antigen processing and presentation				
<i>HLA-DMB</i>	major histocompatibility complex, class II, DM beta	-1.22	6.72x10 ⁻⁵	Dendritic cell maturation
<i>HLA-DQB1</i>	major histocompatibility complex, class II, DQ beta 1	-0.93	0.0366	Dendritic cell maturation
<i>CIITA</i>	class II, major histocompatibility complex, transactivator	-1.39	0.0037	TREM1 signalling
Adhesion molecules				
<i>ITGAL</i>	integrin, alpha L (antigen CD11A (p180), lymphocyte function-associated antigen 1; alpha polypeptide)	-1.36	3.51x10 ⁻⁵	Granulocyte adhesion and diapedesis
<i>ITGAX</i>	integrin, alpha X (complement component 3 receptor 4 subunit)	-0.78	0.0097	TREM1 signalling, Caveolar-mediated endocytosis signalling
<i>ITGA9</i>	integrin, alpha 9	1.14	0.0013	Caveolar-mediated endocytosis signalling
<i>ICAM1</i>	intercellular adhesion molecule 1	0.77	4.96x10 ⁻⁴	TREM1 signalling, Granulocyte adhesion and diapedesis, Atherosclerosis signalling, Dendritic cell maturation, Hepatic fibrosis/hepatic stellate cell activation
Scavenger receptor				
<i>MSR1</i>	mannose receptor, C type 1	-0.81	3.08x10 ⁻⁴	LXR/RXR activation, Atherosclerosis signalling
Collagen degradation				
<i>MMP2</i>	matrix metalloproteinase 2 (gelatinase A, 72kDa gelatinase, 72kDa type IV collagenase)	-1.04	0.0265	Granulocyte adhesion and diapedesis, Hepatic fibrosis/hepatic stellate cell activation
<i>MMP9</i>	matrix metalloproteinase 9 (gelatinase B, 92kDa gelatinase, 92kDa type IV collagenase)	1.30	0.0072	LXR/RXR activation, Granulocyte adhesion and diapedesis, Atherosclerosis signalling, Hepatic fibrosis/hepatic stellate cell activation
<i>MMP19</i>	matrix metalloproteinase 19	0.92	0.0043	Granulocyte adhesion and diapedesis
Immunoregulation/anti-inflammatory				
<i>IL10</i>	interleukin 10	0.90	2.30x10 ⁻⁴	TREM1 signalling, Dendritic cell maturation, Hepatic fibrosis/hepatic stellate cell activation
<i>IGF1</i>	insulin-like growth factor 1 (somatomedin C)	1.57	0.0142	Hepatic fibrosis/hepatic stellate cell activation
<i>PTGS2</i>	prostaglandin-endoperoxide synthase 2 (prostaglandin G/H synthase and cyclooxygenase)	1.04	0.0130	LXR/RXR activation
<i>VEGFA</i>	vascular endothelial growth factor A	0.92	3.87x10 ⁻⁴	Hepatic fibrosis/hepatic stellate cell activation
Chemoattractant				
<i>CCL2</i>	chemokine (C-C motif) ligand 2	2.61	1.79x10 ⁻⁶	TREM1 signalling, LXR/RXR activation, Granulocyte adhesion and diapedesis, Atherosclerosis signalling, Hepatic fibrosis/hepatic stellate cell activation
<i>IL8</i>	interleukin 8, chemokine (C-X-C) ligand 8	1.30	0.0011	TREM1 signalling, Granulocyte adhesion and diapedesis, Atherosclerosis signalling, Hepatic fibrosis/hepatic stellate cell activation
<i>CXCL5</i>	chemokine (C-X-C) ligand 5	2.10	0.0040	Granulocyte adhesion and diapedesis
Complement				
<i>C2</i>	complement component 2	1.24	1.26x10 ⁻⁵	Acute phase response signalling
<i>C3</i>	complement component 3	-1.43	4.84x10 ⁻⁴	LXR/RXR activation, FXR/RXR activation, Acute phase response signalling

Inflammatory				
<i>IL1A</i>	interleukin 1, alpha	0.81	0.0322	LXR/RXR activation, Granulocyte adhesion and diapedesis, Atherosclerosis signalling, Dendritic cell maturation, Hepatic fibrosis/hepatic stellate cell activation, FXR/RXR activation, Acute phase response signalling, IL10 signalling
<i>IL1B</i>	interleukin 1, beta	1.38	0.0041	TREM1 signalling, LXR/RXR activation, Granulocyte adhesion and diapedesis, Atherosclerosis signalling, Dendritic cell maturation, Hepatic fibrosis/hepatic stellate cell activation, FXR/RXR activation, Acute phase response signalling, IL10 signalling
<i>IL1RAP</i>	interleukin 1 receptor accessory protein	0.87	4.16x10 ⁻⁵	LXR/RXR activation, Granulocyte adhesion and diapedesis, Hepatic fibrosis/hepatic stellate cell activation, IL10 signalling
<i>TREM1</i>	triggering receptor expressed on myeloid cells 1	1.04	0.0018	TREM1 signalling
<i>TREM2</i>	triggering receptor expressed on myeloid cells 2	-0.93	0.0074	Dendritic cell maturation
Lipoprotein homeostasis				
<i>APOC1</i>	apolipoprotein C-I	-1.95	0.0014	LXR/RXR activation, Atherosclerosis signalling, FXR/RXR activation
<i>APOE</i>	apolipoprotein E	-1.08	0.0221	LXR/RXR activation, Atherosclerosis signalling, FXR/RXR activation
<i>VLDLR</i>	very low density lipoprotein receptor	0.84	0.0459	FXR/RXR activation
<i>LPL</i>	lipoprotein lipase	-0.99	0.0121	LXR/RXR activation, Atherosclerosis signalling, FXR/RXR activation
<i>PPARG</i>	peroxisome proliferator-activated receptor gamma	-0.99	0.0322	FXR/RXR activation, Acute phase response signalling
Apoptosis				
<i>CASP5</i>	caspase 5, apoptosis-related cysteine peptidase	0.81	0.0483	TREM1 signalling
Other				
<i>A2M</i>	alpha-2-macroglobulin	-1.36	0.0011	Hepatic fibrosis/hepatic stellate cell activation, Acute phase response signalling
<i>CD83</i>	CD83 molecule	-1.09	0.0300	TREM1 signalling, Dendritic cell maturation
<i>EDNRB</i>	endothelin receptor type B	1.22	0.0032	Hepatic fibrosis/hepatic stellate cell activation
<i>FLNA</i>	filamin A, alpha	-1.02	1.47x10 ⁻⁴	Caveolar-mediated endocytosis signalling
<i>FLNB</i>	filamin B, beta	0.80	0.0211	Caveolar-mediated endocytosis signalling
<i>FLOT1</i>	flotillin 1	1.00	8.67x10 ⁻⁵	Caveolar-mediated endocytosis signalling
<i>FPR1</i>	formyl peptide receptor 1	1.74	9.14x10 ⁻⁵	Granulocyte adhesion and diapedesis
<i>FPR2</i>	formyl peptide receptor 2	1.92	3.05x10 ⁻⁶	Granulocyte adhesion and diapedesis
<i>PRKCA</i>	protein kinase C, alpha	0.97	2.34x10 ⁻⁵	Caveolar-mediated endocytosis signalling
<i>RBP1</i>	retinol binding protein 1, cellular	1.23	1.18x10 ⁻⁵	Acute phase response signalling
<i>SERPINA1</i>	serpin peptidase inhibitor, clade A (alpha-1 antiproteinase, antitrypsin), member 1	0.86	1.39x10 ⁻⁵	LXR/RXR activation, Atherosclerosis signalling, FXR/RXR activation, Acute phase response signalling
<i>SERPINF1</i>	serpin peptidase inhibitor, clade F (alpha-2 antiplasmin, pigment epithelium derived factor), member 1	-1.68	1.36x10 ⁻⁴	LXR/RXR activation, FXR/RXR activation, Acute phase response signalling
<i>SOD2</i>	superoxide dismutase 2, mitochondrial	0.98	1.12x10 ⁻⁶	Acute phase response signalling
<i>SOCS3</i>	suppressor of cytokine signaling 3	1.88	2.40x10 ⁻⁴	Acute phase response signalling, IL10 signalling
<i>STAT4</i>	signal transducer and activator of transcription 4	0.95	0.0083	Dendritic cell maturation

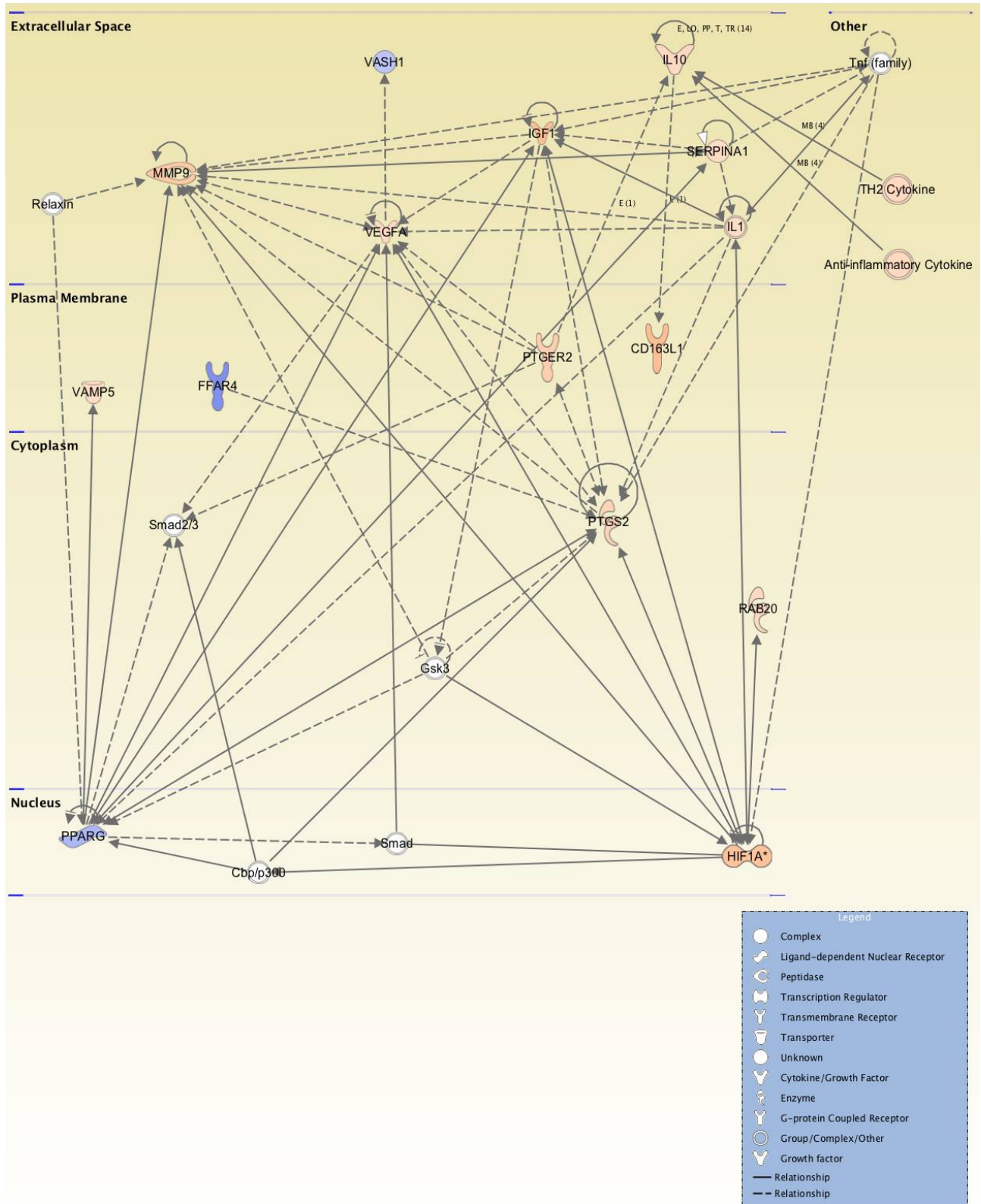


Figure 4.8 MSCs upregulate signalling associated with an M2 macrophage response

A gene network hub of *IL10*, *IGF1* and *VEGFA* signalling and the mediators, constructed using the differentially expressed genes over-represented in the top 10 signalling pathways (listed in Figure 4.7), in the MSC-treated monocytes. Each gene is coloured according to their expression; orange indicates upregulated, blue indicates downregulated. The intensity of the colour indicates the level of gene expression. Each gene is organised based on where the gene product is located within the cell. The continuous line between genes represents a direct relationship between the genes and a dotted line represents an indirect relationship.

Figure 4.9 MSCs upregulate classical monocyte and M2 macrophage-associated phagocytic receptors

A gene network hub of Fc receptor signalling constructed using the differentially expressed genes over-represented in the top 10 signalling pathways (listed in Figure 4.7), in the MSC-treated monocytes. Each gene is coloured according to their expression; orange indicates upregulated, blue indicates downregulated. The intensity of the colour indicates the level of gene expression. Each gene is organised based on where the gene product is located within the cell. The continuous line between genes represents a direct relationship between the genes and a dotted line represents an indirect relationship.

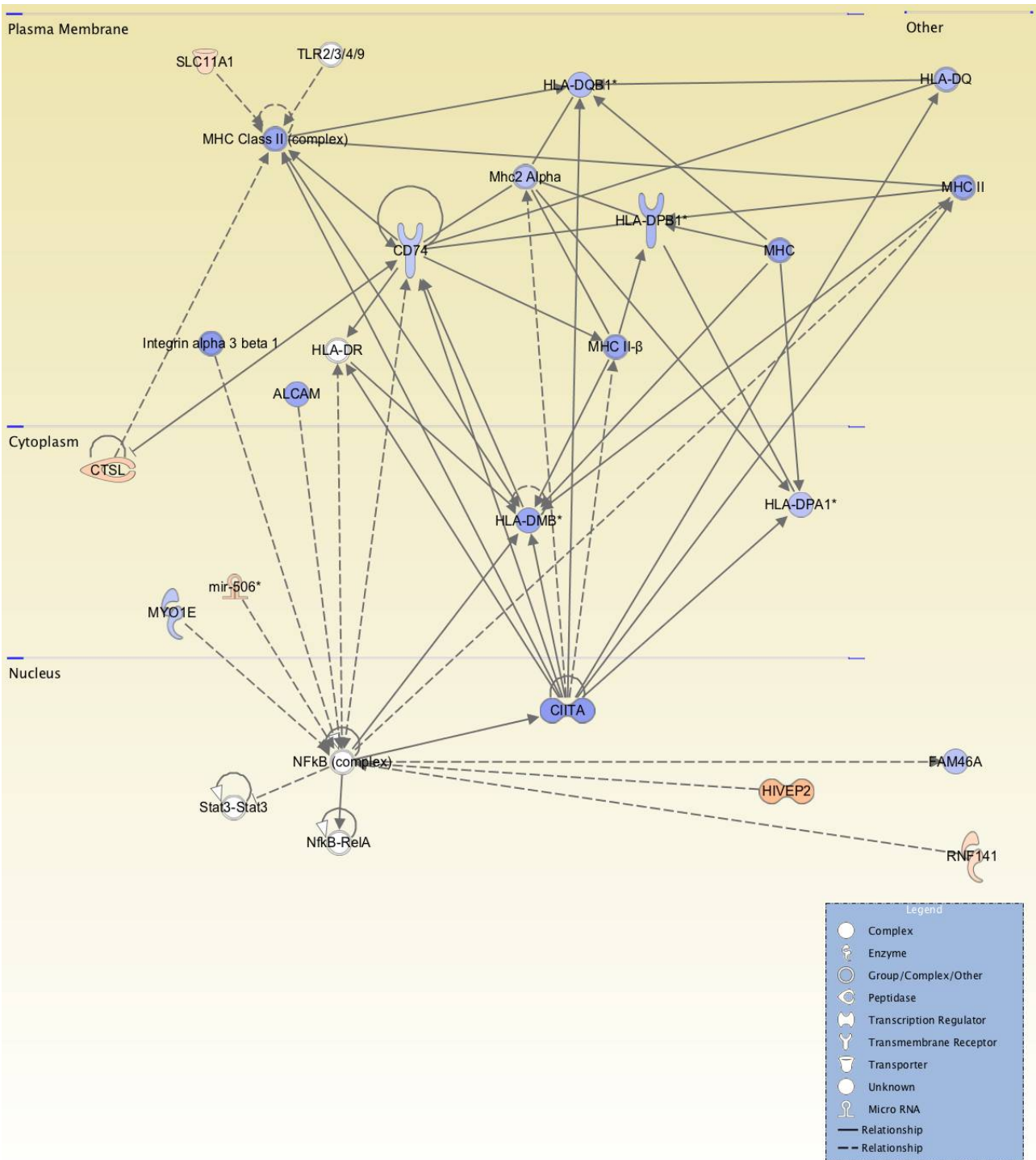


Figure 4.10 MSCs downregulate MHC class II molecules

A gene network hub of MHC class II signalling constructed using the differentially expressed genes over-represented in the top 10 signalling pathways (listed in Figure 4.7), in the MSC-treated monocytes. Each gene is coloured according to their expression; orange indicates upregulated, blue indicates downregulated. The intensity of the colour indicates the level of gene expression. Each gene is organised based on where the gene product is located within the cell. The continuous line between genes represents a direct relationship between the genes and a dotted line represents an indirect relationship.

4.4 Discussion

Inflammation is a key factor involved in the development of diabetic complications. Monocytes and their differentiated tissue progeny, macrophages, are the principle cell types that govern disease pathogenesis and mediate tissue repair (251, 304, 320, 321). Peripheral blood monocytes and macrophages are armed with an extensive repertoire of cell surface markers and exhibit remarkable plasticity, whereby the surrounding cytokine milieu plays a central role in determining their differentiation fate and subsequent activation/polarisation state (322). In addition to monocyte polarity, monocyte-derived macrophages can also be classified into pro-inflammatory and anti-inflammatory subsets known as classical 'M1' and alternative 'M2' macrophages, respectively (322). Manipulating monocyte phenotype in order to reduce inflammation and subsequently insulin resistance could be a promising therapeutic option for type 2 diabetic patients. Here we explore the ability of MSCs to alter the phenotype of monocytes isolated from control and type 2 diabetic subjects.

The current study demonstrated that healthy control subjects had a higher proportion of classical monocytes in circulation, while type 2 diabetic patients had significantly higher proportions of the intermediate and non-classical 'pro-inflammatory' monocyte subsets. This correlates with other studies that have reported that T2D is characterised by increased numbers of circulating monocytes, which display a pro-inflammatory profile and secrete the pro-inflammatory cytokines IL-6, IL-8, TNF- α and IL-1 β (87, 88, 323). In rodents it has been demonstrated that these pro-inflammatory cytokines induce insulin resistance and blocking these cytokines reverses this phenomenon (324-326). Furthermore, monocytes from diabetic patients have demonstrated impaired functionality, involving chemotaxis and phagocytosis (327, 328).

The present study reports that soluble factors produced by MSCs promoted the growth of the T2D monocytes *in vitro*, significantly upregulating monocyte CD14 and CD16 expression

whilst downregulating the HLA-DR expression on both T2D and control monocytes. It is well established that MSCs possess immunomodulatory properties, mediated through their ability to secrete a plethora of growth factors (152). However, this phenomenon is more profound in an inflammatory environment compared to steady state conditions, whereby the MSCs' immunosuppressive properties are primed by inflammatory stimuli (329, 330). Indeed, the current study demonstrated more pronounced immunomodulatory effects of MSCs following co-culture with T2D monocytes. Moreover, the finding that MSCs have the capacity to modulate monocyte phenotype, are in accordance with other studies that have demonstrated immunomodulatory abilities (331, 332). Rocher et al. (331) recently reported that MSCs impair the differentiation of CD14⁺⁺CD16⁻CD64⁺ classical monocytes, from mixed leukocyte reactions, into CD14⁺⁺CD16⁺CD64⁺⁺ intermediate monocytes with decreased levels of MHC class II expression. In addition, Cutler et al. (332) revealed that MSCs decreased the expression of HLA-DR and increased CD14 expression on monocytes in non-activated and alloantigen activated PBMC cultures. These cells also had increased CD206 expression, a marker associated with an anti-inflammatory M2 macrophage phenotype. Furthermore, these findings could be replicated using a Transwell co-culture system or the MSC-conditioned medium alone, indicating the effects were mediated by the MSC-derived soluble factors (332). However, the precise mechanisms in which these MSC-derived soluble factors modulate monocyte phenotype remain to be fully elucidated.

Transcriptional profiling of the monocytes further revealed that MSC treatment significantly altered the expression of several genes associated with the 'classical' monocyte phenotype, whilst downregulating the non-classical associated molecules *ITGAL* and *SPN*, indicating that MSCs impede the differentiation of the monocytes.

There is growing awareness that a shift in macrophage polarisation can resolve inflammation and mediate wound healing. Furthermore, the deregulation of macrophage polarisation contributes to the development of various inflammatory diseases (138, 219, 333, 334). The

present study demonstrated that MSCs upregulated several genes associated with an M2 phenotype, including the cytokines *IL10*, *IGF1* and *VEGF*, known for their potent anti-inflammatory and regenerative abilities, as well as their capacity to protect against diabetes in both mice and humans (335-337). For example, Hong et al. (335) demonstrated that the muscle-specific over-expression of IL-10 in mice, on a high-fat diet, increased insulin sensitivity and exhibited a reduced inflammatory response compared to wild-type control mice. In humans, low IL-10 production was associated with increased plasma glucose, HbA1c and the prevalence of T2D (336). Impaired glucose tolerance and insulin sensitivity also correlated inversely to serum IL-10 levels, indicating that IL-10 may have a protective role in T2D (337). In addition, several studies have demonstrated that IGF-1 administration can improve glycaemic control in T2D patients by enhancing insulin sensitivity and reducing hyperglycaemia and HbA1c (338-340). Further, macrophages expressing IGF-1 and IL-10 have both been shown to dampen inflammation and promote extracellular matrix remodelling and repair of damaged kidneys (138, 219). During the early stages of diabetic nephropathy, elevated expression of VEGF is present within the kidney. However, as the disease advances, VEGF expression and activity declines (341, 342). In a mouse model of type 1 diabetes, the deletion of VEGF-A from glomerular podocytes promoted glomerular injury and resulted in reduced renal function (343). In humans, Tumlin et al. (344) demonstrated that in patients with advanced diabetic nephropathy, a reduction in proteinuria and stabilisation of renal function correlated with increased levels of urinary VEGF. Therefore, in a setting of end-stage diabetic nephropathy, VEGF is beneficial. MSCs also upregulated several M2-associated scavenger receptor genes, which are key players that mediate the remodelling functions of M2 macrophages following tissue damage. There was an increase in *MMP-9* and *MMP-19*, which in the kidney also contributes to extracellular matrix degradation and the attenuation of fibrosis (315, 345). Interestingly, MSCs enhanced *PTGER2* gene expression in the monocytes. It has been demonstrated that MSCs secrete PGE₂, which acts via the EP2 receptor on monocytes, encoded by *PTGER2*. This secreted prostaglandin induces IL-10 production, resulting in immunosuppression (332, 346).

Additionally, *PTGS2*, which also induces the production of PGE₂, was upregulated in the MSC-treated monocytes. Recent studies have shown that it is the MSC-derived PGE₂ that induces macrophage polarisation towards an M2 phenotype (208, 209, 217, 218). However, this effect is lost as a result of PGE₂ ablation or blocking of the PGE₂ receptors, EP2 or EP4 (209, 217). The PTGER2-IL10 signalling pathway was upregulated in the MSC-treated monocytes in this study, indicating that the MSCs were promoting an M2-like gene expression profile in the monocytes. Further, this polarisation was achieved regardless of whether the monocytes were from diabetic patients or healthy controls.

Monocytes and monocyte-derived macrophages are the main inflammatory cells found within kidneys of diabetic patients and animals, with the infiltration and accumulation of these cells being associated with the disease pathogenesis. However, several studies have recently demonstrated that a shift in polarisation state can block the pathological effects of the pro-inflammatory M1 macrophage. Specifically, M2-derived IL-10 can inhibit the pathological effects of TNF- α induced insulin resistance in adipocytes (347). In an experimental model of T2D, the reduction of M1 macrophages and their pro-inflammatory cytokines along with the enhancement of the M2 phenotype resulted in improved insulin signalling and glycaemic control (348). Fadini et al. (334) reported that T2D patients have an imbalanced M1/M2 ratio, which was attributable to a reduction in M2 macrophages. This imbalance directly correlated to waist circumference, HbA1c and DN.

Emerging studies have demonstrated that MSCs are capable of improving β -cell function and consequently insulin sensitivity, ameliorating hyperglycaemia and glomerulosclerosis leading to significantly improved renal function in type 1 and 2 diabetic rodents (162, 316, 349, 350). The administration of MSCs to rats with DN significantly decreased glomerulosclerosis and the expression of fibronectin and collagen I, the main components of the extracellular matrix. In addition, MSCs significantly reduced urinary albumin excretion and creatinine clearance, indicating improved renal function. Blood glucose levels were also significantly

reduced (316, 351). In a phase I clinical trial, three intravenous infusions of MSCs administered one month apart, to patients with T2D, reduced blood glucose levels and Hb1Ac, increased C-peptide and insulin secretion, indicative of an improvement in β -cell function, and improved renal function (310). Together, these studies highlight the ability of MSCs to target the many facets of this multifactorial disease. Their capability to reduce fibrosis, repair damaged tissue and improve renal function make MSCs a prime candidate for a cell-based therapy to treat forms of kidney disease. The additional immunosuppressive properties, which can dampen the inflammatory environment resulting in a downstream improvement in glycaemic control, make them an ideal therapy for T2D patients.

In summary, we report that monocytes from type 2 diabetic patients show different phenotypes to control cells, based on their CD14 and CD16 expression. MSC-derived factors impair the maturation of human monocytes isolated from healthy and type 2 diabetic subjects and promote the polarisation towards a classical, M2 phenotype, as shown by their gene expression profile. As inflammation is associated with the pathogenesis of T2D, reducing and controlling inflammation in these patients is vital. Therefore, manipulating monocyte phenotype and the pro-inflammatory state of T2D patients with the use of MSCs could serve as a useful tool for the development of a novel therapeutic option for patients with T2D.

CHAPTER 5

General Discussion

Chapter 5: General Discussion

The incidence of T2D is dramatically escalating, and with it, the number of patients suffering from kidney disease. Currently, the only treatment options for ESRD include two types of renal replacement therapy: dialysis and transplantation. However, both of these treatments place a significant burden on patient quality of life and healthcare systems. Therefore, there is an urgent need to develop novel therapies for kidney disease patients. MSCs show promise as a cell-based therapy for kidney disease due to their potent immunomodulatory and tissue regenerative properties. This thesis examined the therapeutic ability of MSCs to induce renal repair, using the acute experimental mouse model of renal IR injury. As monocytes and macrophages are the principal immune cells that drive kidney regeneration, the ability of MSCs to modulate monocyte and macrophage polarisation towards a wound-healing phenotype was assessed. In Chapter 2, MSCs were characterised to ensure they conformed to the minimal criteria established by Dominici et al. (150) and the experimental feasibility of using human-derived MSCs in mice was also confirmed. Chapter 3 described the homing patterns of MSCs following administration to mice with IR injury and provided important insight into the MSCs ability to govern renal remodelling and repair. Moreover, it was demonstrated that MSCs could influence macrophage phenotype towards an M2 polarisation state through paracrine mechanisms. Finally, results in Chapter 5 revealed that MSCs retain the ability to modulate the genetic profile and phenotype of monocytes isolated from a chronic inflammatory setting, patients with T2D and ESRD.

The field of MSC research remains ever expanding, since their initial discovery over four decades ago. Friedenstein and colleagues originally isolated MSCs from the bone marrow and proposed that the primary role of these cells was to act as a supportive stroma for HSCs (232). For this reason, the first clinical trial using MSCs exploited this function to promote haematopoietic engraftment in GvHD patients (168). However, MSCs have since been isolated from almost all postnatal and perinatal tissues and possess the same phenotype and

multilineage differentiation potentials as their bone marrow-derived counterparts (156, 352). Additionally, MSCs have demonstrated the ability to induce organ regeneration in a diverse range of applications. Thus, the MSCs' protective mechanisms were re-evaluated and as a consequence, our understanding of their regenerative capabilities has evolved.

In the early 2000s, several publications in the non-bone marrow transplant field suggested that MSCs could exert therapeutic effects through their ability to transdifferentiate, not only into cells of the mesodermal lineage but also endodermal and ectodermal lineages, including cardiomyocytes, lung epithelium, hepatocytes, neurons and pancreatic islets (164, 353-356). Morigi et al. (142) and Herrera et al. (172) reported that following AKI, exogenously administered MSCs integrated within the damaged kidney and transdifferentiated into kidney tubular epithelium, consequently resulting in structural repair and improved function. However, in follow-up studies it was confirmed that only 2 – 2.5% of injected MSCs had differentiated into renal epithelium, as opposed to a previously reported 22% (172, 173). This transdifferentiation phenomenon has been widely disproven through the use of more sensitive techniques (357). Therefore, it is now accepted that MSC transdifferentiation is an extremely rare event and not of any clinical significance.

Under normal homeostasis, intravenous administration of *ex vivo* culture expanded MSCs to rodents results in the cells being trapped in the lungs. Following injury or inflammation, however, MSCs have the capacity to migrate along the inflammatory gradient, preferentially trafficking to sites of tissue damage. Chapter 3 of this thesis used a sensitive *in vivo* cell tracing system to confirm the pattern of cell migration. Following the intravenous administration of MSCs to sham-operated mice, the MSCs remained in the lungs transiently before being systemically cleared. However, when administered to mice with unilateral IR injury, the MSCs selectively homed to the injured kidney. Additionally, following bilateral IR injury, the MSCs homed to both kidneys where they remained for up to 3 days. Interestingly, studies using a range of disease models have shown that MSCs do not need to be present at

the injury site in order to exert their therapeutic effects (282, 358, 359). Further, the administration of MSC-conditioned medium alone is able to promote partial tissue regeneration (174, 360-363). It is now well established that MSCs secrete a myriad of soluble factors that have angiogenic, mitogenic, anti-apoptotic and anti-inflammatory properties and it is these trophic factors that modulate the microenvironment to one allowing regeneration and repair [for review; (277)].

Although MSCs preferentially home to inflammation, a few recent studies have shown that at times, even following injury, MSCs remain trapped in the lungs of mice following intravenous administration (282, 358, 359). This phenomenon is known as the pulmonary first-pass effect (364). The present study also observed this pattern of cell infiltration in some mice that had received kidney IR injury (refer to Chapter 3). Interestingly, however, in the current study the MSCs were able to escape entrapment from the lungs over time and retained the ability to migrate to the injured kidney. The reason why MSCs get trapped in the lung is a controversial topic and is yet to be fully elucidated, with proposed reasons previously discussed in Chapter 3. Future studies are required to determine why MSC lung entrapment occurs and whether the therapeutic efficiency of the MSCs is greater when the cells home to the site of injury, in comparison to the MSCs exerting paracrine effects systemically from the lung. If the efficiency of MSCs is enhanced following homing to the injury site, the route of administration, whether it is local, intravenous or intraarterial, needs to be carefully considered and tailored to each disease in order to achieve maximum therapeutic benefit. Arterial delivery has been demonstrated to result in enhanced MSC engraftment at the injury site, in comparison to intravenous administration, and this is most probably due to the MSCs bypassing the pulmonary first-pass (280). Additionally, methods to enhance site-specific delivery, such as vasodilators, may also need to be employed in some circumstances to improve targeted engraftment (365). Cell dose is another contributing factor that can influence lung entrapment. Delivery of a high number or concentration of MSCs can result in an increased chance of entrapment in the lung capillary bed, i.e.

pulmonary embolism, resulting in death (366). The intravenous delivery of 1.0×10^7 MSCs/ml or above to mice has proven to be fatal (366). As outlined in Chapter 2, we found a single intravenous infusion of 1×10^6 human MSCs (re-suspended in 125 μ l of PBS) to mice with IR injury, a safe and effective dose.

It has previously been shown that MSCs only engraft transiently and further, sustained engraftment is not required for the long-term therapeutic benefits (210, 222, 282, 367). The short-term engraftment of MSCs was also recently confirmed in patients who had received allogeneic MSC infusion, through the analysis of autopsy tissue samples (368). PCR analysis of tissue samples from 18 patients who had received MSCs within a year prior to their death revealed the presence of MSC donor-derived DNA correlated inversely to the time of MSC infusion. The authors therefore concluded that MSCs exert their therapeutic effects through a 'hit and run' mechanism. Results in Chapter 3 also revealed that long-term persistence of the MSCs is not required for kidney repair. Following infusion into mice with acute ischaemic injury, the MSCs localised in the injured kidney/s within 1 hour post-administration, where they promoted structural regeneration and functional recovery by 7 days post-administration. Interestingly, though, the MSCs were not detected in these animals, with the use of bioluminescence imaging, at this day 7 time-point. Our studies utilised a xenogeneic transplant model, therefore the possibility remains that the host's immune system detected and cleared the MSCs by this time-point. Human MSCs are increasingly being used in experimental mouse models, as murine-derived MSCs are extremely unstable *ex vivo*, in contrast to human MSCs that do not exhibit this instability (as demonstrated in Chapter 2). Transplantation of mismatched MSCs across MHC barriers was initially carried out because of the originally reported 'immune privileged' status of MSCs, i.e. low expression of MHC class I and lack of MHC class II expression (153). However, recent findings revealed that following the *in vitro* exposure to the inflammatory cytokine, IFN- γ , MHC class I and II can be upregulated on these cells (154). Moreover, *in vivo* studies have now demonstrated that although the allogeneic transplantation of MSCs into

immunocompetent hosts is not as immunogenic as unmatched fibroblasts, for example, which are rapidly rejected, MSCs are not completely 'immune privileged' and are capable of inducing immune memory (369). Therefore, it has been suggested that MSCs are not completely immune privileged but rather immune evasive (370). Regardless, a growing number of clinical trials have utilised allogeneic MSCs and results have consistently shown transplantation to be safe, with no adverse events reported to date and promising therapeutic benefits (371). Further, clinical trials administering repeated doses of allogeneic MSCs have also been free of any adverse events (310, 372-374). Therefore, future *in vivo* studies directly comparing the immunogenicity and therapeutic efficacy of autologous, allogeneic and xenogeneic MSCs are warranted to gain a better understanding of their true immune status. Furthermore, routine measurements of anti-donor antibodies should be made mandatory in clinical trials in order to determine the effect HLA mismatched MSCs are having on the host's immune system. It was originally proposed that a large bank of allogeneic MSCs from a universal donor could be used in the clinic. This would be of benefit in some clinical scenarios, such as myocardial infarction, stroke or renal IR injury, as generating sufficient numbers of autologous MSCs in such settings would be impractical/impossible. Additionally, customised MSC therapy would be substantially more expensive. However, an optimal approach may be to employ the same system that is used by the blood bank, where a range of donor cells with a diversity of HLA antigens are stored and available for use when required. This cell banking strategy could also potentially decrease the chance of patient sensitisation, prolong MSC persistence in the host and reduce the chances of rejection by the recipient's immune system. This would be of particular importance in a chronic disease setting where prolonging the presence of MSCs and delivering multiple injections of MSCs would most likely be required in order to achieve long-term therapeutic benefits.

Regardless of aetiology, kidney damage results in the infiltration of monocytes and monocyte-derived macrophages that accumulate within the damaged organ. The functional

polarisation state adopted by these infiltrating cells is primarily dependent on the kidney microenvironment. It is now established that monocytes and macrophages are highly heterogeneous and can play both pathogenic and protective roles in acute and chronic kidney disease (108). Therefore, modulating the local kidney environment to influence a reparative monocyte and macrophage phenotype would be of great benefit for kidney disease patients. As MSCs secrete immunosuppressive factors and have previously been shown to modulate the phenotype and effector functions of T-, B-, NK and dendritic cells, we hypothesised that MSCs could influence monocytes and macrophages to adopt an M2 'renoprotective' phenotype. Using an *in vitro* co-culture system, MSCs were found to have the capacity to enhance M2-associated reparative macrophage genes in both M1 and M2 polarised macrophage subsets, through the release of soluble factors. Moreover, gene expression profiling revealed the MSCs retained the ability to polarise monocytes, isolated from a chronic inflammatory setting, i.e. type 2 diabetic patients with ESRD, towards an M2 phenotype, through this same mechanism. Future studies using RT-time PCR or *in situ* hybridisation should be used to validate these gene expression findings and immunohistochemistry or FACS could be utilised to confirm protein expression in these cells. During the course of these studies, Li et al. (219) also demonstrated that MSCs mediated renal regeneration and repair through their ability to polarise macrophages towards an M2 phenotype. Interestingly, these authors showed that MSC-mediated repair was lost when macrophages were depleted 24 hours post-IR.

The focus of future studies will be to delineate the cross-talk that occurs between the MSCs and other cells within the injured kidney and the specific signals that trigger this communication. A key aspect will be to gain insight into the mechanisms by which MSCs direct monocytes and macrophages to adopt an anti-inflammatory, wound healing activation state *in vivo*. The study carried out by Li and colleagues utilised the clodronate liposome macrophage depletion method to demonstrate MSCs mediate renal repair through macrophages (219). It has previously been shown that the clodronate liposome macrophage

depletion method does not effectively deplete circulating monocytes and renal macrophages (375). Notably, CD206⁺ macrophages, i.e. macrophages of the M2 subset, are preserved when this method is used. This is in contrast to diphtheria toxin-mediated monocyte and macrophage depletion, using CD11b diphtheria toxin receptor transgenic mice (375). Therefore, future studies should utilise this monocyte/macrophage depletion method to determine the true effect depletion is having on MSC-mediated repair. Screening of plasma cytokine concentrations in control and MSC-treated animals would also help determine key soluble factors that may be driving kidney repair in this setting. Additionally, long-term studies in chronic renal disease models will determine the prolonged effects of MSC treatment on macrophage populations, the development of fibrosis and renal function.

Within the clinic, IR injury and immune-mediated renal damage following kidney transplantation are inevitable events that greatly impact the functioning of the kidney graft. Delivery of MSCs may aid in mitigating these side effects of organ transplantation and promote graft survival through their ability to induce immune tolerance as well as tissue repair. To date, several clinical trials using autologous or allogeneic MSCs in kidney transplantation have been completed or are underway [see www.clinicaltrials.gov; for review see (374)]. Preliminary results have been promising thus far with MSC treatment improving graft survival and function, lowering the level of immunosuppression required, decreasing the risk of opportunistic infections and reducing rejection (309, 311, 312, 372, 373, 376, 377). Preliminary results from a phase I clinical trial showed that the delivery of allogeneic MSCs to patients undergoing coronary artery bypass or valve repair, who were at high risk of developing AKI, reduced their post-operative length of stay and the development of AKI (171). These positive results have enabled a phase II multicentre clinical trial in cardiac surgery patients who are at risk of AKI (378). Phase I and II clinical trials using MSCs to treat refractory lupus nephritis have also resulted in the recovery and stabilisation of renal function (379-384). A phase I-II randomised controlled clinical trial is currently underway, investigating the safety and efficacy of treating patients with type 2 diabetes and diabetic

nephropathy (CKD stage 3b-4) with allogeneic MSCs (single intravenous infusion; www.clinicaltrials.gov, NCT01843387). Future work following on from the present studies will analyse the phenotype of peripheral blood monocytes from these MSC and placebo-treated patients prior to treatment, 48 to 72 hours post-treatment and 12 weeks post-treatment, in order to determine the short-term and long-term effects of MSC treatment on the profile of circulating monocytes. Genome-wide microarray profiling and FACS analysis will once again be utilised to analyse the gene and protein expression of these isolated cells in order to help determine the surface markers and secreted proteins that are involved. The results of these future studies will provide beneficial insight into the relationship between MSC treatment and the monocyte profile – indicative of the M1/M2 macrophage balance, renal function and the severity of kidney disease.

Conclusion

More than 40 years since the discovery of MSCs, the field of MSC research has rapidly expanded due to their potential benefit in a broad range of clinical applications, yet fundamental questions regarding their mechanisms of action remain unanswered. Nevertheless, several clinical trials using both autologous and allogeneic MSCs have demonstrated safety, efficacy and therapeutic benefits thus far. However, additional studies are required to detail the long-term safety and immunogenicity of MSCs, in order to achieve maximum therapeutic value. Additionally, factors concerning the effectiveness of MSC-based therapy, such as autologous versus allogeneic source, route and timing of administration, dose, and the status of the patient's immune system will have to be considered when tailoring therapies for individual patients in each disease setting.

Undeniably, MSCs hold great potential as a therapeutic option for patients with kidney disease as they have the capacity to target multiple pathophysiological aspects of the disease simultaneously. Therefore, all of these factors need to be carefully considered when designing clinical trials in order to achieve the most effective results. Additionally, it is crucial there is collaboration between researchers and clinicians, as the information gained from both the bench and bedside will together achieve the greatest progress in the field, ultimately producing an improved and better-targeted treatment for kidney disease patients.

REFERENCES

References

1. Munshi R, Hsu C, Himmelfarb J. Advances in understanding ischemic acute kidney injury. *BMC Medicine*. 2011;9(1):11.
2. Nordin BE, Peacock M. Role of kidney in regulation of plasma-calcium. *Lancet*. 1969;2(7633):1280–1283.
3. Wadei HM, Textor SC. The role of the kidney in regulating arterial blood pressure. *Nat Rev Nephrol*. 2012;8(10):602–609.
4. Dunn A, Lo V, Donnelly S. The role of the kidney in blood volume regulation: the kidney as a regulator of the hematocrit. *Am J Med Sci*. 2007;334(1):65–71.
5. Bover J, Cozzolino M. Mineral and bone disorders in chronic kidney disease and end-stage renal disease patients: new insights into vitamin D receptor activation. *Kidney Int Suppl*. 2011;
6. Costantini F, Kopan R. Patterning a complex organ: branching morphogenesis and nephron segmentation in kidney development. *Dev Cell*. 2010;18(5):698–712.
7. Little MH. Regrow or Repair: Potential Regenerative Therapies for the Kidney. *Journal of the American Society of Nephrology*. 2006;17(9):2390–2401.
8. Puelles VG et al. Glomerular number and size variability and risk for kidney disease. *Curr Opin Nephrol Hypertens*. 2011;20(1):7–15.
9. Couser WG, Remuzzi G, Mendis S, Tonelli M. The contribution of chronic kidney disease to the global burden of major noncommunicable diseases. *Kidney Int*. 2011;80(12):1258–1270.
10. Chronic Kidney Disease (CKD). Management in General Practice (2nd edition). *Kidney Health Australia, Melbourne*. 2012: 1–44.
11. International Diabetes Federation. *IDF Diabetes Atlas, 6th edn*. 2013: 1–160.
12. Australian Institute of Health and Welfare. Projections of the incidence of treated end-stage kidney disease in Australia Cat. no. PHE 150. Canberra: AIHW. 2011: 1–72.
13. McDonald S, Clayton P, Hurst K. ANZDATA Registry Report 2012. *Australian and New Zealand Dialysis and Transplant Registry, Adelaide, South Australia*. 2013: 1–235.
14. U.S. Renal Data System (USRDS). 2013 Annual Data Report: Atlas of Chronic Kidney Disease in the United States. *National Institutes of Health, National Institute of Diabetes and Digestive and Kidney Diseases, Bethesda, MD*. 2013: 1–148.
15. Australian Institute of Health and Welfare. Dialysis and kidney transplantation in Australia: 1991-2010. Cat. no. PHE 162. Canberra: AIHW. 2012: 1–59.
16. McDonald S, Leonie E, Brian L. ANZDATA Registry Report 2010. *Australian and New Zealand Dialysis and Transplant Registry, Adelaide, South Australia*. 2010: 1–214.
17. Cass A et al. The economic impact of end-stage kidney disease in Australia: projections to

2020. *Kidney Health Australia*. 2010;

18. U.S. Renal Data System (USRDS). 2013 Annual Data Report: Atlas of End-Stage Renal Disease in the United States. *National Institutes of Health, National Institute of Diabetes and Digestive and Kidney Diseases, Bethesda, MD*. 2013: 1–326.

19. Kramer A et al. Renal replacement therapy in Europe—a summary of the 2010 ERA-EDTA Registry Annual Report. *Clin Kidney J*. 2013;6(1):105–115.

20. Is kidney disease really such an important issue in Europe? *European kidney health alliance*. 2012: 1–3.

21. Stauffer ME, Fan T. Prevalence of anemia in chronic kidney disease in the United States. *PLoS ONE*. 2014;9(1):e84943–e84943.

22. Mehta RL et al. Acute Kidney Injury Network: report of an initiative to improve outcomes in acute kidney injury. *Crit Care*. 2007;11(2):R31.

23. Case J, Khan S, Khalid R, Khan A. Epidemiology of Acute Kidney Injury in the Intensive Care Unit. *Crit Care Res Pract*. 2013;2013(4):1–9.

24. Rosner MH. Acute kidney injury in the elderly. *Clin Geriatr Med*. 2013;29(3):565–578.

25. Hsu CW, Symons JM. Acute kidney injury: can we improve prognosis? *Pediatr Nephrol*. 2010;25(12):2401–2412.

26. Thadhani R, Pascual M, Bonventre JV. Acute renal failure. *N Engl J Med*. 1996;:1–13.

27. Tsagalis G. Update of acute kidney injury: intensive care nephrology. *Hippokratia*. 2010;15(Suppl 1):53–68.

28. Pathophysiology review: acute tubular necrosis. *Nursing*. 2010;40(4):46–47.

29. Arany I, Safirstein RL. Cisplatin nephrotoxicity. *Semin Nephrol*. 2003;23(5):460–464.

30. Goldenberg I, Matetzky S. Nephropathy induced by contrast media: pathogenesis, risk factors and preventive strategies. *CMAJ*. 2005;172(11):1461–1471.

31. Lopez-Novoa JM, Quiros Y, Vicente L, Morales AI, Lopez-Hernandez FJ. New insights into the mechanism of aminoglycoside nephrotoxicity: an integrative point of view. *Kidney Int*. 2010;79(1):33–45.

32. Uchino S et al. Acute renal failure in critically ill patients: a multinational, multicenter study. *JAMA*. 2005;294(7):813–818.

33. Bonventre JV, Yang L. Cellular pathophysiology of ischemic acute kidney injury. *J Clin Invest*. 2011;121(11):4210–4221.

34. Lote CJ, Harper L, Savage CO. Mechanisms of acute renal failure. *Br J Anaesth*. 1996;77(1):82–89.

35. Sharfuddin AA, Molitoris BA. Pathophysiology of ischemic acute kidney injury. *Nat Rev Nephrol*. 2011;7(4):189–200.

36. Wei Q, Dong Z. Mouse model of ischemic acute kidney injury: technical notes and tricks. *Am J Renal Physiol*. 2012;303(11):F1487–94.
37. Kennedy SE, Erlich JH. Murine renal ischaemia-reperfusion injury. *Nephrology (Carlton)*. 2008;13(5):390–396.
38. Liu KD, Brakeman PR. Renal repair and recovery. *Crit Care Med*. 2008;36(4 Suppl):S187–92.
39. Rosen S, Heyman SN. Difficulties in understanding human “acute tubular necrosis”: limited data and flawed animal models. *Kidney Int*. 2001;60(4):1220–1224.
40. Liu KD. Molecular mechanisms of recovery from acute renal failure. *Crit Care Med*. 2003;31(8):S572–S581.
41. Kellerman PS, Clark RA, Hoilien CA, Linas SL, Molitoris BA. Role of microfilaments in maintenance of proximal tubule structural and functional integrity. *Am J Physiol*. 1990;259(2 Pt 2):F279–F285.
42. Molitoris BA, Leiser J, Wagner MC. Role of the actin cytoskeleton in ischemia-induced cell injury and repair. *Pediatr Nephrol*. 1996;11(6):761–767.
43. Zuk A, Bonventre JV, Brown D, Matlin KS. Polarity, integrin, and extracellular matrix dynamics in the postischemic rat kidney. *Am J Physiol*. 1998;275(3 Pt 1):C711–31.
44. Bonventre JV. Kidney injury molecule-1 (KIM-1): a urinary biomarker and much more. *Nephrol Dial Transplant*. 2009;24(11):3265–3268.
45. Lieberthal W, Koh JS, Levine JS. Necrosis and apoptosis in acute renal failure. *Semin Nephrol*. 1998;18(5):505–518.
46. Zuk A, Bonventre JV, Matlin KS. Expression of fibronectin splice variants in the postischemic rat kidney. *Am J Renal Physiol*. 2001;280(6):F1037–F1053.
47. Bonventre JV. Pathophysiology of AKI: injury and normal and abnormal repair. *Contrib Nephrol*. 2010;165:9–17.
48. Blanpain C, Horsley V, Fuchs E. Epithelial Stem Cells: Turning over New Leaves. *Cell Res*. 2007;128(3):445–458.
49. Blanpain C, Lowry WE, Geoghegan A, Polak L, Fuchs E. Self-Renewal, Multipotency, and the Existence of Two Cell Populations within an Epithelial Stem Cell Niche. *Cell Res*. 2004;118(5):635–648.
50. Bussolati B, Tetta C, Camussi G. Contribution of Stem Cells to Kidney Repair. *Am J Nephrol*. 2008;28(5):813–822.
51. Humphreys BD, Bonventre JV. Mesenchymal Stem Cells in Acute Kidney Injury. *Annu Rev Med*. 2008;59(1):311–325.
52. Roufosse C, Cook HT. Stem Cells and Renal Regeneration. *Nephron Exp Nephrol*. 2008;109(2):e39–e45.

53. Elger M et al. Nephrogenesis is induced by partial nephrectomy in the elasmobranch *Leucoraja erinacea*. *J Am Soc Nephrol*. 2003;14(6):1506–1518.
54. Cochrane AL et al. Renal structural and functional repair in a mouse model of reversal of ureteral obstruction. *J Am Soc Nephrol*. 2005;16(12):3623–3630.
55. Poulsom R et al. Bone marrow contributes to renal parenchymal turnover and regeneration. *J Pathol*. 2001;195(2):229–235.
56. Gupta S, Verfaillie C, Chmielewski D, Kim Y, Rosenberg ME. A role for extrarenal cells in the regeneration following acute renal failure. *Kidney Int*. 2002;62(4):1285–1290.
57. Lin F et al. Hematopoietic stem cells contribute to the regeneration of renal tubules after renal ischemia-reperfusion injury in mice. *J Am Soc Nephrol*. 2003;14(5):1188–1199.
58. Lin F, Moran A, Igarashi P. Intrarenal cells, not bone marrow–derived cells, are the major source for regeneration in postischemic kidney. *J Clin Invest*. 2005;115(7):1756–1764.
59. Duffield JS et al. Restoration of tubular epithelial cells during repair of the postischemic kidney occurs independently of bone marrow-derived stem cells. *J Clin Invest*. 2005;115(7):1743–1755.
60. Little MH, Bertram JF. Is there such a thing as a renal stem cell? *J Am Soc Nephrol*. 2009;20(10):2112–2117.
61. Appel D et al. Recruitment of podocytes from glomerular parietal epithelial cells. *J Am Soc Nephrol*. 2009;20(2):333–343.
62. Ronconi E et al. Regeneration of glomerular podocytes by human renal progenitors. *J Am Soc Nephrol*. 2009;20(2):322–332.
63. Sagrinati C et al. Isolation and characterization of multipotent progenitor cells from the Bowman's capsule of adult human kidneys. *J Am Soc Nephrol*. 2006;17(9):2443–2456.
64. Pruszak J, Ludwig W, Blak A, Alavian K, Isacson O. CD15, CD24, and CD29 define a surface biomarker code for neural lineage differentiation of stem cells. *Stem Cells*. 2009;27(12):2928–2940.
65. Shackleton M et al. Generation of a functional mammary gland from a single stem cell. *Nature*. 2006;439(7072):84–88.
66. Miraglia S et al. A novel five-transmembrane hematopoietic stem cell antigen: isolation, characterization, and molecular cloning. *Blood*. 1997;90(12):5013–5021.
67. Shmelkov SV et al. Cytokine preconditioning promotes codifferentiation of human fetal liver CD133+ stem cells into angiomyogenic tissue. *Circulation*. 2005;111(9):1175–1183.
68. Yin AH et al. AC133, a novel marker for human hematopoietic stem and progenitor cells. *Blood*. 1997;90(12):5002–5012.
69. Romagnani P. Toward the identification of a "renopoietic system"? *Stem Cells*. 2009;27(9):2247–2253.

70. Angelotti ML et al. Characterization of renal progenitors committed toward tubular lineage and their regenerative potential in renal tubular injury. *Stem Cells*. 2012;30(8):1714–1725.
71. Smeets B et al. Proximal tubular cells contain a phenotypically distinct, scattered cell population involved in tubular regeneration. *J Pathol*. 2013;229(5):645–659.
72. Wanner N et al. Unraveling the role of podocyte turnover in glomerular aging and injury. *J Am Soc Nephrol*. 2014;25(4):707–716.
73. Berger K et al. The regenerative potential of parietal epithelial cells in adult mice. *J Am Soc Nephrol*. 2014;25(4):693–705.
74. Hakrrouch S et al. Extensive podocyte loss triggers a rapid parietal epithelial cell response. *J Am Soc Nephrol*. 2014;25(5):927–938.
75. Oliver JA, Maarouf O, Cheema FH, Martens TP, Al-Awqati Q. The renal papilla is a niche for adult kidney stem cells. *J Clin Invest*. 2004;114(6):795–804.
76. Oliver JA et al. Proliferation and migration of label-retaining cells of the kidney papilla. *J Am Soc Nephrol*. 2009;20(11):2315–2327.
77. Humphreys BD et al. Intrinsic epithelial cells repair the kidney after injury. *Cell Stem Cell*. 2008;2(3):284–291.
78. Humphreys BD et al. Repair of injured proximal tubule does not involve specialized progenitors. *Proc Natl Acad Sci USA*. 2011;108(22):9226–9231.
79. Bonventre JV. Dedifferentiation and proliferation of surviving epithelial cells in acute renal failure. [Internet]. *J Am Soc Nephrol*. 2003;14 Suppl 1(90001):55S–61.
80. Witzgall R, Brown D, Schwarz C. Localization of proliferating cell nuclear antigen, vimentin, c-Fos, and clusterin in the postischemic kidney. Evidence for a heterogenous genetic response among nephron segments, and a large pool of mitotically active and dedifferentiated cells. *J Clin Invest*. 1994;93:2175–2188.
81. Abbate M, Brown D, Bonventre JV. Expression of NCAM recapitulates tubulogenic development in kidneys recovering from acute ischemia. *Am J Physiol*. 1999;277(3 Pt 2):F454–F463.
82. Imgrund M et al. Re-expression of the developmental gene Pax-2 during experimental acute tubular necrosis in mice. *Kidney Int*. 1999;56(4):1423–1431.
83. Berger K et al. Origin of regenerating tubular cells after acute kidney injury. *Proc Natl Acad Sci USA*. 2014;111(4):1533–1538.
84. Yang J, Zhang L, Yu C, Yang X-F, Wang H. Monocyte and macrophage differentiation: circulation inflammatory monocyte as biomarker for inflammatory diseases. *Biomark Res*. 2014;2(1):1.
85. Meuret G, Bammert J, Hoffmann G. Kinetics of human monocytopoiesis. *Blood*. 1974;44(6):801–816.

86. Heine GH et al. Monocyte subpopulations and cardiovascular risk in chronic kidney disease. *Nat Rev Nephrol.* 2012;8(6):362–369.
87. Yang M et al. Proinflammatory CD14+CD16+ monocytes are associated with microinflammation in patients with type 2 diabetes mellitus and diabetic nephropathy uremia. *Inflammation.* 2012;35(1):388–396.
88. Min D et al. Alterations in monocyte CD16 in association with diabetes complications. *Mediators Inflamm.* 2012;2012(649083):1–10.
89. Williams TM, Wise AF, Alikhan MA, Layton DS, Ricardo SD. Establishing the flow cytometric assessment of myeloid cells in kidney ischemia/reperfusion injury. *Cytometry A.* 2014;85(3):256–267.
90. Sunderkötter C et al. Subpopulations of mouse blood monocytes differ in maturation stage and inflammatory response. *J Immunol.* 2004;172(7):4410–4417.
91. Yona S et al. Fate mapping reveals origins and dynamics of monocytes and tissue macrophages under homeostasis. *Immunity.* 2013;38(1):79–91.
92. Auffray C et al. Monitoring of blood vessels and tissues by a population of monocytes with patrolling behavior. *Science.* 2007;317(5838):666–670.
93. Geissmann F, Jung S, Littman DR. Blood monocytes consist of two principal subsets with distinct migratory properties. *Immunity.* 2003;19(1):71–82.
94. Lin SL, Castaño AP, Nowlin BT, Lopher ML, Duffield JS. Bone marrow Ly6Chigh monocytes are selectively recruited to injured kidney and differentiate into functionally distinct populations. *J Immunol.* 2009;183(10):6733–6743.
95. Passlick B, Flieger D, Ziegler-Heitbrock HW. Identification and characterization of a novel monocyte subpopulation in human peripheral blood. *Blood.* 1989;74(7):2527–2534.
96. Ziegler-Heitbrock L et al. Nomenclature of monocytes and dendritic cells in blood. *Blood.* 2010;116(16):e74–80.
97. Cros J et al. Human CD14dim Monocytes Patrol and Sense Nucleic Acids and Viruses via TLR7 and TLR8 Receptors. *Immunity.* 2009;33(3):375–386.
98. Wong KL et al. Gene expression profiling reveals the defining features of the classical, intermediate, and nonclassical human monocyte subsets. *Blood.* 2011;118(5):e16–e31.
99. Ancuta P et al. Fractalkine preferentially mediates arrest and migration of CD16+ monocytes. *J Exp Med.* 2003;197(12):1701–1707.
100. Belge K-U et al. The proinflammatory CD14+CD16+DR++ monocytes are a major source of TNF. *J Immunol.* 2002;168(7):3536–3542.
101. Ziegler-Heitbrock L. The CD14+ CD16+ blood monocytes: their role in infection and inflammation. *J Leukoc Biol.* 2007;81(3):584–592.
102. Zawada AM et al. SuperSAGE evidence for CD14++CD16+ monocytes as a third monocyte subset. *Blood.* 2011;118(12):e50–61.

103. Wong KL et al. The three human monocyte subsets: implications for health and disease. *Immunol Res.* 2012;53(1-3):41–57.
104. Heine GH et al. CD14+ +CD16+ monocytes but not total monocyte numbers predict cardiovascular events in dialysis patients. *Kidney Int.* 2007;73(5):622–629.
105. Rogacev KS et al. CD14+ +CD16+ monocytes and cardiovascular outcome in patients with chronic kidney disease. *Eur Heart J.* 2011;32(1):84–92.
106. Kimmel PLP et al. Immunologic function and survival in hemodialysis patients. *Kidney Int.* 1998;54(1):236–244.
107. Malaponte G et al. IL-1beta, TNF-alpha and IL-6 release from monocytes in haemodialysis patients in relation to dialytic age. *Nephrol Dial Transplant.* 2002;17(11):1964–1970.
108. Cao Q, Wang Y, Harris DCH. Pathogenic and protective role of macrophages in kidney disease. *Am J Physiol Renal Physiol.* 2013;305(1):F3–F11.
109. Huen SC, Cantley LG. Macrophage-mediated injury and repair after ischemic kidney injury. *Pediatr Nephrol.* [published online ahead of print: January 19, 2014]; doi:10.1007/s00467-013-2726-y
110. Sica A, Mantovani A. Macrophage plasticity and polarization: in vivo veritas. *J Clin Invest.* 2012;122(3):787–795.
111. Nelson PJ et al. The Renal Mononuclear Phagocytic System. *J Am Soc Nephrol.* 2012;23(2):194–203.
112. Krausgruber T et al. IRF5 promotes inflammatory macrophage polarization and TH1-TH17 responses. *Nat Immunol.* 2011;12(3):231–238.
113. Williams TM, Little MH, Ricardo SD. Macrophages in Renal Development, Injury, and Repair. *Semin Nephrol.* 2010;30(3):255–267.
114. Mosser DM, Edwards JP. Exploring the full spectrum of macrophage activation. *Nat Rev Immunol.* 2008;8(12):958–969.
115. Martinez FO, Sica A, Mantovani A, Locati M. Macrophage activation and polarization. *Front Biosci.* 2008;13:453–461.
116. Gordon S, Martinez FO. Alternative Activation of Macrophages: Mechanism and Functions. *Immunity.* 2010;32(5):593–604.
117. Hesse M et al. Differential Regulation of Nitric Oxide Synthase-2 and Arginase-1 by Type 1/Type 2 Cytokines In Vivo: Granulomatous Pathology Is Shaped by the Pattern of l-Arginine Metabolism. *J Immunol.* 2001;
118. Lichtnekert J, Kawakami T, Parks WC, Duffield JS. Changes in macrophage phenotype as the immune response evolves. *Curr Opin Pharmacol.* 2013;13(4):555–564.
119. Fleming BD, Mosser DM. Regulatory macrophages: Setting the Threshold for Therapy. *Eur J Immunol.* 2011;41(9):2498–2502.

120. Moore KW, de Waal Malefyt R, Coffman RL, O'Garra A. Interleukin-10 and the interleukin-10 receptor. *Annu Rev Immunol*. 2001;19(1):683–765.
121. Jenkins JK, Malyak M, Arend WP. The effects of interleukin-10 on interleukin-1 receptor antagonist and interleukin-1 beta production in human monocytes and neutrophils. *Lymphokine Cytokine Res*. 1994;13(1):47–54.
122. Dickensheets HL, Donnelly RP. IFN-gamma and IL-10 inhibit induction of IL-1 receptor type I and type II gene expression by IL-4 and IL-13 in human monocytes. *J Immunol*. 1997;159(12):6226–6233.
123. Anderson CF, Mosser DM. Cutting Edge: Biasing Immune Responses by Directing Antigen to Macrophage Fcγ Receptors. *J Immunol*. 2002;
124. Edwards JP, Zhang X, Frauwirth KA, Mosser DM. Biochemical and functional characterization of three activated macrophage populations. *J Leukoc Biol*. 2006;80(6):1298–1307.
125. Ashcroft GS. Bidirectional regulation of macrophage function by TGF-beta. *Microbes Infect*. 1999;1(15):1275–1282.
126. Li L et al. The chemokine receptors CCR2 and CX3CR1 mediate monocyte/macrophage trafficking in kidney ischemia-reperfusion injury. *Kidney Int*. 2008;74(12):1526–1537.
127. Yu S-J, Oh D-J, Yu S-H. The investigation of macrophage infiltration in the early phase of ischemic acute renal failure in mice. *Korean J Intern Med*. 2008;23(2):64–71.
128. Li L, Okusa MD. Macrophages, dendritic cells, and kidney ischemia-reperfusion injury. *Semin Nephrol*. 2010;30(3):268–277.
129. Lee S et al. Distinct macrophage phenotypes contribute to kidney injury and repair. *J Am Soc Nephrol*. 2011;22(2):317–326.
130. Day YJ. Renal ischemia-reperfusion injury and adenosine 2A receptor-mediated tissue protection: role of macrophages. *Am J Physiol Renal Physiol*. 2004;288(4):F722–F731.
131. Jo SK. Macrophages contribute to the initiation of ischaemic acute renal failure in rats. *Nephrol Dial Transplant*. 2006;21(5):1231–1239.
132. Takada M, Nadeau KC, Shaw GD, Marquette KA, Tilney NL. The cytokine-adhesion molecule cascade in ischemia/reperfusion injury of the rat kidney. Inhibition by a soluble P-selectin ligand. *J Clin Invest*. 1997;99(11):2682–2690.
133. Lemay S, Rabb H, Postler G, Singh AK. Prominent and sustained up-regulation of gp130-signaling cytokines and the chemokine MIP-2 in murine renal ischemia-reperfusion injury. *Transplantation*. 2000;69(5):959–963.
134. Vinuesa E et al. Macrophage involvement in the kidney repair phase after ischaemia/reperfusion injury. *J Pathol*. 2007;214(1):104–113.
135. Lin SL et al. Macrophage Wnt7b is critical for kidney repair and regeneration. *Proc Natl Acad Sci USA*. 2010;107(9):4194–4199.

136. Isbel NM et al. Tubules are the major site of M-CSF production in experimental kidney disease: correlation with local macrophage proliferation. *Kidney Int.* 2001;60(2):614–625.
137. Menke J et al. CSF-1 signals directly to renal tubular epithelial cells to mediate repair in mice. *J Clin Invest.* 2009;119(8):2330–2342.
138. Alikhan MA et al. Colony-stimulating factor-1 promotes kidney growth and repair via alteration of macrophage responses. *Am J Pathol.* 2011;179(3):1243–1256.
139. Ricardo SD, van Goor H, Eddy AA. Macrophage diversity in renal injury and repair. *J Clin Invest.* 2008;118(11):3522–3530.
140. Friedenstein AJ, Chailakhyan RK, Latsinik NV, Panasyuk AF, Keiliss-Borok IV. Stromal cells responsible for transferring the microenvironment of the hemopoietic tissues. Cloning in vitro and retransplantation in vivo. *Transplantation.* 1974;17(4):331–340.
141. Friedenstein AJ, Petrakova KV, Kurolesova AI, Frolova GP. Heterotopic of bone marrow. Analysis of precursor cells for osteogenic and hematopoietic tissues. *Transplantation.* 1968;6(2):230–247.
142. Morigi M et al. Mesenchymal stem cells are renotropic, helping to repair the kidney and improve function in acute renal failure. *J Am Soc Nephrol.* 2004;15(7):1794–1804.
143. Uccelli A, Moretta L, Pistoia V. Immunoregulatory function of mesenchymal stem cells. *Eur J Immunol.* 2006;36(10):2566–2573.
144. Le Blanc K, Ringdén O. Immunomodulation by mesenchymal stem cells and clinical experience. *J Intern Med.* 2007;262(5):509–525.
145. Banfi A et al. Replicative aging and gene expression in long-term cultures of human bone marrow stromal cells. *Tissue Eng.* 2002;8(6):901–910.
146. Banfi A et al. Proliferation kinetics and differentiation potential of ex vivo expanded human bone marrow stromal cells: Implications for their use in cell therapy. *Exp Hematol.* 2000;28(6):707–715.
147. Javazon E. Mesenchymal stem cells: paradoxes of passaging. *Exp Hematol.* 2004;32(5):414–425.
148. Pittenger MF et al. Multilineage potential of adult human mesenchymal stem cells. *Science.* 1999;284(5411):143–147.
149. Tremain N et al. MicroSAGE analysis of 2,353 expressed genes in a single cell-derived colony of undifferentiated human mesenchymal stem cells reveals mRNAs of multiple cell lineages. *Stem Cells.* 2001;19(5):408–418.
150. Dominici M et al. Minimal criteria for defining multipotent mesenchymal stromal cells. The International Society for Cellular Therapy position statement. *Cytotherapy.* 2006;8(4):315–317.
151. Le Blanc K. Mesenchymal stromal cells: Tissue repair and immune modulation. *Cytotherapy.* 2006;8(6):559–561.

152. Uccelli A, Moretta L, Pistoia V. Mesenchymal stem cells in health and disease. *Nat Rev Immunol*. 2008;8(9):726–736.
153. Tse WT, Pendleton JD, Beyer WM, Egalka MC, Guinan EC. Suppression of allogeneic T-cell proliferation by human marrow stromal cells: implications in transplantation. *Transplantation*. 2003;75(3):389–397.
154. Le Blanc K, Tammik C, Rosendahl K, Zetterberg E, Ringden O. HLA expression and immunologic properties of differentiated and undifferentiated mesenchymal stem cells. *Exp Hematol*. 2003;31(10):890–896.
155. Erices A, Conget P, Minguell JJ. Mesenchymal progenitor cells in human umbilical cord blood. *Br J Haematol*. 2000;109(1):235–242.
156. da Silva Meirelles L, Chagastelles PC, Nardi NB. Mesenchymal stem cells reside in virtually all post-natal organs and tissues. *J Cell Sci*. 2006;119(11):2204–2213.
157. Reinders MEJ, Fibbe WE, Rabelink TJ. Multipotent mesenchymal stromal cell therapy in renal disease and kidney transplantation. *Nephrol Dial Transplant*. 2009;25(1):17–24.
158. Zuk PA et al. Human adipose tissue is a source of multipotent stem cells. *Mol Biol Cell*. 2002;13(12):4279–4295.
159. Yamaoka T, Mahara A. Cell rolling column in purification and differentiation analysis of stem cells. *React Funct Polym*. 2011;71(3):362–366.
160. Bartholomew A et al. Mesenchymal stem cells suppress lymphocyte proliferation in vitro and prolong skin graft survival in vivo. *Exp Hematol*. 2002;30(1):42–48.
161. Zappia E. Mesenchymal stem cells ameliorate experimental autoimmune encephalomyelitis inducing T-cell anergy. *Blood*. 2005;106(5):1755–1761.
162. Lee RH et al. Multipotent stromal cells from human marrow home to and promote repair of pancreatic islets and renal glomeruli in diabetic NOD/scid mice. *Proc Natl Acad Sci USA*. 2006;103(46):17438–17443.
163. Urbán VS et al. Mesenchymal stem cells cooperate with bone marrow cells in therapy of diabetes. *Stem Cells*. 2008;26(1):244–253.
164. Ortiz LA et al. Mesenchymal stem cell engraftment in lung is enhanced in response to bleomycin exposure and ameliorates its fibrotic effects. *Proc Natl Acad Sci USA*. 2003;100(14):8407–8411.
165. Ortiz LA et al. Interleukin 1 receptor antagonist mediates the antiinflammatory and antifibrotic effect of mesenchymal stem cells during lung injury. *Proc Natl Acad Sci USA*. 2007;104(26):11002–11007.
166. Orlic D et al. Bone marrow cells regenerate infarcted myocardium. *Nature*. 2001;410(6829):701–705.
167. Nagaya N et al. Intravenous administration of mesenchymal stem cells improves cardiac function in rats with acute myocardial infarction through angiogenesis and myogenesis. *Am J Physiol Heart Circ Physiol*. 2004;287(6):H2670–H2676.

168. Lazarus HM, Haynesworth SE, Gerson SL, Rosenthal NS, Caplan AI. Ex vivo expansion and subsequent infusion of human bone marrow-derived stromal progenitor cells (mesenchymal progenitor cells): implications for therapeutic use. *Bone Marrow Transplant.* 1995;16(4):557–564.
169. Koç ON et al. Rapid hematopoietic recovery after coinfusion of autologous-blood stem cells and culture-expanded marrow mesenchymal stem cells in advanced breast cancer patients receiving high-dose chemotherapy. *J Clin Oncol.* 2000;18(2):307–316.
170. Le Blanc K et al. Treatment of severe acute graft-versus-host disease with third party haploidentical mesenchymal stem cells. *The Lancet.* 2004;363(9419):1439–1441.
171. Tögel FE, Westenfelder C. Treatment of acute kidney injury with allogeneic mesenchymal stem cells: preclinical and initial clinical data. *Regenerative Nephrology.* San Diego, CA, USA: Academic Press; 2011:315-339.
172. Herrera MB et al. Mesenchymal stem cells contribute to the renal repair of acute tubular epithelial injury. *Int J Mol Med.* 2004;14(6):1035–1041.
173. Herrera MB et al. Exogenous mesenchymal stem cells localize to the kidney by means of CD44 following acute tubular injury. *Kidney Int.* 2007;72(4):430–441.
174. Bi B, Schmitt R, Israilova M, Nishio H, Cantley LG. Stromal Cells Protect against Acute Tubular Injury via an Endocrine Effect. *J Am Soc Nephrol.* 2007;18(9):2486–2496.
175. Chen Y et al. Hepatocyte growth factor modification promotes the amelioration effects of human umbilical cord mesenchymal stem cells on rat acute kidney injury. *Stem Cells Dev.* 2011;20(1):103–113.
176. Imberti B et al. Insulin-Like Growth Factor-1 Sustains Stem Cell Mediated Renal Repair. *J Am Soc Nephrol.* 2007;18(11):2921–2928.
177. Semedo P et al. Early modulation of inflammation by mesenchymal stem cell after acute kidney injury. *Int Immunopharmacol.* 2009;9(6):677–682.
178. Tögel F et al. Autologous and Allogeneic Marrow Stromal Cells Are Safe and Effective for the Treatment of Acute Kidney Injury. *Stem Cells Dev.* 2009;18(3):475–486.
179. Tögel F. Administered mesenchymal stem cells protect against ischemic acute renal failure through differentiation-independent mechanisms. *Am J Physiol Renal Physiol.* 2005;289(1):F31–F42.
180. Tögel F et al. Vasculotropic, paracrine actions of infused mesenchymal stem cells are important to the recovery from acute kidney injury. *Am J Physiol Renal Physiol.* 2007;292(5):F1626–F1635.
181. Yuan L et al. VEGF-modified human embryonic mesenchymal stem cell implantation enhances protection against cisplatin-induced acute kidney injury. *Am J Physiol Renal Physiol.* 2011;300(1):F207–F218.
182. Cao H et al. Mesenchymal stem cells derived from human umbilical cord ameliorate ischemia/reperfusion-induced acute renal failure in rats. *Biotechnol Lett.* 2010;32(5):725–732.

183. Eliopoulos N et al. Human marrow-derived mesenchymal stromal cells decrease cisplatin renotoxicity in vitro and in vivo and enhance survival of mice post-intraperitoneal injection. *Am J Physiol Renal Physiol*. 2010;299(6):F1288–98.
184. Hagiwara M, Shen B, Chao L, Chao J. Kallikrein-Modified Mesenchymal Stem Cell Implantation Provides Enhanced Protection Against Acute Ischemic Kidney Injury by Inhibiting Apoptosis and Inflammation. *Hum Gene Ther*. 2008;19(8):807–819.
185. Lange C et al. Administered mesenchymal stem cells enhance recovery from ischemia/reperfusion-induced acute renal failure in rats. *Kidney Int*. 2005;68(4):1613–1617.
186. Morigi M et al. Human bone marrow mesenchymal stem cells accelerate recovery of acute renal injury and prolong survival in mice. *Stem Cells*. 2008;26(8):2075–2082.
187. Semedo P et al. Mesenchymal Stem Cells Ameliorate Tissue Damages Triggered by Renal Ischemia and Reperfusion Injury. *Transplant Proc*. 2007;39(2):421–423.
188. Miller SB, Martin DR, Kissane J, Hammerman MR. Insulin-like growth factor I accelerates recovery from ischemic acute tubular necrosis in the rat. *Proc Natl Acad Sci USA*. 1992;89(24):11876–11880.
189. Miller SB, Martin DR, Kissane J, Hammerman MR. Hepatocyte growth factor accelerates recovery from acute ischemic renal injury in rats. *Am J Physiol Renal Physiol*. 1994;266(1):F129–F134.
190. Liu Y. Hepatocyte growth factor and the kidney. *Curr Opin Nephrol Hypertens*. 2002;11(1):23–30.
191. Hirschberg R, Adler S. Insulin-like growth factor system and the kidney: physiology, pathophysiology, and therapeutic implications. *Am J Kidney Dis*. 1998;31(6):901–919.
192. Schrijvers BF, Flyvbjerg A, De Zeeuw AS. The role of vascular endothelial growth factor (VEGF) in renal pathophysiology. *Kidney Int*. 2004;65(6):2003–2017.
193. Inoue S et al. Immunomodulatory effects of mesenchymal stem cells in a rat organ transplant model. *Transplantation*. 2006;81(11):1589–1595.
194. Devine SM et al. Mesenchymal stem cells are capable of homing to the bone marrow of non-human primates following systemic infusion. *Exp Hematol*. 2001;29(2):244–255.
195. Wynn RF. A small proportion of mesenchymal stem cells strongly expresses functionally active CXCR4 receptor capable of promoting migration to bone marrow. *Blood*. 2004;104(9):2643–2645.
196. Chapel A et al. Mesenchymal stem cells home to injured tissues when co-infused with hematopoietic cells to treat a radiation-induced multi-organ failure syndrome. *J Gene Med*. 2003;5(12):1028–1038.
197. Mahmood A, Lu D, Lu M, Chopp M. Treatment of traumatic brain injury in adult rats with intravenous administration of human bone marrow stromal cells. *Neurosurgery*. 2003;53(3):697–702.

198. Orlic D et al. Mobilized bone marrow cells repair the infarcted heart, improving function and survival. *Proc Natl Acad Sci USA*. 2001;98(18):10344–10349.
199. Brooke G et al. Therapeutic applications of mesenchymal stromal cells. *Semin Cell Dev Biol*. 2007;18(6):846–858.
200. Fox JM, Chamberlain G, Ashton BA, Middleton J. Recent advances into the understanding of mesenchymal stem cell trafficking. *Br J Haematol*. 2007;137(6):491–502.
201. Tögel F, Isaac J, Hu Z, Weiss K, Westenfelder C. Renal SDF-1 signals mobilization and homing of CXCR4-positive cells to the kidney after ischemic injury. *Kidney Int*. 2005;67(5):1772–1784.
202. Honczarenko M et al. Human Bone Marrow Stromal Cells Express a Distinct Set of Biologically Functional Chemokine Receptors. *Stem Cells*. 2006;24(4):1030–1041.
203. Ji JF, He BP, Dheen ST, Tay SSW. Interactions of Chemokines and Chemokine Receptors Mediate the Migration of Mesenchymal Stem Cells to the Impaired Site in the Brain After Hypoglossal Nerve Injury. *Stem Cells*. 2004;22(3):415–427.
204. Ponte AL et al. The In Vitro Migration Capacity of Human Bone Marrow Mesenchymal Stem Cells: Comparison of Chemokine and Growth Factor Chemotactic Activities. *Stem Cells*. 2007;25(7):1737–1745.
205. Zhu H et al. The role of the hyaluronan receptor CD44 in mesenchymal stem cell migration in the extracellular matrix. *Stem Cells*. 2006;24(4):928–935.
206. Göransson V et al. Renal hyaluronan accumulation and hyaluronan synthase expression after ischaemia-reperfusion injury in the rat. *Nephrol Dial Transplant*. 2004;19(4):823–830.
207. Kim J, Hematti P. Mesenchymal stem cell-educated macrophages: A novel type of alternatively activated macrophages. *Exp Hematol*. 2009;37(12):1445–1453.
208. Maggini J et al. Mouse Bone Marrow-Derived Mesenchymal Stromal Cells Turn Activated Macrophages into a Regulatory-Like Profile. *PLoS ONE*. 2010;5(2):e9252.
209. Németh K et al. Bone marrow stromal cells attenuate sepsis via prostaglandin E(2)-dependent reprogramming of host macrophages to increase their interleukin-10 production. *Nat Med*. 2009;15(1):42–49.
210. Ohtaki H et al. Stem/progenitor cells from bone marrow decrease neuronal death in global ischemia by modulation of inflammatory/immune responses. *Proc Natl Acad Sci USA*. 2008;105(38):14638–14643.
211. Zhang Q-Z et al. Human gingiva-derived mesenchymal stem cells elicit polarization of M2 macrophages and enhance cutaneous wound healing. *Stem Cells*. 2010;28(10):1856–1868.
212. Chen L, Tredget EE, Wu PYG, Wu Y. Paracrine Factors of Mesenchymal Stem Cells Recruit Macrophages and Endothelial Lineage Cells and Enhance Wound Healing. *PLoS ONE*. 2008;3(4):e1886.

213. Dayan V et al. Mesenchymal stromal cells mediate a switch to alternatively activated monocytes/macrophages after acute myocardial infarction. *Basic Res Cardiol*. 2011;106(6):1299–1310.
214. François M, Romieu-Mourez R, Li M, Galipeau J. Human MSC suppression correlates with cytokine induction of indoleamine 2,3-dioxygenase and bystander M2 macrophage differentiation. *Mol Ther*. 2011;20(1):187–195.
215. Nakajima HH et al. Transplantation of mesenchymal stem cells promotes an alternative pathway of macrophage activation and functional recovery after spinal cord injury. *J Neurotrauma*. 2012;29(8):1614–1625.
216. Adutler-Lieber S et al. Human Macrophage Regulation Via Interaction With Cardiac Adipose Tissue-Derived Mesenchymal Stromal Cells. *J Cardiovasc Pharmacol Ther*. 2012;18(1):78–86.
217. Furuhashi K et al. Serum-starved adipose-derived stromal cells ameliorate crescentic GN by promoting immunoregulatory macrophages. *J Am Soc Nephrol*. 2013;24(4):587–603.
218. Guo Z et al. Mesenchymal stem cells reprogram host macrophages to attenuate obliterative bronchiolitis in murine orthotopic tracheal transplantation. *Int Immunopharmacol*. 2013;15(4):726–734.
219. Li W et al. Macrophages are involved in the protective role of human umbilical cord-derived stromal cells in renal ischemia–reperfusion injury. *Stem Cell Res*. 2013;10(3):405–416.
220. Abumaree MH et al. Human Placental Mesenchymal Stem Cells (pMSCs) Play a Role as Immune Suppressive Cells by Shifting Macrophage Differentiation from Inflammatory M1 to Anti-inflammatory M2 Macrophages. *Stem Cell Rev and Rep*. 2013;9(5):620–641.
221. Ben-Mordechai T et al. Macrophage Subpopulations Are Essential for Infarct Repair With and Without Stem Cell Therapy. *J Am Coll Cardiol*. 2013;62(20):1890–1901.
222. Mathias LJ et al. Alveolar macrophages are critical for the inhibition of allergic asthma by mesenchymal stromal cells. *J Immunol*. 2013;191(12):5914–5924.
223. Cho D-I et al. Mesenchymal stem cells reciprocally regulate the M1/M2 balance in mouse bone marrow-derived macrophages. *Exp Mol Med*. 2014;46:e70.
224. Gao S et al. Mouse bone marrow-derived mesenchymal stem cells induce macrophage M2 polarization through the nuclear factor- κ B and signal transducer and activator of transcription 3 pathways. *Exp Biol Med*. 2014;239(3):366–375.
225. Bonventre JV. Pathophysiology of AKI: Injury and Normal and Abnormal Repair. In: *Contributions to Nephrology*. Basel: Karger Publishers; 2010:9–17
226. Friedenstein AJ, Gorskaja JF, Kulagina NN. Fibroblast precursors in normal and irradiated mouse hematopoietic organs. *Exp Hematol*. 1976;4(5):267–274.
227. Atoui R, Chiu RC. Concise review: immunomodulatory properties of mesenchymal stem cells in cellular transplantation: update, controversies, and unknowns. *Stem Cells Transl Med*. 2012;1(3):200–205.

228. Li J, Ezzelarab MB, Cooper DKC. Do mesenchymal stem cells function across species barriers? Relevance for xenotransplantation. *Xenotransplantation*. 2012;19(5):273–285.
229. Ren G et al. Concise review: mesenchymal stem cells and translational medicine: emerging issues. *Stem Cells Transl Med*. 2012;1(1):51–58.
230. Trzpis M, Popa ER, McLaughlin P. Spatial and Temporal Expression Patterns of the Epithelial Cell Adhesion Molecule (EpCAM/EGP-2) in Developing and Adult Kidneys. *Nephron Exp Nephrol*. 2007;107(4):e119–e131.
231. Trzpis M et al. Expression of EpCAM is up-regulated during regeneration of renal epithelia. *J Pathol*. 2008;216(2):201–208.
232. Friedenstein AJ, Petrakova KV, Kurolesova AI, Frolova GP. Heterotopic of bone marrow. Analysis of precursor cells for osteogenic and hematopoietic tissues. *Transplantation*. 1968;6(2):230–247.
233. Miura M et al. Accumulated chromosomal instability in murine bone marrow mesenchymal stem cells leads to malignant transformation. *Stem Cells*. 2006;24(4):1095–1103.
234. Tolar J et al. Sarcoma derived from cultured mesenchymal stem cells. *Stem Cells*. 2007;25(2):371–379.
235. Mohseny AB et al. Osteosarcoma originates from mesenchymal stem cells in consequence of aneuploidization and genomic loss of Cdkn2. *J Pathol*. 2009;219(3):294–305.
236. Zhou YF et al. Spontaneous transformation of cultured mouse bone marrow-derived stromal cells. *Cancer Res*. 2006;66(22):10849–10854.
237. Xiao W, Mohseny AB, Hogendoorn PCW, Cleton-Jansen A-M. Mesenchymal stem cell transformation and sarcoma genesis. *Clin Sarcoma Res*. 2012;3(1):10–10.
238. Bernardo ME, Fibbe WE. Mesenchymal stromal cells: sensors and switchers of inflammation. *Cell Stem Cell*. 2013;13(4):392–402.
239. Bernardo ME et al. Human bone marrow–derived mesenchymal stem cells do not undergo transformation after long-term in vitro culture and do not exhibit telomere maintenance mechanisms. *Cancer Res*. 2007;67(19):9142–9149.
240. Prockop DJ et al. Defining the risks of mesenchymal stromal cell therapy. *Cytotherapy*. 2010;12(5):576–578.
241. Klyushnenkova E et al. T cell responses to allogeneic human mesenchymal stem cells: immunogenicity, tolerance, and suppression. *J Biomed Sci*. 2005;12(1):47–57.
242. Lu B et al. Human adult bone marrow-derived somatic cells rescue vision in a rodent model of retinal degeneration. *Exp Eye Res*. 2010;91(3):449–455.
243. Atoui R et al. Marrow stromal cells as universal donor cells for myocardial regenerative therapy: their unique immune tolerance. *Ann Thorac Surg*. 2008;85(2):571–579.

244. Ezquer ME, Ezquer FE, Arango-Rodríguez ML, Conget PA. MSC transplantation: a promising therapeutic strategy to manage the onset and progression of diabetic nephropathy. *Biol Res*. 2012;45(3):289–296.
245. Danchuk S et al. Human multipotent stromal cells attenuate lipopolysaccharide-induced acute lung injury in mice via secretion of tumor necrosis factor- α -induced protein 6. *Stem Cell Res Ther*. 2010;2(3):27–27.
246. Payne NL et al. Distinct immunomodulatory and migratory mechanisms underpin the therapeutic potential of human mesenchymal stem cells in autoimmune demyelination. *Cell Transplant*. 2013;22(8):1409–1425.
247. Ma S et al. Immunobiology of mesenchymal stem cells. *Cell Death Differ*. 2014;21(2):216–225.
248. Duffield JS. Macrophages and Immunologic Inflammation of the Kidney. *Semin Nephrol*. 2010;30(3):234–254.
249. Diamond JR. Macrophages and progressive renal disease in experimental hydronephrosis. *Am J Kidney Dis*. 1995;26(1):133–140.
250. Yoshimoto K et al. CD68 and MCP-1/CCR2 expression of initial biopsies reflect the outcomes of membranous nephropathy. *Nephron Clin Pract*. 2003;98(1):c25–c34.
251. Chow F, Ozols E, Nikolic-Paterson DJ, Atkins RC, Tesch GH. Macrophages in mouse type 2 diabetic nephropathy: correlation with diabetic state and progressive renal injury. *Kidney Int*. 2004;65(1):116–128.
252. Eardley KS et al. The role of capillary density, macrophage infiltration and interstitial scarring in the pathogenesis of human chronic kidney disease. *Kidney Int*. 2008;74(4):495–504.
253. Eardley KS, Cockwell P. Macrophages and progressive tubulointerstitial disease. *Kidney Int*. 2005;68(2):437–455.
254. Otto WR, Wright NA. Mesenchymal stem cells: from experiment to clinic. *Fibrogenesis Tissue Repair*. 2011;4:1–14.
255. Spaggiari GM, Moretta L. Cellular and molecular interactions of mesenchymal stem cells in innate immunity. *Immunol Cell Biol*. 2013;91(1):27–31.
256. Yi TT, Song SUS. Immunomodulatory properties of mesenchymal stem cells and their therapeutic applications. *Arch Pharm Res*. 2012;35(2):213–221.
257. Wang S, Qu X, Zhao RC. Clinical applications of mesenchymal stem cells. *J Hematol Oncol*. 2012;5:1–9.
258. Lange C et al. Accelerated and safe expansion of human mesenchymal stromal cells in animal serum-free medium for transplantation and regenerative medicine. *J Cell Physiol*. 2007;213(1):18–26.
259. Zhang S et al. Purified human bone marrow multipotent mesenchymal stem cells regenerate infarcted myocardium in experimental rats. *Cell Transplant*. 2005;14(10):787–

798.

260. Khakoo AY et al. Human mesenchymal stem cells exert potent antitumorigenic effects in a model of Kaposi's sarcoma. *J Exp Med*. 2006;203(5):1235–1247.
261. Chang YS et al. Human umbilical cord blood-derived mesenchymal stem cells attenuate hyperoxia-induced lung injury in neonatal rats. *Cell Transplant*. 2009;18(8):869–886.
262. Bai L et al. Human bone marrow-derived mesenchymal stem cells induce Th2-polarized immune response and promote endogenous repair in animal models of multiple sclerosis. *Glia*. 2009;57(11):1192–1203.
263. Hung S-C, Pochampally RR, Chen S-C, Hsu S-C, Prockop DJ. Angiogenic effects of human multipotent stromal cell conditioned medium activate the PI3K-Akt pathway in hypoxic endothelial cells to inhibit apoptosis, increase survival, and stimulate angiogenesis. *Stem Cells*. 2007;25(9):2363–2370.
264. Yagi H et al. Bone marrow mesenchymal stromal cells attenuate organ injury induced by LPS and burn. *Cell Transplant*. 2009;19(6):823–830.
265. Stefater JA III, Ren S, Lang RA, Duffield JS. Metchnikoff's policemen: macrophages in development, homeostasis and regeneration. *Trends Mol Med*. 2011;17(12):743–752.
266. Mantovani A et al. The chemokine system in diverse forms of macrophage activation and polarization. *Trends Immunol*. 2004;25(12):677–686.
267. Nozaki Y et al. Tim-1 promotes cisplatin nephrotoxicity. *Am J Physiol Renal Physiol*. 2011;301(5):F1098–104.
268. Samuel CS, Butkus A, Coghlan JP, Bateman JF. The effect of relaxin on collagen metabolism in the nonpregnant rat pubic symphysis: the influence of estrogen and progesterone in regulating relaxin activity. *Endocrinology*. 1996;137(9):3884–3890.
269. Samuel CS. Determination of collagen content, concentration, and sub-types in kidney tissue. *Methods Mol Biol*. 2009;466:223–235.
270. Woessner JF. Quantification of matrix metalloproteinases in tissue samples. *Meth Enzymol*. 1995;248:510–528.
271. Chen Y-T et al. Adipose-derived mesenchymal stem cell protects kidneys against ischemia-reperfusion injury through suppressing oxidative stress and inflammatory reaction. *J Transl Med*. 2011;9:51.
272. Du T et al. The alleviation of acute and chronic kidney injury by human Wharton's jelly-derived mesenchymal stromal cells triggered by ischemia-reperfusion injury via an endocrine mechanism. *Cytotherapy*. 2012;14(10):1215–1227.
273. Park HC et al. Postobstructive regeneration of kidney is derailed when surge in renal stem cells during course of unilateral ureteral obstruction is halted. *Am J Physiol Renal Physiol*. 2010;298(2):F357–F364.
274. Liu X, Shen W, Yang Y, Liu G. Therapeutic implications of mesenchymal stem cells transfected with hepatocyte growth factor transplanted in rat kidney with unilateral ureteral

- obstruction. *J Pediatr Surg*. 2011;46(3):9–9.
275. Asanuma H et al. Arterially delivered mesenchymal stem cells prevent obstruction-induced renal fibrosis. *J Surg Res*. 2011;168(1):e51–e59.
276. Liu Y-L et al. Immunosuppression effects of bone marrow mesenchymal stem cells on renal interstitial injury in rats with unilateral ureteral obstruction. *Cell Immunol*. 2012;:1–9.
277. Wise AF, Ricardo SD. Mesenchymal stem cells in kidney inflammation and repair. *Nephrology*. 2012;17(1):1–10.
278. Liu H et al. The role of SDF-1-CXCR4/CXCR7 axis in the therapeutic effects of hypoxia-preconditioned mesenchymal stem cells for renal ischemia/reperfusion injury. *PLoS ONE*. 2011;7(4):e34608–e34608.
279. Kang SK, Seob Shin Il, Ko MS, Jo JY, Ra JC. Journey of Mesenchymal Stem Cells for Homing: Strategies to Enhance Efficacy and Safety of Stem Cell Therapy. *Stem Cells Int*. 2011;2012:1–11.
280. Tögel F, Yang Y, Zhang P, Hu Z, Westenfelder C. Bioluminescence imaging to monitor the in vivo distribution of administered mesenchymal stem cells in acute kidney injury. *Am J Physiol Renal Physiol*. 2008;295(1):F315–21.
281. Nystedt J et al. Cell surface structures influence lung clearance rate of systemically infused mesenchymal stromal cells. *Stem Cells*. 2013;31(2):317–326.
282. Lee RH et al. Intravenous hMSCs improve myocardial infarction in mice because cells embolized in lung are activated to secrete the anti-inflammatory protein TSG-6. *Cell Stem Cell*. 2009;5(1):54–63.
283. Xinaris C et al. A novel strategy to enhance Mesenchymal Stem Cell migration capacity and promote tissue repair in an injury specific fashion. *Cell Transplant*. 2013;22:423–436.
284. Shi H et al. Glial cell line-derived neurotrophic growth factor increases motility and survival of cultured mesenchymal stem cells and ameliorates acute kidney injury. *Am J Physiol Renal Physiol*. 2008;294(1):F229–F235.
285. Mias CC et al. Ex vivo pretreatment with melatonin improves survival, proangiogenic/mitogenic activity, and efficiency of mesenchymal stem cells injected into ischemic kidney. *Stem Cells*. 2008;26(7):1749–1757.
286. Hung S-C et al. Short-Term Exposure of Multipotent Stromal Cells to Low Oxygen Increases Their Expression of CX3CR1 and CXCR4 and Their Engraftment In Vivo. *PLoS ONE*. 2007;2(5):e416.
287. Cheng Z et al. Targeted migration of mesenchymal stem cells modified with CXCR4 gene to infarcted myocardium improves cardiac performance. *Mol Ther*. 2008;16(3):571–579.
288. Zhen-Qiang F et al. Localized expression of human BMP-7 by BM-MSCs enhances renal repair in an in vivo model of ischemia-reperfusion injury. *Genes Cells*. 2011;17(1):53–64.
289. Kunter U et al. Mesenchymal stem cells prevent progressive experimental renal failure

- but maldifferentiate into glomerular adipocytes. *J Am Soc Nephrol*. 2007;18(6):1754–1764.
290. Catania JM, Chen G, Parrish AR. Role of matrix metalloproteinases in renal pathophysiology. *Am J Physiol Renal Physiol*. 2007;292(3):F905–11.
291. Ichimura T, Hung CC, Yang SA, Stevens JL, Bonventre JV. Kidney injury molecule-1: a tissue and urinary biomarker for nephrotoxicant-induced renal injury. *Am J Physiol Renal Physiol*. 2004;286(3):F552–63.
292. Vaidya VS, Ramirez V, Ichimura T, Bobadilla NA, Bonventre JV. Urinary kidney injury molecule-1: a sensitive quantitative biomarker for early detection of kidney tubular injury. *Am J Physiol Renal Physiol*. 2006;290(2):F517–29.
293. Lu W et al. Exposure to supernatants of macrophages that phagocytized dead mesenchymal stem cells improves hypoxic cardiomyocytes survival. *Int J Cardiol*. 2012;165(2):333–340.
294. Roca H et al. CCL2 and interleukin-6 promote survival of human CD11b+ peripheral blood mononuclear cells and induce M2-type macrophage polarization. *J Biol Chem*. 2009;284(49):34342–34354.
295. Medina RJ et al. Myeloid angiogenic cells act as alternative M2 macrophages and modulate angiogenesis through interleukin-8. *Mol Med*. 2011;17(9-10):1045–1055.
296. Bögels M et al. Carcinoma origin dictates differential skewing of monocyte function. *Oncoimmunology*. 2012;1(6):798–809.
297. Takai H et al. Involvement of glypican-3 in the recruitment of M2-polarized tumor-associated macrophages in hepatocellular carcinoma. *Cancer Biol Ther*. 2009;8(24):2329–2338.
298. Espinoza-Jiménez A, Peón AN, Terrazas LI. Alternatively Activated Macrophages in Types 1 and 2 Diabetes. *Mediators Inflamm*. 2012;2012(3):1–10.
299. Stumvoll M, Goldstein BJ, van Haeften TW. Type 2 diabetes: principles of pathogenesis and therapy. *Lancet*. 2005;365(9467):1333–1346.
300. Fernández-Real JM, Pickup JC. Innate immunity, insulin resistance and type 2 diabetes. *Trends Endocrinol Metab*. 2008;19(1):10–16.
301. Lane PH, Steffes MW, Fioretto P, Mauer SM. Renal interstitial expansion in insulin-dependent diabetes mellitus. *Kidney Int*. 1993;43(3):661–667.
302. Atkins RC, Zimmet P. Diabetic kidney disease: act now or pay later. *Nat Rev Nephrol*. 2010;6(3):134–136.
303. Badawi A et al. Type 2 diabetes mellitus and inflammation: Prospects for biomarkers of risk and nutritional intervention. *Diabetes Metab Syndr Obes*. 2009;3:173–186.
304. Nguyen D et al. Macrophage accumulation in human progressive diabetic nephropathy. *Nephrology*. 2006;11(3):226–231.
305. Du T et al. Modulation of monocyte hyperresponsiveness to TLR ligands by 1,25-

- dihydroxy-vitamin D3 from LADA and T2DM. *Diabetes Res Clin Pract*. 2009;83(2):208–214.
306. Ingersoll MA, Platt AM, Potteaux S, Randolph GJ. Monocyte trafficking in acute and chronic inflammation. *Trends Immunol*. 2011;32(10):470–477.
307. Martinez FO, Gordon S, Locati M, Mantovani A. Transcriptional profiling of the human monocyte-to-macrophage differentiation and polarization: new molecules and patterns of gene expression. *J Immunol*. 2006;177(10):7303–7311.
308. Ancuta P, Liu KY, Misra V, Wacleche VS. Transcriptional profiling reveals developmental relationship and distinct biological functions of CD16+ and CD16- monocyte subsets. *BMC Genomics*. 2009;10(403).
309. Perico N et al. Autologous mesenchymal stromal cells and kidney transplantation: a pilot study of safety and clinical feasibility. *Clin J Am Soc Nephrol*. 2011;6(2):412–422.
310. Jiang R et al. Transplantation of placenta-derived mesenchymal stem cells in type 2 diabetes: a pilot study. *Front Med*. 2011;5(1):94–100.
311. Tan J et al. Induction therapy with autologous mesenchymal stem cells in living-related kidney transplants: a randomized controlled trial. *JAMA*. 2012;307(11):1169–1177.
312. Reinders MEJ et al. Autologous bone marrow-derived mesenchymal stromal cells for the treatment of allograft rejection after renal transplantation: results of a phase I study. *Stem Cells Transl Med*. 2013;2(2):107–111.
313. Jiang X-X et al. Human mesenchymal stem cells inhibit differentiation and function of monocyte-derived dendritic cells. *Blood*. 2005;105(10):4120–4126.
314. Nauta AJ, Kruisselbrink AB, Lurvink E, Willemze R, Fibbe WE. Mesenchymal stem cells inhibit generation and function of both CD34+-derived and monocyte-derived dendritic cells. *J Immunol*. 2006;177(4):2080–2087.
315. Wise AF et al. Human mesenchymal stem cells alter macrophage phenotype and promote regeneration via homing to the kidney following ischemia-reperfusion injury. *Am J Physiol Renal Physiol*. 2014;306(10):F1222–F1235.
316. Lv S-S et al. Mesenchymal stem cells transplantation ameliorates glomerular injury in streptozotocin-induced diabetic nephropathy in rats via inhibiting macrophage infiltration. *Int Immunopharmacol*. 2013;17(2):275–282.
317. Ziegler-Heitbrock HW et al. The novel subset of CD14+/CD16+ blood monocytes exhibits features of tissue macrophages. *Eur J Immunol*. 1993;23(9):2053–2058.
318. Liu H, Shi B, Huang C-C, Eksarko P, Pope RM. Transcriptional diversity during monocyte to macrophage differentiation. *Immunol Lett*. 2008;117(1):70–80.
319. Dong C et al. RNA sequencing and transcriptomal analysis of human monocyte to macrophage differentiation. *Gene*. 2013;519(2):279–287.
320. Tessem JS et al. Critical roles for macrophages in islet angiogenesis and maintenance during pancreatic degeneration. *Diabetes*. 2008;57(6):1605–1617.

321. Nio Y et al. Monocyte chemoattractant protein-1 (MCP-1) deficiency enhances alternatively activated M2 macrophages and ameliorates insulin resistance and fatty liver in lipoatrophic diabetic A-ZIP transgenic mice. *Diabetologia*. 2012;55(12):3350–3358.
322. Alikhan MA, Ricardo SD. Mononuclear phagocyte system in kidney disease and repair. *Nephrology*. 2013;18(2):81–91.
323. Giulietti A et al. Monocytes from type 2 diabetic patients have a pro-inflammatory profile. 1,25-Dihydroxyvitamin D(3) works as anti-inflammatory. *Diabetes Res Clin Pract*. 2007;77(1):47–57.
324. Ruan H, Lodish HF. Insulin resistance in adipose tissue: direct and indirect effects of tumor necrosis factor-alpha. *Cytokine Growth Factor Rev*. 2003;14(5):447–455.
325. Cai D et al. Local and systemic insulin resistance resulting from hepatic activation of IKK-beta and NF-kappaB. *Nat Med*. 2005;11(2):183–190.
326. Ehses JA et al. IL-1 antagonism reduces hyperglycemia and tissue inflammation in the type 2 diabetic GK rat. *Proc Natl Acad Sci USA*. 2009;106(33):13998–14003.
327. Katz S, Klein B, Elian I, Fishman P, Djaldetti M. Phagocytotic activity of monocytes from diabetic patients. *Diabetes Care*. 1983;6(5):479–482.
328. Waltenberger J, Lange J, Kranz A. Vascular endothelial growth factor-A-induced chemotaxis of monocytes is attenuated in patients with diabetes mellitus: A potential predictor for the individual capacity to develop collaterals. *Circulation*. 2000;102(2):185–190.
329. Ryan JM, Barry F, Murphy JM, Mahon BP. Interferon- γ does not break, but promotes the immunosuppressive capacity of adult human mesenchymal stem cells. *Clin Exp Immunol*. 2007;149(2):353–363.
330. Sheng H et al. A critical role of IFN γ in priming MSC-mediated suppression of T cell proliferation through up-regulation of B7-H1. *Cell Res*. 2008;18(8):846–857.
331. Rocher BD, Mencilha AL, Gomes BE, Abdelhay E. Mesenchymal stromal cells impair the differentiation of CD14 $^{++}$ CD16 $^{-}$ CD64 $^{+}$ classical monocytes into CD14 $^{++}$ CD16 $^{+}$ CD64 $^{++}$ activate monocytes. *Cytotherapy*. 2012;14(1):12–25.
332. Cutler AJ, Limbani V, Girdlestone J, Navarrete CV. Umbilical cord-derived mesenchymal stromal cells modulate monocyte function to suppress T cell proliferation. *J Immunol*. 2010;185(11):6617–6623.
333. Olefsky JM, Glass CK. Macrophages, inflammation, and insulin resistance. *Annu Rev Physiol*. 2010;72(1):219–246.
334. Fadini GP et al. An unbalanced monocyte polarisation in peripheral blood and bone marrow of patients with type 2 diabetes has an impact on microangiopathy. *Diabetologia*. 2013;56(8):1856–1866.
335. Hong E-G et al. Interleukin-10 prevents diet-induced insulin resistance by attenuating macrophage and cytokine response in skeletal muscle. *Diabetes*. 2009;58(11):2525–2535.

336. van Exel E et al. Low production capacity of interleukin-10 associates with the metabolic syndrome and type 2 diabetes : the Leiden 85-Plus Study. *Diabetes*. 2002;51(4):1088–1092.
337. Blüher M et al. Association of interleukin-6, C-reactive protein, interleukin-10 and adiponectin plasma concentrations with measures of obesity, insulin sensitivity and glucose metabolism. *Exp Clin Endocrinol Diabetes*. 2005;113(9):534–537.
338. Moses AC, Young SC, Morrow LA, O'Brien M, Clemmons DR. Recombinant human insulin-like growth factor I increases insulin sensitivity and improves glycemic control in type II diabetes. *Diabetes*. 1995;45(1):91–100.
339. Cusi K, DeFronzo R. Recombinant human insulin-like growth factor I treatment for 1 week improves metabolic control in type 2 diabetes by ameliorating hepatic and muscle insulin resistance. *J Clin Endocrinol Metab*. 2000;85(9):3077–3084.
340. Clemmons DR et al. Rh/IGF-I/rhIGFBP-3 administration to patients with type 2 diabetes mellitus reduces insulin requirements while also lowering fasting glucose. *Growth Hormone IGF Res*. 2005;15(4):265–274.
341. Cha DR et al. Role of vascular endothelial growth factor in diabetic nephropathy. *Kidney Int Suppl*. 2000;77(suppl. 77):S104–S112.
342. Hohenstein B et al. Local VEGF activity but not VEGF expression is tightly regulated during diabetic nephropathy in man. *Kidney Int*. 2006;69(9):1654–1661.
343. Sivaskandarajah GA et al. Vegfa protects the glomerular microvasculature in diabetes. *Diabetes*. 2012;61(11):2958–2966.
344. Tumlin JA, Galphin CM, Rovin BH. Advanced diabetic nephropathy with nephrotic range proteinuria: a pilot study of the long-term efficacy of subcutaneous ACTH gel on proteinuria, progression of CKD, and urinary levels of VEGF and MCP-1. *J Diabetes Res*. 2012;2013:489869–489869.
345. Mankhey RW, Wells CC, Bhatti F, Maric C. 17beta-Estradiol supplementation reduces tubulointerstitial fibrosis by increasing MMP activity in the diabetic kidney. *Am J Physiol Regul Integr Comp Physiol*. 2007;292(2):R769–77.
346. Wang D et al. CD14+ monocytes promote the immunosuppressive effect of human umbilical cord matrix stem cells. *Exp Cell Res*. 2010;316(15):2414–2423.
347. Lumeng CN, Bodzin JL, Saltiel AR. Obesity induces a phenotypic switch in adipose tissue macrophage polarization. *J Clin Invest*. 2007;117(1):175–184.
348. Jadhav A, Tiwari S, Lee P, Ndisang JF. The heme oxygenase system selectively enhances the anti-inflammatory macrophage-m2 phenotype, reduces pericardial adiposity, and ameliorated cardiac injury in diabetic cardiomyopathy in zucker diabetic Fatty rats. *J Pharmacol Exp Ther*. 2013;345(2):239–249.
349. Park JH, Hwang I, Hwang SH, Han H, Ha H. Human umbilical cord blood-derived mesenchymal stem cells prevent diabetic renal injury through paracrine action. *Diabetes Res Clin Pract*. 2012;98(3):465–473.

350. Si Y et al. Infusion of Mesenchymal Stem Cells Ameliorates Hyperglycemia in Type 2 Diabetic Rats. *Diabetes*. 2012;61(6):1616–1625.
351. Lv S et al. Mesenchymal stem cells transplantation ameliorates glomerular injury in streptozotocin-induced diabetic nephropathy in rats via inhibiting oxidative stress. *Diabetes Res Clin Pract*. [published online ahead of print: January 14, 2014]; doi:10.1016/j.diabres.2014.01.011
352. Bieback K, Brinkmann I. Mesenchymal stromal cells from human perinatal tissues: From biology to cell therapy. *World J Stem Cells*. 2010;2(4):81–92.
353. Toma C, Pittenger MF, Cahill KS, Byrne BJ, Kessler PD. Human mesenchymal stem cells differentiate to a cardiomyocyte phenotype in the adult murine heart. *Circulation*. 2002;105(1):93–98.
354. Sato Y et al. Human mesenchymal stem cells xenografted directly to rat liver are differentiated into human hepatocytes without fusion. *Blood*. 2005;106(2):756–763.
355. Woodbury D, Schwarz EJ, Prockop DJ, Black IB. Adult rat and human bone marrow stromal cells differentiate into neurons. *J Neurosci Res*. 2000;61(4):364–370.
356. Tang D-Q et al. In vivo and in vitro characterization of insulin-producing cells obtained from murine bone marrow. *Diabetes*. 2004;53(7):1721–1732.
357. Prockop DJ. Repair of tissues by adult stem/progenitor cells (MSCs): controversies, myths, and changing paradigms. *Mol Ther*. 2009;17(6):939–946.
358. Wang N et al. Novel mechanism for mesenchymal stem cells in attenuating peritoneal adhesion: accumulating in the lung and secreting tumor necrosis factor α -stimulating gene-6. *Stem Cell Res Ther*. 2012;3(6):51–51.
359. Oh JY et al. Intravenous mesenchymal stem cells prevented rejection of allogeneic corneal transplants by aborting the early inflammatory response. *Mol Ther*. 2012;20(11):2143–2152.
360. Timmers L et al. Human mesenchymal stem cell-conditioned medium improves cardiac function following myocardial infarction. *Stem Cell Res*. 2011;6(3):206–214.
361. van Koppen AA et al. Human embryonic mesenchymal stem cell-derived conditioned medium rescues kidney function in rats with established chronic kidney disease. *PLoS ONE*. 2011;7(6):e38746–e38746.
362. Cantinieaux D et al. Conditioned medium from bone marrow-derived mesenchymal stem cells improves recovery after spinal cord injury in rats: an original strategy to avoid cell transplantation. *PLoS ONE*. 2013;8(8):e69515.
363. Du Z et al. Mesenchymal stem cell-conditioned medium reduces liver injury and enhances regeneration in reduced-size rat liver transplantation. *J Surg Res*. 2013;183(2):907–915.
364. Fischer UM et al. Pulmonary passage is a major obstacle for intravenous stem cell delivery: the pulmonary first-pass effect. *Stem Cells Dev*. 2009;18(5):683–692.

365. Gao J, Dennis JE, Muzic RF, Lundberg M, Caplan AI. The dynamic in vivo distribution of bone marrow-derived mesenchymal stem cells after infusion. *Cells Tissues Organs*. 2001;169(1):12–20.
366. Kean TJ, Lin P, Caplan AI, Dennis JE. MSCs: Delivery Routes and Engraftment, Cell-Targeting Strategies, and Immune Modulation. *Stem Cells Int*. 2013;2013:732742.
367. Uccelli A, Prockop DJ. Why should mesenchymal stem cells (MSCs) cure autoimmune diseases? *Curr Opin Immunol*. 2010;22(6):768–774.
368. Bahr von L et al. Analysis of tissues following mesenchymal stromal cell therapy in humans indicates limited long-term engraftment and no ectopic tissue formation. *Stem Cells*. 2012;30(7):1575–1578.
369. Zangi L et al. Direct imaging of immune rejection and memory induction by allogeneic mesenchymal stromal cells. *Stem Cells*. 2009;27(11):2865–2874.
370. Ankrum JA, Ong JF, Karp JM. Mesenchymal stem cells: immune evasive, not immune privileged. *Nat Biotechnol*. 2014;32(3):252–260.
371. Millard SM, Fisk NM. Mesenchymal stem cells for systemic therapy: Shotgun approach or magic bullets? *Bioessays*. 2013;35(3):173–182.
372. Vanikar AV, Trivedi HL. Stem cell transplantation in living donor renal transplantation for minimization of immunosuppression. *Transplantation*. 2012;94(8):845–850.
373. Peng Y et al. Donor-derived mesenchymal stem cells combined with low-dose tacrolimus prevent acute rejection after renal transplantation: a clinical pilot study. *Transplantation*. 2013;95(1):161–168.
374. Pileggi A, Xu X, Tan J, Ricordi C. Mesenchymal stromal (stem) cells to improve solid organ transplant outcome: lessons from the initial clinical trials. *Curr Opin Organ Transplant*. 2013;18(6):672–681.
375. Ferenbach DA et al. Macrophage/monocyte depletion by clodronate, but not diphtheria toxin, improves renal ischemia/reperfusion injury in mice. *Kidney Int*. 2012;82(8):928–933.
376. Perico N et al. Mesenchymal stromal cells and kidney transplantation: pretransplant infusion protects from graft dysfunction while fostering immunoregulation. *Transpl Int*. 2013;26(9):867–878.
377. Lee H et al. Intra-osseous injection of donor mesenchymal stem cell (MSC) into the bone marrow in living donor kidney transplantation; a pilot study. *J Transl Med*. 2013;11:96–96.
378. AlloCure. AlloCure Begins Phase 2 Clinical Trial in Acute Kidney Injury [Internet]2012;http://www.allocure.com/clinical/index.php. cited July 31, 2014
379. Sun L et al. Mesenchymal Stem Cell Transplantation Reverses Multiorgan Dysfunction in Systemic Lupus Erythematosus Mice and Humans. *Stem Cells*. 2009;27(6):1421–1432.
380. Sun L et al. Umbilical cord mesenchymal stem cell transplantation in severe and refractory systemic lupus erythematosus. *Arthritis Rheum*. 2010;62(8):2467–2475.

381. Liang J et al. Allogeneic mesenchymal stem cells transplantation in refractory systemic lupus erythematosus: a pilot clinical study. *Ann Rheum Dis*. 2010;69(8):1423–1429.
382. Wang D et al. Double allogeneic mesenchymal stem cells transplantations could not enhance therapeutic effect compared with single transplantation in systemic lupus erythematosus. *Clin Dev Immunol*. 2011;2012:273291–273291.
383. Wang D et al. Allogeneic mesenchymal stem cell transplantation in severe and refractory systemic lupus erythematosus: 4 years of experience. *Cell Transplant*. 2013;22(12):2267–2277.
384. Wang D et al. Umbilical cord mesenchymal stem cell transplantation in active and refractory systemic lupus erythematosus: a multicenter clinical study. *Arthritis Res Ther*. 2014;16(2):R79.

APPENDICES

Review Article

Mesenchymal stem cells in kidney inflammation and repair

ANDREA F. WISE and SHARON D. RICARDO

Monash Immunology and Stem Cell Laboratories (MISCL), Monash University, Melbourne, Victoria, Australia

KEY WORDS:

inflammation, kidney regeneration, stem cell.

Correspondence:

Associate Professor Sharon D Ricardo, Monash Immunology and Stem Cell Laboratories (MISCL), Monash University, Clayton Vic 3800, Australia

Accepted for publication 6 July 2011.

Accepted manuscript online 20 July 2011.

doi:10.1111/j.1440-1797.2011.01501.x

SUMMARY AT A GLANCE

This review discusses the potential therapeutic role of mesenchymal stem cells in kidney disease.

ABSTRACT:

Mesenchymal stem cells are a heterogeneous population of fibroblast-like stromal cells that have been isolated from the bone marrow and a number of organs and tissues including the kidney. They have multipotent and self-renewing properties and can differentiate into cells of the mesodermal lineage. Following their administration *in vivo*, mesenchymal stem cells migrate to damaged kidney tissue where they produce an array of anti-inflammatory cytokines and chemokines that can alter the course of injury. Mesenchymal stem cells are thought to elicit repair through paracrine and/or endocrine mechanisms that modulate the immune response resulting in tissue repair and cellular replacement. This review will discuss the features of mesenchymal stem cells and the factors they release that protect against kidney injury; the mechanisms of homing and engraftment to sites of inflammation; and further elucidate the immunomodulatory effect of mesenchymal stem cells and their ability to alter macrophage phenotype in a setting of kidney damage and repair.

KIDNEY STEM CELLS AND REGENERATION

Understanding the process of endogenous kidney regeneration is important for the development of new therapeutic strategies. Tissue stem/progenitor cells play a vital role in maintaining homeostasis, a process of self-renewal.¹ The rate at which this occurs varies among tissues. For example, epithelial cells of the intestine¹ and skin² have a high cell turnover rate and can completely self-renew within days. In contrast, the kidney has a considerably lower cell turnover rate, with proliferative abilities that differ depending on the specialized cell type.^{3,4}

Unlike mammalian kidneys, where the formation of nephrons ceases at birth, cartilaginous fish have the capacity to form new nephrons after birth through *de novo* nephrogenesis.⁵ Morevoer, following partial nephrectomy, skate fish show proliferation of progenitor cells that results in ongoing kidney development.⁶ In contrast, mammalian adult kidneys undergo compensatory hypertrophy following uninephrectomy without the formation of new nephrons. The mammalian kidney, therefore, has a limited capacity to undergo endogenous cellular replacement and tissue remodelling under normal conditions. Nevertheless, in response to acute injury the adult kidney does have some capacity for repair

and remodelling that can ultimately lead to restoration of renal structure and function.⁷

Acute insults to the kidney such as exposure to toxins, sepsis or ischemia can lead to apoptotic cell death and/or necrosis of the tubular epithelial cells and glomerular podocytes.^{3,8} The kidney's repair response, consisting of cellular replacement of the injured tubular epithelium, is most likely mediated by surviving epithelial cells that neighbour the sites of injury.^{9,10} These epithelial cells dedifferentiate and migrate to injured sites of apoptosis, necrosis and cell detachment, where they subsequently proliferate and redifferentiate into functional tubular epithelial cells.^{3,11} In a setting of chronic injury, glomerular repair is less impressive. Ongoing damage to glomerular cells results in the progressive loss of nephrons, leading to the expansion of the interstitium and development of fibrosis.

It is currently unclear if the kidney contains resident stem cells,¹² although recent reports suggest that progenitor cell population/s originally identified in embryonic kidneys (CD24+CD133+Oct-4+Bmi-1+) exist within the urinary pole of the glomerular parietal epithelium of the Bowman's capsule.^{13–15} These cells, expressing CD24, a surface antigen commonly used for the identification of human stem cells,^{16,17} and CD133, a surface antigen specific for a variety of

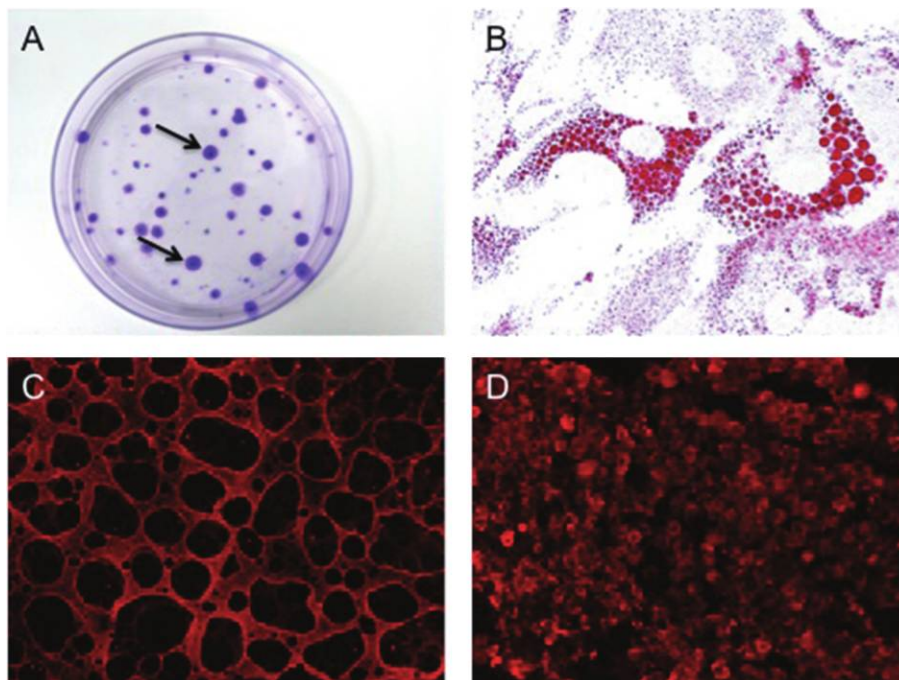


Fig. 1 Mesenchymal stem cells (MSC) show multipotent potential and form colony-forming unit-fibroblasts (CFU-F) in culture (A; arrows) that can differentiate into adipocytes (B), where lipid droplets stain red with Oil Red O (Mag $\times 1000$); bone (C), shown in red with immunostaining for osteopontin (Mag $\times 400$); and cartilage (Mag $\times 200$) stained with collagen II (D).

adult stem cells,^{18–20} may represent a residual kidney progenitor cell population within the parietal epithelium.⁹ The CD24+CD133+podocalyxin+ cells localized to the urinary pole of the parietal epithelium may be responsible for podocyte replacement after injury,^{13,14} a cell type once thought to be post-mitotic and unable to divide.

Cellular loss most often leads to the infiltration of bone marrow (BM)-derived inflammatory cells that may contribute to both tissue destruction or repair depending on the extent of injury.²¹ Mesenchymal stem cells (MSC), derived from the BM, have initiated considerable excitement in their role to promote kidney repair and tissue remodelling through the paracrine secretion of mitogenic and angiogenic factors.

MESENCHYMAL STEM CELLS

Mesenchymal stem cells were originally identified in the BM stroma by Friedenstein and colleagues.^{22,23} MSC therapy has since been reported to ameliorate kidney injury and promote structural repair.²⁴ These undifferentiated adult stem cells are of mesodermal origin and constitute only 0.001–0.01% of the total BM cell population.²⁵ They can be easily isolated from other BM cells *ex vivo* due to their propensity to adhere to plastic and their ability to extensively proliferate *in vitro*.^{25,26} Furthermore, these characteristics allow for the cell expansion of adequate numbers of MSC for potential therapeutic use.⁴ However, as the extensive expansion of MSC in culture can lead to alterations in both phenotype and function, it remains uncertain if *in vitro* cultured MSC differ significantly from the *in vivo* populations.^{26–28}

Mesenchymal stem cells form a heterogeneous population in culture that consists of small immature rapidly self-renewing cells, large, more mature, slowly replicating cells and in some confluent cultures, cuboidal cells.²⁹ Interestingly, it has been shown that single cell-derived clones of MSC can vary in phenotype, gene expression and their differentiation abilities.^{30,31} The *Mesenchymal and Tissue Stem Cell Committee of the International Society of Cellular Therapy* have outlined a combination of morphological, phenotypical and functional characteristics that are required to define these cells.³² As part of their definition, it is essential that MSC adhere to plastic in standard tissue culture conditions, exhibit a fibroblast-like morphology and have the ability to undergo extensive proliferation, resulting in the formation of colonies of fibroblastic cells, termed colony-forming unit-fibroblasts (CFU-F; Fig. 1A).^{32–34} Furthermore, MSC should express the surface antigens CD73, CD90 and CD105 and lack the expression of the hematopoietic markers CD45, CD34, CD14 or CD11b, CD79 α or CD19 and major histocompatibility complex (MHC) class II.³² They also typically express intermediate levels of MHC class I and are negative for the co-stimulatory molecules CD40, CD80 and CD86.³⁵ However, when exposed to inflammatory stimuli, such as interferon (IFN)- γ , their expression of MHC class I and II has been reported to be upregulated.³⁶ Finally, when exposed to the appropriate differentiation conditions, MSCs should have the capacity to differentiate into adipocytes, osteocytes and chondrocytes *in vitro*³² (Fig. 1B–D). More recently MSC have also been detected in adipose, umbilical cord and a number of postnatal organs and tissues, including the kidney, and they have shown a promising ability to protect

against tissue injury and facilitate endogenous tissue repair.^{37–40} Unlike embryonic stem cells and induced pluripotent stem cells, MSC do not form teratomas following transplantation in rodents.⁴¹

MESENCHYMAL STEM CELLS IN TISSUE REGENERATION AND REPAIR

Mesenchymal stem cells have been found to exert a therapeutic effect in a wide array of diseases, acting through their unique immunomodulatory abilities that can alter the pro-inflammatory course of injury. This may involve the secretion of paracrine factors that dampen inflammation and in turn promote tissue remodelling and repair.³⁹ Their ability to modulate the immune response *in vivo* was first reported by Bartholomew *et al.*⁴² who demonstrated that the intravenous administration of allogeneic MSC to baboons resulted in prolonged skin-graft survival. MSC have also been reported to be beneficial in an autoimmune disease setting. In a mouse model of multiple sclerosis termed autoimmune encephalomyelitis (EAE), the administration of MSC at the onset of disease induced peripheral T-cell anergy against the pathogenic peptide myelin oligodendrocyte glycoprotein (MOG), resulting in the amelioration of the progression of injury.⁴³ Furthermore, the administration of MSC to mice with diabetes type 1 resulted in the recovery of damaged insulin producing pancreatic islets and β -cells and decreased blood glucose levels.⁴⁴ Two mechanisms appear to be aiding this recovery. In addition to the production of trophic growth factors, MSC also inhibit the β -cell specific T-cell immune reaction.⁴⁵ In a mouse model of lung fibrosis, MSC reduced local inflammation, collagen accumulation and consequently fibrosis.⁴⁶ Subsequent studies demonstrated that MSC conferred this protection by inhibiting the release of interleukin (IL)-1 α and tumour necrosis factor (TNF)- α through the secretion of IL-1 receptor antagonist (IL-1RA).⁴⁷ The local injection of MSC to mice following coronary ligation induced the regeneration of cardiac tissue and improved myocardial function.⁴⁸ Following intravenous administration, MSC preferentially homed to the infarct site where they promoted angiogenesis and myogenesis and mediated myocardial repair via paracrine mechanisms.⁴⁹ The first phase I clinical trial in humans involved the intravenous infusion of MSC into patients with hematologic malignancies in complete remission resulting in no adverse events.⁵⁰ Subsequent trials in breast cancer patients showed that MSC infusion, following high dose chemotherapy and peripheral-blood progenitor-cell infusion resulted in enhanced hematopoietic engraftment and recovery.⁵¹ The immunosuppressive effects of MSC have also effectively been used to treat a leukaemia patient with severe treatment-resistant grade IV acute graft-versus-host disease (GvHD).⁵² Following the promising results obtained from these trials, MSC have since been clinically trialled in a diverse range of other conditions. Numerous phase I–II and III clinical trials exploring the therapeutic

potential of MSC in conditions such as diabetes type 1, myocardial infarction, ischemic stroke, Crohn's disease, cirrhosis and osteoarthritis have been completed or are currently in progress (see <http://www.clinicaltrials.gov>).

Furthermore, a dose-escalating phase I clinical trial was carried out in on-pump cardiac surgery patients undergoing coronary artery bypass or valve repair, who were at high risk of developing postoperative acute kidney injury (<http://www.clinicaltrials.gov>; NCT00733876). Preliminary results have demonstrated that the MSC therapy resulted in no adverse effects. The postoperative length of stay and readmission rate of MSC-treated patients compared to historical matched controls was reduced by approximately 40%. All MSC-treated patients exhibited normal renal function in comparison to approximately 20% of the historical matched controls that developed acute kidney injury.⁵³ Clinical trials investigating the use of MSC transplantation for the prevention of kidney transplant rejection and graft tolerance (<http://www.clinicaltrials.gov>; NCT00752479, NCT00658073 and NCT00734396), and the treatment of lupus nephritis (<http://www.clinicaltrials.gov>; NCT00698191 and NCT00659217) are also currently underway.

MESENCHYMAL STEM CELLS IN ACUTE KIDNEY DISEASE

Despite the current data showing clinical efficacy, the precise manner in which MSC confer renoprotection is not understood. Initial experimental studies carried out by Morigi *et al.*⁵⁴ and Herrera *et al.*⁵⁵ reported that the exogenous administration of MSC to mice with acute renal injury could promote both structural and functional renal repair via the transdifferentiation of MSC into tubular epithelium. However, follow up studies revealed that only 2.0–2.5% of the injected MSC showed engraftment,⁵⁶ opposed to a previously reported 22% of cells.⁵⁵ These reports demonstrate that the direct engraftment of exogenously administered, transdifferentiating MSC is not the predominant mechanism in which MSC enhance renal repair.

There is increasing evidence that MSC can elicit repair through paracrine and/or endocrine mechanisms, where they release trophic growth factors that modulate the immune response and consequently mediate repair.^{57–64} The ability of MSC to inhibit the release of pro-inflammatory cytokines and secrete a variety of trophic growth factors that, promote angiogenesis, mitogenesis and proliferation while reducing apoptosis may collectively mediate the protective and regenerative effects in the kidney of laboratory rodents (summarized in Table 1).^{54–70}

Recent studies,^{60,62} have shown that the administration of MSC following ischemia-reperfusion (IR) injury result in a significant downregulation of the expression of pro-inflammatory cytokines such as IL-1 β , TNF- α , IFN- γ and suppression of inducible nitric oxide synthase (iNOS) at 24 h post-IR injury. This was coupled with an upregulation of the

Table 1 Summary of studies using mesenchymal stem cells (MSC) isolated from various sources to treat acute kidney injury

Injury model	MSC source	Administration	Features	Reference
Glycerol-induced kidney injury	1 × 10 ⁶ GFP+ mouse BM-MSC – female C57BL/6J mice	i.v. injection	↑ proliferation, ↑ morphological recovery, ↑ renal function	54
Cisplatin-induced kidney injury	2 × 10 ⁵ mouse BM-MSC – male C57BL/6J mice	i.v. injection	↑ renal function, ↑ tubular proliferation, ↑ morphological recovery	55
40 min bilateral IR	1.5 × 10 ⁶ rat BM-MSC – Sprague–Dawley rats	Infused into thoracic aorta via a carotid artery	↑ renal function, ↓ injury score, ↑ preservation of proximal tubular brush border	68
40 min bilateral IR	1 × 10 ⁶ rat BM-MSC	Intra-aortic delivery via left carotid artery	↑ renal function, ↑ proliferative indexes, ↓ apoptotic indexes, ↓ renal injury, ↓ IL-1β, TNF-α, IFN-γ, iNOS, ↑IL-10, bFGF, TGF-α, Bcl-2	62
Cisplatin-induced kidney injury	2 × 10 ⁵ mouse BM-MSC – male C57BL/6J mice	Tail vein or i.p. injection	↑ renal function, ↑ tubular cell proliferation, ↓ tubular cell apoptosis	57
Glycerol-induced kidney injury	1 × 10 ⁶ mouse CD44+ or CD44-/- BM-MSC – C57BL/6J or Cd44tm1Hbg/J mice	Tail vein	CD44+ BM-MSC: ↑ morphological and functional recovery CD44-/- BM-MSC: no significant morphological or functional recovery	56
Cisplatin-induced kidney injury	2 × 10 ⁵ mouse IGF-1 gene silenced BM-MSC – male C57BL/6J mice	i.v. injection	Limited protection of renal function (BUN) and tubular injury	59
60 min bilateral IR	2 × 10 ⁵ rat BM-MSC – male Wistar rats	i.v. injection	↓ serum creatinine and plasma urea, ↑ PCNA nuclei in MSC treated kidneys, ↑ IL-4, ↓ IL-1β	70
30 min unilateral IR	1 × 10 ⁵ rat MSC	Intra-arterially infused	↓ apoptosis in kidney regions with MSC still present in microvasculature 24 h post-IR	63
40 min bilateral IR	1 × 10 ⁶ Kallikrein-modified BM-MSC – male Wistar rats	Intra-aortic delivery via left carotid artery	↓ serum creatinine and urea nitrogen, ↓ apoptosis, ↓ tubular injury	67
Cisplatin-induced kidney injury	5 × 10 ⁵ human BM-MSC	Tail vein	↑ renal function, ↑ proliferative score, ↓ proximal tubular epithelial cell injury, ↓ apoptotic score, ↓ mortality	69
60 min bilateral IR	2 × 10 ⁵ rat BM-MSC – male Wistar rats	i.v. injection	↓ serum creatinine, ↑ renal function, low expression of IL-1β, IL-6, TNF-α, high expression IL-4 and IL-10	60
58 min bilateral IR	VEGF knockdown BM-MSC – hPAP transgenic F344 rats	Intra-aortic delivery via left carotid artery	↑ mortality, delayed functional recovery	61
60 min bilateral IR	1 × 10 ⁶ human umbilical cord-MSC	Intra-aortic delivery via left carotid artery	↓ serum creatinine and urea nitrogen, ↓ caspase-3, IL-1β and TNF-α, ↑ proliferative score	65
Cisplatin-induced kidney injury	5 × 10 ⁶ human BM-MSC	i.p. injection	Prolonged survival, ↓ urea nitrogen, ↓ apoptosis, ↑ proliferation	66
Cisplatin-induced kidney injury	5 × 10 ⁵ VEGF-hMSC	Tail vein	↑ proliferation, ↓ apoptosis, ↑ renal function, improved morphology and prolonged survival	64
60 min bilateral IR	1 × 10 ⁶ human umbilical cord HGF-MSC	Intra-aortic delivery via left carotid artery	↓ apoptosis, ↓ tubular casts, ↑ proliferation, ↑ renal function	58

bFGF, basic fibroblast growth factor; BM-MSC, bone marrow-mesenchymal stem cell; BUN, blood urea nitrogen; HGF, hepatic growth factor; IGF, insulin-like growth factor; IL, interleukin; iNOS, inducible nitric oxide synthase; i.p., intraperitoneal; IR, ischemia reperfusion; i.v., intravenous; PCNA, proliferating cell nuclear antigen; TGF, transforming growth factor; TNF, tumour necrosis factor; VEGF, vascular endothelial growth factor.

anti-inflammatory cytokines IL-4, IL-10, basic fibroblast growth factor (bFGF), transforming growth factor (TGF)-α and Bcl-2, which resulted in a reduction in renal injury, increased tubular epithelial proliferation and improved renal function. These findings indicate that MSC are capable of modulating the inflammatory immune response soon after the initiation of injury, shifting it from a pro-inflammatory T_H1 profile to an anti-inflammatory T_H2 one.^{60,62} Moreover, the areas of the kidney where MSC were still present at 24 h post-IR injury were associated with reduced apoptosis com-

pared to regions that no longer contained these cells.⁶³ This suggests that MSC are capable of secreting anti-apoptotic factors that protect surrounding renal cells from undergoing apoptosis following renal insult. To further elucidate their protective mechanisms, MSC, were co-cultured *in vitro* with cisplatin-treated proximal tubular epithelial cells (PTEC).⁵⁹ These co-culture assays, using Transwell membranes, showed that the protective effects of MSC on PTEC proliferation were not due to cell-to-cell contact but more likely the production of MSC-derived trophic factors.⁵⁹

Importantly, the administration of MSC-conditioned medium to mice with cisplatin-induced injury was also found to reduce tubular cell apoptosis and improve kidney structure and function.⁵⁷ This further supports the notion that MSC secrete factors that mediate renoprotection in a paracrine manner. MSC-conditioned medium has been reported to contain hepatocyte growth factor (HGF), insulin-like growth factor 1 (IGF-1) and vascular endothelial growth factor (VEGF).^{62,63} Both HGF and IGF-1 have anti-apoptotic and mitogenic properties that can accelerate cellular repair when administered to mice with kidney IR injury.⁷¹⁻⁷⁴ In addition to the cellular survival effects of VEGF that decrease apoptosis and promote endothelial and epithelial proliferation, VEGF can also mediate vasodilation, matrix remodeling, monocyte chemotaxis and angiogenesis.^{63,75}

Imberti *et al.*⁵⁹ provided *in vitro* evidence that MSC-derived IGF-1 is the principle mediator responsible for renal repair. The addition of an anti-IGF-1 antibody to MSC and PTEC co-cultures resulted in the attenuation of PTEC proliferation. Furthermore, the co-culture of IGF-1 silenced MSC and PTEC also resulted in the attenuation of PTEC proliferation and increased apoptosis. The *in vivo* administration of IGF-1 silenced MSC to mice with cisplatin-induced injury resulted in limited improvements in renal regeneration and repair.⁵⁹ Furthermore, human umbilical cord-derived MSC (hucMSC) overexpressing HGF (HGF-hucMSC) showed enhanced therapeutic effects when administered to mice with IR injury, compared to hucMSC treatment.⁵⁸ In addition, Yuan *et al.*⁶⁴ demonstrated that the *in vitro* co-culture of human embryonic MSC overexpressing VEGF (VEGF-hMSC) with cisplatin-injured tubular epithelial cells (TCMK-1) resulted in enhanced protection, in comparison with co-cultures involving hMSC. Moreover, the administration of VEGF-hMSC to mice with cisplatin-induced injury, resulted in decreased apoptosis and increased proliferation, enhanced functional recovery and prolonged survival compared to hMSC treated mice.⁶⁴ Tögel *et al.*⁶¹ also demonstrated that the administration of VEGF knockdown MSC to animals with IR injury resulted in a decline in the rate of functional renal repair and increased mortality rates.

While results in the laboratory have shown great potential for MSC to exert immunomodulatory effects and promote regeneration and repair following disease, it should not be ignored that some studies have demonstrated that the therapeutic effect of MSC can vary.^{66,76}

HOMING OF MESENCHYMAL STEM CELLS

In steady state, intravenously injected MSC migrate to the BM.^{77,78} In the setting of inflammatory damage, MSC preferentially home to the site of inflammation where they then migrate across the endothelium and enter the injured organ,^{46,56,79-81} to some extent analogous to leukocyte trafficking (Fig. 2). The *in vivo* tracking of fluorescently labelled MSC have demonstrated that these cells infiltrate the peri-

tubular capillaries and glomeruli of kidneys with IR injury within 10 min of injection, with no cells evident by 72 h.⁶² The precise mechanisms of MSC homing to sites of tissue injury are not fully understood. However, Bi *et al.*⁵⁷ reported that the beneficial effects of administering MSC to mice with cisplatin-induced injury were also observed when MSC-conditioned media was administered without the cells. This implies that the mechanisms in which MSC confer protection is not entirely attributed to their ability to home and engraft to the site of kidney damage. The study highlights that MSC are also capable of mediating protection via an endocrine manner.⁵⁷

Mesenchymal stem cells have numerous chemokine receptors that may assist in their migration to sites of inflammation.^{82,83} Following ischemic injury, the expression of the chemokine stromal cell-derived factor-1 (SDF-1), also known as CXCL12, is upregulated within the kidney.⁸⁴ MSC express the SDF-1 receptor CXCR4, which is further upregulated under hypoxic conditions.^{85,86} In addition, when MSC are pre-incubated with TNF- α they show an increased migratory capacity towards SDF-1 indicating that a SDF-1/CXCR4 interaction may mediate the localization of exogenously injected MSC to sites of tissue injury.^{87,88} Ponte *et al.*⁸⁸ tested the ability of MSC to home towards 16 different growth factors and chemokines *in vitro* and found that platelet-derived growth factor-AB (PDGF-AB) and IGF-1 were the most potent chemoattractants for MSC. CD44 is another candidate that has been shown to play a vital role in MSC trafficking.^{56,89} CD44 on MSC binds to hyaluronic acid (HA), which is significantly upregulated in the kidney following ischemic injury.^{56,90} Supportive studies by Herrera *et al.*⁵⁶ show that the injection of either MSC derived from CD44 null mice, or MSC incubated with a CD44 blocking antibody or soluble HA, did not migrate to the kidney following glycerol induced damage. However, MSC homing was restored when these CD44-negative cells were transfected with wild-type CD44, indicating that CD44/HA interactions are required for the migration of MSC to the kidney following injury.⁵⁶

DO MESENCHYMAL STEM CELLS ACT VIA MACROPHAGES?

Monocyte-derived macrophages comprise a heterogeneous population of cells that play a fundamental role in immune and non-immune-mediated renal disease, host defence and allograft responses. Macrophages are key regulators of the innate immune system, where they can detect, phagocytose and destroy foreign antigens.⁹¹ Apart from tissue destruction, it is now known that macrophages also play an important role in tissue homeostasis, cellular replacement and repair through the clearance of apoptotic cells and cellular debris. They also produce mediators that downregulate inflammation and promote remodelling and regeneration.

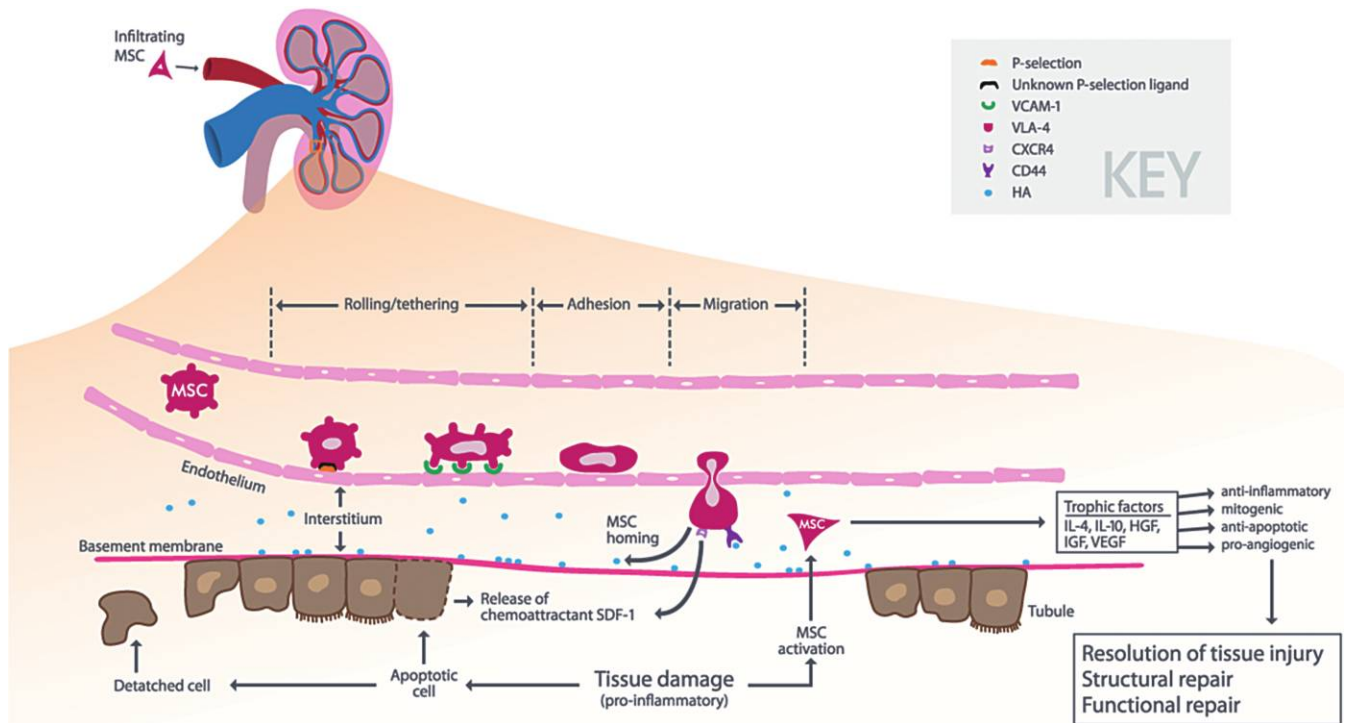


Fig. 2 Representative diagram depicting MSC homing to a kidney with acute damage. The precise mechanisms that facilitate MSC homing are still unclear. However, various growth factors, cytokines, chemokines and chemokine receptors are proposed to play key roles in the migratory process. Following acute insult, there is upregulation of SDF-1 and HA within the kidney. MSC express CXCR4 and CD44, which bind SDF-1 and HA, respectively. Following intravenous administration, MSC can bind to P-selectin and roll along the endothelium of blood vessels, preferentially migrating along the SDF-1 and HA gradient to sites of inflammation. Thereafter, MSC firmly adhere to the endothelial wall via VLA-4 and VCAM-1 and transmigrate across the endothelium into the kidney where they secrete an array of trophic factors that promote structural and functional repair and mediate tissue remodelling. HA, hyaluronic acid; MSC, mesenchymal stem cell; SDF-1, stromal cell-derived factor-1; VCAM-1, vascular cell adhesion molecule-1; VLA-4, very late antigen-4. IL, interleukin; HGF, hepatocyte growth factor; IGF, insulin-like growth factor; VEGF, vascular endothelial growth factor.

The immunomodulatory effects of MSC on T lymphocytes, B lymphocytes, natural killer cells and dendritic cells have been extensively investigated (for review^{34,92}). However, less is known about their ability to modulate macrophage phenotype and function. The activation state that governs macrophage function is dependent on the inflammatory stimuli received from the tissue microenvironment. As the process of repair shifts from the initial inflammatory phase to that of remodelling, macrophages subsequently exhibit varying polarization states and exert a diverse range of functional activities.⁹³ Although a variety of classification methods have been proposed, macrophages are typically believed to exist in one of two opposing polarization states, that is, the M1 ‘classically activated’ subset or M2 ‘alternatively activated’ subset.⁹⁴

M1 polarization is achieved through a combination of events. The first ‘priming’ step involves exposure of the macrophage to IFN- γ .⁹¹ The second signal requires the exposure to either a microbial product, such as lipopolysaccharide (LPS), or proinflammatory cytokines, such as TNF, to the macrophage, resulting in M1 activation.⁹¹ M1 macrophages are characterized by their enhanced ability to phagocytose and present antigen through the upregulation of MHC class

II and the co-stimulatory molecules CD80 and CD86.⁹⁵ They secrete numerous pro-inflammatory cytokines, particularly IL-12 and IL-23, which induce the downstream production of the toxic intermediates nitric oxide and reactive oxygen species (ROS) as well as promoting the killing and degradation of intracellular microorganisms.^{91,96}

It was previously believed that Th2 derived cytokines had a deactivating effect on macrophages.⁹⁷ However, in 1992, Stein *et al.*⁹⁸ demonstrated that macrophages exposed to IL-4 took on an ‘alternative’ phenotype, characterized by reduced secretion of proinflammatory cytokines. It has since been reported that exposure to IL-13, IL-10, TGF- β , glucocorticoids and immune complexes in combination with IL-1 β or LPS can also induce an M2 alternative polarization state.⁹⁴ In contrast to their classically activated counterpart, M2 macrophages are involved in dampening the inflammatory response, while exhibiting enhanced scavenging abilities that promote tissue remodelling and repair. It has recently been shown that M2 macrophages produce several factors that promote angiogenesis, mediate wound healing, extracellular matrix (ECM) deposition and tissue remodelling. For example, they express high levels of IGF-1, which provides signals for repair and stimulates re-epithelialization;

fibronectin (FN)-1, which mediates ECM deposition; and the TGF- β matrix associated protein MP78/70 (β IG-H3) that promotes fibrogenesis.^{99–101}

Recent studies have demonstrated that MSC interact with macrophages and have the potential to promote M2 polarization.^{102–106} The *in vitro* co-culture of human MSC and macrophages resulted in an alternatively activated macrophage phenotype described as mannose receptor (MR)^{high}, IL-10^{high}, IL-6^{high}, TNF- α ^{low} and IL-12^{low} with enhanced phagocytic activity.^{102,106} In addition, it has been shown that MSC-conditioned medium can promote macrophages to adapt a regulatory-like M2 phenotype characterized by a significantly reduced production of pro-inflammatory cytokines and an enhanced production of IL-10 and phagocytic function.¹⁰³

The *in vivo* treatment of wounds with BM-MSC conditioned medium has been reported to enhance wound healing, a process associated with an increased infiltration of macrophages.¹⁰⁷ Following the systemic administration of human gingiva-derived MSC (GMSC) to mice with an excisional skin wound, GMSC homed to the wound site and were found in close proximity with macrophages. Subsequent analysis of this macrophage phenotype revealed an increased expression of the M2 macrophage markers Fizz1 and arginase-1, highlighting the ability of MSC to interact with macrophages and promote M2 polarization.¹⁰⁶ In a mouse model of transient global ischemia, the administration of BM-MSC resulted in neuroprotection. Further investigation demonstrated an upregulation of the M2 markers Ym-1, IGF-1, galactin-3 and MHCII in the microglia/macrophages.¹⁰⁵ Moreover, Nemeth *et al.*¹⁰⁴ showed that MSC administered to mice with cecal ligation and puncture (CLP)-induced sepsis homed to the lung where they were found surrounded by macrophages. To further support the argument for the importance of macrophages in the MSC reparative response, when MSC were administered to mice with CLP-induced sepsis following macrophage depletion, injury protection was lost.¹⁰⁴

CONCLUSION

Since the initial excitement surrounding the multilineage potential and self-renewal properties of MSC, their therapeutic potential to elicit tissue regeneration has now been exploited both experimentally and in a wide range of potential clinical applications. MSC can home to damaged tissue where they exert potent immunosuppressive effects and secrete soluble factors that modify the pro-inflammatory cascade to promote tissue remodelling and cellular replacement, which subsequently protects the kidney from further injury. The interaction of MSC with macrophages may play a vital role in their downstream anti-inflammatory and immunomodulatory effects. However, the specific cell cross-talk between MSC and damaged kidney cells and the molecular mechanisms responsible for their unique immunogenicity

remain poorly defined. Furthermore, the optimal delivery methods for engraftment, long-term safety and their ability to modify the tissue microenvironment in a setting of fibrosis require additional consideration.

REFERENCES

1. Blanpain C, Horsley V, Fuchs E. Epithelial stem cells: Turning over new leaves. *Cell* 2007; **128**: 445–58.
2. Blanpain C, Lowry WE, Geoghegan A, Polak L, Fuchs E. Self-renewal, multipotency, and the existence of two cell populations within an epithelial stem cell niche. *Cell* 2004; **118**: 635–48.
3. Bussolati B, Tetta C, Camussi G. Contribution of stem cells to kidney repair. *Am. J. Nephrol.* 2008; **28**: 813–22.
4. Humphreys BD, Bonventre JV. Mesenchymal stem cells in acute kidney injury. *Annu. Rev. Med.* 2008; **59**: 311–25.
5. Roufosse C, Cook HT. Stem cells and renal regeneration. *Nephron Exp. Nephrol.* 2008; **109**: E39–E45.
6. Elger M, Hentschel H, Litteral J *et al.* Nephrogenesis is induced by partial nephrectomy in the elasmobranch *Leucoraja erinacea*. *J. Am. Soc. Nephrol.* 2003; **14**: 1506–18.
7. Cochrane AL, Kett MM, Samuel CS *et al.* Renal structural and functional repair in a mouse model of reversal of ureteral obstruction. *J. Am. Soc. Nephrol.* 2005; **16**: 3623–30.
8. Kelly KJ, Molitoris BA. Acute renal failure in the new millennium: Time to consider combination therapy. *Semin. Nephrol.* 2000; **20**: 4–19.
9. Romagnani P. Toward the identification of a 'renopoeitic system'? *Stem Cells* 2009; **27**: 2247–53.
10. Humphreys BD, Valerius MT, Kobayashi A *et al.* Intrinsic epithelial cells repair the kidney after injury. *Cell Stem Cell* 2008; **2**: 284–91.
11. Bonventre JV. Dedifferentiation and proliferation of surviving epithelial cells in acute renal failure. *J. Am. Soc. Nephrol.* 2003; **14**: S55–S61.
12. Little MH, Bertram JF. Is there such a thing as a renal stem cell? *J. Am. Soc. Nephrol.* 2009; **20**: 2112–7.
13. Appel D, Kershaw D, Smeets B, Yuan G, Fuss A, Frye B. Recruitment of podocytes from glomerular parietal epithelial cells. *J. Am. Soc. Nephrol.* 2009; **20**: 333–43.
14. Ronconi E, Sagrinati C, Angelotti ML *et al.* Regeneration of glomerular podocytes by human renal progenitors. *J. Am. Soc. Nephrol.* 2009; **20**: 322–32.
15. Sagrinati C, Netti GS, Mazzinghi B *et al.* Isolation and characterization of multipotent progenitor cells from the Bowman's capsule of adult human kidneys. *J. Am. Soc. Nephrol.* 2006; **17**: 2443–56.
16. Pruszk J, Ludwig W, Blak A, Alavian K, Isacson O. CD15, CD24, and CD29 define a surface biomarker code for neural lineage differentiation of stem cells. *Stem Cells* 2009; **27**: 2928–40.
17. Shackleton M, Vaillant F, Simpson KJ *et al.* Generation of a functional mammary gland from a single stem cell. *Nature* 2006; **439**: 84–8.
18. Miraglia S, Godfrey W, Yin AH *et al.* A novel five-transmembrane hematopoietic stem cell antigen: Isolation, characterization, and molecular cloning. *Blood* 1997; **90**: 5013–21.
19. Shmelkov SV, Meeus S, Moussazadeh N *et al.* Cytokine preconditioning promotes codifferentiation of human fetal liver CD133+ Stem cells into angiomyogenic tissue. *Circulation* 2005; **111**: 1175–83.

20. Yin AH, Miraglia S, Zanjani ED *et al.* AC133, a novel marker for human hematopoietic stem and progenitor cells. *Blood* 1997; **90**: 5002–12.
21. Ricardo SD, van Goor H, Eddy AA. Macrophage diversity in renal injury and repair. *J. Clin. Invest.* 2008; **118**: 3522–30.
22. Friedenstein AJ, Chailakhyan RK, Latsinik NV. Stromal cells responsible for transferring the microenvironment of the hemopoietic tissues. Cloning *in vitro* and retransplantation *in vivo*. *Transplantation* 1974; **17**: 331–40.
23. Friedenstein AJ, Petrakova KV, Kurolesova AI, Frolova GP. Heterotopic of bone marrow. Analysis of precursor cells for osteogenic and hematopoietic tissues. *Transplantation* 1968; **6**: 230–47.
24. Morigi M, Imberti B, Zoja C *et al.* Mesenchymal stem cells are renotropic, helping to repair the kidney and improve function in acute renal failure. *J. Am. Soc. Nephrol.* 2004; **15**: 1794–804.
25. Uccelli A, Moretta L, Pistoia V. Immunoregulatory function of mesenchymal stem cells. *Eur. J. Immunol.* 2006; **36**: 2566–73.
26. Le Blanc K, Ringden O. Immunomodulation by mesenchymal stem cells and clinical experience. *J. Intern. Med.* 2007; **262**: 509–25.
27. Banfi A, Bianchi G, Notaro R, Luzzatto L, Cancedda R, Quarto R. Replicative aging and gene expression in long-term cultures of human bone marrow stromal cells. *Tissue Eng.* 2002; **8**: 901–10.
28. Banfi A, Muraglia A, Dozin B, Mastrogiacomo M, Cancedda R, Quarto R. Proliferation kinetics and differentiation potential of *ex vivo* expanded human bone marrow stromal cells: Implications for their use in cell therapy. *Exp. Hematol.* 2000; **28**: 707–15.
29. Javazon EH, Beggs KJ, Flake AW. Mesenchymal stem cells: Paradoxes of passaging. *Exp. Hematol.* 2004; **32**: 414–25.
30. Pittenger MF, Mackay AM, Beck SC *et al.* Multilineage potential of adult human mesenchymal stem cells. *Science* 1999; **284**: 143–7.
31. Treman N, Korkko J, Ibberson D, Kopen GC, DiGirolamo C, Phinney DG. MicroSAGE analysis of 2,353 expressed genes in a single cell-derived colony of undifferentiated human mesenchymal stem cells reveals mRNAs of multiple cell lineages. *Stem Cells* 2001; **19**: 408–18.
32. Dominici M, Le Blanc K, Mueller I *et al.* Minimal criteria for defining multipotent mesenchymal stromal cells. The International Society for Cellular Therapy position statement. *Cytotherapy* 2006; **8**: 315–7.
33. Le Blanc K. Mesenchymal stromal cells: Tissue repair and immune modulation. *Cytotherapy* 2006; **8**: 559–61.
34. Uccelli A, Moretta L, Pistoia V. Mesenchymal stem cells in health and disease. *Nat. Rev. Immunol.* 2008; **8**: 726–36.
35. Tse WT, Pendleton JD, Beyer WM, Egalka MC, Guinan EC. Suppression of allogeneic T-cell proliferation by human marrow stromal cells: Implications in transplantation. *Transplantation* 2003; **75**: 389–97.
36. Le Blanc K, Tammik C, Rosendahl K, Zetterberg E, Ringden O. HLA expression and immunologic properties of differentiated and undifferentiated mesenchymal stem cells. *Exp. Hematol.* 2003; **31**: 890–6.
37. Erices A, Conget P, Minguell JJ. Mesenchymal progenitor cells in human umbilical cord blood. *Br. J. Haematol.* 2000; **109**: 235–42.
38. Meirelles LDS, Chagastelles PC, Nardi NB. Mesenchymal stem cells reside in virtually all post-natal organs and tissues. *J. Cell Sci.* 2006; **119**: 2204–13.
39. Reinders MEJ, Fibbe WE, Rabelink TJ. Multipotent mesenchymal stromal cell therapy in renal disease and kidney transplantation. *Nephrol. Dial. Transplantat.* 2010; **25**: 17–24.
40. Zuk PA, Zhu M, Ashjian P *et al.* Human adipose tissue is a source of multipotent stem cells. *Mol. Biol. Cell* 2002; **13**: 4279–95.
41. Yamaoka T, Mahara A. Cell rolling column in purification and differentiation analysis of stem cells. *React. Func. Polym.* 2011; **71**: 362–6.
42. Bartholomew A, Sturgeon C, Siatskas M *et al.* Mesenchymal stem cells suppress lymphocyte proliferation *in vitro* and prolong skin graft survival *in vivo*. *Exp. Hematol.* 2002; **30**: 42–8.
43. Zappia E, Casazza S, Pedemonte E *et al.* Mesenchymal stem cells ameliorate experimental autoimmune encephalomyelitis inducing T-cell anergy. *Blood* 2005; **106**: 1755–61.
44. Lee RH, Seo MJ, Reger RL *et al.* Multipotent stromal cells from human marrow home to and promote repair of pancreatic islets and renal glomeruli in diabetic NOD/scid mice. *Proc. Natl. Acad. Sci. USA* 2006; **103**: 17438–43.
45. Urban VS, Kiss J, Kovacs J *et al.* Mesenchymal stem cells cooperate with bone marrow cells in therapy of diabetes. *Stem Cells* 2008; **26**: 244–53.
46. Ortiz LA, Gambelli F, McBride C *et al.* Mesenchymal stem cell engraftment in lung is enhanced in response to bleomycin exposure and ameliorates its fibrotic effects. *Proc. Natl. Acad. Sci. USA* 2003; **100**: 8407–11.
47. Ortiz LA, DuTreil M, Fattman C *et al.* Interleukin 1 receptor antagonist mediates the antiinflammatory and antifibrotic effect of mesenchymal stem cells during lung injury. *Proc. Natl. Acad. Sci. USA* 2007; **104**: 11002–7.
48. Orlic D, Kajstura J, Chimenti S *et al.* Bone marrow cells regenerate infarcted myocardium. *Nature* 2001; **410**: 701–5.
49. Nagaya N, Fujii T, Iwase T *et al.* Intravenous administration of mesenchymal stem cells improves cardiac function in rats with acute myocardial infarction through angiogenesis and myogenesis. *Am. J. Physiol. Heart Circ. Physiol.* 2004; **287**: H2670–H6.
50. Lazarus HM, Haynesworth SE, Gerson SL, Rosenthal NS, Caplan AI. *Ex-vivo* expansion and subsequent infusion of human bone-marrow-derived stromal progenitor cells (mesenchymal progenitor cells) – implications for therapeutic use. *Bone Marrow Transplant.* 1995; **16**: 557–64.
51. Koc ON, Gerson SL, Cooper BW *et al.* Rapid hematopoietic recovery after coinfusion of autologous-blood stem cells and culture-expanded marrow mesenchymal stem cells in advanced breast cancer patients receiving high-dose chemotherapy. *J. Clin. Oncol.* 2000; **18**: 307–16.
52. Le Blanc K, Rasmuson I, Sundberg B *et al.* Treatment of severe acute graft-versus-host disease with third party haploidentical mesenchymal stem cells. *Lancet* 2004; **363**: 1439–41.
53. Togel F, Westenfelder C. Treatment of acute kidney injury with allogeneic mesenchymal stem cells: preclinical and initial clinical data. In: Goligorsky M (ed.). *Regenerative Nephrology*, 1st edn. San Diego, CA, USA: Academic Press, 2011; 315–39.
54. Morigi M, Imberti B, Zoja C *et al.* Mesenchymal stem cells are renotropic, helping to repair the kidney and improve function in acute renal failure. *J. Am. Soc. Nephrol.* 2004; **15**: 1794–804.
55. Herrera MB, Bussolati B, Bruno S, Fonsato V, Romanazzi GM, Camussi G. Mesenchymal stem cells contribute to the renal repair of acute tubular epithelial injury. *Int. J. Mol. Med.* 2004; **14**: 1035–41.
56. Herrera MB, Bussolati B, Bruno S *et al.* Exogenous mesenchymal stem cells localize to the kidney by means of CD44 following acute tubular injury. *Kidney Int.* 2007; **72**: 430–41.
57. Bi B, Schmitt R, Israilova M, Nishio H, Cantley LG. Stromal cells protect against acute tubular injury via an endocrine effect. *J. Am. Soc. Nephrol.* 2007; **18**: 2486–96.

58. Chen Y, Qian H, Zhu W *et al.* Hepatocyte growth factor modification promotes the amelioration effects of human umbilical cord mesenchymal stem cells on rat acute kidney injury. *Stem Cells Dev.* 2011; **20** (1): 103–13.
59. Imberti B, Morigi M, Tomasoni S *et al.* Insulin-like growth factor-1 sustains stem cell-mediated renal repair. *J. Am. Soc. Nephrol.* 2007; **18**: 2921–8.
60. Semedo P, Palasio CG, Oliveira CD *et al.* Early modulation of inflammation by mesenchymal stem cell after acute kidney injury. *Int. Immunopharmacol.* 2009; **9**: 677–82.
61. Togel F, Cohen A, Zhang P, Yang Y, Hu Z, Westenfelder C. Autologous and allogeneic marrow stromal cells are safe and effective for the treatment of acute kidney injury. *Stem Cells Dev.* 2009; **18**: 475–85.
62. Togel F, Hu ZM, Weiss K, Isaac J, Lange C, Westenfelder C. Administered mesenchymal stem cells protect against ischemic acute renal failure through differentiation-independent mechanisms. *Am. J. Physiol. Renal Physiol.* 2005; **289**: F31–F42.
63. Togel F, Weiss K, Yang Y, Hu Z, Zhang P, Westenfelder C. Vasculotropic, paracrine actions of infused mesenchymal stem cells are important to the recovery from acute kidney injury. *Am. J. Physiol. Renal Physiol.* 2007; **292**: F1626–35.
64. Yuan L, Wu M-J, Sun H-Y *et al.* VEGF-modified human embryonic mesenchymal stem cell implantation enhances protection against cisplatin-induced acute kidney injury. *Am. J. Physiol. Renal Physiol.* 2011; **300**: F207–F18.
65. Cao HL, Qian H, Xu WR *et al.* Mesenchymal stem cells derived from human umbilical cord ameliorate ischemia/reperfusion-induced acute renal failure in rats. *Biotechnol. Lett.* 2010; **32**: 725–32.
66. Eliopoulos N, Zhao J, Bouchentouf M *et al.* Human marrow-derived mesenchymal stromal cells decrease cisplatin renotoxicity *in vitro* and *in vivo* and enhance survival of mice post-intraperitoneal injection. *Am. J. Physiol. Renal Physiol.* 2010; **299**: F1288–F98.
67. Hagiwara M, Shen B, Chao L, Chao JLM. Kallikrein-modified mesenchymal stem cell implantation provides enhanced protection against acute ischemic kidney injury by inhibiting apoptosis and inflammation. *Hum. Gene Ther.* 2008; **19**: 807–19.
68. Lange C, Togel F, Itrich H *et al.* Administered mesenchymal stem cells enhance recovery from ischemia/reperfusion-induced acute renal failure in rats. *Kidney Int.* 2005; **68**: 1613–17.
69. Morigi M, Inrona M, Imberti B *et al.* Human bone marrow mesenchymal stem cells accelerate recovery of acute renal injury and prolong survival in mice. *Stem Cells* 2008; **26**: 2075–82.
70. Semedo P, Wang PM, Andreucci TH *et al.* Mesenchymal stem cells ameliorate tissue damages triggered by renal ischemia and reperfusion injury. *Transplant. Proc.* 2007; **39**: 421–3.
71. Miller SB, Martin DR, Kissane J, Hammerman MR. Insulin-like growth factor I accelerates recovery from ischemic acute tubular necrosis in the rat. *Proc. Natl. Acad. Sci. USA* 1992; **89**: 11876–80.
72. Miller SB, Martin DR, Kissane J, Hammerman MR. Hepatocyte growth factor accelerates recovery from acute ischemic renal injury in rats. *Am. J. Physiol.* 1994; **266**: F129–F34.
73. Liu YH. Hepatocyte growth factor and the kidney. *Curr. Opin. Nephrol. Hypertens.* 2002; **11**: 23–30.
74. Hirschberg R, Adler S. Insulin-like growth factor system and the kidney: Physiology, pathophysiology, and therapeutic implications. *Am. J. Kidney Dis.* 1998; **31**: 901–19.
75. Schrijvers BF, Flyvbjerg A, De Zeeuw AS. The role of vascular endothelial growth factor (VEGF) in renal pathophysiology. *Kidney Int.* 2004; **65**: 2003–17.
76. Inoue S, Popp FC, Koehl GE *et al.* Immunomodulatory effects of mesenchymal stem cells in a rat organ transplant model. *Transplantation* 2006; **81**: 1589–95.
77. Devine SM, Bartholomew AM, Mahmud N *et al.* Mesenchymal stem cells are capable of homing to the bone marrow of non-human primates following systemic infusion. *Exp. Hematol.* 2001; **29**: 244–55.
78. Wynn RF, Hart CA, Corradi-Perini C *et al.* A small proportion of mesenchymal stem cells strongly expresses functionally active CXCR4 receptor capable of promoting migration to bone marrow. *Blood* 2004; **104**: 2643–5.
79. Chapel A, Bertho JM, Bensedhoum M *et al.* Mesenchymal stem cells home to injured tissues when co-infused with hematopoietic cells to treat a radiation-induced multi-organ failure syndrome. *J. Gene Med.* 2003; **5**: 1028–38.
80. Mahmood A, Lu DY, Lu M, Chopp M. Treatment of traumatic brain injury in adult rats with intravenous administration of human bone marrow stromal cells. *Neurosurgery* 2003; **53**: 697–702.
81. Orlic D, Kajstura J, Chimenti S *et al.* Mobilized bone marrow cells repair the infarcted heart, improving function and survival. *Proc. Natl. Acad. Sci. USA* 2001; **98**: 10344–9.
82. Brooke G, Cooka M, Blair C *et al.* Therapeutic applications of mesenchymal stromal cells. *Semin. Cell Dev. Biol.* 2007; **18**: 846–58.
83. Fox JM, Chamberlain G, Ashton BA, Middleton J. Recent advances into the understanding of mesenchymal stem cell trafficking. *Br. J. Haematol.* 2007; **137**: 491–502.
84. Togel F, Isaac J, Hu ZM, Weiss K, Westenfelder C. Renal SDF-1 signals mobilization and homing of CXCR4-positive cells to the kidney after ischemic injury. *Kidney Int.* 2005; **67**: 1772–84.
85. Honczarenko M, Le Y, Swierkowski M, Ghiran I, Glodek AM, Silberstein LE. Human bone marrow stromal cells express a distinct set of biologically functional chemokine receptors. *Stem Cells* 2006; **24**: 1030–41.
86. Hung SC, Pochampally RR, Hsu SC *et al.* Short-term exposure of multipotent stromal cells to low oxygen increases their expression of CX3CR1 and CXCR4 and their engraftment *in vivo*. *PLoS ONE* 2007; **2**: e416.
87. Ji JF, He BP, Dheen ST, Tay SSW. Interactions of chemokines and chemokine receptors mediate the migration of mesenchymal stem cells to the impaired site in the brain after hypoglossal nerve injury. *Stem Cells* 2004; **22**: 415–27.
88. Ponte AL, Marais E, Gallay N *et al.* The *in vitro* migration capacity of human bone marrow mesenchymal stem cells: Comparison of chemokine and growth factor chemotactic activities. *Stem Cells* 2007; **25**: 1737–45.
89. Zhu H, Mitsuhashi N, Klein A *et al.* The role of the hyaluronan receptor CD44 in mesenchymal stem cell migration in the extracellular matrix. *Stem Cells* 2006; **24**: 928–35.
90. Goransson V, Johnsson C, Jacobson A, Heldin P, Hallgren R, Hansell P. Renal hyaluronan accumulation and hyaluronan synthase expression after ischaemia-reperfusion injury in the rat. *Nephrol. Dial. Transplant.* 2004; **19**: 823–30.
91. Wilson HM, Walbaum D, Rees AJ. Macrophages and the kidney. *Curr. Opin. Nephrol. Hypertens.* 2004; **13**: 285–90.
92. Nauta AJ, Fibbe WE. Immunomodulatory properties of mesenchymal stromal cells. *Blood* 2007; **110**: 3499–506.
93. Stout RD, Jiang CC, Matta B, Tietzel I, Watkins SK, Suttles J. Macrophages sequentially change their functional phenotype in response to changes in microenvironmental influences. *J. Immunol.* 2005; **175**: 342–9.

94. Ricardo SD, van Goor H, Eddy AA. Macrophage diversity in renal injury and repair. *J. Clin. Invest.* 2008; **118**: 3522–30.
95. Martinez FO, Sica A, Mantovani A, Locati M. Macrophage activation and polarization. *Front. Biosci.* 2008; **13**: 453–61.
96. Williams TM, Little MH, Ricardo SD. Macrophages in renal development, injury, and repair. *Semin. Nephrol.* 2010; **30**: 255–67.
97. Gordon S. Alternative activation of macrophages. *Nat. Rev. Immunol.* 2003; **3**: 23–35.
98. Stein M, Keshav S, Harris N, Gordon S. Interleukin 4 potentially enhances murine macrophage mannose receptor activity: A marker of alternative immunologic macrophage activation. *J. Exp. Med.* 1992; **176**: 287–92.
99. Tsuboi R, Shi CM, Sato C, Cox GN, Ogawa H. Co-administration of insulin-like growth factor (IGF)-I and IGF-binding protein-1 stimulates wound healing in animal models. *J. Invest. Dermatol.* 1995; **104**: 199–203.
100. Gratchev A, Guillot P, Hakiy N *et al.* Alternatively activated macrophages differentially express fibronectin and its splice variants and the extracellular matrix protein beta IG-H3. *Scand. J. Immunol.* 2001; **53**: 386–92.
101. Kratz G, Lake M, Gidlund M. Insulin like growth factor-1 and -2 and their role in the re-epithelialisation of wounds; interactions with insulin like growth factor binding protein type 1. *Scand. J. Plast. Reconstr. Surg. Hand Surg.* 1994; **28**: 107–12.
102. Kim J, Hematti P. Mesenchymal stem cell-educated macrophages: A novel type of alternatively activated macrophages. *Exp. Hematol.* 2009; **37**: 1445–53.
103. Maggini J, Mirkin G, Bognanni I *et al.* Mouse bone marrow-derived mesenchymal stromal cells turn activated macrophages into a regulatory-like profile. *PLoS ONE* 2010; **5**: e9252.
104. Nemeth K, Leelahavanichkul A, Yuen PST *et al.* Bone marrow stromal cells attenuate sepsis via prostaglandin E-2-dependent reprogramming of host macrophages to increase their interleukin-10 production. *Nat. Med.* 2009; **15**: 42–9.
105. Ohtaki H, Ylostalo JH, Foraker JE *et al.* Stem/progenitor cells from bone marrow decrease neuronal death in global ischemia by modulation of inflammatory/immune responses. *Proc. Natl. Acad. Sci. USA* 2008; **105**: 14638–43.
106. Zhang QZ, Su WR, Shi SH *et al.* Human gingiva-derived mesenchymal stem cells elicit polarization of M2 macrophages and enhance cutaneous wound healing. *Stem Cells* 2010; **28**: 1856–68.
107. Chen L, Tredget EE, Wu PY, Wu Y. Paracrine factors of mesenchymal stem cells recruit macrophages and endothelial lineage cells and enhance wound healing. *PLoS ONE* 2008; **3**: e1886.

Human mesenchymal stem cells alter macrophage phenotype and promote regeneration via homing to the kidney following ischemia-reperfusion injury

Andrea F. Wise,¹ Timothy M. Williams,¹ Mensiena B. G. Kiewiet,¹ Natalie L. Payne,²
Christopher Siatskas,¹ Chrishan S. Samuel,³ and Sharon D. Ricardo¹

¹Department of Anatomy and Developmental Biology, Monash University, Clayton, Victoria, Australia; ²Australian Regenerative Medicine Institute, Monash University, Clayton, Victoria, Australia; and ³Department of Pharmacology, Monash University, Clayton, Victoria, Australia

Submitted 19 December 2013; accepted in final form 6 March 2014

Wise AF, Williams TM, Kiewiet MB, Payne NL, Siatskas C, Samuel CS, Ricardo SD. Human mesenchymal stem cells alter macrophage phenotype and promote regeneration via homing to the kidney following ischemia-reperfusion injury. *Am J Physiol Renal Physiol* 306: F1222–F1235, 2014. First published March 12, 2014; doi:10.1152/ajprenal.00675.2013.—Mesenchymal stem cells (MSCs) ameliorate injury and accelerate repair in many organs, including the kidney, although the reparative mechanisms and interaction with macrophages have not been elucidated. This study investigated the reparative potential of human bone marrow-derived MSCs and traced their homing patterns following administration to mice with ischemia-reperfusion (IR) injury using whole body bioluminescence imaging. The effect of MSCs on macrophage phenotype following direct and indirect coculture was assessed using qPCR. Human cytokine production was measured using multiplex arrays. After IR, MSCs homed to injured kidneys where they afforded protection indicated by decreased proximal tubule kidney injury molecule-1 expression, blood urea nitrogen, and serum creatinine levels. SDS-PAGE and immunofluorescence labeling revealed MSCs reduced collagen $\alpha_1(I)$ and IV by day 7 post-IR. Gelatin zymography confirmed that MSC treatment significantly increased matrix metalloproteinase-9 activity in IR kidneys, which contributed to a reduction in total collagen. Following direct and indirect coculture, macrophages expressed genes indicative of an anti-inflammatory “M2” phenotype. MSC-derived human GM-CSF, EGF, CXCL1, IL-6, IL-8, MCP-1, PDGF-AA, and CCL5 were identified in culture supernatants. In conclusion, MSCs home to injured kidneys and promote repair, which may be mediated by their ability to promote M2 macrophage polarization.

ischemia-reperfusion injury; mesenchymal stem cells; macrophage

SINCE THE INITIAL EXCITEMENT surrounding the multilineage potential and self-renewal properties of mesenchymal stem (stromal) cells (MSCs), their therapeutic potential to elicit tissue regeneration has been explored experimentally and in a wide range of clinical applications (45). MSCs are capable of modulating inflammation through interacting with a variety of immune cells (53, 68). These immunomodulatory properties, in combination with their tissue-regenerative capabilities, have created great enthusiasm for these cells to be used as a treatment for a wide variety of pathological conditions ranging from autoimmune to chronic inflammatory diseases (for a review, see Refs. 45, 62, and 68). MSCs reside in most postnatal organs and tissues and can be isolated and expanded in culture (13). Unlike embryonic stem (ES) cells and induced pluripotent stem (iPS) cells, MSCs typically do not form

tumors following transplantation in rodents and are free of the ethical limitations associated with ES cell research.

Human MSCs have been shown to ameliorate the symptoms of inflammatory diseases in rodent models (4, 9, 24, 27, 41, 70); however, the mechanisms responsible for their protective and regenerative effects are not completely understood. The interaction of MSCs with macrophages may play a vital role in their downstream anti-inflammatory and immunomodulatory effects, yet the specific cell cross talk MSCs have with infiltrating macrophages and damaged kidney cells, along with the cytokines that contribute to their unique immunomodulatory properties, remains poorly defined.

MSCs secrete a broad range of cytokines, including macrophage chemoattractants, as well as a variety of factors with renoprotective and reparative capabilities. These include anti-inflammatory, antiapoptotic, mitogenic, antifibrotic, and proangiogenic agents, which most likely govern repair via paracrine and endocrine pathways (5, 19, 21, 67). In a setting of acute kidney injury (AKI), transplanted MSCs localized within peritubular capillaries, adjacent to the renal tubules, and glomeruli (56). However, the survival of MSCs and timing of administration leading to the interplay between MSCs and macrophages, along with their ability to modify the tissue microenvironment in a setting where aberrant wound healing-induced collagen accumulation leads to fibrosis, have yet to be elucidated.

Macrophages comprise a heterogeneous population that is governed by the inflammatory cues in the surrounding microenvironment (54). Although initially recognized as contributing to the pathogenesis of kidney injury, macrophages may also play a vital role in the remodeling phase of kidney regeneration following acute damage (30, 61, 63). Subsequently, macrophages have been broadly classified into one of two opposing polarization states: classically activated “M1” and alternatively activated “M2” populations (38). M1 macrophages secrete numerous proinflammatory cytokines and are involved in pathogen clearance whereas M2 macrophages secrete anti-inflammatory cytokines that mediate wound healing and tissue remodeling (38).

This study investigated the therapeutic potential of human bone marrow (BM)-derived MSCs in conjunction with their homing patterns following intravenous (iv) administration to mice with ischemia-reperfusion (IR) injury using whole body bioluminescence imaging. In addition, the effect of MSCs on macrophage phenotype and the soluble factors produced following direct and indirect coculture experiments were assessed.

Address for reprint requests and other correspondence: S. D. Ricardo, Dept. of Anatomy and Developmental Biology, Level 3, Bldg. 75, Monash Univ., Clayton, Victoria 3800, Australia (sharon.ricardo@monash.edu).

MATERIALS AND METHODS

Mesenchymal stem cell culture. Human BM-derived MSCs purchased from the Tulane Center for Stem Cell Research and Regenerative Medicine (Tulane University, New Orleans, LA) and enhanced green fluorescent protein (eGFP) and firefly luciferase (fluc) eGFP⁺fluc⁺ MSCs were cultured as previously described (47). Karyotype analysis was performed on MSCs at passage 3 (Southern Cross Pathology, Clayton, Australia). The clonogenic potential of MSCs was tested using a colony-forming unit-fibroblast (CFU-F) assay, and colonies were stained with 3% (wt/vol) crystal violet (Sigma-Aldrich, St. Louis, MO).

Multilineage differentiation. To demonstrate multilineage differentiation potential, MSCs were differentiated toward osteogenic, adipogenic, and chondrogenic lineages using a human functional identification kit (R&D Systems, Minneapolis, MN). Following differentiation, osteocytes were stained with Alizarin red S (Sigma-Aldrich), adipocytes with fatty acid binding protein-4 (FABP-4; R&D Systems), and chondrocytes with aggrecan (R&D Systems).

Flow cytometry. Immunophenotypic analysis of MSCs by flow cytometry was performed using the following fluorochrome-conjugated anti-human antibodies: CD73-PE, CD90-PerCP-Cy5.5, CD105-Alexa Fluor 647, CD14-APC (eBioscience), CD19-FITC, CD34-APC, CD45-APC, and HLA-DR-FITC. All antibodies were purchased from BD Biosciences (San Jose, CA) unless otherwise indicated. Cell population data was acquired using a FACSCanto II flow cytometer (BD Biosciences) and analyzed using Flowlogic Software (Invivo Technologies, Mentone, Australia).

Experimental design. All animal studies were approved by the Monash University Animal Ethics Committee, which adheres to the Australian Code of Practice for the Care and Use of Animals for Scientific Purposes. For IR injury, male 6- to 8-wk-old C57BL/6J mice (Monash Animal Services, Clayton, Australia) were anesthetized with 2.5% (vol/vol) inhaled isoflurane (Abbott Australasia Pty, Kurnell, Australia), and injury was induced by clamping the left renal pedicle for 40 min (unilateral) or both renal pedicles for 25 min (bilateral) with a microvascular clamp (0.4–0.1 mm; S&T Fine Science Tools, Foster City, CA) through a flank incision. Following reperfusion, mice were injected iv with 1×10^6 MSCs resuspended in 120 μ l PBS or a vehicle control (120 μ l PBS alone). A third group of mice served as a sham-operated control group, whereby the animals were anesthetized and a flank incision made without clamping the renal pedicle. Mice that received bilateral IR injury were placed in metabolic cages to obtain 24-h urine samples. Urinary kidney injury molecule (Kim)-1 was measured with a Kim-1 mouse ELISA (Abcam, Cambridge, UK). Concentrations of blood urea nitrogen (BUN) and serum creatinine were measured 3 days post-IR using the i-STAT CHEM8+ cartridges and the i-STAT system ($n = 8$; Abbott, Ontario, Canada).

Bioluminescence imaging. Mice ($n = 5$) were anesthetized with 2.5% (vol/vol) isoflurane, injected intraperitoneally (ip) with 200 μ l D-luciferin (15 mg/ml in PBS; VivoGlo Luciferin, Promega, San Luis Obispo, CA) and imaged 10 min after injection using the Xenogen IVIS 200 system (Xenogen, Alameda, CA) on days 0 (1-h post-IR injection), 1, and 3 post-IR. Regions of interest (ROI) were drawn, and luciferase signal intensities were analyzed using Living Image 3.2 software (Xenogen).

Histology and immunofluorescence labeling. Histopathology was assessed on formalin-fixed, 4- μ m-thick paraffin sections stained with hematoxylin and eosin (H&E). Semiquantification of histopathology was performed after taking five fields of view/kidney section within the corticomedullary region ($n = 3$; 3 sections/mouse; $\times 400$). Proximal tubular damage and protein cast formation were assessed, and the percentage of kidney damage was graded on a scale of 0 to 4 (refer to Table 1).

To assess proliferation, kidney sections were stained with mouse anti-PCNA (DakoCytomation, Glostrup, Denmark) and rabbit anti-mouse Ki67 (Abcam) primary antibodies followed by Alexa Fluor

Table 1. Injury scale used to grade kidney damage following IR injury

Scale	Percentage of Kidney Damage
0	Normal tubules and no protein casts
0.5	Minor tubular damage and protein cast formation
1.0	Involvement of <10% corticomedullary region
2.0	Involvement of 10% to 25% of corticomedullary region
2.5	Involvement of 26% to 50% of corticomedullary region
3.0	Involvement of 51% to 75% of corticomedullary region
4.0	Widespread damage >75% of corticomedullary region

IR, ischemia-reperfusion.

488 donkey anti-mouse (Molecular Probes, Eugene, OR) and Alexa Fluor 555 goat anti-rabbit (Molecular Probes) secondary antibodies. For proximal tubule Kim-1 expression, immunohistochemical staining was performed with rat anti-mouse Kim-1 (R&D Systems) using the avidin-biotin complex (ABC) method as described previously (43). The area of 3,3'-diaminobenzidine staining per unit area of tissue was measured using a custom macro from the image-analysis software ImageJ/FIJI, version 1.48d. Areas of positive staining were quantified in five nonoverlapping, randomly selected fields of view ($n = 3$, 3 sections/mouse; $\times 400$ magnification).

For the visualization of type IV collagen, kidney sections were stained with a goat anti-human collagen type IV primary antibody (Southern Biotech, Birmingham, AL) followed by an Alexa Fluor 647 chicken anti-goat antibody (Molecular Probes) and for macrophage staining, a rat anti-mouse F4/80 antibody (AbD Serotec, Oxford, UK) followed by an Alexa Fluor 555 goat anti-rat antibody (Molecular Probes). Sections were counterstained with 4,6-diamidino-2-phenylindole (Molecular Probes) and viewed with a Provis AX70 fluorescence microscope (Olympus, Tokyo, Japan). Fluorescence images were captured with an F-view II digital camera (Soft Imaging System, Munster, Germany).

Hydroxyproline, SDS-PAGE, and zymographic analyses. A kidney from each animal was divided into portions containing both cortex and medulla for use in each assay. The total collagen content (% collagen content/dry weight tissue) in the kidney ($n = 3$ /group) was measured using a hydroxyproline assay as previously described (49). In brief, kidneys were lyophilized to measure dry weight, hydrolyzed in 6 M hydrochloric acid, and hydroxyproline levels were determined by measuring the absorbance of hydrolyzed samples at 558 nm, using a Digital Spectrophotometer (Varian, Palo Alto, CA) (50). Total collagen content was determined by multiplying the hydroxyproline measurements by a factor of 6.94.

SDS-PAGE analysis was used to detect changes in interstitial collagen subtypes within the kidney (50). The supernatants from pepsin-digested kidneys were analyzed on 5% (wt/vol) acrylamide gels with 3.5% (wt/vol) acrylamide stacking gels. The α_1 (III) chains were separated from the α_1 (I) collagen chains with interrupted electrophoresis with delayed reduction of type III collagen. The gels were stained with 0.1% Coomassie blue R-250 overnight at 4°C and then destained with 30% (vol/vol) methanol containing 7% (vol/vol) acetic acid. Densitometry was performed with a calibrated imaging densitometer (Gel Scan-710, Bio-Rad, Hercules, CA), and data were analyzed using Quantity-One software (Bio-Rad).

Matrix metalloproteinase (MMP)-2 and MMP-9 activity was assessed by gelatin zymography (65). Zymographs consisted of 7.5% (wt/vol) acrylamide gels containing 1 mg/ml gelatin. The gels were stained with 0.1% (wt/vol) Coomassie blue R-250 overnight at 37°C and then destained with 7% (vol/vol) acetic acid. Clear bands indicated gelatinolytic activity, where the enzymes had digested the substrate. Densitometry of these MMP bands was performed, and data were analyzed using Quantity-One software.

MSC and macrophage coculture. BM was isolated from male 6- to 8-wk-old C57BL/6J mice and cultured in DMEM/F12 (Invitrogen,

Camarillo, CA) supplemented with 10% FBS, 10 mM L-glutamine, 100 $\mu\text{g}/\text{ml}$ penicillin/streptomycin, and 100 U/ml mouse recombinant colony-stimulating factor (CSF)-1 (Chiron) to generate macrophages. On *day 7*, the purity of the BM-derived macrophages was $>95\%$ when checked by flow cytometry.

For coculture experiments, macrophages were primed with 120 ng/ml of IFN- γ (R&D Systems) and 10 ng/ml LPS (Sigma-Aldrich) to induce an M1 phenotype or with 20 ng/ml IL-4 (Invitrogen) to induce an M2 phenotype. The macrophages were then washed with PBS before MSCs were plated indirectly, on a 0.4- μm pore size Transwell (Corning Life Sciences, Pittsford, PA), or directly and cultured for 48 h. Following 24 h of coculture, 1 ml of the coculture supernatant was collected and screened for human MSC-derived cytokines, using a MILLIPLEX_{MAP} Human Cytokine/Chemokine Panel (Millipore).

Real-time quantification PCR gene expression analysis. Macrophages were sorted by fluorescence-activated cell sorting (FACS) from the cocultures using the conjugated anti-mouse antibodies CD45-FITC (BD Biosciences) and F4/80-APC (BD Biosciences). RNA was extracted using an RNeasy Micro Kit (Qiagen, Hilden, Germany) according to the manufacturer's guidelines. RNA samples were reverse transcribed using a High Capacity cDNA Reverse Transcription Kit (Applied Biosystems, Foster City, CA), and real-time quantitative PCR (qPCR) for each target gene was performed in duplicate on cDNA samples using TaqMan Universal PCR Master Mix (Applied Biosystems) and TaqMan Gene Expression Assays (Applied Biosystems; see Table 2). The threshold cycle (Ct) values were normalized against endogenous control β -actin to determine ΔCt .

Statistical analyses. Statistical analyses of the data were performed using GraphPad Prism software version 5.0 (GraphPad Software, San Diego, CA). An unpaired *t*-test was used to analyze data between two groups. Comparisons among three groups were performed by one-way ANOVA followed by Tukey's multiple comparison tests. All data were expressed as means \pm SE. $P < 0.05$ was considered statistically significant.

RESULTS

Characterization of MSCs. Human MSCs were initially characterized to confirm their cellular identity using the minimal criteria established by Dominici et al. (14). In vitro, cultured MSCs adhered to plastic, had a spindle-shaped morphology (Fig. 1A), displayed a normal karyotype (Fig. 1B), and formed CFU-F (Fig. 1C). Functionally, MSCs differentiated into osteocytes, adipocytes, and chondrocytes as evidenced by positive staining with Alizarin red (Fig. 1D), FABP-4 (Fig. 1E), and aggrecan (Fig. 1F), respectively. Finally, MSCs were uniformly positive for the canonical MSC markers CD73, CD90, and CD105 and lacked the expression of the hematopoietic markers CD14, CD19, CD34, CD45, and HLA-DR (Fig. 1G).

MSCs home to the injured kidney following unilateral and bilateral IR injury. eGFP⁺fluc⁺ MSCs were FACS sorted to enrich for the number of eGFP⁺fluc⁺ MSCs (Fig. 2A), with the purity of the postsorted cells also determined by flow cytometry (Fig. 2A). eGFP expression was confirmed visually using fluorescence microscopy (Fig. 2B). Using a noninvasive bioluminescent imaging technique, eGFP⁺fluc⁺ MSCs were tracked in vivo following iv administration immediately following surgery in mice with unilateral or bilateral IR injury and in sham-operated control mice (see diagram in Fig. 2C).

Following sham surgery, MSCs accumulated only in the lungs, likely the result of being trapped in the pulmonary capillaries (Fig. 3A). Bioluminescence measurements in the sham-operated control mice decreased over the 3-day time

Table 2. Real-time PCR TaqMan gene expression assays

Gene Symbol	Assay ID
<i>Actb</i>	Mm00607939_s1
<i>Arg1</i>	Mm00475988_m1
<i>Chi3l3</i>	Mm00657889_m1
<i>Fizz1 (Retnla)</i>	Mm00445108_m1
<i>Ccl2</i>	Mm00441242_m1
<i>Mrc1</i>	Mm00485148_m1

course (2.038×10^7 photons $\cdot\text{s}^{-1}\cdot\text{cm}^{-2}\cdot\text{sr}^{-1}$ on *day 0* to 3.362×10^6 photons $\cdot\text{s}^{-1}\cdot\text{cm}^{-2}\cdot\text{sr}^{-1}$ on *day 1* as per mouse in Fig. 3A). No signal was detected at *day 3*. In contrast, following unilateral and bilateral IR injury, MSCs homed to the site of damage via two routes: directly to the kidney(s), as detected at the *day 0* imaging time point (Fig. 3, B and D, respectively), or to the kidney(s) via the lungs (Fig. 3, C and E, respectively). The localization of the MSCs in the kidney was confirmed by imaging the lateral aspect of the mouse (images not shown) before the kidneys were excised and imaged *ex vivo*. Examples of each of the MSC homing patterns with detected fluc signals in sham and IR mice are shown in Fig. 3. The fluc signal following direct homing to the kidney with unilateral IR injury was marginally decreased from *day 0* to *day 1* (4.436×10^7 to 3.828×10^7 photons $\cdot\text{s}^{-1}\cdot\text{cm}^{-2}\cdot\text{sr}^{-1}$) and further by *day 3* (1.953×10^7 photons $\cdot\text{s}^{-1}\cdot\text{cm}^{-2}\cdot\text{sr}^{-1}$; Fig. 3B). In contrast to the unilateral model, the fluc signal with bilateral IR injury gradually increased from 5.109×10^7 photons $\cdot\text{s}^{-1}\cdot\text{cm}^{-2}\cdot\text{sr}^{-1}$ on *day 1* to 1.706×10^8 photons $\cdot\text{s}^{-1}\cdot\text{cm}^{-2}\cdot\text{sr}^{-1}$ on *day 3*. At 7 days post-IR, the fluc signal was no longer detected in either the unilateral or bilateral models. In the mice where MSCs were observed to accumulate in the lungs before migrating to the damaged kidney(s) following unilateral or bilateral IR injury (Fig. 3, C and E), the majority of injected cells had localized in the lungs at 1 h postadministration. However, the MSCs further migrated from the lungs to the injured kidney(s) (imaged on *days 1* and *3*), with the majority of cells being present in the kidney(s) at *day 3*. Again, at *day 7*, no cells were detected.

MSCs promote structural and functional regeneration. Compared to sham-operated mice, at 7 days following IR injury there was widespread tubular epithelial cell damage within the kidney, evidenced by numerous protein casts, interstitial matrix expansion, and extracellular matrix deposition along with a marked infiltration of inflammatory cells (Fig. 4A). In contrast, the administration of MSCs to mice with IR injury promoted structural regeneration, including reduced inflammation and reestablishment of the tubular epithelium. Semiquantitative examination of kidney sections revealed a significant reduction in the number of protein casts ($P < 0.001$) and proximal tubule epithelial cell damage ($P < 0.001$; Fig. 4B) by 5 days following MSC injection. Structural regeneration of the MSC-treated kidneys was associated with a significant increase in tubular epithelial cell proliferation demonstrated at the *day 3* time point, as assessed with Ki67 and PCNA immunostaining (Fig. 4, C and D). This MSC-mediated repair was further evidenced by functional recovery. BUN and serum creatinine concentrations were measured 3 days post-MS administration (Fig. 5, A and B). At 3 days after bilateral IR surgery, BUN levels had increased over twofold compared with sham-operated controls (18.1 ± 1.9 vs. 8.4 ± 0.4 mmol/l; $P < 0.001$) and serum creatinine

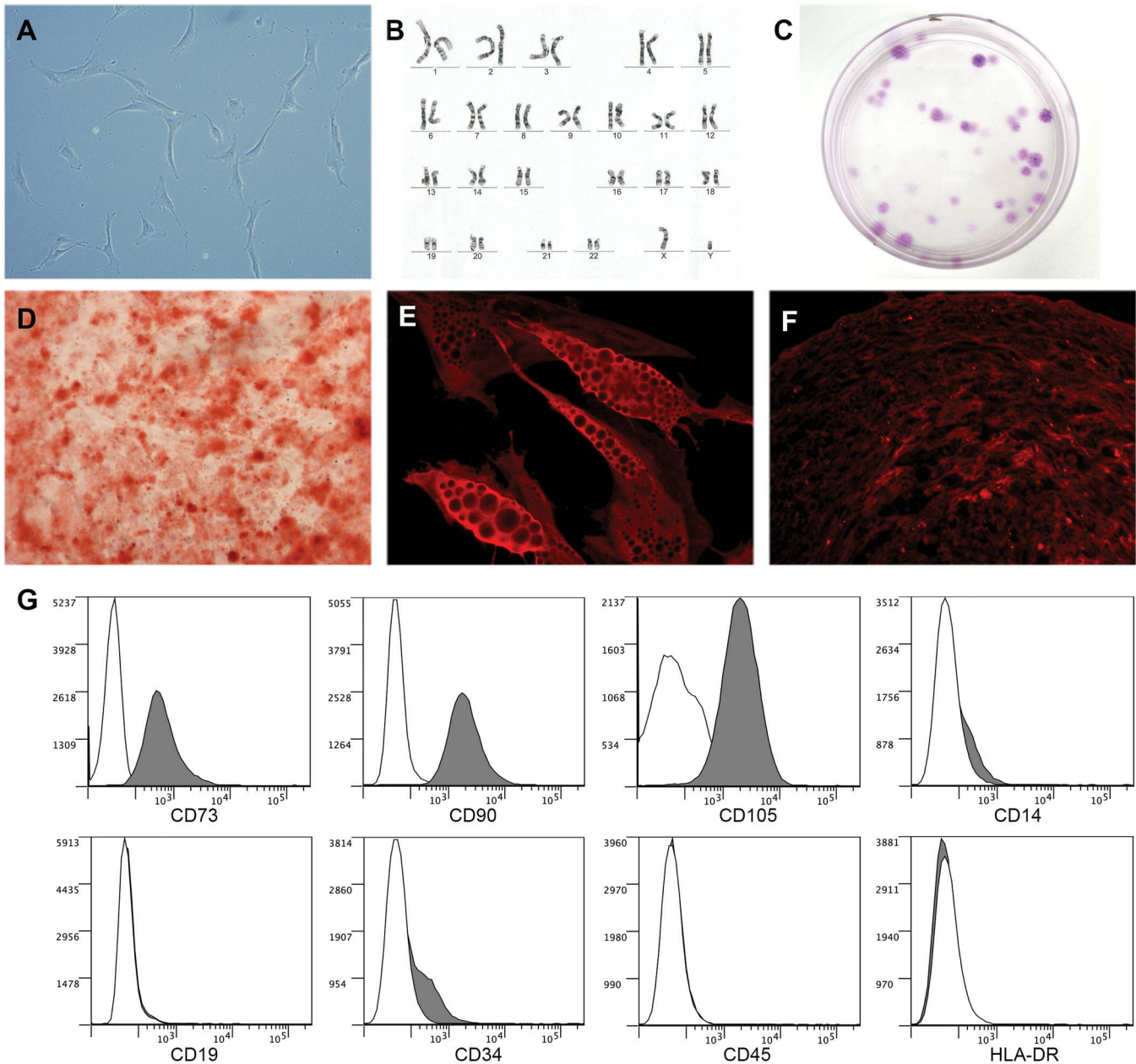


Fig. 1. In vitro characterization of human mesenchymal stem cells (MSCs). MSCs adhered to plastic in standard tissue culture conditions (magnification $\times 200$; A), displayed a normal 46XY karyotype (B), and formed colony-forming unit-fibroblasts (CFU-F), demonstrated by crystal violet staining, following 14 days in vitro culture (C). MSCs possessed multilineage differentiation potential in vitro, differentiating into osteocytes, indicated by the formation of calcium-rich deposits detected with alizarin red staining (magnification $\times 50$; D), adipocytes, identified by the presence of lipid vacuoles and fatty acid binding protein-4 staining (magnification $\times 400$; E), and chondrocytes, visualized by the presence of aggrecan staining (magnification $\times 200$; F). MSCs expressed the cell surface antigens CD73, CD90, and CD105, however, and lacked the expression of CD14, CD19, CD34, CD45, and HLA-DR (G).

1.5-fold higher than sham levels (34.7 ± 3.1 vs. 22.4 ± 2.1 $\mu\text{mol/l}$; $P < 0.05$). In MSC-treated mice, both the BUN and serum creatinine concentrations were comparable to baseline measurements and were significantly lower than the vehicle-treated controls (Fig. 5, A and B). In addition, immunohistochemical staining revealed increased expression of Kim-1, a marker of proximal tubular injury, on the apical membrane of proximal tubule cells 3 days after IR injury, compared with sham-operated kidneys (Fig. 5C), while Kim-1 expression was markedly reduced in MSC-treated mice. Notably, urinary Kim-1, assessed by an ELISA, was significantly increased at 7

days post-IR compared with sham-operated control mice ($P < 0.001$) but returned to baseline levels in MSC-treated mice ($P < 0.01$; Fig. 5D).

MSCs reduce collagen accumulation in the injured kidney. MSC therapy following IR injury reduced interstitial collagen accumulation as assessed by hydroxyproline assay, SDS-PAGE, and type IV collagen immunofluorescence labeling. IR injury resulted in a gradual but significant increase in the total collagen concentration at 3 ($P < 0.05$), 5 ($P < 0.001$), and 7 ($P < 0.001$) days postinjury compared with sham-operated controls (Fig. 6A). At 5 days post-IR injury, MSC treatment

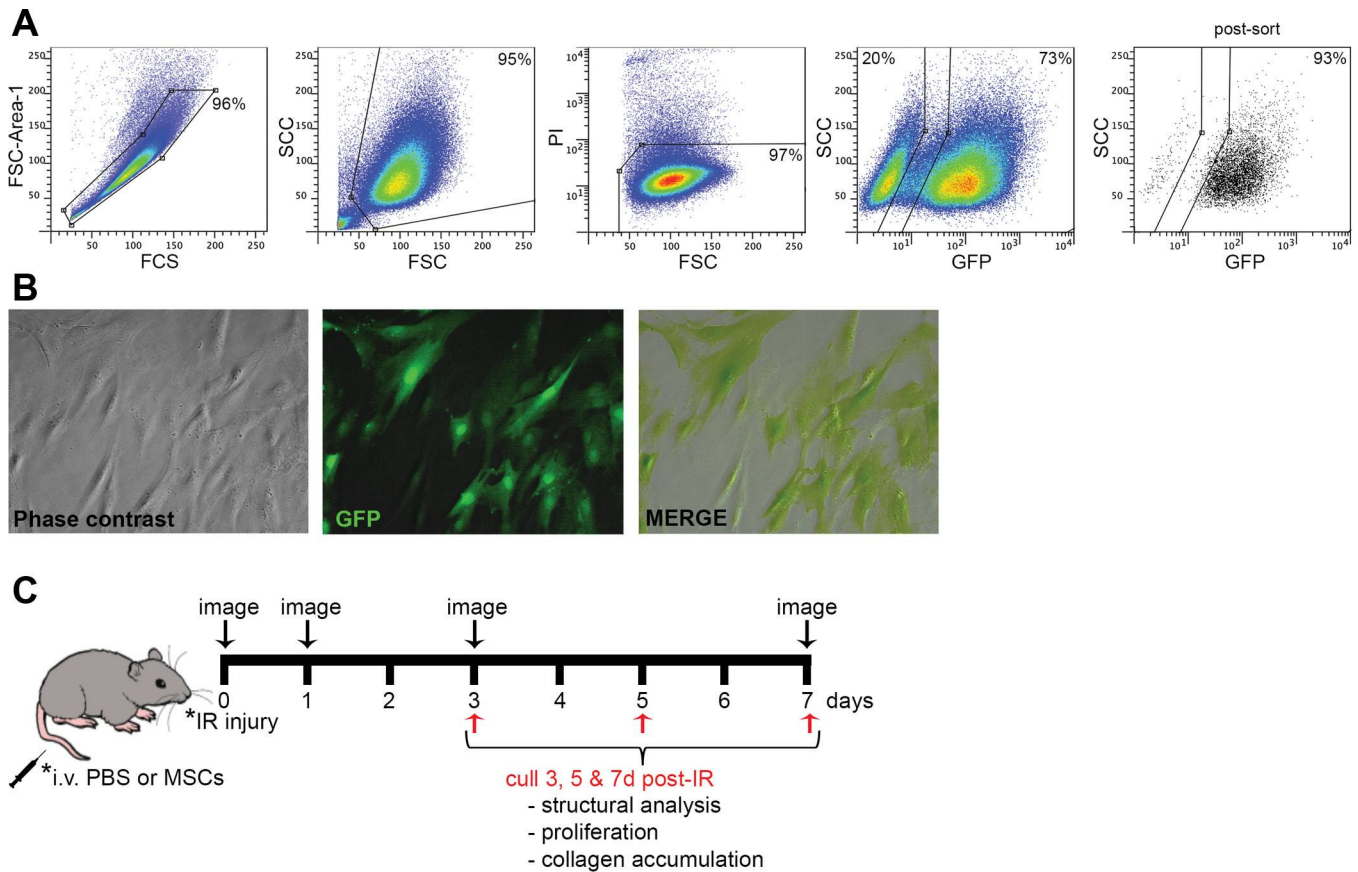


Fig. 2. Isolation of enhanced green fluorescent protein+ firefly luciferase+ (eGFP+fluc+) MSCs and experimental design for in vivo bioluminescence tracing. eGFP+fluc+ MSCs were FACS sorted based on their forward and side light-scattering properties, viability using propidium iodide (PI), and eGFP expression (A). Representative micrographs are shown of the MSCs demonstrating eGFP expression (magnification $\times 200$; B) and a schematic diagram of the experimental timeline following the induction of unilateral (40 min) or bilateral (25 min) ischemia-reperfusion (IR) injury with and without MSC treatment (C).

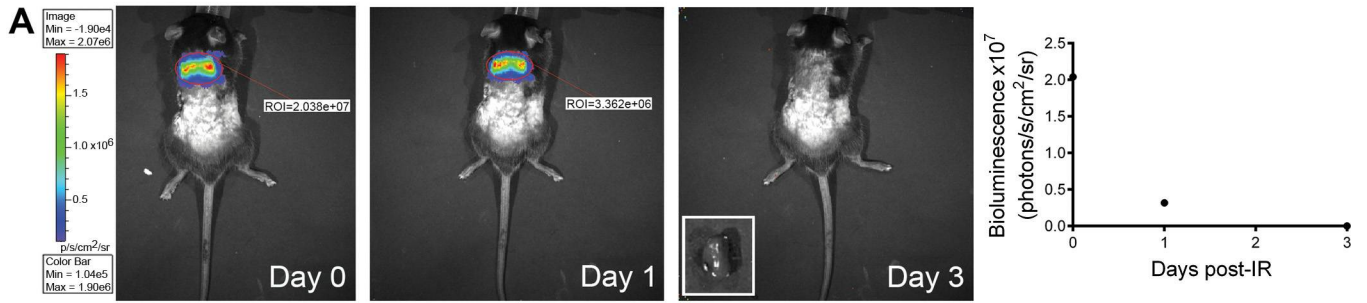
significantly decreased the total renal collagen concentration ($P < 0.05$) compared with vehicle-treated mice. SDS-PAGE revealed the predominant interstitial collagen subtypes within the kidney were type 1 collagen [$\alpha_1(I)$ and $\alpha_2(I)$ monomers and dimers of two $\alpha_1(I)$ chains ($\beta 11$) or $\alpha_1(I)$ and $\alpha_2(I)$ monomers ($\beta 12$)], and a small amount of type V collagen (Fig. 6B). Scanning densitometry further revealed a decrease in the accumulation of the collagen subtype $\alpha_1(I)$ in MSC-treated kidneys compared with the vehicle-treated controls at 5 and 7 days postinjury (Fig. 6B), which reached significance ($P < 0.05$) at day 7. Immunofluorescence microscopy was utilized to visualize type IV collagen and macrophage (F4/80) localization within the kidney (Fig. 6D). At day 7, an accumulation of interstitial collagen was evident in vehicle-treated kidneys. In comparison, type IV collagen appeared as a delicate framework surrounding the glomeruli and reepithelialized tubules of MSC-treated kidneys, with a pattern of expression comparable to kidneys from sham-operated control mice.

Gelatin zymography revealed that IR injury resulted in a significant increase in latent and active MMP-2 levels compared with sham-operated control kidneys at both 5 ($P < 0.001$) and 7 ($P < 0.001$) days postinjury (Fig. 6C). In comparison, the latent and active forms of MMP-2 in the MSC-treated kidneys remained significantly lower than in the vehicle-treated kidneys at both days 5 and 7. Active MMP-9 was also significantly increased in vehicle-treated kidneys at 3 ($P < 0.001$), 5 ($P < 0.01$), and 7 ($P < 0.05$) days postinjury compared with the sham-operated kidneys (Fig. 6C). Notably, MSC treatment resulted in a significant increase in active MMP-9 at 3 days postinjury ($P < 0.05$) compared with its vehicle-treated counterpart.

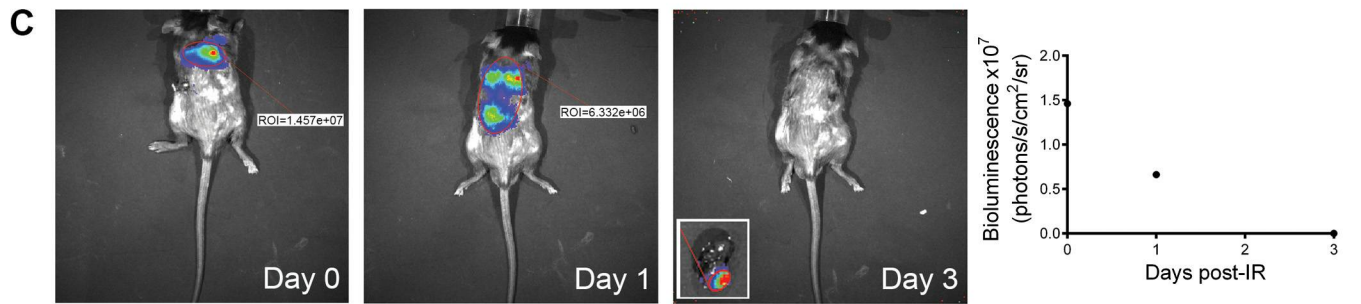
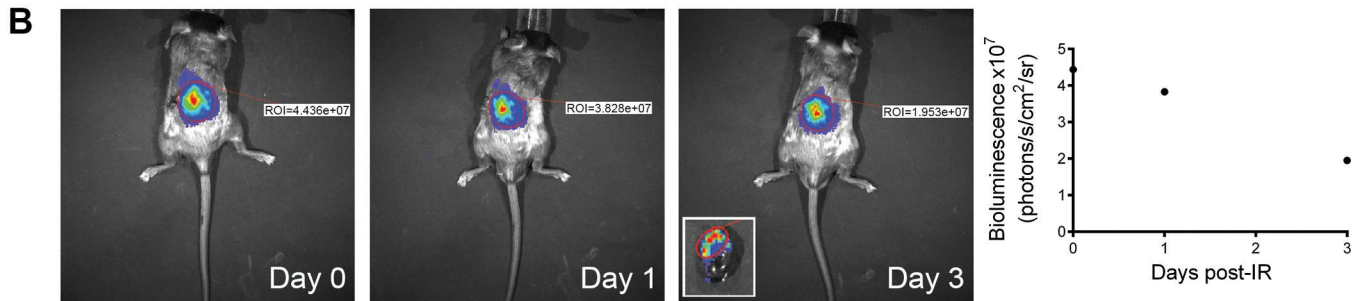
MSCs alter macrophage phenotype following in vitro coculture. Direct and indirect coculture of MSCs with macrophages resulted in an MSC-dependent polarization of macrophages toward an M2 phenotype. BM-derived murine macrophages that had been stimulated to display an M1 or M2 phenotype in vitro were cocultured

Fig. 3. MSCs traffic to the injured kidney(s) following unilateral and bilateral IR injury. Representative images of the distribution of MSCs 0, 1, and 3 days post-intravenous injection in sham-operated control mice, showing the accumulation of these cells in the lungs (A) and in mice with unilateral or bilateral IR injury, where the cells homed directly to the injured kidney (B and D, respectively) or to the injured kidney via the lungs (C and E, respectively). The region of interest (ROI) indicates photon emission within the red-circled area. Red indicates areas with the highest photon emission density, and blue indicates the areas with the lowest. The in vivo ROIs for each animal on days 0, 1, and 3 are displayed in each corresponding graph.

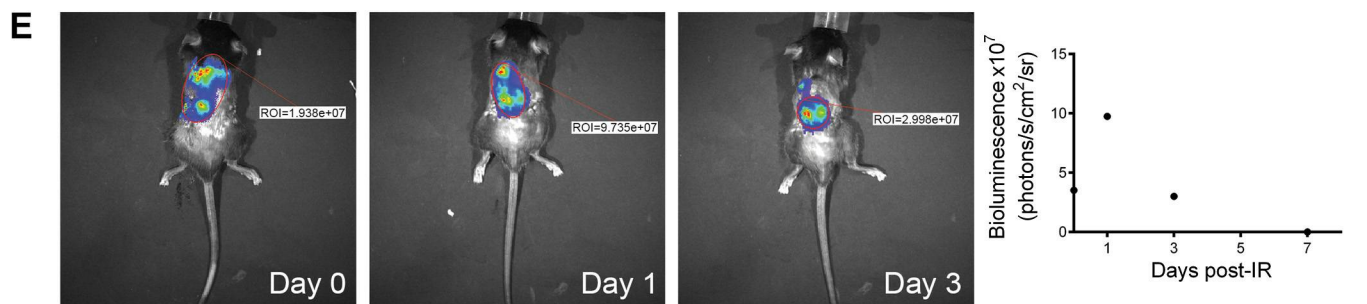
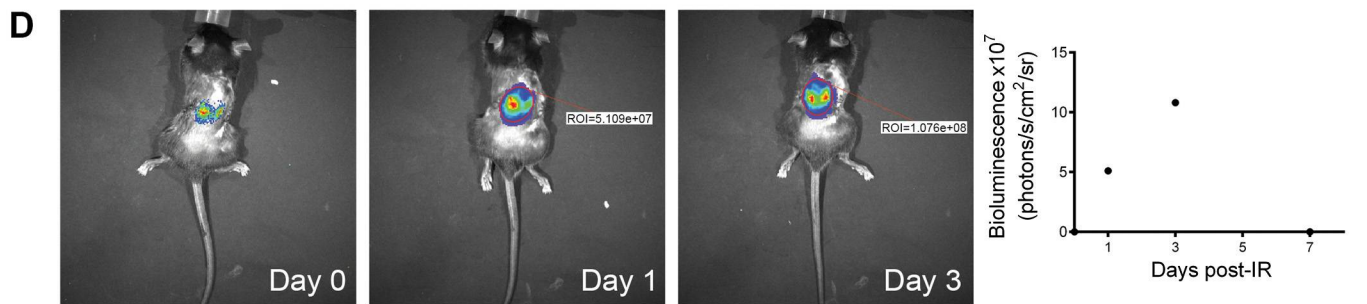
Sham



Unilateral IR injury



Bilateral IR injury



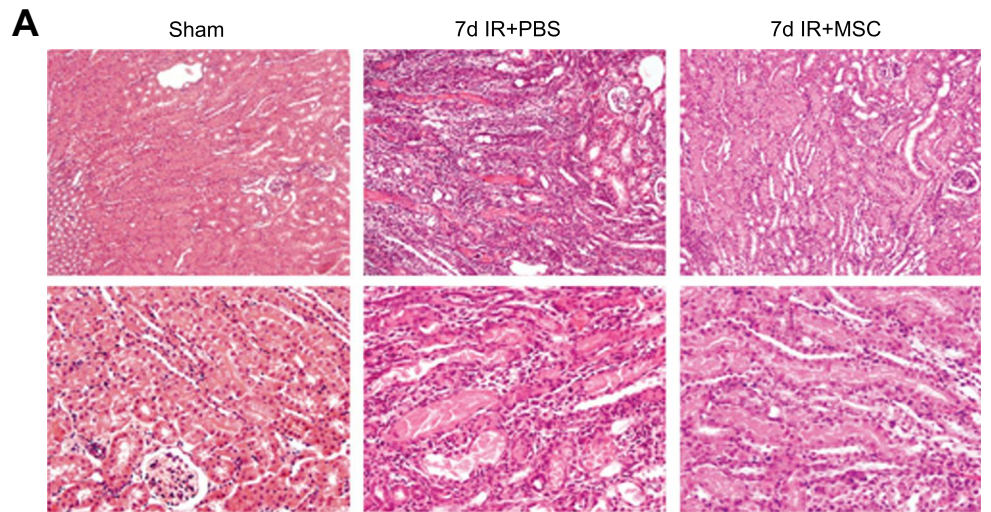
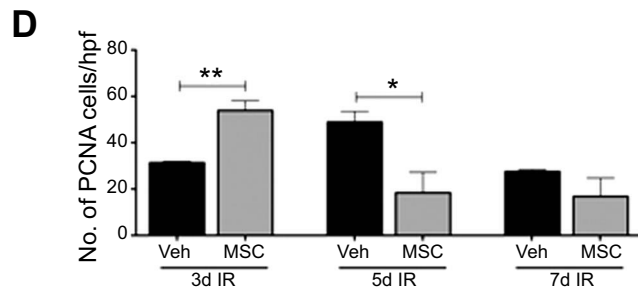
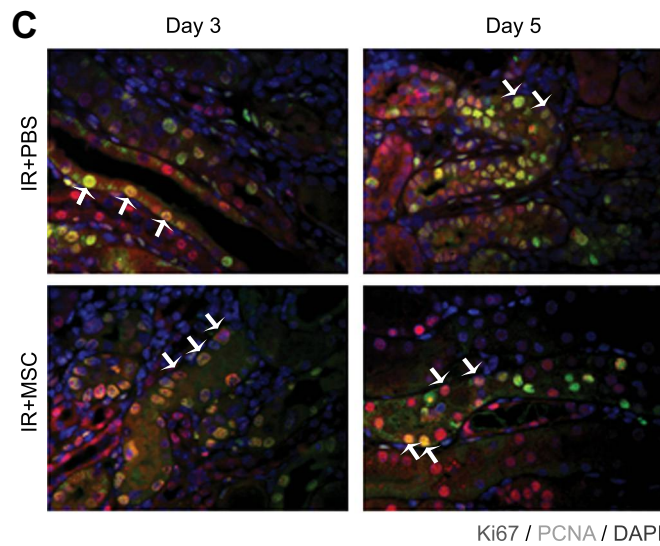
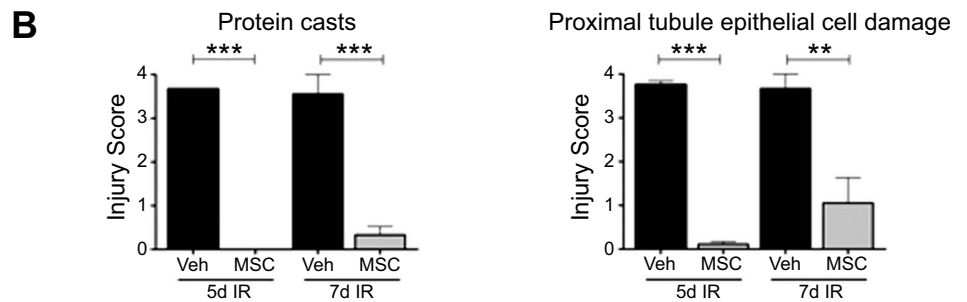


Fig. 4. MSC treatment following IR injury accelerates structural repair in adult mice. Representative micrographs of hematoxylin and eosin (H&E)-stained sections show the histoarchitecture of the corticomedullary region from sham and unilateral IR kidneys with and without MSC treatment, 7 days postinjury (magnification $\times 200$ and $\times 400$; A). Semiquantitative analysis of kidney injury from IR kidneys with and without MSC treatment 5 and 7 days post-IR is displayed graphically (B). Tubular epithelial cell proliferation was demonstrated with Ki67 (red) and PCNA (green) immunofluorescence labeling in kidneys with and without MSC treatment (C). PCNA expression was quantified at 3, 5, and 7 days following IR injury (magnification $\times 400$; D). Veh, vehicle; cells/hpf, cells per high-power field. Values are means \pm SE; $n = 3$. * $P < 0.05$. ** $P < 0.01$. *** $P < 0.001$.



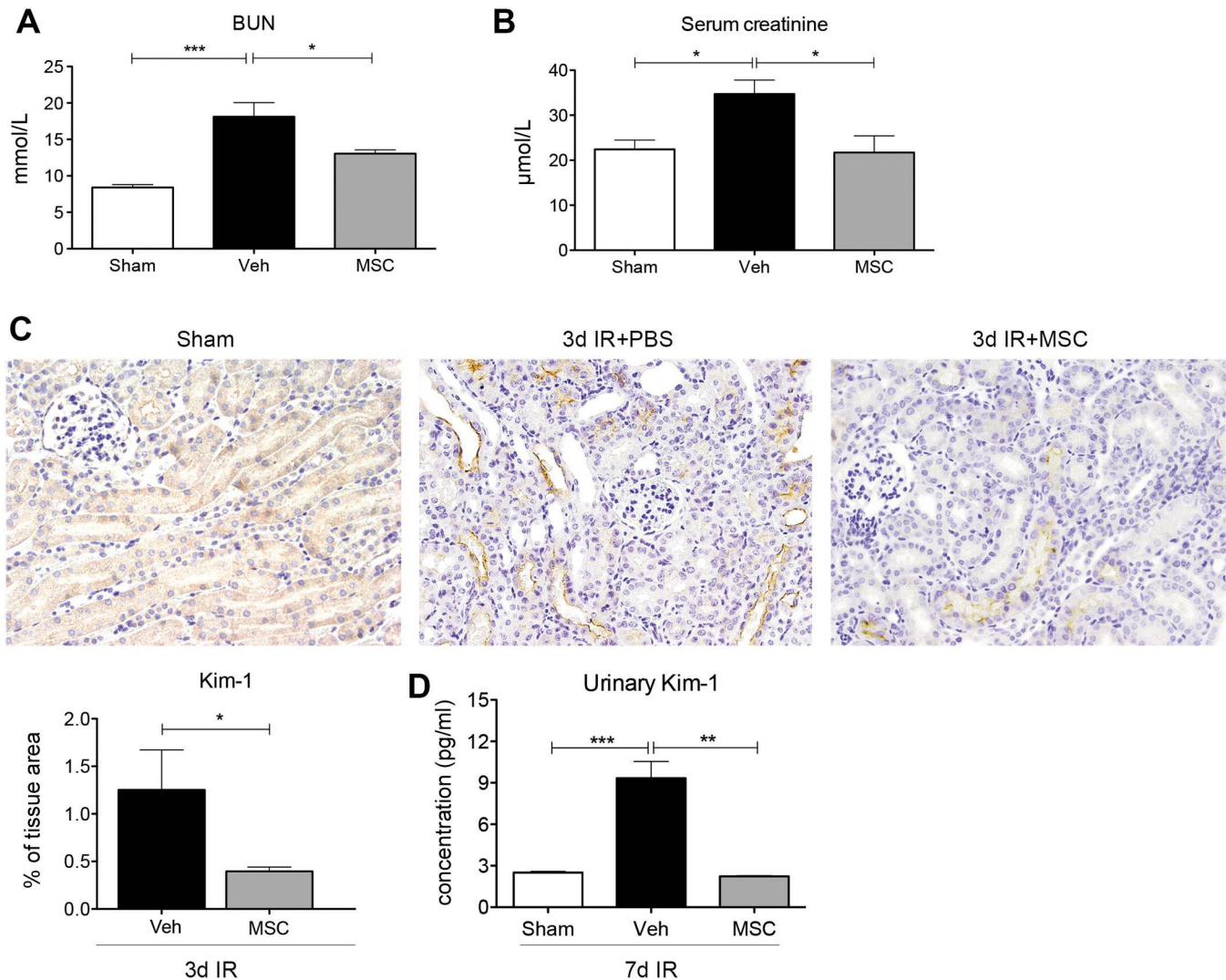


Fig. 5. MSCs improve kidney function and reduce the expression and excretion of Kim-1 in the kidney following IR injury. Functional analysis is shown measuring blood urea nitrogen (BUN; *A*) and serum creatinine (*B*) in sham and bilateral IR mice with and without MSC treatment 3 days postinjury. Representative micrographs and semiquantification of Kim-1 expression in sham and IR kidneys 3 days following MSC treatment are shown (magnification $\times 400$; *C*). Urinary Kim-1 levels from days 6–7 was significantly increased in mice with IR but returned to baseline levels following MSC treatment (*D*). Values are means \pm SE. ** $P < 0.01$. *** $P < 0.001$.

with MSCs for 48 h either directly or indirectly using a Transwell coculture system (see diagram in Fig. 7*A*). qPCR analysis of macrophage gene expression showed that the direct coculture of M1 macrophages with MSCs caused an upregulation of the M2-associated gene, *Arg1* (Fig. 7*B*). Another M2-associated gene, *Ccl2*, was also upregulated following the indirect coculture of M1 macrophages with MSCs (Fig. 7*B*). Furthermore, an enhanced expression of the M2-associated genes, *Arg1*, *Chi3l3*, *Ccl2*, and *Fizz1* (also known as *Retnla*), was observed following both the direct and indirect coculture of M2 macrophages with MSCs (Fig. 7*B*).

The MSC-macrophage coculture medium was then screened using a panel of human cytokines and chemokines (Table 3). The human soluble factors EGF, granulocyte macrophage colony-stimulating factor (GM-CSF), CXCL1, IL-6, IL-8, monocyte chemoattractant protein (MCP)-1, PDGF-AA, and CCL5 were detected in the coculture supernatants, suggesting these factors may play a role in the MSC-mediated shift in macrophage polarization.

DISCUSSION

The therapeutic efficacy of MSCs derived from various sources including BM (41), adipose (11), umbilical cord (7), embryos (69), and Wharton's jelly (15) to treat cisplatin- (5, 17, 41)-, glycerol (18, 42)-, unilateral ureteral obstruction (UUO) (2, 34, 35, 46)-, and IR (28, 51, 56, 57)-induced experimental models of AKI have been investigated (for a review, see Ref. 64). However, the mechanisms by which MSCs elicit repair remain largely unknown. Following injury, MSCs have the capacity to migrate along an inflammatory cytokine gradient, governed largely by chemokines and their receptors, to the site of damage (18, 23, 33, 58). The present study demonstrated that MSCs administered to sham-operated mice migrated directly to the lungs, where they remained and were cleared within 3 days. In comparison, MSCs administered to mice following IR had the potential to home directly to the injured kidney(s), where they remained for up to 3 days postadministration and exerted beneficial effects over the lon-

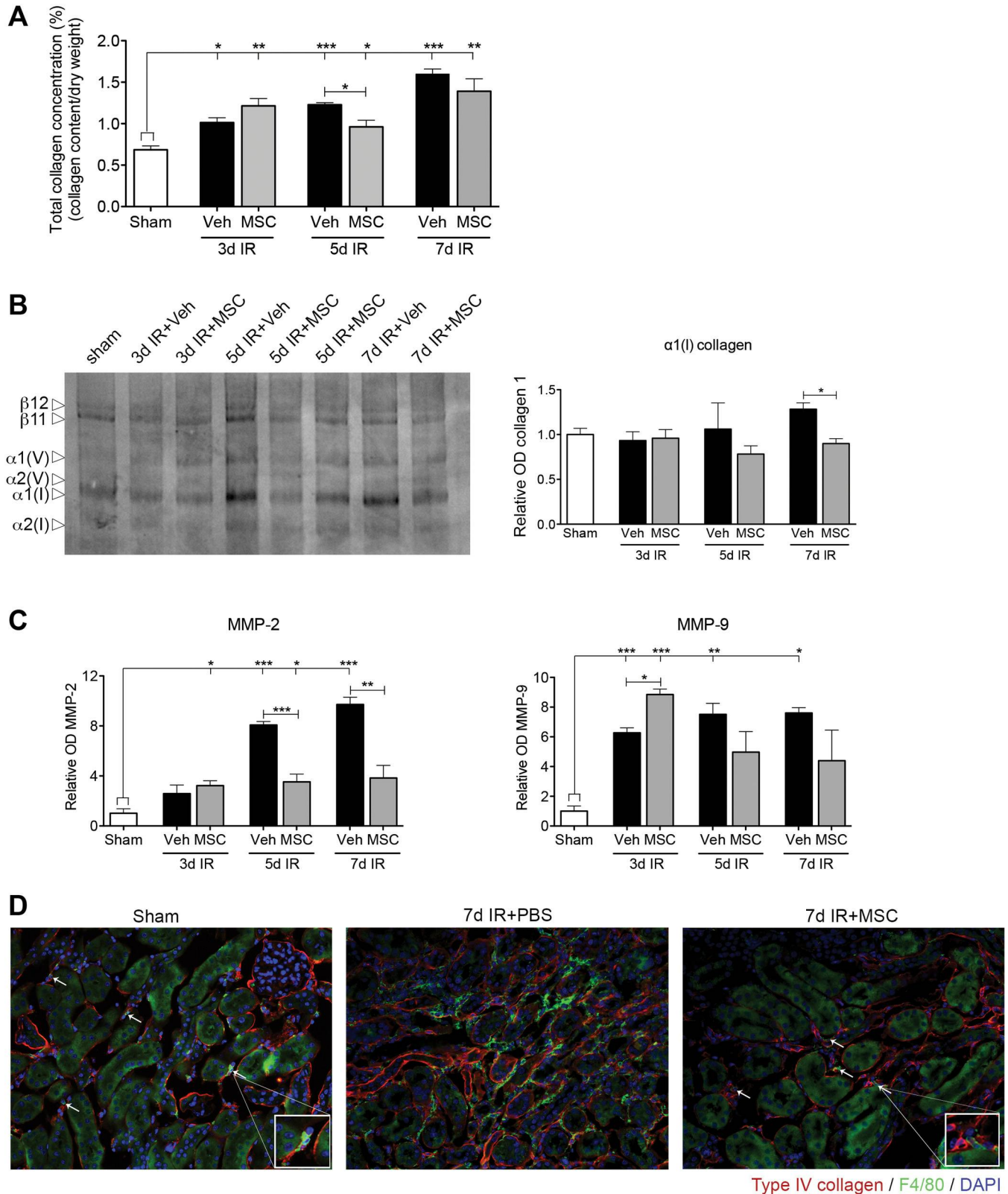


Fig. 6. MSCs reduce collagen accumulation in the kidney following IR injury. *A*: total kidney collagen concentration (% collagen content/dry weight tissue) in sham and IR kidneys with and without MSC treatment. *B*: SDS-PAGE analysis and densitometry of sham and IR kidneys 3, 5, and 7 days after vehicle or MSC treatment. *C*: densitometry of matrix metalloproteinase (MMP)-2 and MMP-9 in sham and IR kidneys 3, 5, and 7 days following IR injury with vehicle or MSC treatment. *D*: representative fluorescence micrographs showing type IV collagen (red) and F4/80 (green) staining in sham and IR kidneys 7 days after vehicle or MSC treatment (magnification $\times 200$). OD, optical density. Values are means \pm SE; $n = 3$. * $P < 0.05$. ** $P < 0.01$. *** $P < 0.001$.

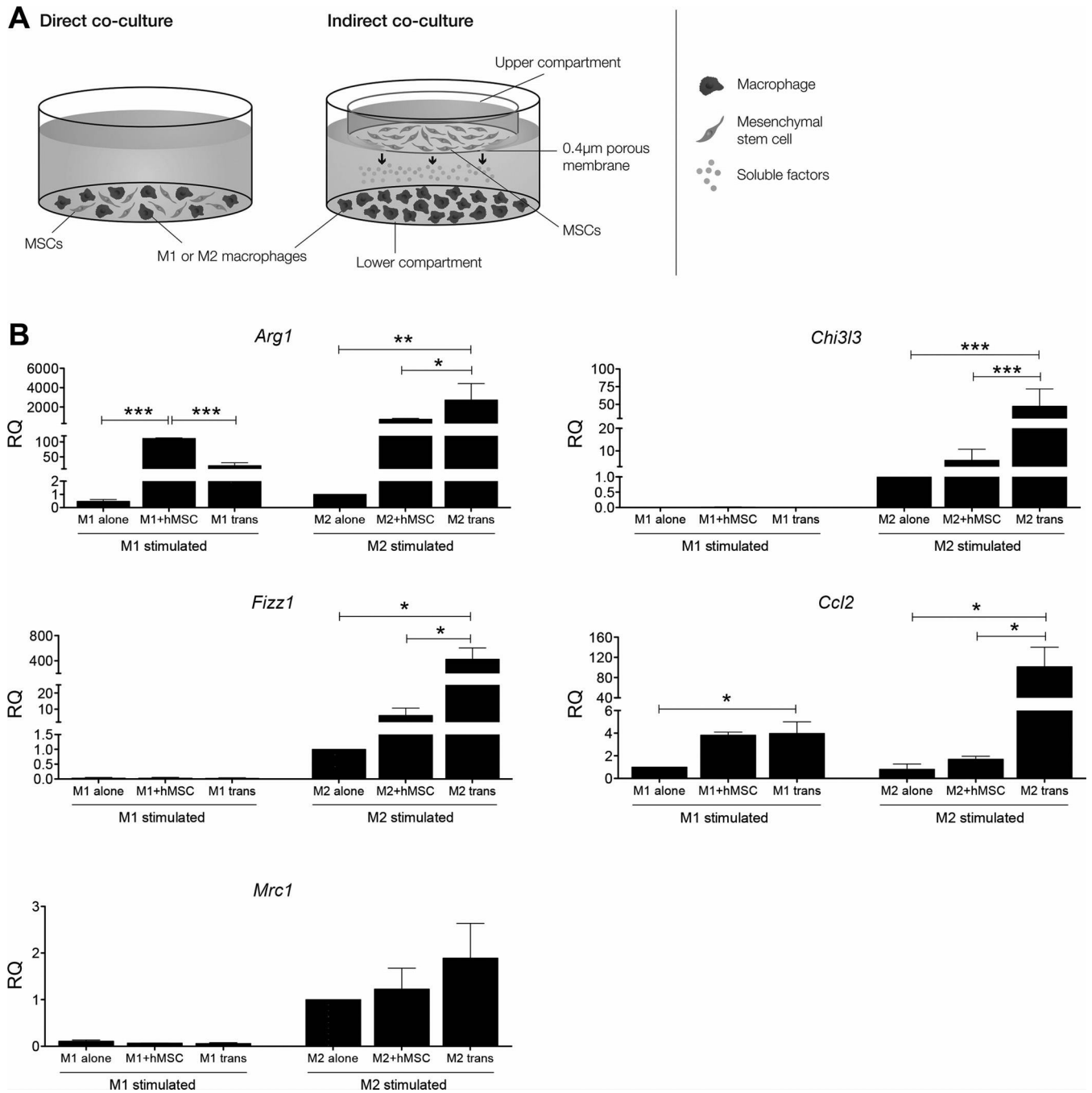


Fig. 7. MSCs can alter macrophage phenotype following in vitro coculture. *A*: schematic diagram of the coculture system used to culture macrophages and MSCs. *B*: qPCR analysis of anti-inflammatory “M2” gene expression in mouse bone marrow-derived M1- and M2-stimulated macrophages cocultured for 48 h either directly (M1 or M2+MSC) or indirectly (M1 or M2 trans) with MSCs. RQ, relative quantification; trans, Transwell. Values are means \pm SE; $n = 3$. * $P < 0.05$. ** $P < 0.01$. *** $P < 0.001$.

ger term. These findings are consistent with previously published work (59). While some MSCs still traveled to the lung, these cells retained the ability to migrate to the injured kidney(s) within the first 3 days following IR injury. The localization of the MSCs in the lungs of mice has been confirmed in previous studies in other experimental models (29, 44). Cell size is believed to contribute to the initial entrapment of the MSCs within the pulmonary capillaries, due to the small diameter of the vessels. In addition, adhesion molecules ex-

pressed by MSCs and the corresponding receptors expressed on the lung endothelia may also contribute to the MSC lung entrapment and dislodgment (44). Although tissue-specific homing has been demonstrated in a number of different conditions, long-term engraftment of the MSCs has rarely been shown. Consequently, several studies have investigated strategies aimed at enhancing the MSC migratory properties, survival, and consequently regenerative capacity through preconditioning with various growth factors such as IGF-1 (66), glial

Table 3. Human cytokines secreted following 24 h of MSC and mouse bone marrow-derived macrophage coculture in vitro

Cytokine, pg/ml	Coculture Conditions					
	M1+MSC direct	M1+MSC Transwell	Significance	M2+MSC direct	M2+MSC Transwell	Significance
EGF	8.3 ± 5.0	16.6 ± 3.2	NS	2.57 ± 2.6	0	NS
Eotaxin	0	0	NS	0	0	NS
FGF2	0	0	NS	0	0	NS
Flt-3L	0	0	NS	0	0	NS
Fractalkine	0	0	NS	0	0	NS
G-CSF	0	0	NS	0	0	NS
GM-CSF	3.5 ± 0.2	0	†	0	0	NS
GRO (CXCL1)	67.8 ± 3.6	0	†	30.8 ± 5.1	0	†
IFN-α2	0	0	NS	0	0	NS
IFN-γ	0	0	NS	0	0	NS
IL-1α	0	0	NS	0	0	NS
IL-1β	0	0	NS	0	0	NS
IL-1Rα	0	0	NS	0	0	NS
IL-2	0	0	NS	0	0	NS
IL-3	0	0	NS	0	0	NS
IL-4	0	0	NS	0	0	NS
IL-5	0	0	NS	0	0	NS
IL-6	732.6 ± 22.6	193.9 ± 10.7	†	423.2 ± 38.3	88.7 ± 3.7	†
IL-7	0	0	NS	0	0	NS
IL-8	133.5 ± 7.7	23.2 ± 4.0	†	68.3 ± 11.9	6.8 ± 0.4	*
IL-9	0	0	NS	0	0	NS
IL-10	0	0	NS	0	0	NS
IL12p40	0	0	NS	0	0	NS
IL12p70	0	0	NS	0	0	NS
IL-13	0	0	NS	0	0	NS
IL-15	0	0	NS	0	0	NS
IL-17A	0	0	NS	0	0	NS
IP10 (CXCL10)	0	0	NS	0	0	NS
MCP-1 (CCL2)	433.1 ± 16.1	103.9 ± 8.7	†	86.1 ± 11.8	51.3 ± 2.7	†
MCP-3 (CCL7)	0	0	NS	0	0	NS
MDC (CCL22)	0	0	NS	0	0	NS
MIP-1α (CCL3)	0	0	NS	0	0	NS
MIP-1β (CCL4)	0	0	NS	0	0	NS
PDGF-AA	38.1 ± 2.5	13.5 ± 1.0	†	35.2 ± 1.0	15.5 ± 0.2	†
PDGF-BB	0	0	NS	0	0	NS
RANTES (CCL5)	0	16.2 ± 1.0	†	0	3.58 ± 0.9	*
sCD40Lα	0	0	NS	0	0	NS
sIL-2Rα	0	0	NS	0	0	NS
TGF-α	0	0	NS	0	0	NS
TNF-α	0	0	NS	0	0	NS
TNF-β	0	0	NS	0	0	NS

Values are means ± SE; *n* = 3. MSC, mesenchymal stem cell; G-CSF, granulocyte colony-stimulating factor; GM-CSF, granulocyte macrophage colony-stimulating factor; IL-1RA, IL-1 receptor antagonist; IP-10, IFN-γ-induced protein; MCP-1, monocyte chemotactic protein; MDC, macrophage-derived chemokine; MIP, monocyte inflammatory protein; RANTES, regulated and normal T cell expressed and secreted; sCD40L, soluble CD40 ligand; sIL-2Rα, soluble IL-2 receptor-α; TGF, transforming growth factor; NS, not significant. **P* < 0.01. †*P* < 0.001.

cell-derived neurotrophic factor (GDNF) (52), melatonin (40), exposure to hypoxia (20), or genetic modification (10, 12, 16, 69, 71).

The current study utilized the xenogeneic transplantation of MSCs into immunocompetent mice without the use of immunosuppressant agents. Although there are extensive data demonstrating the immunomodulatory properties of MSCs in vitro, it is unclear why these cells remain tolerated by the host's immune system following xenogeneic transplantation (3). In the current study, the possibility that the host's immune system cleared the transplanted MSCs by the *day 7* time point cannot be discounted. Nevertheless, numerous studies have demonstrated extraordinary regenerative efficacy following successful transplantation of human MSCs into mice in several disease models (31). However, the type of MSC transplantation (allogeneic vs. autologous), tissue of origin (BM, adipose, umbilical cord), isolation method (enzymatic vs. mechanical), delivery

route (systemic vs. local), dose, and timing of administration are also key factors that may influence the renoprotective effect of MSC therapy and need to be carefully considered before clinical application. For example, in an experimental model of glomerulonephritis, the administration of MSCs improved renal function but resulted in long-term maldifferentiation into glomerular adipocytes (26). These findings raise considerable concerns surrounding the safety of MSC-based therapies, and so it is imperative that studies looking into their long-term safety and unwanted differentiation are performed.

In this study, we demonstrate that following migration to the kidney in response to IR injury, MSCs promoted tubular epithelial cell proliferation, resulting in structural repair and tissue remodeling concurrent with a reduction in collagen. MMPs are enzymes that are involved in extracellular matrix remodeling via collagen degradation (8). The identification of an MSC-induced increase in MMP-9 at *day 3* and decrease in

MMP-2 at days 5 and 7 provides insight into the temporal pattern of MSC-mediated tissue remodeling. In addition to structural improvement, proximal tubular Kim-1 expression and urinary Kim-1 levels were assessed, as a direct measure of kidney injury. Both demonstrated significant improvements in the severity of injury at 3 and 7 days post-MSC treatment. Kim-1 is a sensitive AKI biomarker useful for detecting early disease onset and can provide useful insight into the state of injury before the production of classic indicators of nephrotoxicity, such as serum creatinine levels (22, 60).

MSCs have unique immunomodulatory properties and their trophic effects on T, B, natural killer, and dendritic cells have been thoroughly investigated (53, 68). However, the effect of MSCs on macrophage polarization and the consequences of this cell-cell interaction in altering the proinflammatory course of injury remains largely unknown. Our findings are consistent with other studies that have demonstrated the ability of MSCs to polarize macrophages toward an M2 phenotype in vitro (1, 25, 32, 36, 37). However, the influence MSCs have on the phenotypic and functional characteristics of macrophages is often variable. For example, MSCs have been shown to both upregulate and inhibit the expression of IL-6. Similarly, macrophage phagocytic activity has been both enhanced and suppressed by MSCs (1, 25, 32, 37).

Li et al. (32) demonstrated that MSC repair requires the infiltration of macrophages after the induction of IR injury. Given this important observation, we show herein that MSCs significantly enhanced the expression of M2-associated macrophage genes in both M1 and M2 macrophage subsets in vitro. Furthermore, MSC-induced M2 polarization was evident in both direct and indirect coculture systems, indicating that the alteration of macrophage phenotype was mediated through paracrine mechanisms. Screening of the coculture supernatants detected the presence of MSC-derived EGF, GM-CSF, CXCL1, IL-6, IL-8, MCP-1/CCL2, PDGF-AA, and RANTES/CCL5, all of which, except for EGF, GM-CSF, CXCL1, and PDGF-AA, have previously been shown to promote M2 polarization (1, 6, 39, 48, 55). Interestingly, CXCL1 was only detected in the direct coculture system, indicating that its production required direct cell-to-cell contact. Conversely, RANTES/CCL5 was only detected in the Transwell coculture system, signifying that the direct cell-to-cell contact inhibited the release of this chemokine. Although the enhancement of an M2 phenotype was facilitated through paracrine mechanisms, with the exception of EGF and RANTES/CCL5, direct coculture did result in increased levels of MSC-secreted soluble factors.

In summary, whole body bioluminescence imaging to trace MSCs delivered to mice with unilateral or bilateral IR injury demonstrated a unique pattern of infiltration where MSCs either homed directly to the injured kidney(s) or mobilized from the lungs to the injured kidney(s). MSC therapy was renoprotective and promoted kidney repair, as indicated by decreased proximal tubule Kim-1 expression and urinary Kim-1 levels. In addition, MSC therapy stimulated somatic tubular epithelial cell proliferation and significantly reduced aberrant collagen accumulation, resulting in improved kidney function. This highlights the therapeutic potential of MSCs in ameliorating the progression of kidney disease, of which established fibrosis is a common characteristic. MSCs are thought to elicit repair through paracrine and/or endocrine

mechanisms that modulate the immune response, leading to tissue repair and cellular replacement. Our results provide important insights into the production of various cytokines, chemokines, and enzymes resulting from macrophage-MSC interactions and how these govern the inflammatory and remodeling phases of AKI. However, determining the optimal delivery methods for engraftment, testing long-term safety, and understanding their ability to modify the tissue microenvironment in a setting of progressive fibrosis require further consideration.

ACKNOWLEDGMENTS

We thank Professor Claude Bernard for intellectual input and Keith Schulze from Monash Micro Imaging, Monash University, for technical support.

GRANTS

This study was funded by a Project Grant (1003806) from the National Health and Medical Research Council (NHMRC) of Australia. C. S. Samuel is supported by Monash University Mid-Career and NHMRC Senior Research Fellowships.

DISCLOSURES

No conflicts of interest, financial or otherwise, are declared by the authors.

AUTHOR CONTRIBUTIONS

Author contributions: A.F.W., C.S.S., and S.D.R. provided conception and design of research; A.F.W., T.M.W., M.B.G.K., N.L.P., and C.S. performed experiments; A.F.W., T.M.W., M.B.G.K., and C.S.S. analyzed data; A.F.W., T.M.W., M.B.G.K., and S.D.R. interpreted results of experiments; A.F.W. prepared figures; A.F.W. drafted manuscript; A.F.W., T.M.W., C.S.S., and S.D.R. edited and revised manuscript; A.F.W., T.M.W., M.B.G.K., N.L.P., C.S., C.S.S., and S.D.R. approved final version of manuscript.

REFERENCES

1. Adutler-Lieber S, Ben-Mordechai T, Naftali-Shani N, Asher E, Loberman D, Raanani E, Leor J. Human macrophage regulation via interaction with cardiac adipose tissue-derived mesenchymal stromal cells. *J Cardiovasc Pharmacol Ther* 18: 78–86, 2012.
2. Asanuma H, Vanderbrink BA, Campbell MT, Hile KL, Zhang H, Meldrum DR, Meldrum KK. Arterially delivered mesenchymal stem cells prevent obstruction-induced renal fibrosis. *J Surg Res* 168: e51–e59, 2011.
3. Atoui R, Chiu RC. Concise review: immunomodulatory properties of mesenchymal stem cells in cellular transplantation: update, controversies, and unknowns. *Stem Cells Transl Med* 1: 200–205, 2012.
4. Bai L, Lennon DP, Eaton V, Maier K, Caplan AI, Miller SD, Miller RH. Human bone marrow-derived mesenchymal stem cells induce Th2-polarized immune response and promote endogenous repair in animal models of multiple sclerosis. *Glia* 57: 1192–1203, 2009.
5. Bi B, Schmitt R, Israilova M, Nishio H, Cantley LG. Stromal cells protect against acute tubular injury via an endocrine effect. *J Am Soc Nephrol* 18: 2486–2496, 2007.
6. Bögels M, Braster R, Nijland PG, Gül N, van de Luitgaarden W, Fijneman RJ, Meijer GA, Jimenez CR, Beelen RH, van Egmond M. Carcinoma origin dictates differential skewing of monocyte function. *Oncimmunology* 1: 798–809, 2012.
7. Cao H, Qian H, Xu W, Zhu W, Zhang X, Chen Y, Wang M, Yan Y, Xie Y. Mesenchymal stem cells derived from human umbilical cord ameliorate ischemia/reperfusion-induced acute renal failure in rats. *Bio-technol Lett* 32: 725–732, 2010.
8. Catania JM, Chen G, Parrish AR. Role of matrix metalloproteinases in renal pathophysiology. *Am J Physiol Renal Physiol* 292: F905–F911, 2007.
9. Chang YS, Oh W, Choi SJ, Sung DK, Kim SY, Choi EY, Kang S, Jin HJ, Yang YS, Park WS. Human umbilical cord blood-derived mesenchymal stem cells attenuate hyperoxia-induced lung injury in neonatal rats. *Cell Transplant* 18: 869–886, 2009.
10. Chen Y, Qian H, Zhu W, Zhang X, Yan Y, Ye S, Peng X, Li W, Xu W. Hepatocyte growth factor modification promotes the amelioration

- effects of human umbilical cord mesenchymal stem cells on rat acute kidney injury. *Stem Cells Dev* 20: 103–113, 2011.
11. **Chen YT, Sun CK, Lin YC, Chang LT, Chen YL, Tsai TH, Chung SY, Chua S, Kao YH, Yen CH, Shao PL, Chang KC, Leu S, Yip HK.** Adipose-derived mesenchymal stem cell protects kidneys against ischemia-reperfusion injury through suppressing oxidative stress and inflammatory reaction. *J Transl Med* 9: 51, 2011.
 12. **Cheng Z, Ou L, Zhou X, Li F, Jia X, Zhang Y, Liu X, Li Y, Ward CA, Melo LG, Kong D.** Targeted migration of mesenchymal stem cells modified with CXCR4 gene to infarcted myocardium improves cardiac performance. *Mol Ther* 16: 571–579, 2008.
 13. **da Silva Meirelles L, Chagastelles PC, Nardi NB.** Mesenchymal stem cells reside in virtually all post-natal organs and tissues. *J Cell Sci* 119: 2204–2213, 2006.
 14. **Dominici M, Le Blanc K, Mueller I, Slaper-Cortenbach I, Marini F, Krause D, Deans R, Keating A, Prockop D, Horwitz E.** Minimal criteria for defining multipotent mesenchymal stromal cells. The International Society for Cellular Therapy position statement. *Cytotherapy* 8: 315–317, 2006.
 15. **Du T, Cheng J, Zhong L, Zhao XF, Zhu J, Zhu YJ, Liu GH.** The alleviation of acute and chronic kidney injury by human Wharton's jelly-derived mesenchymal stromal cells triggered by ischemia-reperfusion injury via an endocrine mechanism. *Cytotherapy* 14: 1215–1227, 2012.
 16. **Hagiwara M, Shen B, Chao L, Chao J.** Kallikrein-modified mesenchymal stem cell implantation provides enhanced protection against acute ischemic kidney injury by inhibiting apoptosis and inflammation. *Hum Gene Ther* 19: 807–819, 2008.
 17. **Herrera MB, Bussolati B, Bruno S, Fonsato V, Romanazzi GM, Camussi G.** Mesenchymal stem cells contribute to the renal repair of acute tubular epithelial injury. *Int J Mol Med* 14: 1035–1041, 2004.
 18. **Herrera MB, Bussolati B, Bruno S, Morando L, Mauriello-Romanazzi G, Sanavio F, Stamenkovic I, Biancone L, Camussi G.** Exogenous mesenchymal stem cells localize to the kidney by means of CD44 following acute tubular injury. *Kidney Int* 72: 430–441, 2007.
 19. **Humphreys BD, Bonventre JV.** Mesenchymal stem cells in acute kidney injury. *Annu Rev Med* 59: 311–325, 2008.
 20. **Hung SC, Pochampally RR, Hsu SC, Sanchez C, Chen SC, Spees J, Prockop DJ.** Short-term exposure of multipotent stromal cells to low oxygen increases their expression of CX3CR1 and CXCR4 and their engraftment in vivo. *PLoS One* 2: e416, 2007.
 21. **Hung SC, Pochampally RR, Chen SC, Hsu SC, Prockop DJ.** Angiogenic effects of human multipotent stromal cell conditioned medium activate the PI3K-Akt pathway in hypoxic endothelial cells to inhibit apoptosis, increase survival, and stimulate angiogenesis. *Stem Cells* 25: 2363–2370, 2007.
 22. **Ichimura T, Hung CC, Yang SA, Stevens JL, Bonventre JV.** Kidney injury molecule-1: a tissue and urinary biomarker for nephrotoxicant-induced renal injury. *Am J Physiol Renal Physiol* 286: F552–F563, 2004.
 23. **Kang SK, Shin IS, Ko MS, Jo JY, Ra JC.** Journey of mesenchymal stem cells for homing: strategies to enhance efficacy and safety of stem cell therapy. *Stem Cells Int* 2012: 1–11, 2012.
 24. **Khakoo AY, Pati S, Anderson SA, Reid W, Elshal MF, Rovira II, Nguyen AT, Malide D, Combs CA, Hall G, Zhang J, Raffeld M, Rogers TB, Stetler-Stevenson W, Frank JA, Reitz M, Finkel T.** Human mesenchymal stem cells exert potent antitumorigenic effects in a model of Kaposi's sarcoma. *J Exp Med* 203: 1235–1247, 2006.
 25. **Kim J, Hematti P.** Mesenchymal stem cell-educated macrophages: a novel type of alternatively activated macrophages. *Exp Hematol* 37: 1445–1453, 2009.
 26. **Kunter U, Rong S, Boor P, Eitner F, Müller-Newen G, Djuric Z, van Roeyen CR, Konieczny A, Ostendorf T, Villa L, Milovanceva-Popovska M, Kerjaschki D, Floege J.** Mesenchymal stem cells prevent progressive experimental renal failure but maldifferentiate into glomerular adipocytes. *J Am Soc Nephrol* 18: 1754–1764, 2007.
 27. **Lange C, Cakiroglu F, Spiess AN, Cappallo-Obermann H, Dierlamm J, Zander AR.** Accelerated and safe expansion of human mesenchymal stromal cells in animal serum-free medium for transplantation and regenerative medicine. *J Cell Physiol* 213: 18–26, 2007.
 28. **Lange C, Tögel F, Itrich H, Clayton F, Nolte-Ernsting C, Zander AR, Westenfelder C.** Administered mesenchymal stem cells enhance recovery from ischemia/reperfusion-induced acute renal failure in rats. *Kidney Int* 68: 1613–1617, 2005.
 29. **Lee RH, Pulin AA, Seo MJ, Kota DJ, Ylostalo J, Larson BL, Semprun-Prieto L, Delafontaine P, Prockop DJ.** Intravenous hMSCs improve myocardial infarction in mice because cells embolized in lung are activated to secrete the anti-inflammatory protein TSG-6. *Cell Stem Cell* 5: 54–63, 2009.
 30. **Lee S, Huen S, Nishio H, Nishio S, Lee HK, Choi BS, Ruhrberg C, Cantley LG.** Distinct macrophage phenotypes contribute to kidney injury and repair. *J Am Soc Nephrol* 22: 317–326, 2011.
 31. **Li J, Ezzelarab MB, Cooper DK.** Do mesenchymal stem cells function across species barriers? Relevance for xenotransplantation. *Xenotransplantation* 19: 273–285, 2012.
 32. **Li W, Zhang Q, Wang M, Wu H, Mao F, Zhang B, Ji R, Gao S, Sun Z, Zhu W, Qian H, Chen Y, Xu W.** Macrophages are involved in the protective role of human umbilical cord-derived stromal cells in renal ischemia-reperfusion injury. *Stem Cell Res* 10: 405–416, 2013.
 33. **Liu H, Liu S, Li Y, Wang X, Xue W, Ge G, Luo X.** The role of SDF-1-CXCR4/CXCR7 axis in the therapeutic effects of hypoxia-preconditioned mesenchymal stem cells for renal ischemia/reperfusion injury. *PLoS One* 7: e34608, 2011.
 34. **Liu X, Shen W, Yang Y, Liu G.** Therapeutic implications of mesenchymal stem cells transfected with hepatocyte growth factor transplanted in rat kidney with unilateral ureteral obstruction. *J Pediatr Surg* 46: 9–9, 2011.
 35. **Liu YL, Wang YD, Zhuang F, Xian SL, Fang JY, Su W, Zhang W.** Immunosuppression effects of bone marrow mesenchymal stem cells on renal interstitial injury in rats with unilateral ureteral obstruction. *Cell Immunol* 276: 144–152, 2012.
 36. **Lu W, Fu C, Song L, Yao Y, Zhang X, Chen Z, Li Y, Ma G, Shen C.** Exposure to supernatants of macrophages that phagocytized dead mesenchymal stem cells improves hypoxic cardiomyocytes survival. *Int J Cardiol* 165: 330–340, 2013.
 37. **Maggini J, Mirkin G, Bognanni I, Holmberg J, Piazzón IM, Nepomnaschy I, Costa H, Cañones C, Raiden S, Vermeulen M, Geffner JR.** Mouse bone marrow-derived mesenchymal stromal cells turn activated macrophages into a regulatory-like profile. *PLoS One* 5: e9252, 2010.
 38. **Mantovani A, Sica A, Sozzani S, Allavena P, Vecchi A, Locati M.** The chemokine system in diverse forms of macrophage activation and polarization. *Trends Immunol* 25: 677–686, 2004.
 39. **Medina RJ, O'Neill CL, O'Doherty TM, Knott H, Guduric-Fuchs J, Gardiner TA, Stitt AW.** Myeloid angiogenic cells act as alternative M2 macrophages and modulate angiogenesis through interleukin-8. *Mol Med* 17: 1045–1055, 2011.
 40. **Mias C, Trouche E, Seguelas MH, Calcagno F, Dignat-George F, Sabatier F, Piercecchi-Marti MD, Daniel L, Bianchi P, Calise D, Bourin P, Parini A, Cussac D.** Ex vivo pretreatment with melatonin improves survival, proangiogenic/mitogenic activity, and efficiency of mesenchymal stem cells injected into ischemic kidney. *Stem Cells* 26: 1749–1757, 2008.
 41. **Morigi M, Inrona M, Imberti B, Corna D, Abbate M, Rota C, Rottoli D, Benigni A, Perico N, Zoja C, Rambaldi A, Remuzzi A, Remuzzi G.** Human bone marrow mesenchymal stem cells accelerate recovery of acute renal injury and prolong survival in mice. *Stem Cells* 26: 2075–2082, 2008.
 42. **Morigi M, Imberti B, Zoja C, Corna D, Tomasoni S, Rottoli D, Angioletti S, Benigni A, Perico N, Alison M, Remuzzi G.** Mesenchymal stem cells are renoprotective, helping to repair the kidney and improve function in acute renal failure. *J Am Soc Nephrol* 15: 1794–1804, 2004.
 43. **Nozaki Y, Nikolic-Paterson DJ, Yagita H, Akiba H, Holdsworth SR, Kitching AR.** Tim-1 promotes cisplatin nephrotoxicity. *Am J Physiol Renal Physiol* 301: F1098–F1104, 2011.
 44. **Nystedt J, Anderson H, Tikkanen J, Pietilä M, Hirvonen T, Takalo R, Heiskanen A, Satomaa T, Natunen S, Lehtonen S, Hakkarainen T, Korhonen M, Laitinen S, Valmu L, Lehenkari P.** Cell surface structures influence lung clearance rate of systemically infused mesenchymal stromal cells. *Stem Cells* 31: 317–326, 2013.
 45. **Otto WR, Wright NA.** Mesenchymal stem cells: from experiment to clinic. *Fibrogenesis Tissue Repair* 4: 1–14, 2011.
 46. **Park HC, Yasuda K, Ratliff B, Stoessel A, Sharkovska Y, Yamamoto I, Jasmin JF, Bachmann S, Lisanti MP, Chander P, Goligorsky MS.** Postobstructive regeneration of kidney is derailed when surge in renal stem cells during course of unilateral ureteral obstruction is halted. *Am J Physiol Renal Physiol* 298: F357–F364, 2010.
 47. **Payne NL, Sun G, McDonald C, Layton D, Moussa L, Emerson-Webber A, Veron N, Siatskas C, Herszfeld D, Price J, Bernard CC.**

- Distinct immunomodulatory and migratory mechanisms underpin the therapeutic potential of human mesenchymal stem cells in autoimmune demyelination. *Cell Transplant* 22: 1409–1425, 2013.
48. **Roca H, Varsos ZS, Sud S, Craig MJ, Ying C, Pienta KJ.** CCL2 and interleukin-6 promote survival of human CD11b+ peripheral blood mononuclear cells and induce M2-type macrophage polarization. *J Biol Chem* 284: 34342–34354, 2009.
 49. **Samuel CS, Butkus A, Coghlan JP, Bateman JF.** The effect of relaxin on collagen metabolism in the nonpregnant rat pubic symphysis: the influence of estrogen and progesterone in regulating relaxin activity. *Endocrinology* 137: 3884–3890, 1996.
 50. **Samuel CS.** Determination of collagen content, concentration, and subtypes in kidney tissue. *Methods Mol Biol* 466: 223–235, 2009.
 51. **Semedo P, Palasio CG, Oliveira CD, Feitoza CQ, Gonçalves GM, Cenedeze MA, Wang PM, Teixeira VP, Reis MA, Pacheco-Silva A, Câmara NO.** Early modulation of inflammation by mesenchymal stem cell after acute kidney injury. *Int Immunopharmacol* 9: 677–682, 2009.
 52. **Shi H, Patschan D, Dietz GP, Bähr M, Plotkin M, Goligorsky MS.** Glial cell line-derived neurotrophic growth factor increases motility and survival of cultured mesenchymal stem cells and ameliorates acute kidney injury. *Am J Physiol Renal Physiol* 294: F229–F235, 2008.
 53. **Spaggiari GM, Moretta L.** Cellular and molecular interactions of mesenchymal stem cells in innate immunity. *Immunol Cell Biol* 91: 27–31, 2013.
 54. **Stefater JA III, Ren S, Lang RA, Duffield JS.** Metchnikoff's policemen: macrophages in development, homeostasis and regeneration. *Trends Mol Med* 17: 743–752, 2011.
 55. **Takai H, Ashihara M, Ishiguro T, Terashima H, Watanabe T, Kato A, Suzuki M.** Involvement of glypican-3 in the recruitment of M2-polarized tumor-associated macrophages in hepatocellular carcinoma. *Cancer Biol Ther* 8: 2329–2338, 2009.
 56. **Tögel F, Hu Z, Weiss K, Isaac J, Lange C, Westenfelder C.** Administered mesenchymal stem cells protect against ischemic acute renal failure through differentiation-independent mechanisms. *Am J Physiol Renal Physiol* 289: F31–F42, 2005.
 57. **Tögel F, Cohen A, Zhang P, Yang Y, Hu Z, Westenfelder C.** Autologous and allogeneic marrow stromal cells are safe and effective for the treatment of acute kidney injury. *Stem Cells Dev* 18: 475–486, 2009.
 58. **Tögel F, Isaac J, Hu Z, Weiss K, Westenfelder C.** Renal SDF-1 signals mobilization and homing of CXCR4-positive cells to the kidney after ischemic injury. *Kidney Int* 67: 1772–1784, 2005.
 59. **Tögel F, Yang Y, Zhang P, Hu Z, Westenfelder C.** Bioluminescence imaging to monitor the in vivo distribution of administered mesenchymal stem cells in acute kidney injury. *Am J Physiol Renal Physiol* 295: F315–F321, 2008.
 60. **Vaidya VS, Ramirez V, Ichimura T, Bobadilla NA, Bonventre JV.** Urinary kidney injury molecule-1: a sensitive quantitative biomarker for early detection of kidney tubular injury. *Am J Physiol Renal Physiol* 290: F517–F529, 2006.
 61. **Vinuesa E, Hotter G, Jung M, Herrero-Fresneda I, Torras J, Sola A.** Macrophage involvement in the kidney repair phase after ischaemia/reperfusion injury. *J Pathol* 214: 104–113, 2007.
 62. **Wang S, Qu X, Zhao RC.** Clinical applications of mesenchymal stem cells. *J Hematol Oncol* 5: 1–9, 2012.
 63. **Williams TM, Little MH, Ricardo SD.** Macrophages in renal development, injury, and repair. *Semin Nephrol* 30: 255–267, 2010.
 64. **Wise AF, Ricardo SD.** Mesenchymal stem cells in kidney inflammation and repair. *Nephrology (Carlton)* 17: 1–10, 2011.
 65. **Woessner JF Jr.** Quantification of matrix metalloproteinases in tissue samples. *Methods Enzymol* 248: 510–528, 1995.
 66. **Xinaris C, Morigi M, Benedetti V, Imberti B, Fabricio AS, Squarcina E, Benigni A, Gagliardini E, Remuzzi G.** A novel strategy to enhance mesenchymal stem cell migration capacity and promote tissue repair in an injury specific fashion. *Cell Transplant* 22: 423–436, 2013.
 67. **Yagi H, Soto-Gutierrez A, Kitagawa Y, Tilles AW, Tompkins RG, Yarmush ML.** Bone marrow mesenchymal stromal cells attenuate organ injury induced by LPS and burn. *Cell Transplant* 19: 823–830, 2009.
 68. **Yi T, Song SU.** Immunomodulatory properties of mesenchymal stem cells and their therapeutic applications. *Arch Pharm Res* 35: 213–221, 2012.
 69. **Yuan L, Wu MJ, Sun HY, Xiong J, Zhang Y, Liu CY, Fu LL, Liu DM, Liu HQ, Mei CL.** VEGF-modified human embryonic mesenchymal stem cell implantation enhances protection against cisplatin-induced acute kidney injury. *Am J Physiol Renal Physiol* 300: F207–F218, 2011.
 70. **Zhang S, Jia Z, Ge J, Gong L, Ma Y, Li T, Guo J, Chen P, Hu Q, Zhang P, Liu Y, Li Z, Ma K, Li L, Zhou C.** Purified human bone marrow multipotent mesenchymal stem cells regenerate infarcted myocardium in experimental rats. *Cell Transplant* 14: 787–798, 2005.
 71. **Zhen-Qiang F, Bing-Wei Y, Yong-Liang L, Xiang-Wei W, Shan-Hong Y, Yuan-Ning Z, Wei-Sheng J, Wei C, Ye G.** Localized expression of human BMP-7 by BM-MSCs enhances renal repair in an in vivo model of ischemia-reperfusion injury. *Genes Cells* 17: 53–64, 2011.



Establishing the Flow Cytometric Assessment of Myeloid Cells in Kidney Ischemia/Reperfusion Injury

Timothy M. Williams,¹ Andrea F. Wise,¹ Maliha A. Alikhan,² Daniel S. Layton,³ Sharon D. Ricardo^{1*}

¹Department of Anatomy and Developmental Biology, Monash University, Victoria, Australia

²Monash Centre for Inflammatory Diseases, Monash University, Victoria, Australia

³Monash Antibody Technologies Facility, Monash University, Victoria, Australia

Received 13 June 2013; Revised 1 November 2013; Accepted 6 November 2013

Grant sponsor: National Health and Medical Research Council (NHMRC); Grant number: 1003806; Grant sponsor: the Alport Foundation of Australia.

Additional Supporting Information may be found in the online version of this article.

*Correspondence to: Sharon D. Ricardo; Department of Anatomy and Developmental Biology, Level 3, Building 75, Monash University, Clayton, Victoria 3800, Australia

Published online 21 November 2013 in Wiley Online Library (wileyonlinelibrary.com)

DOI: 10.1002/cyto.a.22420

© 2013 International Society for Advancement of Cytometry

• Abstract

Polychromatic flow cytometry is a powerful tool for assessing populations of cells in the kidney through times of homeostasis, disease and tissue remodeling. In particular, macrophages have been identified as having central roles in these three settings. However, because of the plasticity of myeloid cells it has been difficult to define a specific immunophenotype for these cells in the kidney. This study developed a gating strategy for identifying and assessing monocyte and macrophage subpopulations, along with neutrophils and epithelial cells in the healthy kidney and following ischemia/reperfusion (IR) injury in mice, using antibodies against CD45, CD11b, CD11c, Ly6C, Ly6G, F4/80, CSF-1R (CD115), MHC class II, mannose receptor (MR or CD206), an alternatively activated macrophage marker, and the epithelial cell adhesion marker (EpcAM or CD326). Backgating analysis and assessment of autofluorescence was used to extend the knowledge of various cell types and the changes that occur in the kidney at various time-points post-IR injury. In addition, the impact of enzymatic digestion of kidneys on cell surface markers and cell viability was assessed. Comparisons of kidney myeloid populations were also made with those in the spleen. These results provide a useful reference for future analyses of therapies aimed at modulating inflammation and enhancing endogenous remodeling following kidney injury. © 2013 International Society for Advancement of Cytometry

• Key terms

monocyte; macrophage; kidney; ischemia/reperfusion injury

INTRODUCTION

A common feature of the progression of immune and nonimmune kidney disease of diverse aetiology is the infiltration of inflammatory macrophages (1). Macrophage numbers have shown to correlate with disease progression, making them a useful tool in predicting disease outcome (1–3). More recently, macrophage heterogeneity has been shown to correspond to the diverse roles that these cells play in both the initiation of tissue fibrosis and the positive role in wound healing and tissue remodeling (4,5). Monocytes recruited in response to inflammatory cues can undergo differentiation into two broad macrophage subsets based on phenotype, function, and polarization state. The classically activated or M1 macrophage is the pro-inflammatory cell type closely associated with the innate immune response, whereas the alternatively activated or M2 macrophage possesses a range of anti-inflammatory and wound healing capabilities (6–8). In part, achieving wound repair and tissue remodeling requires an appropriate balance between the M1 and M2 polarization states.

Traditionally, studies investigating the number of infiltrating macrophages in damaged kidneys have relied on immunohistochemistry (IHC) and immunofluores-

cence (IF) techniques to assess kidney histopathology, cell morphology, and receptor expression. However, flow cytometry is becoming an increasingly important tool, particularly because of the ability to evaluate a panel of cell surface and intracellular markers on individual cells at a rate of over 10,000 cells/second. Eight-color polychromatic flow cytometry in conjunction with two nonfluorescent parameters, forward and side light scattering, is now common and with the latest flow cytometers measuring up to 20 parameters, the information obtainable from each experiment is destined to grow, and with it the need for more rigorous methods of data analysis (9). However, even with improving technology, there remain a number of key challenges related to the preparation of kidney samples for flow cytometry, the selection of appropriate target markers and the informative analysis of the resulting data, which need to be addressed.

The aim of this study was to assess the impact of enzymes (used to produce a kidney single cell suspension) and ischemia/reperfusion (IR) injury on cell yield, viability, surface marker expression, and autofluorescence. Gating strategies were created that best characterize various myeloid cell types, especially where particular receptors were expressed at low levels. The panel of monocyte-, macrophage-, dendritic cell (DC)- and granulocyte-associated markers used included CD11b, CD11c, Ly6C, Ly6G, major histocompatibility complex class II (MHCII), colony stimulating factor-1 receptor (CSF-1R or CD115), mannose receptor (MR or CD206), and F4/80. Particular emphasis of the study was on the assessment of kidney myeloid cell analysis in the inflammatory phase of IR injury, which is characterized by widespread epithelial cell death, an influx of pro-inflammatory cells and heightened inflammatory cytokine production.

In addition, the apoptotic and necrotic epithelial cells of the damaged kidney tubular epithelium, related to the reduced glomerular filtration that follows injury, leads to the accumulation of tubular casts (10). This hallmark of acute kidney injury results in autofluorescence and nonspecific background signals, which leads to difficulties in interpretation of flow cytometric data that is unique to the kidney. Unless addressed, this can lead to erroneous analysis. The intrinsic autofluorescent properties of kidney cells also apply to macrophages because of their propensity to phagocytose cellular debris.

Finally, backgating analysis was used to define and extend the knowledge of myeloid subpopulations in terms of their co-expression of multiple markers and for their spatial location on parent dot plots. This study clarifies and addresses the anomalies encountered when assessing myeloid cells in the kidney, as compared to the more commonly assessed primary and secondary lymphoid organs, while forming a comparative base for which various therapies aimed at manipulating cell numbers and function can be referenced.

MATERIALS AND METHODS

Animals and Surgery

Male 6–8 week old (20–25 g) C57BL/6J mice obtained from Monash Animal Services (Melbourne, Australia) were

used. All studies were approved by the Monash University Animal Ethics Committee and were performed in accordance with the *Australian Code of Practice for the Care and Use of Animals for Scientific Purposes*. Mice were anesthetized with 2.0% inhaled isoflurane (Abbott Australasia, Sydney, Australia) before the left renal pedicle was occluded using a vascular clamp (0.4–1.0 mm; Fine Science Tools, Heidelberg, Germany) for 40 min via a flank incision to induce unilateral IR injury ($n = 5$ mice/group/time-point). Following removal of the clamp, reperfusion was visually confirmed prior to wound closure using silk suture (size 5-0, Ethicon, NJ, USA). An additional group of mice served as a sham-operated control group where the animals were anaesthetized and a flank incision was performed without renal pedicle clamping.

Digestion and Preparation of the Kidney and Spleen for Flow Cytometry

Mice were culled using a CO₂ cull chamber at 6 hours, 1 day or 7 days after IR injury. The spleen and left kidney were removed and placed in cold FACS buffer (PBS supplemented with 0.2% BSA, 0.02% NaN₃ and 5 mM EDTA).

Spleens were cleaned of any connective tissue and mechanically digested in cold FACS buffer to produce a single cell suspension. Mechanical digestion (MD) was achieved by making small incisions in the side of the spleen before gently pressing the organ between two frosted glass slides.

Kidneys were decapsulated and finely chopped with surgical scissors before enzymatic digestion (ED) in 1 mL of dissociation media consisting of HBSS (Sigma-Aldrich, St. Louis, MO, USA) supplemented with 3 mg/mL collagenase/dispase (Roche Applied Science, Penzberg, Germany), 0.2 mg/mL DNase type 1 (Roche Applied Science), 50 μ M CaCl₂, preheated to 37°C. The samples were mixed on a rotary tube suspension mixer (20 RPM; Ratek Instruments, Melbourne, Australia) at 37°C for 20 min and then mechanically digested using a 1000 μ L pipette tip. The samples were mixed for two further 5 min periods (20 RPM) with mechanical dissociation in between. After 30 min, mechanical dissociation with an 18-gauge needle resulted in a single cell suspension. Nine mL of cold FACS buffer was added in order to inhibit enzyme activity.

ED for kidneys and MD for spleens were used for all aspects of this study except for the comparison between ED and MD (Section “Using Enzymes to Aid in the Digestion of the Kidney is more Suitable than MD Alone” and Fig. 1) where both ED and MD were performed on each of the organs.

All single cell suspensions were incubated for 1 min with 1 mL of red blood cell lysis buffer (8.3 g/L Na₄Cl, 10 mM Tris-HCl, pH7.5) to remove red blood cells. All samples were filtered with a 40 μ m nylon cell strainer (BD Bioscience, San Jose, USA) prior to antibody labeling.

Cell Counts and Viability

For flow cytometry cell preparation, cell counts and viability determination were performed using a Z2 Coulter Counter (Beckman Coulter, USA). In addition, for the ED

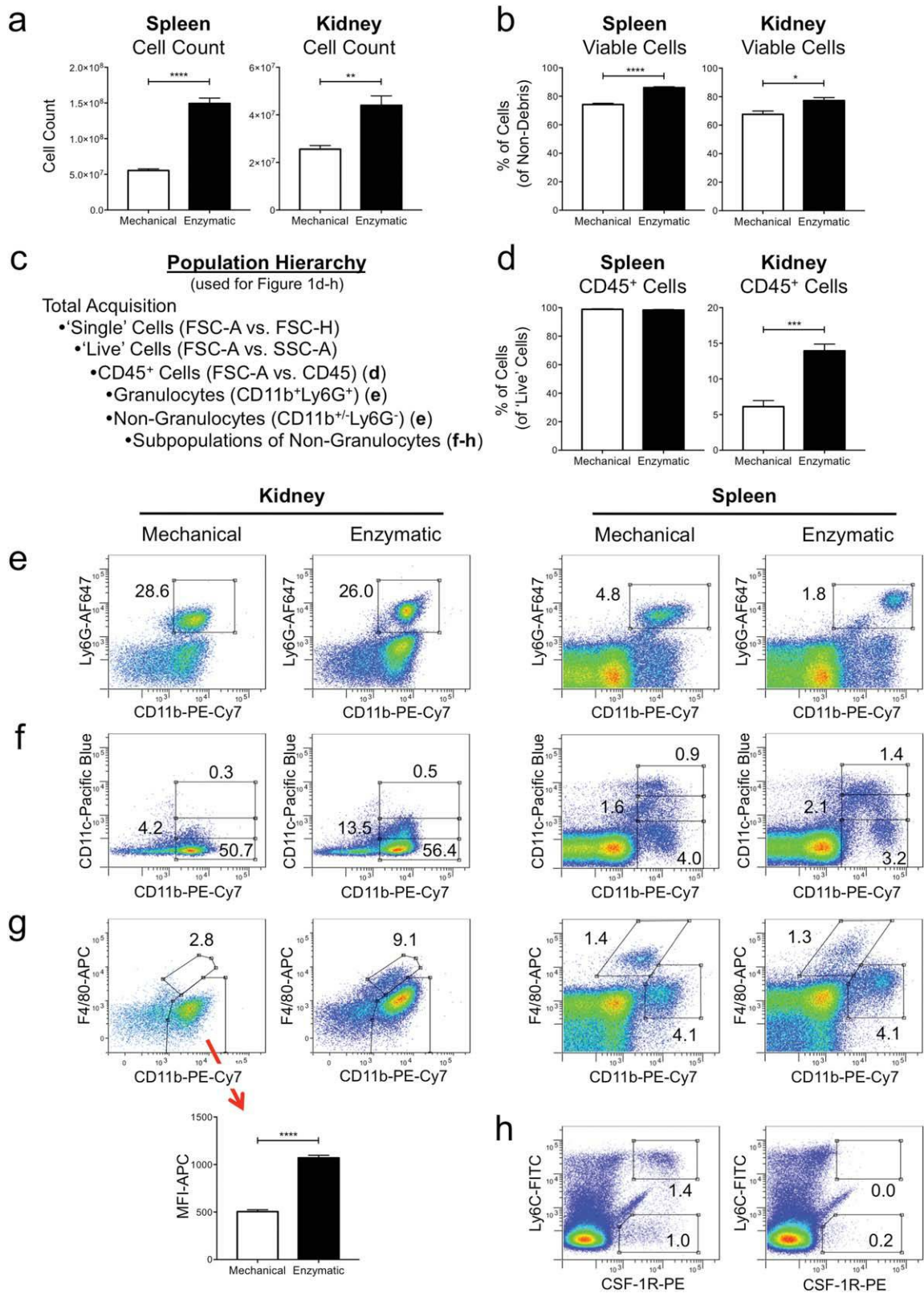


Figure 1.

versus MD study, propidium iodide (PI) was also used to determine cell viability.

Antibody Labeling

Three million cells from kidney or spleen single cell suspensions were incubated for 20 min at 4°C in the dark with the following fluorochrome-conjugated antimouse antibodies: anti-CD45 APC-Cy7 (clone 30-F11; Biolegend, San Diego, USA) and PE-Cy5 (clone 30-F11; BD Biosciences), anti-CD11b PE-Cy7 (clone M1/70; BD Biosciences), anti-CD11c Pacific Blue (clone N418; Biolegend), anti-I-A/I-E (MHCII) PE-Cy5 (clone M5/114.15.2; Biolegend), anti-CSF-1R (CD115) PE (clone AFS98; eBioscience, San Diego, USA), anti-F4/80 APC (clone BM8; eBioscience), anti-Ly6G Alexa Fluor 647 (clone 1A8; Biolegend), anti-Ly6C FITC (clone HK1.4; Biolegend), anti-CD206 (mannose receptor) Alexa Fluor 488 (clone C068C2; Biolegend), and anti-EpCAM (CD326) PE-Cy7 (clone G8.8; Biolegend). Fc receptor block (anti-CD16/32 antibody) was added to all antibody cocktails. Intracellular MR labeling involved the use of a CytoFix/CytoPerm kit (BD Biosciences). Following surface receptor labeling, cells were permeabilized and incubated with antibody for 30 min at 4°C in the dark before being washed twice in 1× Perm/Wash buffer (BD Biosciences) and resuspend in FACS buffer. Isotype matched controls were used for each antibody in a fluorescence minus one (FMO) manner.

Flow Cytometric Acquisition and Analysis

Data were acquired on a BD FACS Canto II flow cytometer (BD Biosciences) equipped with 405, 488, and 633 nm excitation lasers in conjunction with FACS Diva acquisition software (BD Biosciences). Compensation was performed with single color controls for each organ using the same conjugated antibodies used in the study. Data analysis was performed using FlowLogic FCS analysis software (Inivai Technologies, Melbourne, Australia).

Statistical Analysis

Statistical analysis was performed using GraphPad Prism software version 6.0c (GraphPad Software, San Diego, USA). A Student's *t*-test (unpaired, two-tailed, with Welch's correction) was used to analyze data between two groups. A one-way analysis of variance with a Tukey's multiple comparisons

test was used to analyze data contained in three groups. Data are displayed as means ± SEM. *P* < 0.05 was considered statistically significant.

RESULTS

Using Enzymes to Aid in the Digestion of the Kidney is more Suitable than MD Alone

Using enzymes (collagenase/dispase, DNase type I) to aid in the digestion of kidney tissue risks cleaving particular cell surface receptors. In addition, optimal primary and secondary lymphoid organ cell preparations are often achieved with MD alone. It was therefore necessary to test whether ED is indeed required for kidney dissociation. Ten mice received 40 min unilateral IR injury and 24 hours later the spleen and injured kidney were removed. One group of 5 mice had both organs digested with the aid of enzymes, whereas the remaining mice had their organs digested purely by mechanical means. Once digested, cells from each organ were labeled with antibodies against CD45, CD11b, CD11c, Ly6C, Ly6G, MHCII, F4/80, and CSF-1R, and assessed using flow cytometry. Our data show that in both the spleen and the kidney, ED yielded a higher viable cell count compared to MD (spleen MD: 5.54×10^7 , spleen ED: 1.49×10^8 , *P* < 0.0001; kidney MD: 2.56×10^7 , kidney ED: 4.40×10^7 , *P* = 0.0025) (Fig. 1a). Furthermore, propidium iodide staining revealed that ED yielded greater viability for both spleen and kidney cells (spleen MD: 74.2%, spleen ED: 86.1%, *P* < 0.0001; kidney MD: 67.7%, kidney ED: 77.3%, *P* = 0.0153) (Fig. 1b). In assessing hematopoietic cells (as per the gating hierarchy described in Fig. 1c), we found no difference in the proportion of CD45⁺ leukocytes in the spleen with the different digestion methods (MD: 98.8%, ED: 98.3%). However, ED of the kidney resulted in a significantly greater proportion of CD45⁺ cells compared to MD (MD: 6.1%, ED: 13.9%, *P* = 0.0003) (Fig. 1d). Within the CD45⁺ cell pool in the kidney, the digestion method caused no difference in the proportion of Ly6G⁺ granulocytes (MD: 28.6%, ED: 26.0%). However, in the spleen, ED significantly reduced the proportion of this cell type (MD: 4.8%, ED: 1.8%, *P* = 0.0241) (Fig. 1e). In both organs, ED significantly increased the expression (mean fluorescence intensity) of both

Figure 1. Using enzymes to aid in the digestion of the kidney is more suitable than mechanical digestion alone. To compare the effects of two different organ digestion methods, spleens and kidneys from mice at 24 hours post-IR injury were subjected to either mechanical digestion (MD) or enzymatic digestion (ED). For both organs, ED yielded a higher cell count (a). ED also resulted in a greater proportion of viable cells as assessed using propidium iodide (b). The gating hierarchy used to assess viable cells, CD45⁺ cells, Ly6G⁺ granulocytes, and subpopulations of CD11b⁺Ly6G⁺ cells is shown (c). There was no difference in the proportion of CD45⁺ cells in the spleen between ED and MD. However, ED yielded a greater proportion of CD45⁺ cells in the kidney compared to MD (d). The digestion method had no impact on the proportion of CD11b⁺Ly6G⁺ granulocytes in the kidney but significantly reduced the proportion of granulocytes in the spleen (e). In the spleen ED resulted in a greater proportion of CD11b⁺CD11c^{high} and CD11b⁺CD11c^{low} cells compared to MD (f). However, ED increased CD11b expression and resulted in less well-defined CD11c populations (f). The CD11b⁺CD11c^{high} group was largely absent in the kidney, while ED greatly increased the proportion of the CD11b⁺CD11c^{low} population (f). There was no significant difference in the proportions between the CD11b⁺CD11c populations in either organ with regards to the digestion method (f). The proportion of F4/80⁺ cells was significantly greater in the kidney following ED compared to MD (g). No difference was observed in this population in the spleen between MD and ED (g). The MFI of the CD11b⁺F4/80^{low} population in the kidney (depicted graphically) was significantly increased following ED compared to MD (g). CSF-1R expression was dramatically reduced in the spleen following ED compared to MD for both Ly6C^{high} and Ly6C⁺ populations (h). Numbers on dot plots represent proportions of parent populations. Statistical analysis was performed using a Student's *t*-test (unpaired, two-tailed, with Welch's correction); ***P* < 0.01, ****P* < 0.001, *****P* < 0.0001. Data are displayed as means ± SEM (*n* = 5/group).

Ly6G and CD11b on this population, as seen in the dot plots (Fig. 1e) (data not shown).

After excluding the granulocytes, three populations of CD11b⁺ cells were assessed in conjunction with CD11c expression (Fig. 1f). In the spleen, ED resulted in a greater proportion of CD11b⁺CD11c^{high} DCs (MD: 0.9%, ED: 1.4%, $P = 0.0034$), although the populations were less well defined compared to those acquired following MD (Fig. 1f). There were very few cells that shared this phenotype in the kidney, regardless of the digestion method.

The proportion of a second population, which expressed low levels of CD11c, was statistically higher following ED in both the kidney (MD: 4.2%, ED: 13.5%, $P = 0.0003$) and spleen (MD: 1.6%, ED: 2.1%, $P = 0.0084$) (Fig. 1f).

There was no significant difference in the proportion of CD11b⁺CD11c⁻(Ly6G⁻) cells between the two groups in either the kidney (MD: 50.7%, ED: 56.4%) or spleen (MD: 4.0%, ED: 3.2%) (Fig. 1f).

F4/80 expression was assessed on the same CD11b⁺Ly6G⁻ population with a notable difference identified between the two digestion methods in the kidney. With MD, the F4/80⁺ cells were barely detectable but made up over 9% of CD11b⁺Ly6G⁻ cells following ED (MD: 2.8%, ED: 9.1%, $P < 0.0001$) (Fig. 1g). In the spleen there was no difference in the proportion of F4/80⁺ cells (MD: 1.4%, ED: 1.3%) although the population appeared more dispersed following ED (Fig. 1g). In addition, the two digestion methods resulted in substantial differences in the CD11b⁺F4/80^{low/-} populations in the kidney. Once gated, the MFI for the F4/80-APC parameter was assessed and shown to be significantly greater following ED (MD: 505 MFI, ED: 1070 MFI, $P < 0.0001$) (Fig. 1g).

In the spleen, ED reduced the expression of two CSF-1R⁺ populations: a Ly6C^{high}CSF-1R⁺ (MD: 1.38%, ED: 0.03%, $P = 0.0073$) and a Ly6C⁻CSF-1R⁺ population (MD: 1.0%, ED: 0.2%, $P < 0.0001$) (Fig. 1h). Very few CSF-1R⁺ cells were detected in either group in the kidney (data not shown). It must be noted that a change in the proportion of one population can affect the proportion of other populations. However, ED does appear important for assessing F4/80 expression in the kidney, while dramatically reducing surface CSF-1R expression, as demonstrated in the spleen. With this knowledge, a suitable gating strategy was created to clearly identify subpopulations of CD11b⁺ cells in the kidney, both in the steady state and in the inflammatory phase following IR injury.

Gating Strategy for Myeloid Cells in the Kidney

With up to eight-color flow cytometry commonly employed to assess cell phenotypes, there are inevitably many different theoretical subsets that can be defined in any experiment. Here we describe a gating procedure designed to clearly identify important myeloid cell populations in the kidney, accounting for the high potential for autofluorescence, particularly following injury. Figure 2a outlines the population hierarchy used to distinguish between CD11b⁺Ly6G⁺ granulocytes and CD11b⁺Ly6G⁻ nongranulocytes. Initially, a

polygon gate was created on the FSC-A vs. FSC-H plot to select the ‘Single’ cells that passed by the lasers individually (Fig. 2b). CD45⁺ cells from the resulting daughter population were subsequently viewed against FSC-A. These cells represent a viable CD45⁺ population as compared with a similar population identified using propidium iodide to exclude dead cells (data not shown). These CD45⁺ cells were colored red and viewed on a FSC-A vs. SCA-A plot. The coloring of this population enabled a ‘Live’ gate to be drawn on the FSC-A vs. SCA-A plot, to select viable hematopoietic cells and exclude debris (Fig. 2b). This is otherwise difficult to achieve when assessing cells in the kidney as compared to those from lymphoid organs because of the low proportion of CD45⁺ cells. This same technique can also be employed to aid in the creation of the initial ‘Single’ cells gate. A population of CD45⁺CD11b⁺ cells (encompassing resident and infiltrating myeloid cells) was selected from the ‘Live’ cell pool (Fig. 2b). The plots in Figure 2b represent the cells in the kidney 6 hours post-IR surgery, which is characterized by an influx of CD45⁺ cells. Granulocytes were identified in the resulting daughter population based on the positive expression of Ly6G (also Ly6C^{low}) (Fig. 2c) with their proportion being significantly higher at 6 hrs post-IR injury (sham-IR: 23.0%, IR: 28.3%, $P = 0.0222$). An inverse gate effectively excluded the granulocytes for further analysis of myeloid cell subpopulations. Examples from sham-IR and IR kidneys at 6 hours post-surgery are shown (Fig. 2c).

Gating Strategy for Myeloid Cell Subpopulations in the Kidney

The gating strategy used to interrogate CD11b⁺Ly6G⁻ subsets shown in Figure 3a extends from the gating procedure described in Section “Gating Strategy for Myeloid Cells in the Kidney”. Expression of the antigen-presenting molecule MHCII was compared to other markers to identify subpopulations of monocytes and macrophages. An intracellular antibody against MR was used to identify M2 macrophages (Fig. 3b). A quadrant gate was used to identify two MR⁺ populations based on a combination of MR and MHCII expression. While most mature M2 macrophages co-express MHCII (16.9% of CD45⁺CD11b⁺Ly6G⁻ cells at 24 hrs post-IR injury), there was a population of MHCII⁻ cells in which MR was detected (8.5%). The example shown is from a kidney assessed 24 hours following IR injury, prior to the recognized tissue remodeling phase, where M2 macrophages are the predominant macrophage population (11).

CD11b⁺Ly6G⁻ cells were also examined for their expression of the monocyte-associated marker Ly6C (Fig. 3c), the historical mature macrophage marker F4/80 (Fig. 3d) and the DC-associated marker CD11c (Fig. 3e). These markers were all compared to the expression of MHCII. Both a Ly6C^{high} (sham-IR: 3.8%, IR: 27.9%, $P = 0.0004$) and a Ly6C^{low} (sham-IR: 1.4%, IR: 4.5%, $P = 0.0257$) population not expressing MHCII were identified with a much greater proportion in the IR injured kidney. Ly6C is a marker of monocyte immaturity and expression is lost as monocytes transition into macrophages. A general population of Ly6C⁺ cells expressing MHCII was seen (sham-IR: 3.3%, IR: 11.0%, $P = 0.0066$),

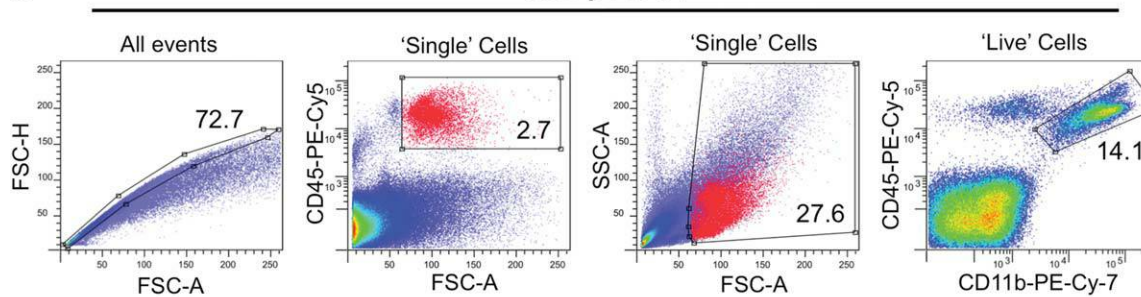
a Population Hierarchy

Total Acquisition

- 'Single' Cells (FSC-A vs. FSC-H) (b)
- 'Live' Cells (FSC-A vs. SSC-A) (b)
- CD45⁺CD11b⁺ Cells (CD11b vs. CD45) (b)
 - Granulocytes (Ly6C^{low}Ly6G⁺) (c)
 - Non-Granulocytes (Ly6C^{+/−}Ly6G[−]) (c)

b

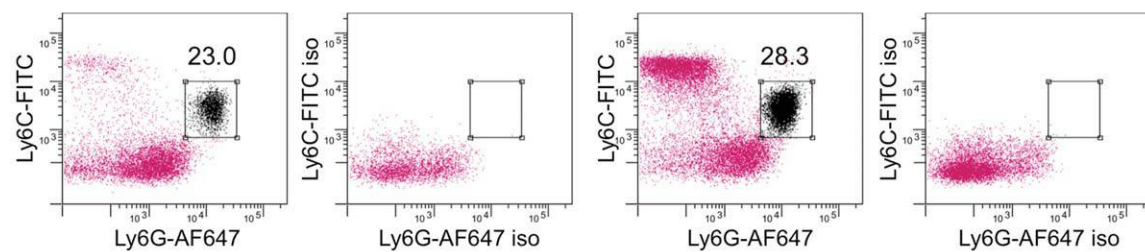
6hrs post-IR



c

Sham-IR

6hrs post-IR



■ CD45⁺ Cells
■ Granulocytes
■ CD11b⁺Ly6G[−] Cells

Figure 2. Gating strategy for assessing myeloid cells in the kidney. The population hierarchy shows the CD11b⁺ gating strategy (a). 'Single' cells (excluding doublets and triplets) were selected with a polygon gate on a FSC-A vs. FSC-H dot plot (b). CD45⁺ cells were gated on the resulting daughter population on a FSC-A vs. CD45 dot plot. These cells were colored (red) and viewed on a FSC-A vs. SSC-A dot plot (b). A 'Live' cell gate (which excludes debris) was created with the aid of the colored CD45⁺ cells (b). CD45⁺CD11b⁺ cells were selected with a polygon gate (b). Granulocytes were selected by gating on Ly6C^{low}Ly6G⁺ cells (c). An inverse gate to select CD11b⁺Ly6C^{+/−}Ly6G[−] cells (pink) was used to gate out granulocytes (black) for further analysis of myeloid cell subsets (c). Plots in b are from a kidney taken 6 hours post-IR injury. Plots in c are from kidneys taken 6 hours post-IR surgery from IR and sham-IR animals. Numbers on dot plots represent proportions of parent populations.

indicating a population of maturing monocytes, which appear to down-regulate their expression of Ly6C and up-regulate MHCII concomitantly (Fig. 3c). F4/80 has historically been regarded as a mature macrophage marker (12). However, more recent reports have shown that it is not expressed on all macrophage populations and has been identified on some Ly6C⁺ monocytes along with a range of other myeloid cells, revoking its status as a sole identifier of macrophages (13–16). When viewed against MHCII, three F4/80⁺ populations were identified (Fig. 3d). The classical F4/80⁺MHCII^{high} mature macrophage was prominent in both sham-IR and IR groups

(gated population) (sham-IR: 59.0%, IR: 30.5%, $P = 0.0001$). When viewed as an overlay containing F4/80 stained cells and an isotype control antibody, an F4/80⁺MHCII^{low} and an F4/80⁺MHCII^{high} population were made evident, particularly following IR-injury (Fig. 3d). The latter population also corresponded with the Ly6C^{high} monocyte population when these cells were gated on a MHCII vs. Ly6C plot and colored (green) (Fig. 3d).

There is much discussion surrounding the similarities and differences between macrophages and DCs. In this model, a clearly defined CD11b⁺CD11c^{high} population, generally

recognized as DCs, was not observed in the kidney (Fig. 3e). There were cells that expressed a low level of CD11c but this population differs from the distinct CD11c^{high} DCs seen in other organs, such as the spleen. For this reason, CD11c expression was viewed on the CD45⁺CD11b⁺ population, rather than as an initial differentiating marker for macro-

phages and DCs. To further investigate the changes to these cells following IR injury, the entire MHCII^{high} population was gated and the change in the MFI for the anti-CD11c antibody analyzed. As seen in the overlay plots for both the sham-IR and the IR groups at 6 hours postsurgery, antibody labeling exists at levels above the isotype control. There is also a

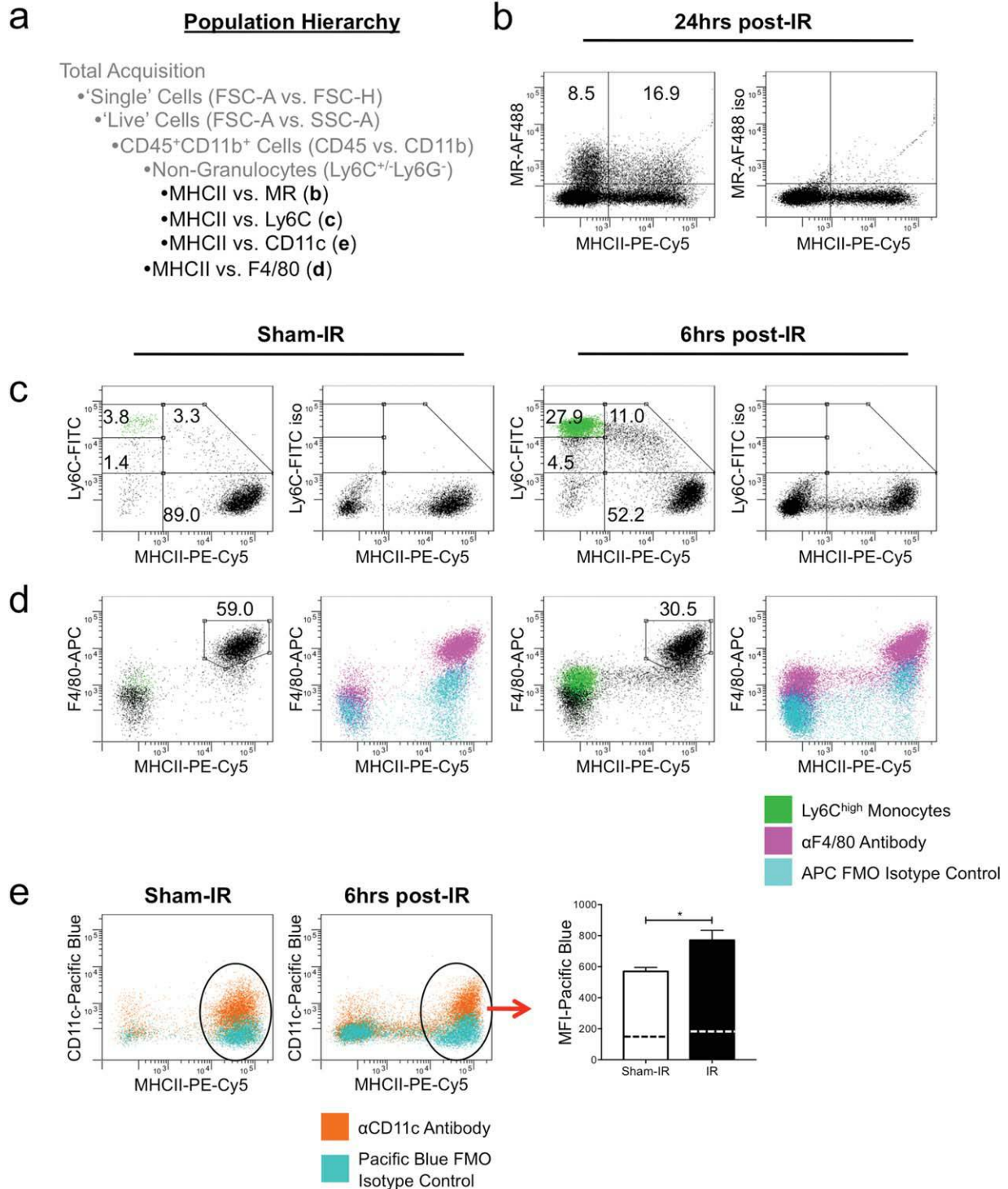


Figure 3.

significant increase in the MFI of this parameter following IR injury (sham-IR: 570 MFI, IR: 770 MFI, $P = 0.031$) (Fig. 3e).

Kidney and Spleen Ly6C⁺, Ly6G⁺, and MHCII⁺ Cell Population Comparison

Backgating analysis was used to further characterize various myeloid subpopulations in the kidney. Comparisons were also made between these cells and their counterparts in the spleen. Figure 4a shows Ly6G⁺(Ly6C^{low}) granulocytes (dark blue). These cells are also displayed on the grandparent FSC-A vs. SSC-A plot (Figure 4b). Granulocytes in the spleen appear similar to those in the sham-IR and IR kidneys 6 hours post-surgery. However, they compose a greater proportion of the CD45⁺CD11b⁺ pool (spleen: 72.5%, sham-IR kidney: 23.0%, IR kidney: 28.3%).

In a similar fashion, MHCII⁺Ly6C⁻ cells (red) (Fig. 4a) were backgated and overlaid onto the same FSC-A vs. SSC-A plots (Fig. 4b) (spleen: 34.2%, sham-IR kidney: 89.0%, IR kidney: 52.2% of the CD45⁺CD11b⁺Ly6G⁻ pool). A far greater proportion and number of Ly6C^{high} cells (green) were present in the IR kidney compared to the sham-IR kidneys (spleen: 31.2%, sham-IR kidney: 3.8%, IR kidney: 27.9% of the CD45⁺CD11b⁺Ly6G⁻ pool) (Fig. 4a). There were distinctly fewer MHCII⁺Ly6C^{low} cells (purple) compared to the Ly6C^{high} population (spleen: 9.2%, sham-IR kidney: 1.4%, IR kidney: 4.5% of the CD45⁺CD11b⁺Ly6G⁻ pool) (Fig. 4a). The maturing or transitioning monocytes (MHCII^{low}Ly6C⁺, light blue) are also most prevalent in the IR compared to the sham-IR kidneys (spleen: 12.4%, sham-IR kidney: 3.3%, IR kidney: 11.0% of the CD45⁺CD11b⁺Ly6G⁻ pool) (Fig. 4a). All of the Ly6C expressing cells from both organs present in a similar fashion on the FSC-A vs. SCA-A plots, as do the MHCII⁺ populations. The granulocyte population in the spleen appears to be composed of cells with a greater range of size and granularity compared to that in the kidney (Fig. 4b).

Assessing Epithelial Cells and Autofluorescence in the Post-Ischemic Kidney

Epithelial proliferation leading to regeneration and repair is central to processes of healing following various forms of kidney disease, including IR injury (17). As such, the pan epithelial marker EpCAM was used to assess the impact of IR injury on epithelial cell populations. To assess EpCAM⁺ cells,

'Single' cells were gated, followed by 'Live' cells (to exclude debris), as depicted in the population hierarchy (Fig. 5a). EpCAM expression was then compared to CD45 expression, with a gate placed around the CD45⁺EpCAM⁺ population (Fig. 5b). The proportion of EpCAM⁺ cells had already significantly decreased at 6 hours post-IR injury (sham-IR: 16.3%, IR: 9.6%, $P=0.0001$) and fell further as seen at day 7 postinjury (sham-IR: 14.3%, IR: 5.9%, $P=0.0001$). Autofluorescence can pose a problem, as is evident when the kidneys taken 6 hours post-IR are displayed alongside those taken 7 days postinjury, where prominent autofluorescence is visible in the IR anti-EpCAM antibody and isotype control groups (Fig. 5b). The autofluorescence was not present in the IR group 6 hours postinjury. For the day 7 time-point, a modified EpCAM⁺ gate was created in order to exclude the autofluorescence from the EpCAM⁺ population. This method can also be employed for clearly distinguishing CD45⁺ cells from the rest of the kidney cells. Backgating analysis of the EpCAM⁺, autofluorescent and CD45⁺ cells was performed to view their location on the parent FSC-A vs. SSC-A dot plot (Fig. 5c). The difference between the different cell types is clear, with the CD45⁺ cells forming a tighter group further along the forward scatter axis compared to the EpCAM⁺ cells and autofluorescent events.

Autofluorescence increases progressively with time after IR injury. Figure 5d shows autofluorescent cells, after gating on CD45⁺CD11b⁺ cells, on a Ly6C vs. MHCII plot from a sham-IR kidney along with injured kidneys at 24 hours and 7 days post-IR. The autofluorescent populations were backgated and shown in pink on the CD11b vs. CD45 parent plot. At 7 days post-IR the autofluorescence is very difficult to distinguish from nonautofluorescent CD11b⁺ cells. Empty channels may be useful for gating out autofluorescence that is associated with IR-induced damage. The increase in the autofluorescence increased almost threefold between 24 hours and 7 days post-IR injury (sham-IR: 1.3%, 24 hrs post-IR: 7.8%, 7 days post-IR: 21.2%) (Fig. 5e).

DISCUSSION

Identifying and characterizing macrophage functional/polarization states is necessary to understand processes of disease progression and healing. Here, we have described a polychromatic flow cytometry analysis strategy, taking into

Figure 3. Gating strategy for CD11b⁺ cell subpopulations in the kidney. The gating hierarchy (continued from Figure 2) shows the procedure used to assess CD11b⁺ cells following the exclusion of Ly6G⁺ granulocytes (a). M2 macrophages, defined as being MR⁺, were assessed in conjunction with the expression of MHCII (b). Subsequent monocyte/macrophage subsets were defined based on the cellular expression of MHCII, Ly6C, F4/80 and CD11c (c–e). Ly6C was used to distinguish monocytes at various maturation stages. Ly6C^{high} cells (MHCII⁻) are immature monocytes. The marker is down regulated as the cells mature. A prominent Ly6C^{high} (MHCII⁻) population is present at 6hrs post-IR injury (green) (c), along with a smaller Ly6C^{low}MHCII⁻ population (c). A maturing or transitioning population of MHCII^{low}Ly6C⁺ cells exist, particularly following IR-injury (c). A prominent Ly6C^{high}MHCII^{high} population exists in kidneys following both sham-IR and IR-surgery (c). MHCII can also be used to distinguish between three F4/80⁺ populations. A prominent F4/80⁺MHCII^{high} population was identified (gated cells) (d). The dot plot overlay shows this population (pink) compared with an isotype control antibody (light blue) (d). The overlay also helped identify populations of F4/80⁺MHCII^{low} and F4/80⁺MHCII⁻ cells. The latter corresponds to the Ly6C^{high} population (green) (d). Low levels of CD11c expression can make it difficult to distinctly categorize CD11c⁺ cells in the kidney, as opposed to its expression when examined in lymphoid organs or the blood. Here the CD11c labeled cells (orange) were overlaid with an isotype control (light blue) (e). In addition, the MFI of the CD11c-Pacific Blue antibody was assessed for the MHCII^{high} population. These data are displayed graphically with the MFI for the isotype controls indicated using a broken line (e). Appropriate isotype controls (iso) are displayed. Numbers on dot plots represent proportions of parent populations. Statistical analysis was performed using a Student's *t*-test (unpaired, two-tailed, with Welch's correction); * $P < 0.05$. Data are displayed as means \pm SEM ($n = 5$ /group).

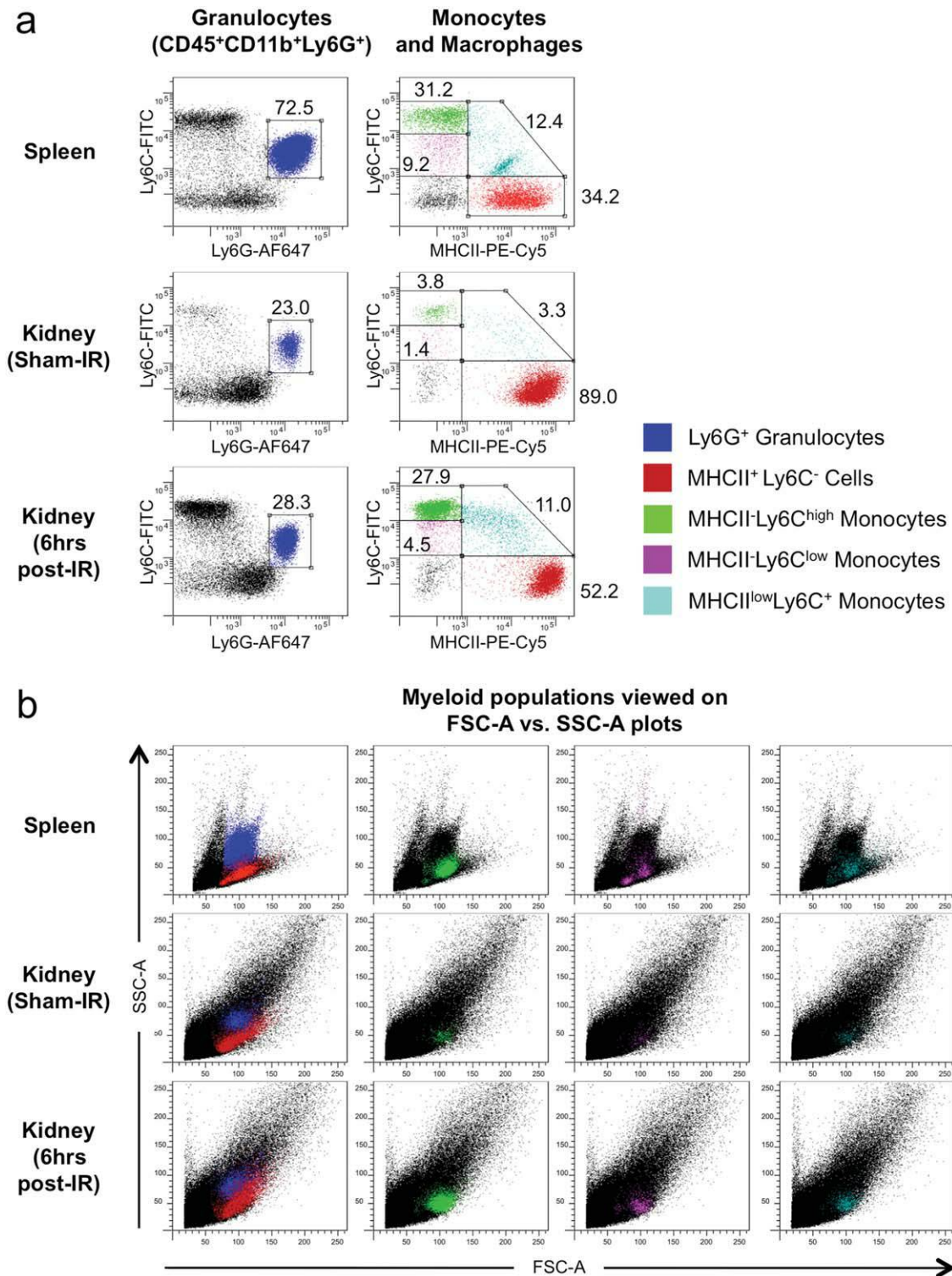


Figure 4. Kidney and spleen Ly6C⁺, Ly6G⁺ and MHCII⁺ cell population comparison. Backgating analysis of flow cytometry data was used to compare the relative positioning of Ly6G⁺ granulocytes (dark blue), MHCII⁺ Ly6C⁻ cells (red), MHCII⁺ Ly6C^{high} cells (green), MHCII⁺ Ly6C^{low} cells (purple) and maturing or transitioning monocytes (MHCII^{low} Ly6C⁺) (light blue) (a). Backgating analysis of these populations shows their profiles on FSC-A vs. SSC-A dot plots (b). Examples from spleen and kidneys at 6 hours post-sham-IR and IR surgery. Numbers on dot plots represent proportions of parent populations.

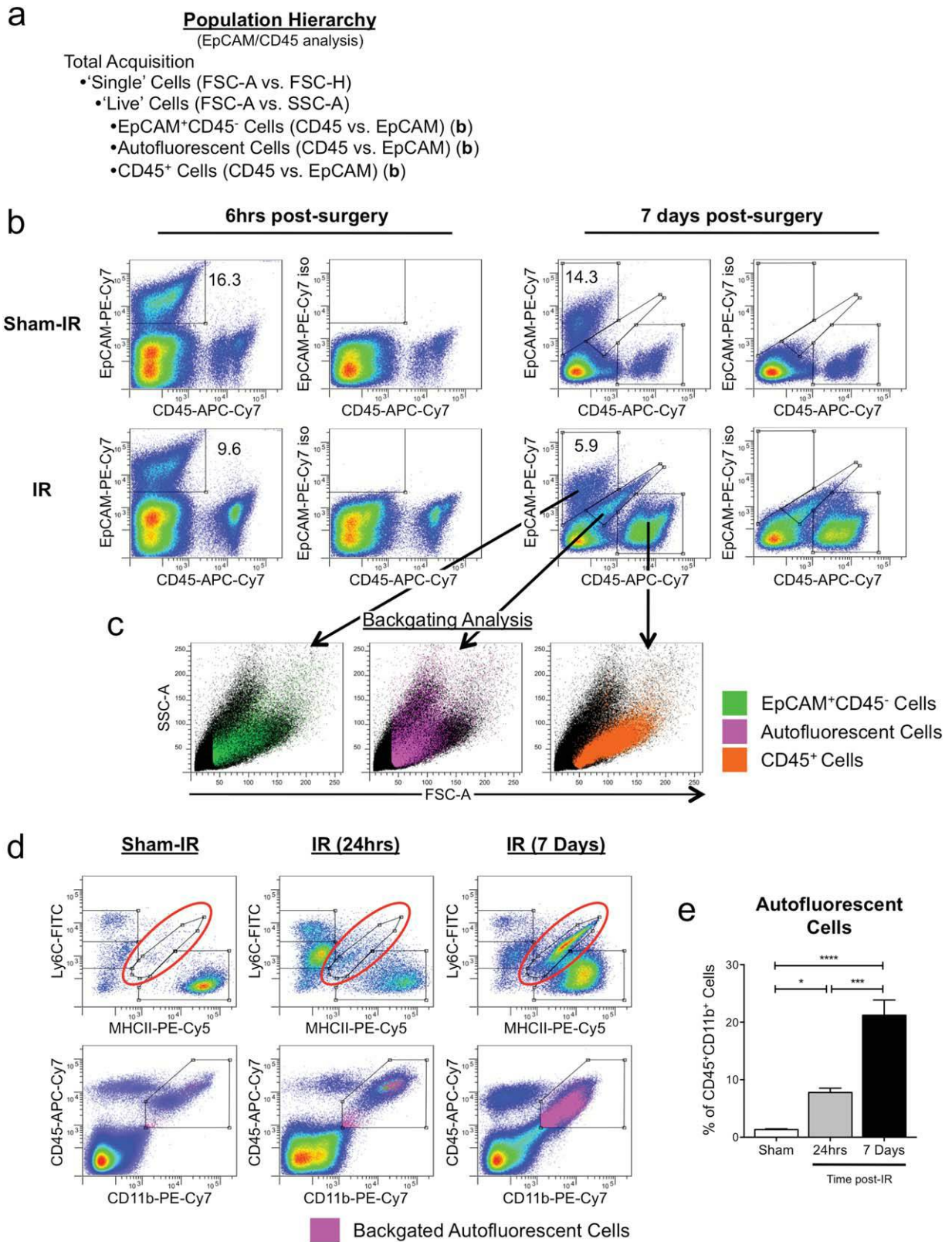


Figure 5.

account light scattering and autofluorescent characteristics, to assess infiltrating and resident cells in the uninjured kidney and in the inflammatory phase following IR injury. Performing backgating analysis along with coloring populations and viewing them against multiple parameters will lead to more detailed phenotypic and functional descriptions. This includes information regarding the maturation state of the cell, its autofluorescent properties and functional capacity, which can be linked to other data, such as cytokine production and enzyme activity. This is particularly relevant to tissue macrophages because of their heterogeneity, especially in the disease setting where they play central roles in inflammation and tissue remodeling.

One marker that we focused on was Ly6C, as its expression can be used to define monocyte maturation and function, with Ly6C^{high} pro-inflammatory cells down regulating the marker as they mature into Ly6C^{low} macrophages (18). In addition, the activation of monocytes at various maturation stages leads to mature macrophages of distinct functional states (18). Following unilateral ureteral obstruction, Ly6C^{high} cells have been shown to home to kidneys where they differentiate into monocytes/macrophages of distinct functional states, indeed identified by the level of Ly6C expression (19). Our data showed that the initial inflammatory phase of the IR model involves a dramatic increase in the proportion and number of Ly6C^{high} monocytes. As such, assessing changes in this population with various treatments or in fact targeting this cell type directly may impact the degree of injury or provide increased potential for regeneration. A number of studies have used antibodies against Gr-1, a complex formed by both Ly6C and Ly6G, to separate monocytes from granulocytes (20). Confirmed here in the kidney, using separate antibodies against Ly6C and Ly6G allows for an easier delineation of monocytes and granulocytes, and where applicable allows for further separation of the granulocyte pool into neutrophils and eosinophils (21). Monocyte populations have also been defined by their expression of the chemokine receptors, CX₃CR1 and CCR2 (22,23). CD11b⁺CCR2^{low}Gr1^{int}Ly6C^{high}CX₃CR1^{high} monocytes migrate to normal tissues, whereas inflammatory monocytes with a CD11b⁺CCR2^{high}Gr1^{int}Ly6C^{high}CX₃CR1^{low} phenotype home to injured tissues (24).

We also chose to assess MR expression as it is a useful identifier of M2 macrophages (4,25). Indeed, mannose receptor 2 has been shown to be upregulated on macrophages following unilateral ureteral obstruction and is believed to play a role in modulating fibrosis through binding and internalizing

collagen via an extracellular fibronectin type II domain (26,27). Interestingly, this study showed that two populations of MR⁺ cells (MHCII⁻ and MHCII⁺) exist in the kidney at 24 hours post-IR injury. Again, targeting or manipulating this cell type may help promote kidney remodeling and regeneration. When considering assessing MR expression with flow cytometry, it should be noted that MR is expressed weakly on the cell surface (28). Membrane permeabilization may result in more effective labeling, although this does not allow for isolation of a potential viable M2 population via FACS.

Autofluorescence is another characteristic of kidney IR injury that needs to be considered carefully. Myeloid cells, particularly those expressing CD11b, CD11c and high levels of F4/80, exhibit autofluorescence at a range of excitation and emission wavelengths (14). Certain myeloid populations can even be defined based on their autofluorescence signature. However, if a full panel of fluorochromes is being used then there is a risk of erroneous emission signals. Using an FMO approach for antibody controls is useful for identifying and minimizing the effects of autofluorescence (29). This study showed that autofluorescence increases over time in kidney IR injury and can be potentially problematic when assessing both hematopoietic and nonhematopoietic populations. Measuring autofluorescence may also prove to be a useful indicator of injury and repair, especially if assessed over a longer time-course and correlated with other injury biomarkers.

The subtle differential expression of markers such as MHCII may also prove to be important in characterizing macrophage subsets and determining functional capabilities. Even the notion of a DC has been challenged in recent times with some evidence suggesting that they might be more closely associated with macrophages than previously thought. This study highlights the difference in the expression of the classical DC marker, CD11c, between the spleen and the kidney, and that the lack of a clear CD11c population may mean that examining CD11c on subpopulations may be more useful than trying to, for example, separate the CD45⁺ population into macrophages and DCs. The assessment of CD11c expression in this study also demonstrates the usefulness of measuring MFI for a particular antibody in lieu of, or in addition to, population proportions, especially when the expression is low or when shifts in expression levels are subtle.

Part of the challenge in using flow cytometry to assess subpopulations of cells in the kidney is choosing an appropriate panel of markers to investigate. This is further complicated knowing that different digestion methods may enhance

Figure 5. Assessing epithelial cells and autofluorescence in the post-ischemic kidney. The population hierarchy resulting from the EpCAM⁺ epithelial gating analysis is shown (a). Following the gating of 'Single' cells (FSC-A vs. FSC-H) and 'Live' cells (FSC-A vs. SSC-A) (data not shown), EpCAM⁺ epithelial cells were selected for their expression of EpCAM and for a lack of expression of the hematopoietic marker CD45 (b). With the progression of time in the IR model, autofluorescence becomes increasingly prominent. In this example, at 7 days post-IR, the EpCAM⁺ gate was altered so as not to include autofluorescent cells (b). Backgating analysis shows the difference in the FSC-A vs. SSC-A profile of CD45⁻EpCAM⁺, autofluorescent and CD45⁺ populations (c). An autofluorescent population appeared when examining the CD45⁺CD11b⁺ cell pool in the kidney following IR injury (d). On the MHCII vs. Ly6C dot plots, autofluorescence became more prominent with time after injury (d). This autofluorescent population was backgated and displayed in pink on the parent CD11b vs. CD45 plot (d). The increase in the proportion of this autofluorescent population with time (after injury) is shown graphically (e). Numbers on dot plots represent proportions of parent populations. Statistical analysis was performed using a one-way analysis of variance with a Tukey's multiple comparisons test; ***P* < 0.01, ****P* < 0.001, *****P* < 0.0001. Data are displayed as means ± SEM (*n* = 5/group).

detection of a particular cell type or negatively impact individual markers or receptors. The ED protocol described in this paper was optimized for the combination of enzymes used (collagenase/dispase, DNase type 1). The enzyme concentrations and incubation times, along with the method of mechanical dissociation (size of pipette tip and timing of the dissociations), were all methodically tested to achieve an optimal digestion as determined by cell counts, viability and flow cytometric profiles. This study demonstrated that ED is indeed required to achieve greater viable and CD45⁺ cells yields and to most effectively study cells expressing markers such as F4/80. However, variations in dissociation media may be required for different disease models, as some are characterized by inflammation, cell infiltrate, and cell death, whilst others may centre on fibrosis and collagen deposition. The combination of collagenase/dispase and DNase type 1 appeared to impact negatively on CSF-1R expression, as seen on Ly6C^{high} and Ly6C⁺ cells in the spleen, again highlighting the need to optimize digestion methods for each specific study.

Equally as rapid as the advancements in flow cytometer technology, is the development of new fluorochromes and viability dyes. These are providing narrower emission spectra allowing for greater clarity in population identification. There is also now a range of viability dyes available for a large variety of excitation and emission wavelengths. The interactive tools available online, such as spectra viewers and panel builders are also very useful in creating optimal antibody cocktails.

CONCLUSION

This study has highlighted some of the advantages and limitations associated with assessing kidney cells using flow cytometry, particularly in the IR injury model. This can be an incredibly powerful tool but requires a tested and systematic approach, including the method for organ digestion, antibody selection (target antigen and fluorochrome) and specific gating strategies. Other analytical techniques, including IHC, IF, and PCR should be used in conjunction with flow cytometry data to provide a complete depiction of cell types present together with localization in the tissue in which they reside. The obvious extension of the use of flow cytometry to analyze cell populations is the sorting of live populations for further investigations *in vitro* or in adoptive transfer experiments.

ACKNOWLEDGMENTS

Timothy M. Williams and Daniel S. Layton have been involved in the development of FlowLogic FCS analysis software.

LITERATURE CITED

- Duffield JS. Macrophages and immunologic inflammation of the kidney. *Semin Nephrol* 2010;30:234–254. Available at: <http://eutils.ncbi.nlm.nih.gov/entrez/eutils/eflink.fcgi?dbfrom=pubmed&id=20620669&retmode=ref&cmd=prlinks>.
- Nguyen D, Ping F, Mu W, Hill P, Atkins RC, Chadban SJ. Macrophage accumulation in human progressive diabetic nephropathy. *Nephrology (Carlton, Vic)* 2006;11:226–231.
- Chow F, Ozols E, Nikolic-Paterson DJ, Atkins RC, Tesch GH. Macrophages in mouse type 2 diabetic nephropathy: correlation with diabetic state and progressive renal injury. *Kidney Int* 2004;65:116–128.
- Ricardo SD, van Gooor H, Eddy AA. Macrophage diversity in renal injury and repair. *J Clin Invest* 2008;118:3522–3530.
- Williams TM, Little MH, Ricardo SD. Macrophages in renal development, injury, and repair. *Semin Nephrol* 2010;30:255–267.
- Mantovani A, Sica A, Sozzani S, Allavena P, Vecchi A, Locati M. The chemokine system in diverse forms of macrophage activation and polarization. *Trends Immunol* 2004;25:677–686.
- Martinez FO, Helming L, Gordon S. Alternative activation of macrophages: An immunologic functional perspective. *Annu Rev Immunol* 2009;27:451–483.
- Mosser DM, Edwards JP. Exploring the full spectrum of macrophage activation. *Nat Rev Immunol* 2008;8:958–969.
- Chattopadhyay PK, Roederer M. Cytometry: Today's technology and tomorrow's horizons. *Methods* 2012;57:251–258.
- Zuk AA, Bonventre JV, Brown DD, Matlin KSK. Polarity, integrin, and extracellular matrix dynamics in the posts ischemic rat kidney. *Am J Physiol* 1998;275:C711–C731.
- Lee S, Huen S, Nishio H, Nishio S, Lee HK, Choi B-S, Ruhrberg C, Cantley LG. Distinct macrophage phenotypes contribute to kidney injury and repair. *J Am Soc Nephrol* 2011;22:317–326.
- Austyn JM, Gordon SS. F4/80, a monoclonal antibody directed specifically against the mouse macrophage. *Eur J Immunol* 1981;11:805–815.
- Taylor PRP, Brown GDG, Geldhof ABA, Martinez-Pomares LL, Gordon SS. Pattern recognition receptors and differentiation antigens define murine myeloid cell heterogeneity *ex vivo*. *Eur J Immunol* 2003;33:2090–2097.
- Mitchell AJ, Pradel LC, Chasson L, Van Rooijen N, Grau GE, Hunt NH, Chimini G. Technical advance: Autofluorescence as a tool for myeloid cell analysis. *J Leukoc Biol* 2010;88:597–603.
- Nonaka K, Saio M, Suwa T, Frey AB, Umemura N, Imai H, Ouyang G-F, Osada S, Balazs M, Adany R, Kawaguchi Y, Yoshida K, Takami T. Skewing the Th cell phenotype toward Th1 alters the maturation of tumor-infiltrating mononuclear phagocytes. *J Leukoc Biol* 2008;84:679–688.
- Stables MJ, Shah S, Camon EB, Lovering RC, Newson J, Bystrom J, Farrow S, Gilroy DW. Transcriptomic analyses of murine resolution-phase macrophages. *Blood* 2011;118:e192–208.
- Alikhan MA, Jones CV, Williams TM, Beckhouse AG, Fletcher AL, Kett MM, Sakkal S, Samuel CS, Ramsay RG, Deane JA, Wells CA, Little MH, Hume DA, Ricardo SD. Colony-stimulating factor-1 promotes kidney growth and repair via alteration of macrophage responses. *Am J Pathol* 2011;179:1243–1256.
- Sunderkötter C, Nikolic T, Dillon MJ, van Rooijen N, Stehling M, Drevets DA, Leenen PJM. Subpopulations of mouse blood monocytes differ in maturation stage and inflammatory response. *J Immunol* 2004;172:4410–4417.
- Lin SL, Castaño AP, Nowlin BT, Lupher ML, Duffield JS. Bone marrow Ly6Chigh monocytes are selectively recruited to injured kidney and differentiate into functionally distinct populations. *J Immunol* 2009;183:6733–6743.
- Fleming TJT, Fleming MLM, Malek TRT. Selective expression of Ly-6G on myeloid lineage cells in mouse bone marrow. RB6–8C5 mAb to granulocyte-differentiation antigen (Gr-1) detects members of the Ly-6 family. *J Immunol* 1993;151:2399–2408.
- Rose S, Misharin A, Perlman H. A novel Ly6C/Ly6G-based strategy to analyze the mouse splenic myeloid compartment. *Cytometry Part A* 2012;81A:343–350.
- Geissmann F, Jung S, Littman DR. Blood monocytes consist of two principal subsets with distinct migratory properties. *Immunity* 2003;19:71–82.
- Li L, Huang L, Sung S-SJ, Vergis AL, Rosin DL, Rose CE, Lobo PI, Okusa MD. The chemokine receptors CCR2 and CX3CR1 mediate monocyte/macrophage trafficking in kidney ischemia–reperfusion injury. *Kidney Int* 2008;74:1526–1537.
- Tacke F, Randolph GJ. Migratory fate and differentiation of blood monocyte subsets. *Immunobiology* 2006;211:609–618.
- Gordon S. Alternative activation of macrophages. *Nat Rev Immunol* 2003;3:23–35.
- Kushiyama T, Oda T, Yamada M, Higashi K, Yamamoto K, Sakurai Y, Miura S, Kumagai H. Alteration in the phenotype of macrophages in the repair of renal interstitial fibrosis in mice. *Nephrology (Carlton, Vic)* 2011;16:522–535.
- Lopez-Guisa JM, Cai X, Collins SJ, Yamaguchi I, Okamura DM, Bugge TH, Isacke CM, Emson CL, Turner SM, Shankland SJ, Eddy AA. Mannose receptor 2 attenuates renal fibrosis. *J Am Soc Nephrol* 2012;23:236–251.
- Martinez-Pomares LL, Reid DMD, Brown GDG, Taylor PRP, Stillion RJR, Linehan SAS, Zamze SS, Gordon SS, Wong SYCS. Analysis of mannose receptor regulation by IL-4, IL-10, and proteolytic processing using novel monoclonal antibodies. *J Leukoc Biol* 2003;73:604–613.
- Perfetto SP, Chattopadhyay PK, Roederer M. Seventeen-colour flow cytometry: unravelling the immune system. *Nat Rev Immunol* 2004;4:648–655.

Detailed Zymography methodology for Chapter 3

As gelatin is the preferred substrate for gelatinases (MMP-2 and MMP-9), their expression/activity were determined by gelatin zymography; a gel electrophoresis method that exploits the incorporation of gelatin into the acrylamide gel (65). Briefly, protein extracts from kidney tissues (containing 15ug of total protein) were mixed with sample loading buffer (containing 62.5mM Tris/HCl, pH 6.8, 2% (w/v) SDS, 10% (w/v) glycerol and 0.01% (w/v) bromophenol blue) in a volumetric ratio of 1:4, for 1 hour at room temperature, prior to gel loading. Samples were electrophoresed on 7.5% (wt/vol) acrylamide separating gels containing 1 mg/ml gelatin and 3.5% acrylamide stacking gels. Completed gels were washed with 0.25% (w/v) Triton X-100 and incubated with an incubation buffer containing 50mM Tris-Hcl (pH 7.5), 10mM CaCl₂, 1% (w/v) Triton X-100, 0.02% (w/v) NaN₃ and 1μM ZnCl₂ overnight at 37°C. Gels were then stained with 0.1% (wt/v) Coomassie blue R-250 in 40% isopropanol for 1 hour and then destained with 7% (v/v) acetic acid to reveal clear bands of gelatinolytic activity. Densitometry of these MMP bands was performed using a GS710 Densitometer (Bio-Rad Laboratories) and data were analyzed using Quantity-One software.